



HAL
open science

Analysis and design of space-time block codes for coded MIMO transmissions

Ammar El Falou

► **To cite this version:**

Ammar El Falou. Analysis and design of space-time block codes for coded MIMO transmissions. Networking and Internet Architecture [cs.NI]. Télécom Bretagne, Université de Bretagne-Sud, 2013. English. NNT: . tel-00908835

HAL Id: tel-00908835

<https://theses.hal.science/tel-00908835>

Submitted on 25 Nov 2013

HAL is a multi-disciplinary open access archive for the deposit and dissemination of scientific research documents, whether they are published or not. The documents may come from teaching and research institutions in France or abroad, or from public or private research centers.

L'archive ouverte pluridisciplinaire **HAL**, est destinée au dépôt et à la diffusion de documents scientifiques de niveau recherche, publiés ou non, émanant des établissements d'enseignement et de recherche français ou étrangers, des laboratoires publics ou privés.

Sous le sceau de l'Université européenne de Bretagne

Télécom Bretagne

En habilitation conjointe avec l'Université de L'Université de Bretagne-Sud

École Doctorale – SICMA

Analysis and design of space-time block codes for coded MIMO transmissions

Thèse de Doctorat

Mention : « Science et Technologies de l'Information et de la Communication (STIC) »

Présentée par **Ammar El Falou**

Département : Électronique

Laboratoire : Lab – STICC Pôle : CACS

Directeur de thèse : Catherine Douillard

Soutenue le 23 Mai 2013

Jury :

Mme. Ghaya Rekaya-Ben Othman, Professeur, ComElec, Télécom ParisTech (Rapporteur)
M. Olivier Berder, Maître de Conférences HDR, CAIRN, ENSSAT (Rapporteur)
Mme. Maryline Héléard, Professeur, IETR, INSA Rennes (Examinateur)
M. Jean-Pierre Cances, Professeur, ELT, ENSIL (Examinateur)
Mme. Laura Condé, Maître de Conférences, Lab-STICC, UBS (Examinateur)
Mme. Catherine Douillard, Professeur, Télécom Bretagne (Directeur de thèse)
Mme. Charlotte Langlais, Maître de Conférences, Télécom Bretagne (Encadrant)
M. Charbel Abdel Nour, Maître de Conférences, Télécom Bretagne (Co-encadrant)

“La diversité crée la richesse !”

Abstract

Most of the modern wireless communication systems as WiMAX, DVB-NGH, WiFi, HSPA+, LTE and 4G have adopted the use of multiple antennas at the transmitter and the receiver, called multiple-input multiple-output (MIMO). Space time coding for MIMO systems is a promising technology to increase the data rate and enhance the reliability of wireless communications. The diversity-multiplexing tradeoff (DMT) characterizes the interplay between data rate and reliability achieved by any transmission over MIMO channels.

Space-time block codes (STBCs) are commonly designed according to the rank-determinant criteria suitable at high signal to noise ratios (SNRs). In contrast, wireless communication standards employ MIMO technology with capacity-approaching forward-error correcting (FEC) codes like turbo codes and low-density parity-check (LDPC) codes, ensuring low error rates even at low SNRs.

In this thesis, we investigate the design of STBCs for MIMO systems with capacity-approaching FEC codes. Conventional STBC design criteria are asymptotic while capacity-approaching FEC codes achieve their desired performance at a specific SNR depending on the coding rate. We start by optimizing a low complexity maximum-likelihood (ML)-detection STBC according to the trace criterion, accurate at low SNRs. The resulting STBC outperforms the original STBC in the context of a WiMAX system especially with low coding rates. Afterwards, we propose a non-asymptotic STBC design criterion based on the bitwise mutual information (BMI) maximization between transmitted and soft estimated bits at a specific target SNR. We optimize several conventional STBCs according to the BMI criterion. Their design parameters are shown to be SNR-dependent leading to the proposal of adaptive STBCs. Among them, our proposed adaptive trace-orthonormal based STBC shows identical or better performance than standard WiMAX profiles for all coding rates. In addition to performance, the complexity is an important issue for practical communication systems. Therefore, we assess the complexity of the WiMAX receiver. Moreover, the proposed adaptive trace-orthonormal STBC is proven to be ML-detected with a low complexity at low SNRs. The proposal of adaptive STBCs is important for system design as they can always provide the best performance with the lowest complexity compared to conventional non-adaptive STBCs.

The first part of our study assumes that transmit and receive antennas are perfectly uncorrelated. This assumption depends on the communication environment and is not always valid *e.g.*, in indoor case or for mobile phones. Thereby, to complete our study, we investigate the effect of spatial correlation between antennas on the performance of

coded MIMO systems. The correlation effect differs depending on the employed MIMO codes. We show that the BMI criterion can always be used to classify and select the suitable MIMO code depending on the communication environment.

Afterwards, we examine MIMO systems using more than dual transmit antennas. In order to limit the system complexity increase, we consider that an antenna selection (AS) is performed where the transmission is only done via best antennas. In the MIMO literature, the AS for MIMO systems has been studied only for the case of uncoded systems where it has been proved that it provides large diversity and SNR gains. In this thesis, the benefits of AS technology for coded MIMO systems are addressed. We start by designing adaptive STBCs for MIMO systems employing the AS then we show that, although no additional diversity gain is observed in this context, a substantial SNR gain of more than 3 dB is obtained with respect to a conventional WiMAX system.

Conventional STBCs are designed according to the rank-determinant criteria in a way achieving the asymptotic DMT frontier. Recently, the finite-SNR DMT has been proposed as a novel framework to characterize the DMT at finite SNRs. Our last contribution consists of the derivation of the exact finite-SNR DMT for MIMO channels with dual antennas at the transmitter ($2 \times N_r$) and/or the receiver ($N_t \times 2$). Both uncorrelated and correlated Rayleigh fading channels are considered. It is shown that at realistic SNRs, achievable diversity gains are significantly lower than asymptotic values. This finite-SNR could provide new insights on the design of STBCs at operational SNRs.

Résumé

Les systèmes de communication modernes sans fil tels que WiMAX, DVB-NGH, WiFi, HSPA+, LTE et 4G ont adopté l'utilisation de plusieurs antennes en émission et réception. Dans ces systèmes dits *Multiple Input Multiple Output* (MIMO), le codage espace-temps est une technologie prometteuse permettant d'augmenter le débit et la fiabilité des communications sans fil. Le compromis diversité-gain de multiplexage ou *Diversity-Multiplexing Tradeoff* (DMT) caractérise l'interaction entre le débit et la fiabilité d'une transmission sur les canaux MIMO.

Les codes espace-temps en blocs ou *Space Time Block Codes* (STBCs) sont souvent conçus selon les critères du rang et du déterminant, appropriés pour les rapports signal sur bruit (RSB) élevés. En revanche, les standards définissent l'utilisation du codage MIMO en association avec un codage correcteur d'erreur puissant ou *Forward Error Correction* (FEC) comme un turbo code ou un code *Low-Density Parity-Check* (LDPC) garantissant de faibles taux d'erreurs même pour des faibles valeurs de RSB.

Dans cette thèse, nous étudions la construction des STBCs pour les systèmes MIMO utilisant un FEC puissant. Les critères de construction classiques des STBCs sont asymptotiques alors que les codes FEC sont construits pour fonctionner à un RSB spécifique habituellement dans la gamme des bas RSB. Nous avons par conséquent commencé par optimiser un STBC de faible complexité de détection selon le critère de la trace, approprié aux bas RSBs. Le code obtenu surpasse le code original dans le contexte du système WiMAX, en particulier pour les faibles rendements de codage FEC. Puis nous proposons un critère de construction non-asymptotique des STBCs, basé sur la maximisation de l'information mutuelle entre les bits émis et reçus, dite *Bitwise Mutual Information* (BMI). Selon le critère de la BMI, nous optimisons plusieurs STBCs. Nous proposons des STBCs adaptatifs grâce à l'optimisation de leurs paramètres selon le RSB. Parmi eux, nous construisons un code adaptatif basé sur la structure du STBC trace-orthonormal. Le code proposé donne des performances identiques ou meilleures que les codes du standard WiMAX pour tous les rendements de codage FEC. En plus de la performance, la complexité est un enjeu important pour les systèmes pratiques. Par conséquent, nous nous intéressons également à la complexité du récepteur WiMAX. Nous montrons notamment que la détection du code trace-orthonormal adaptatif obtenu est moins complexe pour les faibles RSBs. La construction de codes adaptatifs constitue un enjeu important pour les systèmes pratiques car ils offrent de meilleures performances pour une complexité de détection moindre.

La première partie de l'étude considère que les antennes en émission et en réception sont parfaitement décorréelées. Cette hypothèse dépend de l'environnement et n'est pas toujours valable, par exemple en *indoor* ou pour les téléphones mobiles. Ainsi, pour compléter l'étude, nous étudions l'effet de la corrélation entre les antennes sur les systèmes MIMO codés. L'effet de la corrélation varie selon le code MIMO utilisé. Le critère de la BMI peut toujours servir pour classifier et sélectionner le code MIMO approprié en fonction de l'environnement de communication.

Ensuite, nous nous intéressons aux systèmes MIMO utilisant plus de deux antennes à l'émission. Afin de limiter l'augmentation de complexité du système, nous considérons qu'une sélection d'antenne ou *Antenna Selection* (AS) est effectuée afin de n'utiliser que les meilleures antennes. Dans la littérature MIMO, l'AS n'est étudiée que pour les systèmes MIMO sans codage FEC où il est montré qu'elle donne des gains à la fois en diversité et en RSB par rapport à un système 2×2 classique. Dans cette thèse, nous étudions les avantages de l'AS pour les systèmes MIMO codés. Nous construisons des codes adaptatifs puis nous montrons que, bien qu'aucun gain de diversité ne soit observé dans ce contexte, un gain en RSB dépassant 3 dB est obtenu par rapport au système WiMAX 2×2 classique sans AS.

Les STBCs classiques sont construits de manière à atteindre la frontière du DMT asymptotique. Récemment, un DMT dépendant du RSB ou *finite-SNR DMT* a été proposé visant à caractériser le DMT selon le RSB. Notre dernière contribution consiste à dériver le *finite-SNR DMT* exact pour les systèmes MIMO ayant deux antennes en émission et/ou en réception. Les canaux Rayleigh non corrélés et corrélés sont considérés. Pour les RSB opérationnels, nous montrons que les gains de diversité atteints sont largement inférieurs aux valeurs asymptotiques. Ce *finite-SNR DMT* peut s'avérer être un nouvel outil de grande utilité pour construire des STBCs efficaces pour différentes valeurs de RSBs opérationnels.

Acknowledgments

If this PhD work has been completed, it is largely thanks to the kindness and cooperation of all the people who enlighten me with their information and experience, all these who made possible this work, all these who directly or indirectly supported me during these three years.

I thank them a lot and I wish to recall the names of all whose help has been particularly invaluable:

I thank, first of all, my supervisors at Telecom Bretagne: Dr. Charlotte Langlais, Dr. Charbel Abdel Nour and Prof. Catherine Douillard, and at Concordia University: Prof. Walaa Hamouda, for all provided aids, all assigned works, all given advices, for their support, kindness, encouragement, dynamism and large attention.

I also thank the head and the team members of the Electronics Department at Telecom Bretagne, who supported and helped me, with an extreme amiability.

Furthermore, I gratefully acknowledge the council of the Region Bretagne for providing me a grant to fund my PhD works.

A special thanks to the committee members, Prof. Ghaya ReKay-Ben Othman, Dr. Olivier Berder, Prof. Maryline H elard, Prof. Jean-Pierre Cances and Dr. Laura Conde for reading and reporting my manuscript.

I do not forget to thank my friends in Brest: Hani, Walid, Georges, Khodor, Amina, Dalal, Roua, Ha ifa, Aur elie, Yasser, Jad, Ali, Mohamad, Alya, Oscar, Salim, Rachid, Purush; in Montreal: Firas, Hassan, Mazen; in Lannion: Abdul Rahman, Mohamad, Samer and in all over the world, with whom I spent unforgettable moments.

Finally, the largest thanks, I address to my dear family, who supported and encouraged me during my years of study, that without their guidance nothing would have been possible. A tender thought to my nieces and nephews who embellished my life by their innocence !

شكرا

Résumé de la thèse

Chapitre 1 : Introduction aux systèmes MIMO codés

Les communications sans fil ont connu une évolution considérable et sont devenues essentielles dans notre vie quotidienne. En 2012, le nombre d'abonnés mobiles dans le monde a dépassé les six milliards [ITU12]. Avec cette croissance des appareils et applications sans fil, le défi pour la communauté scientifique reste toujours de concevoir des systèmes de communication qui assurent une transmission fiable avec des débits élevés, ainsi qu'une grande efficacité spectrale et énergétique.

Une solution incontournable pour augmenter le débit sans allouer de bande passante supplémentaire est de passer vers un système utilisant plusieurs antennes en émission et en réception dit système *Multiple Input Multiple Output* (MIMO). Ce système offre une efficacité spectrale supérieure (gain de multiplexage) et de meilleures performances (gain de diversité spatiale) par rapport à un système émettant sur une seule antenne en émission et en réception appelé système *Single Input Single Output* (SISO) [TSC98, ZT03]. Ainsi, les standards des systèmes de communication modernes tels que WiMAX, DVB-NGH, WiFi, HSPA+, LTE et 4G, définissent l'utilisation de système MIMO codé, incluant généralement un code à fort pouvoir de correction [OC07, Nua07, BCC⁺07, DG07, SOZ11].

Pour bénéficier de ces gains de multiplexage et de diversité, un codage spécifique connu sous le nom de codage spatio-temporel ou *Space-Time Coding* (STC) est réalisé à l'émission [TSC98]. Parmi les codes utilisés pour les systèmes MIMO, on trouve les codes spatio-temporels en bloc dits *Space-Time Block Codes* (STBC) où une combinaison linéaire de plusieurs symboles - dans le domaine des valeurs complexes - est envoyée via les antennes d'émission sur une durée définie généralement courte. En revanche, l'utilisation du codage STC augmente la complexité du système surtout à la réception. Les systèmes pratiques favorisent les codes à faible complexité pour avoir des récepteurs à faible latence.

Les codes espace-temps en bloc sont généralement conçus selon les critères du rang et du déterminant, appropriés pour les rapports signal sur bruit (RSB) élevés [TSC98]. En revanche, les codes correcteurs d'erreurs puissants garantissent des faibles taux d'erreurs

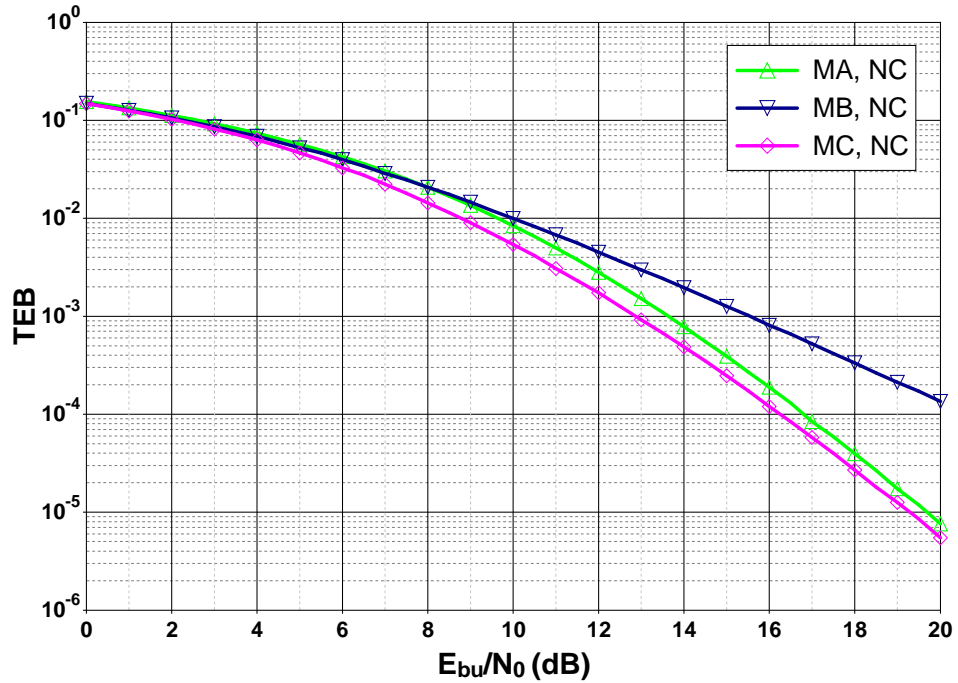


FIGURE 1: TEB des profils MIMO du système WiMAX: MA avec une modulation MAQ-16 et MB, MC avec une modulation MAQ-4; Canal de Rayleigh MIMO quasi-statique.

même pour des faibles valeurs de RSB.

La question qui se pose est donc la suivante : est-ce que les codes espace-temps optimisés selon les critères du rang et du déterminant sont adaptés aux systèmes MIMO codés ?

Considérons par exemple le système WiMAX [Nua07]. Ce système utilise les codes MIMO du standard IEEE 802.16e-2005 [IEE06]. Deux profils sont obligatoires pour la voie descendante. Le premier est le code d'Alamouti [Ala98] appelé matrice A (MA). Il est à diversité pleine mais à rendement unitaire. Le deuxième profil est le multiplexage spatial [WFGV98] appelé matrice B (MB), qui a un rendement plein. Afin de bénéficier des gains de diversité et de multiplexage, un autre profil, variante du code d'or [BRV05], appelé matrice C (MC), est inclus dans le standard IEEE 802.16-e. Pour les RSBs élevés, le code d'or est connu comme étant le meilleur STBC pour les systèmes MIMO ayant deux antennes en émission et deux antennes en réception noté 2×2 .

La figure 1 présente le taux d'erreur binaire (TEB) des profils MIMO du système WiMAX en fonction du RSB transmis un canal de Rayleigh quasi-statique. Afin de transmettre à la même efficacité spectrale, une modulation MAQ-16 est utilisée pour la matrice A et une MAQ-4 est utilisée pour les matrice B et matrice C. Les résultats obtenus montrent que la pente des courbes de TEB est plus élevée pour la matrice A et la matrice C par rapport à la matrice B. Par conséquent, ces systèmes surpassent le code matrice B à des RSB élevés. Sur la base du TEB et sans codage de canal, le code

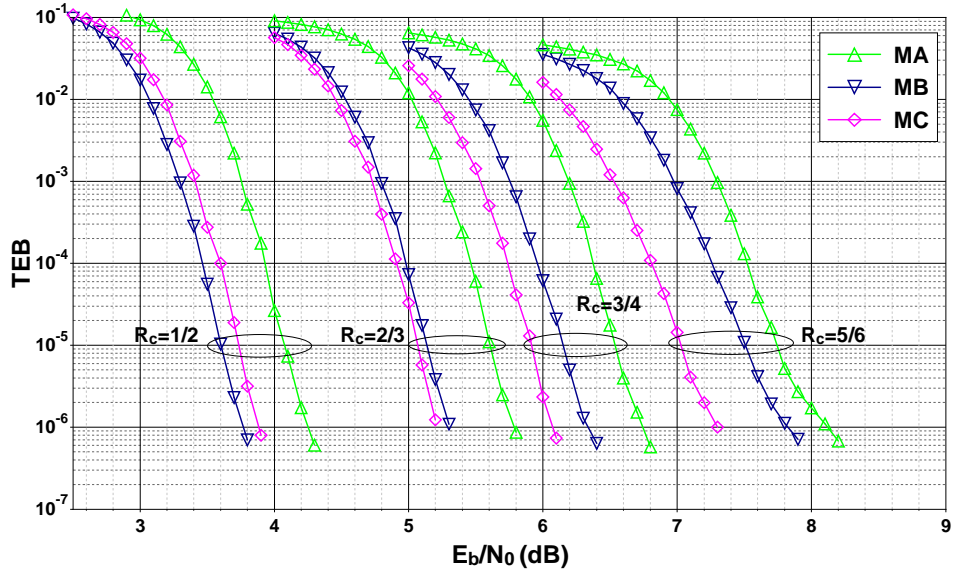


FIGURE 2: TEB du système WiMAX codé; Code FEC: le turbocode 8-états double binaire avec des rendements ($R_c = 1/2, 2/3, 3/4, 5/6$) après 8 itérations du turbo décodage; Profils MIMO : MA avec une modulation MAQ-16 et MB, MC avec une modulation MAQ-4; Canal de Rayleigh MIMO quasi-statique.

matrice C devrait donc être choisie.

En revanche, la figure 2 présente le TEB du système WiMAX MIMO complet c.à.d. en considérant les différents profils MIMO associés au code FEC, le turbocode 8-états double binaire, pour plusieurs rendements de codage R_c . Ces résultats montrent que les codes espace-temps conventionnels ne sont pas adaptés aux systèmes MIMO codés. En effet, le choix du code MIMO varie selon le rendement de codage FEC R_c . En particulier, le code matrice C altère les performances des terminaux ayant un faible rendement de codage. Pour cela, nous traitons dans cette thèse de l'analyse et de la conception de codes espace-temps en bloc pour des transmissions MIMO codées.

Chapitre 2: Amélioration des STBCs normalisés pour les systèmes MIMO codés: Vers des STBCs adaptatifs

Dans ce chapitre, nous étudions la construction des STBCs pour les systèmes MIMO utilisant un FEC puissant. Les critères de construction classiques des STBCs sont asymptotiques alors que les codes FEC sont conçus pour fonctionner à un RSB spécifique habituellement dans la gamme des bas RSBs. Nous avons par conséquent commencé par optimiser un STBC de faible complexité de détection appelé matrice D (MD) [SS07, SSB⁺08] selon le critère de la trace [TC01, CYV01], approprié aux bas RSBs. Le code obtenu surpasse le code original dans le contexte du système WiMAX, en particulier pour les faibles rendements de codage FEC [EALD11].

Le critère de la trace reste asymptotique car il cible une gamme de RSB. Cependant, les systèmes de communications fonctionnent pour un RSB spécifique. Pour cela, nous proposons un nouveau critère de construction non-asymptotique des STBCs, basé sur la maximisation de l'information mutuelle entre les bits émis et reçus, dite *Bitwise Mutual Information* (BMI). Selon le critère de la BMI, nous optimisons plusieurs STBCs. Cela conduit à la proposition de STBCs adaptatifs grâce à l'optimisation de leurs paramètres selon le RSB.

Le premier code adaptatif proposé est le code matrice D adaptatif [ELAD12b]. Après une évaluation de la complexité du récepteur WiMAX, plus particulièrement du détecteur MIMO et du décodeur FEC, nous montrons que le code matrice D adaptatif peut être un bon compromis offrant une bonne performance et une complexité tolérable pour les systèmes MIMO codés.

Ensuite, nous construisons un code adaptatif [ELAD12a] basé sur la structure du STBC trace-orthonormal [ZLW07]. Ce code permet de passer de manière continue du multiplexage spatial, adapté pour les faibles RSB et donc pour les rendements de codage faibles, au code d'or, optimal à fort RSB. La figure 3 montre que le code adaptatif proposé donne des performances identiques ou meilleures que les codes du standard WiMAX pour tous les rendements de codage FEC.

En plus de la performance, la complexité est un enjeu important pour les systèmes pratiques. Nous montrons que la détection du code trace-orthonormal adaptatif obtenu est moins complexe pour les faibles RSBs.

La construction de codes adaptatifs est importante pour les systèmes pratiques car ils offrent de meilleures performances, et ce sans augmenter la complexité du système.

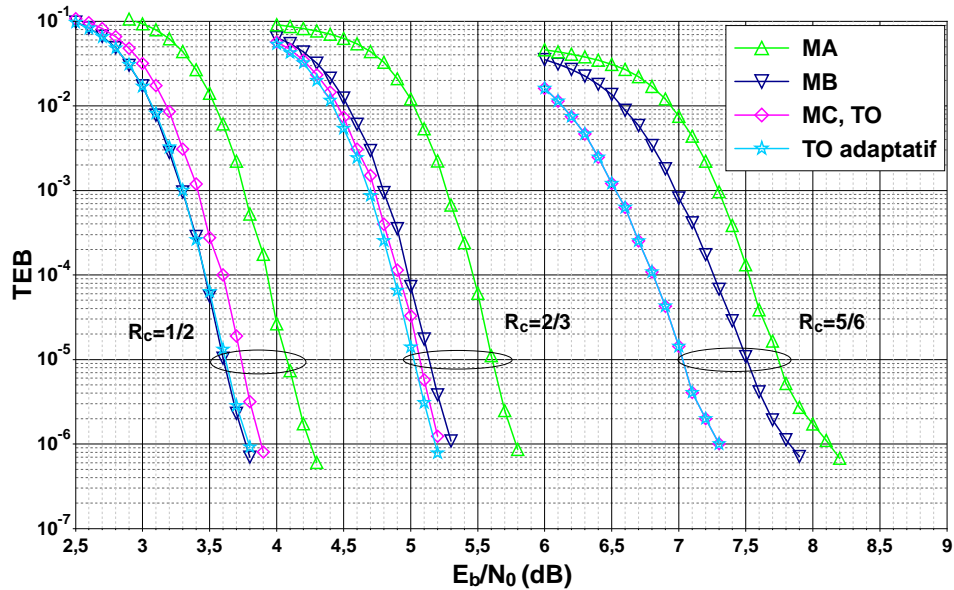


FIGURE 3: TEB des profils du système WiMAX codé et du code trace-orthonormal adaptatif; Code FEC: le turbocode 8-états double binaire avec des rendements ($R_c = 1/2, 2/3, 5/6$) après 8 itérations du turbo décodage; Profils MIMO : MA avec une modulation MAQ-16 et MB, MC avec une modulation MAQ-4; Canal de Rayleigh MIMO quasi-statique.

Chapitre 3: Effet de la corrélation spatiale et la sélection d'antenne sur les systèmes MIMO codés

L'étude faite dans le Chapitre 2 considère que les antennes en émission et en réception sont parfaitement décorréelées. Cette hypothèse dépend de l'environnement et n'est pas toujours valable, par exemple en *indoor* ou pour les téléphones mobiles. Ainsi, pour compléter l'étude, nous étudions, dans la première partie du Chapitre 3, l'effet de la corrélation entre les antennes sur les systèmes MIMO codés. Nous montrons que les faibles corrélations sont équivalentes à une perte en RSB alors que les corrélations élevées conduisent à une dégradation considérable de performance. De plus, l'effet de la corrélation varie selon le code MIMO utilisé. Le critère de la BMI peut toujours servir pour classifier et sélectionner le code MIMO approprié en fonction de l'environnement de communication.

Ensuite dans la deuxième partie du Chapitre 3, nous nous intéressons aux systèmes MIMO utilisant plus de deux antennes à l'émission. Afin de limiter l'augmentation de complexité du système, nous considérons qu'une sélection d'antenne ou *Antenna Selection* (AS) est effectuée afin de n'utiliser que les meilleures antennes. Dans la littérature MIMO, l'AS n'est étudiée que pour les systèmes MIMO sans codage FEC où il est montré qu'elle donne des gains à la fois en diversité et en RSB par rapport à un système 2×2 classique. Pour cela, nous étudions les avantages de l'AS pour les systèmes MIMO codés

Système MIMO	$R_c = 1/2$	$R_c = 5/6$
$(2/3) \times 2$	3	3.4
$(2/4) \times 2$	5.1	5.4
$(2/5) \times 2$	6.35	6.8

TABLE 1: Gains de la technologie de sélection d'antenne en dB par rapport au système WiMAX 2×2 classique, pour un TEB cible à 10^{-5} .

utilisant 2 parmi N_t antennes d'émission et 2 antennes de réception noté $(2/N_t) \times 2$. Pour ces systèmes, nous construisons des codes adaptatifs. Bien qu'aucun gain de diversité ne soit observé dans ce contexte, nous montrons qu'un gain important en RSB est obtenu par rapport au système WiMAX 2×2 classique sans AS. Le tableau 1 récapitule ces gains pour un TEB cible égal à 10^{-5} .

Chapitre 4: Compromis diversité-gain de multiplexage sur les canaux de Rayleigh MIMO

Le compromis diversité-gain de multiplexage ou *Diversity-Multiplexing Tradeoff* (DMT) [ZT03] définit la borne supérieure sur les gains de diversité et de multiplexage atteinte par un STC sur un canal MIMO. En d'autres termes, il caractérise l'interaction entre le débit et la fiabilité d'une transmission sur les canaux MIMO. Les STBCs classiques sont construits de manière à atteindre la frontière du DMT asymptotique. En effet, un déterminant non nul est une condition suffisante pour atteindre la frontière de ce compromis [EKP⁺06, ORBV06].

Les travaux présentés dans les chapitres précédents montrent qu'une étude dépendante du RSB est plus convenable pour les systèmes pratiques. Récemment, un DMT dépendant du RSB ou *finite-SNR DMT* a été proposé visant à caractériser le DMT selon le RSB [Nar06]. Dans le Chapitre 4, nous dérivons l'expression exacte de la probabilité de coupure et du *finite-SNR DMT* pour les systèmes MIMO ayant deux antennes en émission et/ou en réception. Les canaux de Rayleigh non corrélés [EHL⁺13] et corrélés sont considérés.

Nous montrons, pour le système 2×2 , que nos résultats en termes de probabilité de coupure et de *finite-SNR DMT* sont identiques à ceux obtenus par des simulations Monte Carlo pour les canaux non corrélés et corrélés. Puis, nous prouvons que la diversité maximale atteinte à un RSB fini et obtenue lorsque le gain de multiplexage r tend vers 0, est la même pour les canaux non corrélés et corrélés, indépendamment de la valeur de corrélation spatiale. Ensuite, nous considérons le *finite-SNR DMT* pour les canaux corrélés où nous montrons que le gain de diversité est légèrement dégradé à faibles et moyennes corrélations spatiales alors qu'il est fortement dégradé pour les corrélations élevées. De plus, nous montrons que l'écart entre les courbes de DMT pour les faibles et fortes corrélations augmente avec l'augmentation du nombre d'antennes. En outre, nous étudions la différence entre les systèmes $N_t \times 2$ et $2 \times N_r$. Nous montrons que les antennes de réception offrent un gain en diversité supérieur à celui offert par les antennes d'émission surtout pour les faibles et moyens RSB. Dans tous les cas, le *finite-SNR DMT* converge vers le DMT asymptotique lorsque le RSB tend vers l'infini.

D'une manière générale, nous montrons que, pour les RSB opérationnels, les gains de diversité atteints sont largement inférieurs aux valeurs asymptotiques. Ce *finite-SNR DMT* peut s'avérer être un nouvel outil de grande utilité pour construire des STBCs efficaces pour différentes valeurs de RSBs opérationnels.

Conclusions et perspectives

Après avoir rappelé et illustré que les STBCs optimisés selon les critères du rang et du déterminant ne sont pas nécessairement optimaux pour les systèmes MIMO codés, nous avons proposé un nouveau critère de construction des STBCs basé sur l'information mutuelle au niveau binaire. Selon ce critère, nous avons construit des codes adaptatifs qui offrent toujours les meilleures performances pour tous les rendements de codage, et ce sans augmenter la complexité du système. Nous avons adressé les canaux non corrélés et corrélés. Puis, nous avons évalué le gain offert par la technologie de sélection d'antenne pour les systèmes MIMO codés. Enfin, nous avons dérivé l'expression exacte de la probabilité de coupure et du *finite-SNR DMT* pour les canaux de Rayleigh non-corrélés et corrélés ayant deux antennes en émission et/ou en réception.

Présentons maintenant les perspectives principales de ce travail. La première consiste à étendre la construction des codes adaptatifs à des systèmes ayant un nombre d'antennes plus élevé. En effet, les normes des systèmes de communications modernes définissent l'utilisation d'un nombre d'antennes élevé allant jusqu'à 4×4 pour le WiMAX et 8×8 pour le LTE-A. La deuxième piste de travail concerne l'extension à d'autres canaux comme le canal de Rice, à des détecteurs MIMO moins complexe comme le décodeur sphère, MMSE, ZF. La troisième perspective consiste à dériver le *finite-SNR DMT* pour les codes adaptatifs. L'obtention d'une formulation exacte permettrait d'en déduire une méthode analytique d'optimisation des codes. Enfin, ce travail peut être appliqué au contexte d'un système coopératif, vu comme un système MIMO virtuel. Un système utilisant un codage spatio-temporel distribué associé à un codage de canal classique/distribué est à adresser.

Contents

Abstract	iv
Résumé	vi
Acknowledgments	viii
Résumé de la thèse	x
List of Figures	xxii
List of Tables	xxvi
Abbreviations	xxviii
Notations	xxxii
Introduction	2
1 Introduction to Coded MIMO Systems	6
1.1 Coded MIMO System Model	7
1.1.1 Noise Model	9
1.1.2 Fading Model	9
1.1.3 MIMO Channel Model	10
1.2 MIMO Channel Capacity	11
1.2.1 Entropy and Mutual Information	11
1.2.2 Channel Capacity and Outage Probability	12
1.3 Diversity Techniques	14
1.3.1 Diversity-Multiplexing Tradeoff for MIMO systems	15
1.4 Space-Time Coding for MIMO Systems	16
1.4.1 Space-Time Block Codes	17
1.4.2 Conventional Rank-Determinant Design Criteria	18
1.4.3 Conventional MIMO Codes	18
1.4.3.1 ML-Detection of STBCs	22
1.5 Background on Capacity-Approaching Channel Coding	24
1.5.1 Convolutional Codes	24
1.5.2 The WiMAX 8-State Double Binary Turbo Code	25

1.5.3	Log-Likelihood Ratios	26
1.5.4	Iterative (Turbo) Decoding	27
1.5.5	EXtrinsic Information Transfer Charts	28
1.5.6	FlexiCodes	30
1.6	An Example of Coded MIMO System: WiMAX	31
1.6.1	Bit Error Rate of Uncoded Transmission	32
1.6.2	Bit Error Rate of Coded Transmission	32
1.7	Chapter Summary	33
2	Improving Standardized STBCs for Coded MIMO Systems: Towards Adaptive STBCs	34
2.1	Matrix D Space-Time Block Code	35
2.1.1	Original Low Complexity Detector	35
2.1.2	Soft Detection for MD STBC	37
2.1.2.1	Original Detector Impairments	37
2.1.2.2	Proposed Soft Detector for MD STBC	37
2.1.2.3	Comparison Between Detectors	39
2.1.3	Robustness of the Detector with respect to Erasure Events	39
2.2	Matrix D STBC for Coded MIMO Communication Systems	40
2.2.1	Trace Criterion	40
2.2.2	MD STBC Optimization according to the Trace Criterion	41
2.2.3	Performance Evaluation	42
2.2.3.1	BER Curves of the Uncoded MIMO System	42
2.2.3.2	BER Curves of the Coded MIMO System	43
2.2.3.3	Erasure Effects on the BER of the Coded MIMO System	44
2.3	On the Complexity of the WiMAX Receiver	45
2.3.1	ML-Detection Complexity Assessment	45
2.3.2	Turbo Decoding Complexity Assessment	46
2.3.3	WiMAX Receiver Complexity Assessment	47
2.4	Bitwise Mutual Information Criterion	48
2.4.1	Why Bitwise Mutual Information?	48
2.4.2	Criterion Definition	49
2.4.3	Criterion Validation	50
2.5	Proposal of Adaptive Space-Time Block Codes	50
2.5.1	Adaptive Matrix D STBC	51
2.5.2	Adaptive Trace-Orthonormal STBC	54
2.5.2.1	Presentation of Adaptive Trace-Orthonormal STBC	54
2.5.2.2	Analysis of the Transmitted Constellations	56
2.5.2.3	Complexity Reduction of ML-Detection	58
2.6	Performance Evaluation of the Proposed Adaptive TO STBC for a WiMAX System	59
2.6.1	Adaptive TO STBC Parameter Computation for Coded Systems	59
2.6.2	BMI Study of the Adaptive TO STBC	60
2.6.3	Closed-Loop System	60
2.6.3.1	4-QAM Modulation	61
2.6.3.2	16-QAM Modulation	62
2.6.3.3	Higher Order Modulations	62

2.6.3.4	Conclusion	63
2.6.4	Broadcast Transmission: Open-Loop System	63
2.7	Performance Evaluation with FlexiCode	65
2.8	Chapter Summary	65
3	Effect of Spatial Correlation and Antenna Selection on Coded MIMO Systems	68
3.1	Effect of Spatial Correlation on Coded MIMO Systems	70
3.1.1	Modeling Spatially Correlated Channels	70
3.1.2	BMI Study of the Effect of Spatial Correlation	70
3.1.2.1	Correlation between Transmit Antennas	71
3.1.2.2	Correlation between Receive Antennas	71
3.1.2.3	Correlation between both Transmit and Receive Antennas	72
3.1.2.4	Discussion on the Obtained Results	72
3.1.3	Adaptive TO STBC Design for Spatially Correlated Systems	73
3.1.4	Enhanced Spatial Multiplexing Scheme	73
3.1.5	BER Performance of the Proposed Adaptive STBCs	75
3.1.5.1	Low Transmit Correlation	75
3.1.5.2	High Transmit Correlation	76
3.1.6	BER Performance of the Enhanced Spatial Multiplexing Scheme	76
3.1.6.1	High Transmit Correlation	77
3.1.6.2	Full Transmit Correlation	77
3.1.7	Conclusions on the Effect of Spatial Correlation	79
3.2	Antenna Selection for Coded MIMO Systems	80
3.2.1	Transmit Antenna Selection	80
3.2.1.1	Antenna Selection Algorithm	81
3.2.2	BER Curves of the Uncoded MIMO System with Transmit AS	81
3.2.3	Transmit AS for Coded MIMO systems: Adaptive STBCs design	83
3.2.3.1	Adaptive Matrix D STBC	83
3.2.3.2	Adaptive Trace-Orthonormal STBC	83
3.2.4	BER Performance of the Coded MIMO System with Transmit AS	84
3.3	Chapter Summary	86
4	Finite-SNR Diversity- Multiplexing Tradeoff for Rayleigh MIMO Channels	88
4.1	Background on Finite-SNR DMT	89
4.1.1	Finite-SNR DMT for Orthogonal Space-time Block Codes	90
4.1.2	Finite-SNR DMT for 2×2 MIMO Channels	92
4.2	Finite-SNR DMT for MIMO Channels with Dual Antennas	93
4.2.1	Mutual Information for $N_t \times 2$ and $2 \times N_r$ MIMO Systems	93
4.2.2	Finite-SNR DMT for Uncorrelated Flat Rayleigh Channels	94
4.2.2.1	Mutual Information pdf Derivation	94
4.2.2.2	Outage Probability Derivation	95
4.2.2.3	Analytical Expression of Finite-SNR DMT	96
4.2.3	Finite-SNR DMT for Correlated Flat Rayleigh Channel	96
4.2.3.1	Mutual Information pdf Derivation	97
4.2.3.2	Outage Probability Derivation	98

4.2.3.3	Analytical Expression of Finite-SNR DMT	98
4.3	Numerical Results	99
4.3.1	2×2 MIMO System	99
4.3.2	MIMO System with $n \geq 3$	101
4.4	Chapter Summary	104
Conclusions and perspectives		106
A	Optimization of Matrix D STBC Parameter according to the BMI Criterion	110
B	Optimization of Trace-Orthonormal STBC Parameter according to the BMI Criterion	112
C	Transmitted Constellation for Trace-Orthonormal STBC	114
D	Derivation of Finite-SNR DMT for uncorrelated Rayleigh MIMO Channels	116
	Bibliography	120
	List of Publications	120

List of Figures

1	TEB des profils MIMO du système WiMAX: MA avec une modulation MAQ-16 et MB, MC avec une modulation MAQ-4; Canal de Rayleigh MIMO quasi-statique.	xi
2	TEB du système WiMAX codé; Code FEC: le turbocode 8-états double binaire avec des rendements ($R_c = 1/2, 2/3, 3/4, 5/6$) après 8 iterations du turbo décodage; Profils MIMO : MA avec une modulation MAQ-16 et MB, MC avec une modulation MAQ-4; Canal de Rayleigh MIMO quasi-statique.	xii
3	TEB des profils du système WiMAX codé et du code trace-orthonormal adaptatif; Code FEC: le turbocode 8-états double binaire avec des rendements ($R_c = 1/2, 2/3, 5/6$) après 8 iterations du turbo décodage; Profils MIMO : MA avec une modulation MAQ-16 et MB, MC avec une modulation MAQ-4; Canal de Rayleigh MIMO quasi-statique.	xiv
1.1	Structure of the system at the transmitter and the receiver.	7
1.2	The optimal diversity-multiplexing tradeoff of a MIMO system.	16
1.3	Structure of an 8-state binary encoder.	25
1.4	Structure of a turbo encoder.	26
1.5	Structure of an 8-state double binary RSC encoder.	26
1.6	Iterative decoding of a parallel concatenated convolutional code.	28
1.7	EXIT chart at $E_b/N_0 = 2.6$ dB of the 8-state double binary turbo code with rate $R_c = 1/2$; 4-QAM modulation; flat Rayleigh fading channel. . . .	30
1.8	Structure of the Flexicode encoder.	30
1.9	BER for 2×2 WiMAX MIMO profiles: MA with 16-QAM modulation and MB, MC with 4-QAM modulation; quasi-static flat Rayleigh fading MIMO channel.	31
1.10	BER of turbo coded 2×2 WiMAX system; 8-state double binary turbo code ($R_c = 1/2, 2/3, 3/4, 5/6$) with 8 turbo decoding iterations; MIMO profiles: Alamouti code (MA) with 16-QAM and spatial multiplexing (MB), Golden code (MC) with 4-QAM; quasi-static flat Rayleigh fading MIMO channel.	32
2.1	BER for the concatenation of the WiMAX 8-state double binary turbo code ($R_c = 1/2, k = 4,800$) and the MD STBC detected with: original, proposed and full complexity soft detectors; 4-QAM modulation; quasi-static flat Rayleigh fading MIMO channel.	39
2.2	Minimum trace and minimum determinant of the MD STBC as a function of its design parameter φ ; 4-QAM modulation.	41

2.3	BER for the uncoded (UC) system (only MIMO system); MIMO profiles: Spatial multiplexing (MB), Golden code (MC), original MD [SS07], MD($\varphi = 135^\circ$) and MD($\varphi = 125^\circ$); 4-QAM modulation; quasi-static flat Rayleigh fading MIMO channel.	42
2.4	BER of turbo coded system; 8-state double binary turbo code ($R_c = 1/2, 5/6$) with 8 turbo decoding iterations; MIMO profiles: Alamouti code (MA) with 16-QAM modulation and spatial multiplexing (MB), Golden code (MC), original MD [SS07], MD($\varphi = 135^\circ$) and MD($\varphi = 125^\circ$) with 4-QAM modulation; quasi-static flat Rayleigh fading MIMO channel.	43
2.5	BER of turbo coded system; 8-state double binary turbo code ($R_c = 5/6$) with 8 turbo decoding iterations; MIMO profiles: Alamouti code (MA) with 16-QAM modulation and spatial multiplexing (MB), Golden code (MC), original MD [SS07], MD($\varphi = 135^\circ$) and MD($\varphi = 125^\circ$) with 4-QAM modulation; quasi-static flat Rayleigh fading erased MIMO channel with erasure probability = 0.2.	45
2.6	Average number of turbo decoding iterations per frame \bar{N} for $R_c = 5/6$; MIMO profiles: Alamouti code (MA) with 16-QAM modulation and spatial multiplexing (MB), Golden code (MC), original MD [SS07] and MD($\varphi = 125^\circ$) with 4-QAM modulation; $N_{\max} = 8$ decoding iterations.	47
2.7	Normalized number of occurrences for the detected soft bit $\hat{c}_i = \Pr(c_i = 1)$ at $E_{bu}/N_0 = 0$ dB; MIMO profiles : spatial multiplexing (MB) and Golden code (MC); 4-QAM modulation.	49
2.8	BMI of some well-known 2×2 MIMO codes at high E_{bu}/N_0 ; 4-QAM modulation.	51
2.9	BMI at $E_{bu}/N_0 = 12$ dB and minimum determinant of MD STBC as a function of its design parameter φ ; 4-QAM modulation.	52
2.10	BMI at $E_{bu}/N_0 = 0$ dB and minimum determinant of MD STBC as a function of its design parameter φ ; 4-QAM modulation.	52
2.11	BER of turbo coded system; 8-state double binary turbo code ($R_c = 1/2, 2/3, 5/6$) with 8 turbo decoding iterations and information frame size $k = 4,800$ bits; MIMO profiles: Alamouti code (MA) with 16-QAM modulation and spatial multiplexing (MB), Golden code (MC), Matrix D (MD) and adaptive MD with 4-QAM modulation; quasi-static flat Rayleigh fading MIMO channel.	54
2.12	BMI at $E_{bu}/N_0 = -3$ dB and minimum determinant of TO STBC as a function of its design parameter θ ; 4-QAM modulation.	55
2.13	BMI at $E_{bu}/N_0 = 12$ dB and minimum determinant of TO STBC as a function of its design parameter θ ; 4-QAM modulation.	55
2.14	BMI of full-rate WiMAX MIMO profiles and adaptive TO code as a function of E_{bu}/N_0 ; 4-QAM modulation.	60
2.15	BER of turbo coded system; 8-state double binary turbo code ($R_c = 1/2, 2/3, 5/6$) with 8 turbo decoding iterations and information frame size $k = 4,800$ bits; MIMO profiles: Alamouti code (MA) with 16-QAM modulation and spatial multiplexing (MB), Golden code (MC) & original TO, Matrix D (MD) and adaptive TO with 4-QAM modulation; quasi-static flat Rayleigh fading MIMO channel.	61

2.16	BER of turbo coded system; 8-state double binary turbo code ($R_c = 1/2, 5/6$) with 8 turbo decoding iterations and information frame size $k = 10,800$ bits; MIMO profiles: Alamouti code (MA) with 256-QAM and spatial multiplexing (MB), Golden code (MC) & original TO, Matrix D (MD) and adaptive TO with 16-QAM; quasi-static flat Rayleigh fading MIMO channel.	62
2.17	Uncoded BER for 2×2 MIMO profiles: Spatial multiplexing (MB), Golden code (MC) and Matrix D (MD); quasi-static flat Rayleigh fading channel.	63
2.18	BER of coded MIMO system; FlexiCode ($R_c = 1/2, 2/3, 3/4$) with 10 turbo decoding iterations and an information frame size $k = 5,399$ bits; MIMO profiles: spatial multiplexing (MB), Golden code (MC) & original TO, and adaptive TO with 4-QAM modulation; quasi-static flat Rayleigh fading MIMO channel.	65
3.1	BER of turbo coded system; 8-state double binary turbo code with 8 turbo decoding iterations and information frame size $k = 4,800$ bits; MIMO profiles: Alamouti code (MA) with 16-QAM modulation and spatial multiplexing (MB), Golden code (MC) & original TO, Matrix D (MD) and adaptive TO with 4-QAM modulation; quasi-static flat correlated Rayleigh fading MIMO channel with $\rho_t = 0.3$	75
3.2	BER of turbo coded system; 8-state double binary turbo code with 8 turbo decoding iterations and information frame size $k = 4,800$ bits; MIMO profiles: Alamouti code (MA) with 16-QAM modulation and spatial multiplexing (MB), Golden code (MC) & original TO, Matrix D (MD) and adaptive TO with 4-QAM modulation; quasi-static flat correlated Rayleigh fading MIMO channel with $\rho_t = 0.7$	77
3.3	BER of turbo coded system; 8-state double binary turbo code with 8 turbo decoding iterations and information frame size $k = 4,800$ bits; MIMO profiles: Alamouti code with 256-QAM modulation and spatial multiplexing (SM), $\mathbf{X}_{\theta=45^\circ}^{\text{TO}}$ (TO 45), enhanced spatial multiplexing (eSM) [MKV ⁺ 12], proposed eSM with 16-QAM modulation; quasi-static flat correlated Rayleigh fading MIMO channel with $\rho_t = 0.7$	78
3.4	BER of turbo coded system; 8-state double binary turbo code ($R_c = 1/2$) with 8 turbo decoding iterations and information frame size $k = 4,800$ bits; MIMO profiles: Alamouti code with 256-QAM modulation and spatial multiplexing (SM), $\mathbf{X}_{\theta=45^\circ}^{\text{TO}}$ (TO 45), enhanced spatial multiplexing (eSM) [MKV ⁺ 12] with 16-QAM modulation; quasi-static flat correlated Rayleigh fading MIMO channel with $\rho_t = 1$	78
3.5	Uncoded BER of spatial multiplexing with dashed blue curves and Golden code with solid pink curves; dual transmit AS among $N_t = 2, 3, 4$ and 5; 4-QAM modulation; quasi-static uncorrelated flat Rayleigh fading MIMO channel.	82
3.6	BER of turbo coded $(2/3) \times 2$ system; 8-state double binary turbo code ($R_c = 1/2, 5/6$) with 8 turbo decoding iterations and information frame size $k = 4,800$ bits; MIMO profiles: Alamouti code (MA) with 16-QAM modulation and spatial multiplexing (MB), Golden code (MC) & original TO, Matrix D (MD) and adaptive TO with 4-QAM modulation; quasi-static uncorrelated flat Rayleigh fading channel.	85

3.7	BER of turbo coded $(2/5) \times 2$ system; 8-state double binary turbo code ($R_c = 1/2, 5/6$) with 8 turbo decoding iterations and information frame size $k = 4,800$ bits; MIMO profiles: Alamouti code (MA) with 16-QAM modulation and spatial multiplexing (MB), Golden code (MC) & original TO, Matrix D (MD) and adaptive TO with 4-QAM modulation; quasi-static uncorrelated flat Rayleigh fading channel.	86
4.1	Asymptotic and exact finite-SNR DMT curves for 2×2 uncorrelated flat Rayleigh MIMO channel with and without Alamouti code at various SNRs.	92
4.2	Outage probability for different multiplexing gains $r = 0.5, 1$; $N_t = N_r = 2$, uncorrelated and correlated ($\rho_t = 0.0043 + j0.9789$ as in [Nar06]) flat Rayleigh fading with dashed and solid lines respectively.	99
4.3	Asymptotic and exact finite-SNR DMT curves for 2×2 correlated flat Rayleigh MIMO channel with low $\rho_t = 0.1$, medium $\rho_t = 0.7$ and high $\rho_t = 0.0043 + j0.9789$ (as in [Nar06]) correlations at various SNRs.	100
4.4	Outage probability for MIMO systems with multiplexing gain $r \rightarrow 0$; 2×2 , 2×3 and 2×4 , in uncorrelated and correlated ($\rho_t = 0.0043 + j0.9789$) flat Rayleigh fading channels (dashed and solid lines respectively).	101
4.5	Asymptotic and exact finite-SNR DMT curves for 3×2 MIMO channel with solid lines and 2×3 MIMO channel with dashed lines at various SNRs.	102
4.6	Asymptotic and exact finite-SNR DMT curves for 5×2 MIMO channel with solid lines and 2×5 MIMO channel with dashed lines at various SNRs.	102
4.7	Exact finite-SNR DMT curves for 2×5 correlated flat Rayleigh MIMO channel with a low $\rho_t = 0.1$ and high $\rho_t = 0.0043 + j0.9789$ correlations at various SNRs (dashed and solid lines respectively).	104
A.1	Polynomial interpolation between φ values obtained according to the BMI criterion.	111
B.1	Polynomial interpolation between θ values obtained according to the BMI criterion.	113

List of Tables

1	Gains de la technologie de sélection d'antenne en dB par rapport au système WiMAX 2×2 classique, pour un TEB cible à 10^{-5}	xv
1.1	Comparison between the minimum determinant of some well-known full-rate 2×2 MIMO codes.	22
2.1	ML-detection complexity per coded bit of 2×2 WiMAX MIMO profiles in terms of floating point additions and multiplications.	46
2.2	ML-detection complexity per coded bit of 2×2 WiMAX MIMO profiles in terms of floating point additions and multiplications for 4-QAM and 16-QAM modulations.	48
2.3	LUT providing $\theta_{\text{opt}}^{4\text{-QAM}}$ as a function of the coding rate R_c for the 8-state double binary turbo code with 8 turbo decoding iterations at a target BER = 10^{-5} ; 4-QAM modulation.	64
3.1	Transmit AS gains in dB with respect to a coded WiMAX MIMO system at a target BER = 10^{-5}	85
A.1	MD STBC parameter φ optimized according to the BMI criterion as a function of E_{bu}/N_0 ; 4-QAM modulation.	111
B.1	TO STBC parameter θ optimized according to the BMI criterion as a function of E_{bu}/N_0 ; 4-QAM modulation.	113

Abbreviations

3G	Third Generation
4G	Fourth Generation
AMC	Adaptive Modulation and Coding
AS	Antenna Selection
AWGN	Additive White Gaussian Noise
BER	Bit Error Rate
BICM	Bit Interleaved Coded Modulation
BIM	Bitwise Mutual Information
CRC	Cyclic Redundancy Check
CSI	Channel State Information
DMT	Diversity-Multiplexing Tradeoff
DSL	Digital Subscriber Line
DV	Dayal-Varanasi
DVB	Digital Video Broadcasting
DVB-NGH	Digital Video Broadcasting-Next Generation Handheld
DVB-RCS	Digital Video Broadcasting-Return Channel via Satellite
DVB-RCT	Digital Video Broadcasting-Return Channel Terrestrial
eSM	enhanced Spatial Multiplexing
FD	Full Diversity
FEC	Forward Error Correcting
FER	Frame Error Rate

FP	F loating P oint
FR	F ull R ate
GC	G olden C ode
GSM	G lobal S ystem for M obile
HSPA	H igh S peed P acket A ccess
HSPA+	E volved H igh S peed P acket A ccess
HTW-PGA	H ottinen T irkkonen W ichman- P aredes G ershman A lkhansari
i.i.d.	independent and identically distributed
LDPC	L ow- D ensity- P arity- C heck
LD-STBC	L inear D ispersion- S pace- T ime B lock C ode
LOS	L ine O f S ight
LLR	L og- L ikelihood R atio
LTE	L ong T erm E volution
LTE-A	L ong T erm E volution- A dvanced
LUT	L ook U p T able
MA	M atrix A
MAP	M aximum A P osteriori
MB	M atrix B
MC	M atrix C
MCS	M odulation and C oding S cheme
MD	M atrix D
MIMO	M ultiple- I nput M ultiple- O utput
MISO	M ultiple- I nput S ingle- O utput
ML	M aximum L ikelihood
MMSE	M inimum M ean S quare E rror
NVD	N on V anishing D eterminant
OFDM	O rthogonal F requency D ivision M ultiplexing
OSTBC	O rthogonal S pace- T ime B lock C ode

pdf	probability density function
PEP	Pairwise Error Probability
PSTBC	Perfect Space-Time Block Code
QAM	Quadrature Amplitude Modulation
QoS	Quality of Service
RF	Radio-Frequency
RSC	Recursive Systematic Convolutional
SIMO	Single-Input Multiple-Output
SISO	Single-Input Single-Output
SM	Spatial Multiplexing
SNR	Signal-to-Noise Ratio
SOVA	Soft Output Viterbi Algorithm
SPC	Single Parity Check
SR	Srinath-Rajan
STBC	Space-Time Block Code
STTC	Space-Time Trellis Code
TO	Trace-Orthonormal
UBER	Uncoded Bit Error Rate
UMTS	Universal Mobile Telecommunication System
V-BLAST	Vertical-Bell Laboratories Layered Space- Time
WiMAX	Worldwide interoperability for Microwave Access
WLAN	Wireless Local Area Network
YW	Yao-Wornell
ZF	Zero Forcing

Notations

x^*	Complex conjugate of x
\mathbf{x}	Vector \mathbf{x}
\mathbf{A}	Matrix \mathbf{A}
\mathbf{A}^H	Hermitian (conjugate transpose) of the matrix \mathbf{A}
$\ \mathbf{A}\ _F$	Frobenius norm of the matrix \mathbf{A}
N_t	Number of transmit antennas
N_r	Number of receive antennas
\mathbf{b}	Information word
\mathbf{c}	Interleaved codeword
E_b	Energy per information bit
E_{bu}	Energy per bit for uncoded MIMO system <i>i.e.</i> , without FEC code
N_0	Total noise power
σ^2	Variance of the Gaussian noise
\mathbf{H}	MIMO channel matrix
\mathbf{X}	Transmitted code
\mathbf{Y}	Received code
\mathbf{N}	AWGN noise
h_{ij}	Channel coefficient between i -th receive antenna and j -th transmit antenna
T	Coherence time
ρ	Received SNR per receive antenna
E	Expectation operation (mean)

R	System rate
H	Entropy
I	Mutual information
C	Channel capacity
P_{out}	Outage probability
\mathcal{C}	Encoder
P_e	Maximum likelihood error probability
r	Multiplexing gain
d	Diversity gain
$d(r)$	Diversity-multiplexing tradeoff
$d(r, \rho)$	Finite-SNR diversity-multiplexing tradeoff
R_c	FEC code rate
Π	Interleaver
L	LLR
\mathcal{C}^{-1}	Decoder
\mathbf{I}	Identity matrix
j	Imaginary unit, $j^2 = -1$
\Re	Real part of a complex number
\Im	Imaginary part of a complex number
ρ_t	Spatial correlation coefficient at the transmitter side
ρ_r	Spatial correlation coefficient at the receiver side
ψ	Number of selected antennas

إلى إخوتي و أخواتي
إلى أبي
إلى أمي ...

Introduction

The theory of electromagnetic waves has been proposed by Maxwell in 1861. Their existence has been demonstrated by Hertz in 1887. In 1895, Marconi established the first radio link in his attic laboratory, allowing him to ring a bell two rooms away purely by striking a telegraph key that created electromagnetic waves. Several years later, Shannon has founded in his pioneering work *A Mathematical Theory of Communication* [Sha48] the basics of information theory where he defined the capacity of digital communication systems. Since then, wireless communication systems have witnessed a tremendous evolution and have become vital in our everyday life. For instance, the number of worldwide mobile subscribers surpasses 6 billion by the end of 2011 [ITU12]. With this growth of wireless devices and applications, the challenge for the wireless research community has always been to design communication systems which continue to achieve reliable transmission, high data rates, high spectral and power efficiency and are able to mitigate the fading and interference effects. A way to overcome this challenge is by exploiting diversity in time, in frequency or space.

Forward error correcting (FEC) codes, exploiting time and frequency diversities, are usually introduced in communication chains to increase the link reliability and the spectral efficiency. The most relevant FEC codes are those which closely approach the channel capacity known by capacity-approaching FEC codes. In 1993, Berrou *et al.* proposed the turbo code known as the first implementable capacity-approaching FEC code [BGT93]. Afterwards, MacKay *et al.* rediscovered in 1996 the capacity-approaching low-density parity-check (LDPC) code [MN96] previously proposed by Gallager in 1962 [Gal62]. Turbo codes and LDPC codes are competing where one of them is usually adopted in recently standardized telecommunication systems *e.g.*, WiMAX, WiFi, DVB, HSPA+, LTE and 4G.

In order to fulfill the large traffic increase without expanding the bandwidth, the use of multiple antennas at the transmitter and the receiver sides called multiple-input multiple-output (MIMO) has been introduced. MIMO technology increases the channel capacity and consequently the achievable data rates and the spectral efficiency. The first analysis of a MIMO cellular scenario composed by a base station with multiple antennas and single-antenna mobile terminals, transmitting in the same frequency band, is due to

[Win87]. In 1994, Paulraj and Kailath presented one of the first examples of practical application of MIMO for broadcast TV [PK94]. In 1996, Foschini introduced the concept of layered space-time scheme referred as Bell laboratories layered space-time (BLAST) [Fos96]. In 1998, a new version of BLAST scheme called vertical-BLAST (V-BLAST) was proposed in [WFGV98]. The V-BLAST scheme, also known as spatial multiplexing (SM), shows that it is possible, under some channel conditions, to transmit up to $\min(N_t, N_r)$ independent data streams (where N_t and N_r are the number of transmit and receive antennas, respectively) thereby immensely increasing the spectral efficiency. The SM scheme is a full-rate (FR) code *i.e.*, can achieve the MIMO channel capacity derived by Teletar in 1995 later published in 1999 [Tel99].

Also, MIMO is a well-known technology to exploit the diversity in time and space. A maximal diversity of $N_t N_r$ equal to the number of available independent paths can be achieved. Space-time coding for MIMO systems improves the coverage, enhances the quality of service (QoS) and offers lower bit error rates (BER) [DG07]. In 1998, Alamouti introduced the first space-time code (STC) achieving the maximal diversity or full-diversity (FD) STC for $2 \times N_r$ MIMO systems [Ala98]. Afterwards, Tarokh *et al.* extended the work of Alamouti by proposing orthogonal STCs for a higher number of transmit antennas [TJC99]. Orthogonal STCs achieves the maximal diversity but they are not always FR. Therefore, Hassibi and Hochwald introduced in 2002 the linear dispersion (LD) STCs aiming at maximizing the symbol-wise mutual information and achieving the channel capacity [HH02]. In 2003, Zheng and Tse proved that diversity gain and multiplexing gain can be achieved simultaneously with a fundamental tradeoff between them called the diversity-multiplexing tradeoff (DMT) [ZT03]. FR-FD LD-STCs are conventionally designed according to the well-known rank-determinant criteria proposed by Tarokh *et al.* in [TSC98]. A nonzero minimum determinant is a sufficient condition to reach the frontier of the asymptotic DMT [EKP⁺06, ORBV06]. For this purpose, several FR-FD space-time block codes (STBCs) have been proposed in [YW03, DV05, BRV05, ORBV06, ESK07, ZLW07, SS07]. In order to benefit from diversity and multiplexing gains, MIMO technology has also been adopted in recently standardized telecommunication systems *e.g.*, WiMAX, WiFi, DVB, HSPA+, LTE and 4G [SOZ11].

Wireless telecommunication standards define the use of capacity-approaching FEC coding and MIMO coding. MIMO codes are conventionally designed according the asymptotic rank-determinant criteria efficient at high signal to noise ratios (SNRs). In contrast, capacity-approaching FEC codes ensure low error rates even at low SNRs. Recently, several papers have stated that an analysis based only on the performance of MIMO systems without FEC codes could be misleading, and reveals to be insufficient to predict the performance of coded MIMO systems *i.e.*, when a powerful FEC code is concatenated with a MIMO code [MRLRB07, KSB09, LJ10, MKV⁺12, MRLB12]. In

this thesis, we focus on the design of STBCs for practical communication systems. The improvement of the end-to-end BER is targeted.

In addition to performance, the complexity is an important issue for standard communication systems. Therefore, unlike [GGB08], the use of iterative MIMO detection is usually avoided. Furthermore, the use of low complexity detection MIMO codes is favored. The receiver is implemented in the user terminal whose size and price should be, when focusing on the downlink, kept reasonable. A performance loss can be tolerated in favor of reducing the MIMO detection complexity. Several MIMO codes have been designed for this purpose [HTW03, SS07, SSB⁺08, PGGA08, Ism11]. In this thesis, we also focus on the assessment of the receiver complexity and the design of STBCs enjoying a low complexity maximum likelihood (ML) detection.

In general, our work aim to analyze and design STBCs for coded MIMO transmissions, with a constraint of low complexity detection. The rest of this thesis is organized as follows:

Contributions and Outline

In Chapter 1, we review the basic concepts and motivations of the work of this thesis. First, we present the coded MIMO system model under consideration. Then we review the basic information theoretic tools as mutual information, channel capacity and outage probability. Afterwards, we present the diversity techniques and the diversity-multiplexing tradeoff. Furthermore, we review conventional MIMO codes and their design criteria. We complete the chapter by describing capacity-approaching FEC codes used in this thesis. Finally, we assess the performance of a coded WiMAX system which motivates our work.

In Chapter 2, we start by the presentation a low ML-detection complexity STBC called Matrix D [SS07, SSB⁺08]. The first contribution in this chapter consists of the adaptation of this code for coded MIMO systems. We start by the proposal of a soft detector for the Matrix D STBC with the same complexity order as the original one. Then we optimize this code according to the trace criterion efficient at low SNRs. We show that the proposed code overcomes the original one in the context of a coded WiMAX system. Furthermore, we assess the computational complexity of MIMO ML-detection and FEC decoding in a WiMAX receiver. Afterwards, we propose a non-asymptotic STBC design criterion based on the bitwise mutual information (BMI) optimization between transmitted and soft detected bits at a specific target SNR. After its validation, we optimize several conventional STBCs according to the proposed BMI criterion. Their design parameters are shown to be SNR-dependent leading to the proposal of adaptive STBCs. Designed adaptive Matrix D STBC overcomes the original one for all coding rates. Furthermore, based on the trace-orthonormal STBC structure described in

[ZLW07], we propose an adaptive trace-orthonormal STBC. Finally, we prove the superiority of the proposed adaptive trace-orthonormal STBC with respect to conventional WiMAX profiles in terms of performance and detection complexity.

Chapter 3 comprises two separate parts. In the first part, we study the effect of spatial correlation between antennas. Actually, in Chapter 2 we considered the case of an uncorrelated MIMO Rayleigh fading channel. This assumption is valid when the spacing between antennas is greater than the half-wavelength which is not always feasible due to physical constraints *e.g.*, mobile phones and small tablets. Based on a BMI study, we assess the effect of spatial correlation on the performance of coded MIMO systems. We show that low correlations are equivalent to a simple SNR loss while high correlations can lead to substantial performance degradation. The correlation effect differs depending on the used MIMO codes where some MIMO codes are shown to be more resistant against spatial correlation than others. The BMI criterion serves as a useful tool to classify, design and select the suitable MIMO code depending on the communication environment.

In the second part of Chapter 3, we consider the case of MIMO systems using more than dual transmit antennas. In order to limit the system complexity increase, we consider an antenna selection (AS) where only suitable antennas are used. In the MIMO literature, the AS is only studied for the case of MIMO systems without FEC codes where it has been shown to provide diversity and SNR gains. In this part, the benefits of AS technology for coded MIMO systems are addressed. We start by designing adaptive STBCs. Then we show that, although no additional diversity gain is observed in this context, a substantial SNR gain of more than 3 dB is obtained with respect to a conventional turbo coded WiMAX system without AS.

Conventional STBCs are designed to reach the frontier of the asymptotic DMT. Our previous work proved that it is more accurate to design STBCs using an SNR-dependent criterion such as the proposed BMI criterion. Recently, the finite-SNR DMT has been proposed as a novel framework to characterize the tradeoff between diversity and multiplexing gains at finite-SNRs. In Chapter 4, we derive the exact finite-SNR DMT for MIMO channels with dual antennas at the transmitter ($2 \times N_r$) and/or at the receiver ($N_t \times 2$). We consider the case of both uncorrelated and correlated Rayleigh fading channels. Afterwards, we show that achievable diversity gains at realistic SNRs are significantly lower than asymptotic values. This finite-SNR characterizes MIMO systems at operational SNRs and could provide new insights on the design of SNR-dependent STBCs.

Finally, the contents of this thesis are summarized and perspective works are provided. Parts of our contributions have been published in [EALD11, ELAD12b, ELAD12a, EHL⁺13, ELAD13] and the rest is under preparation.

Chapter 1

Introduction to Coded MIMO Systems

Until the last decade, low rate voice communication was the main service provided by wireless networks. Nowadays, the data/IP traffic demand is growing and gaining importance. The user-perceived data rates are still under the *quality of service* (QoS) requirements, and far from rates offered by other technologies like *digital subscriber line* (DSL) over fixed telephony lines. Actually, wireless signals suffer from degradations due to multipath fading and user mobility which leads to a QoS decrease. Spatial, temporal and frequency diversity techniques are used to combat these degradations. In order to increase the link reliability and the channel spectral efficiency, *capacity-approaching* error correcting encoding like *turbo codes* and *low-density parity-check* (LDPC) codes, incorporated in *multiple-input multiple-output* (MIMO) systems have been adopted in most of the recently developed wireless communication systems e.g., *long term evolution* (LTE), LTE-Advanced, *Worldwide Interoperability for Microwave Access* (WiMAX), WiFi, *Digital Video Broadcasting-Next Generation Handheld* (DVB-NHG) and 4G.

Space-time block codes (STBCs) for MIMO systems are conventionally designed according to the well-known rank-determinant design criteria suitable at high signal to noise ratios (SNRs). Besides, practical communication systems introduce capacity-approaching *forward error correcting* (FEC) codes in the transmission chain. Such FEC codes ensure low error rates even at low SNRs. Therefore, a simple aggregation of conventional STBCs and capacity-approaching FEC codes is not necessarily judicious. This thesis deals with developing appropriate methods aiming at suitably designing STBCs for coded MIMO systems.

This chapter gives an overview of the basic concepts and motivations of the work of this thesis. In Section 1.1, we present the coded MIMO system model under consideration. Basic information theoretic tools are reviewed in Section 1.2. Thereafter, diversity

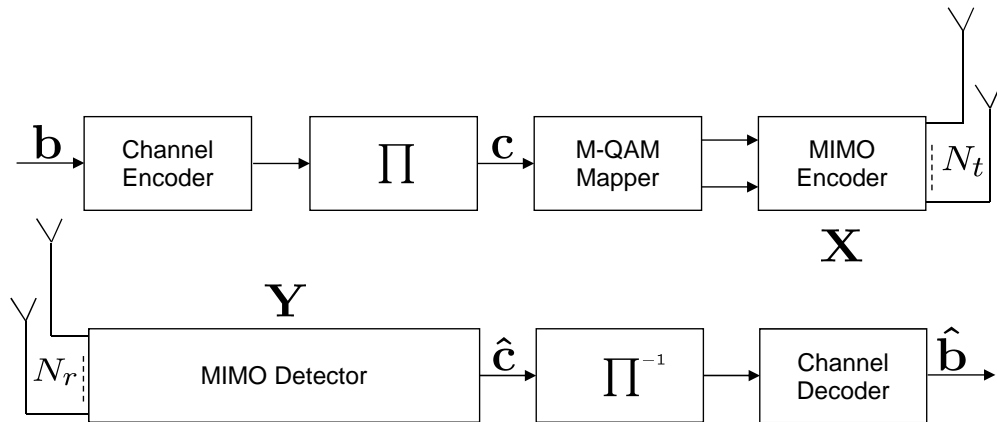


FIGURE 1.1: Structure of the system at the transmitter and the receiver.

techniques used to combat the channel fading, and diversity-multiplexing tradeoff defining the upper bound achievable by any transmission over a MIMO system, are given in Section 1.3. In Section 1.4, we present conventional STBCs for MIMO systems and their design criteria. Furthermore, in Section 1.5, we describe the capacity-approaching FEC codes precisely those used in the sequel of the thesis: the 8-state double binary turbo code and the Flexicode. In Section 1.6, we consider the WiMAX system as an example of coded MIMO system. Presented performance for the turbo coded WiMAX system motivates the work in the course of this thesis.

1.1 Coded MIMO System Model

In this section, we present the MIMO system model considered throughout this thesis. The fundamental purpose of a communication system is the reconstruction at one point or *destination*, either exactly or approximately a message transmitted at another point or *source*. The message or the *information word* is transmitted over a physical medium or *channel*. Figure 1.1 illustrates a simplified diagram of a digital MIMO communication system with N_t transmit antennas and N_r receive antennas. It essentially consists of two parts: a *transmitter* which operates on the message to produce a signal suitable for transmission over the channel, and a *receiver* which performs the inverse operation of that done by the transmitter, *i.e.*, reconstructs the message from the signal. More precisely, we have:

Transmitter side the source transmits an information word \mathbf{b} of length k ,

$$\mathbf{b} = (b_1, b_2, \dots, b_k).$$

Packet \mathbf{b} is encoded by a channel encoder. The channel encoder generates and adds redundancy to the information to make it robust against errors and channel impairments. The channel code rate is defined by $R_c = k/n$ which corresponds to the ratio of the number of information bits k to the number of total coded bits n . In order to protect the transmitted information from *burst errors*, the resulting codeword is interleaved with a random interleaver Π following a *bit-interleaved coded modulation* (BICM) scheme [CTB98]. The interleaved codeword of length n is denoted by \mathbf{c} ,

$$\mathbf{c} = (c_1, c_2, \dots, c_n).$$

The elements of \mathbf{b} and \mathbf{c} belong to the binary *Galois field* $GF(2)$, *i.e.*, $b_i, c_i \in \{0, 1\}$. The binary sequence \mathbf{c} is mapped onto a Gray encoded M -QAM constellation whose complex symbols are denoted by S_i , where $M = 2^m$ is the modulation order and m denotes the number of bits per symbol. MIMO encoding is used to increase the rate and improve the reliability of the transmitted data, by *space-time encoding* these QAM symbols. The mapper feeds a block of $N_t \times T$ QAM symbols to the MIMO encoder. Afterwards, encoder output denoted by the matrix $\mathbf{X}_{[N_t \times T]}$ is transmitted via N_t antennas over the channel during T channel use periods.

Receiver side The destination receives on the N_r antennas during T channel use periods a corrupted version $\mathbf{Y}_{[N_r \times T]}$ of the MIMO code \mathbf{X} . The MIMO detector and the decoder try to recover the information packet \mathbf{b} from the received signals. The MIMO detector estimates the transmitted M -QAM symbols and feeds an estimated version $\hat{\mathbf{c}}$ of the codeword \mathbf{c} . Deinterleaved version of $\hat{\mathbf{c}}$ is provided to the channel decoder which generates an estimate $\hat{\mathbf{b}}$ of the original packet \mathbf{b} . An *error* occurs when the i -th estimated bit \hat{b}_i is different from the original bit b_i . The *bit error rate* (BER) is defined as the number of errors divided by the total number of transmitted bits.

During its propagation, the transmitted signal is distorted by several phenomena. The main channel impairments corrupting the transmitted signal are noise, path loss propagation, shadowing and fading. The path loss is defined as the signal power attenuation resulting from propagation over long distances. It mainly depends on the propagation environment (free space, urban, rural, etc.) and the distance between the transmitter and the receiver. Furthermore, the obscuration of the signal by large obstructions such as hills or buildings is known as shadowing or slow fading. The received power change caused by shadowing is often modeled using a log-normal distribution with a standard deviation depending on the environment. In fact, path loss and shadowing are average quantities while the instantaneous received signal power is a much more rapidly varying random quantity [DG07]. This variation is due to the noise and the multipath fading effects. The instantaneous *signal-to-noise ratio* is defined as the

ratio of the received power to the noise power. In the following, with the understanding that the path loss and shadowing determine the average operational SNR, we will be concerned with the *small-scale* variations. Thereafter, we briefly describe the statistical model of noise and multipath fading before modeling the MIMO channel under consideration.

1.1.1 Noise Model

For a wireless telecommunication system, the noise is generally modeled as a random variable added to the received signals. The main sources of noise are thermal noise generated by the thermal agitation of electrons in electronic components and amplifiers at the receiver and the transmitter, channel interference from other communication systems, climatic conditions and even cosmic radiation. By invoking the central limit theorem, this noise is statistically modeled as a white complex Gaussian random variable with *probability density function* (pdf) $\sim CN(0, \sigma^2)$. $CN(\mu, \sigma^2)$ denotes the complex Gaussian pdf with mean μ and variance σ^2 . The total noise power spectral density is $N_0 = \sigma^2$. The noise model is known as *additive white Gaussian noise* (AWGN).

1.1.2 Fading Model

In wireless telecommunications, multipath propagation is a common phenomenon that occurs when the signal reaches the receiving antenna by more than one path. Causes of multipath include signal diffractions, refractions and reflections by the presence of obstacles (hills, buildings, etc.) as well as transmitter or receiver mobility. These multiple paths may combine destructively which induces fading. Fading is modeled differently according to the received signals at the destination. When there is no predominant path between the transmitter and the receiver, fading is modeled with a Rayleigh distribution referred to as *Rayleigh fading*. The fluctuation of the signal amplitude is therefore Rayleigh distributed. Besides, when there is a predominant path, often a *line of sight* (LoS) path, between the transmitter and the receiver, fading is modeled with a Ricean distribution [Pät02].

Small-scale fading is simultaneously characterized by the *time-spreading* of the signal or *signal dispersion* and the *time-variance* of the channel. The coherence bandwidth is defined as the frequency separation beyond which two signals experience different fading characteristics. The signal dispersion induces *inter-symbol interference*. The signal dispersion manifestations lead to *flat fading* or *frequency-selective fading* degradations [Sk101]. From a frequency domain point of view,

- Flat fading occurs when the coherence bandwidth of the channel is larger than the signal bandwidth. Therefore, all frequency components of the signal experience the same magnitude fading.

- Frequency-selective fading occurs when the coherence bandwidth of the channel is smaller than the signal bandwidth. Different frequency components of the signal therefore experience decorrelated or correlated fading.

Furthermore, the channel coherence time is defined as the time interval during which the channel response is invariant. The time-variance of the channel is related to the mobility of the transmitter, the receiver and the obstacles between them. One can distinguish three types of fading channel:

- *Fast fading channel* where the channel changes independently every channel use period.
- *Quasi-static fading channel* where the channel remains constant during the transmission of one codeword of length T and changes independently across codewords.
- *Block fading channel* where the channel remains constant during the transmission of a given number of sub-blocks of the codeword. The quasi-static channel is a special case of this type of channel.

In this thesis, we will consider only quasi-static flat Rayleigh fading channels. In fact, many systems such as WiFi, WiMAX, DVB or LTE uses the *orthogonal frequency division multiplexing* (OFDM) technique which transforms frequency-selective channels into parallel narrowband flat fading channels [vNP00].

1.1.3 MIMO Channel Model

We consider a MIMO system with N_t transmit antennas, N_r receive antennas operating over a narrowband quasi-static flat Rayleigh fading channel. A coherent MIMO system is considered where a perfect *channel state information* (CSI) knowledge is assumed only at the receiver, but not at the transmitter.

The channel input-output relation is completely defined by

$$\mathbf{Y} = \mathbf{H}\mathbf{X} + \mathbf{N} \quad (1.1)$$

where the $\mathbf{H}_{[N_r \times N_t]}$ represents the MIMO channel. A complex white Gaussian noise $\mathbf{N}_{[N_r \times T]}$ with *independent and identically distributed* (i.i.d.) entries and pdf $\sim CN(0, \sigma^2)$ is added to the received signals.

In general, a spatial correlation exists between antennas. The MIMO spatially correlated Rayleigh channel is considered following the well-known Kronecker model validated for both indoor and outdoor environment [KSP⁺02, YBO⁺04]. According to this model,

the correlation between transmit antennas and receive antennas are assumed independent and separable. The channel matrix can be factorized as

$$\mathbf{H} = \mathbf{R}_{\text{Rx}}^{1/2} \mathbf{H}_w \mathbf{R}_{\text{Tx}}^{1/2H}, \quad (1.2)$$

where \mathbf{H}_w represents the uncorrelated Rayleigh fading channel and its entries h_{ij} are assumed to be i.i.d. circularly symmetric Gaussian random variables with pdf $\sim CN(0, 1)$. h_{ij} corresponds to the channel coefficient between receive antenna i and transmit antenna j . \mathbf{R}_{Rx} and \mathbf{R}_{Tx} are the $N_r \times N_r$ and $N_t \times N_t$ correlation matrices at the receiver and the transmitter respectively. Note that $\mathbf{R}_{\text{Rx}}^{1/2}$ and $\mathbf{R}_{\text{Tx}}^{1/2}$ can be computed by Cholesky factorization.

In Chapter 2 and Chapter 3 Section 3.2, we assume an ideal uncorrelated MIMO system *i.e.*, $\mathbf{H} = \mathbf{H}_w$. This assumption is valid when the spacing between antennas is greater than the half-wavelength $\lambda/2$ [WSG94, BEFN04]. However, in practical systems, a correlation between transmit and/or receive antennas can exist and may lead to a substantial degradation in the system performance. The effect of the correlation on the system is discussed in Chapter 3.

1.2 MIMO Channel Capacity

This section introduces the basic definitions of information theory first introduced by Shannon in [Sha48]. We start by the definition of the *entropy* and the *mutual information*. Then, we provide the notions of *capacity* and *outage* which define the limits of any reliable transmission over the channel.

1.2.1 Entropy and Mutual Information

We first introduce the concept of entropy, which is a measure of uncertainty associated with a random variable. Let X be a discrete random variable belonging to an alphabet \mathcal{X} with a probability mass function $p(x) = \Pr(X = x)$, $x \in \mathcal{X}$. The entropy $H(X)$ of a discrete random variable X is defined by

$$H(X) = - \sum_{x \in \mathcal{X}} p(x) \log_2 p(x) \quad (1.3)$$

The entropy quantifies the expected value of information associated with a realization of the random variable and is typically measured in bits¹.

¹In the equation (1.3) we use \log_2 then the entropy is measured in bits. If we use the natural logarithm \log_e then the entropy is measured in nats.

Similarly, the joint entropy $H(X, Y)$ of a pair of discrete random variables (X, Y) with joint distribution $p(x, y)$, where y takes values in an alphabet \mathcal{Y} , is defined as

$$H(X, Y) = - \sum_{x \in \mathcal{X}} \sum_{y \in \mathcal{Y}} p(x, y) \log_2 p(x, y) \quad (1.4)$$

We also define the conditional entropy of Y given the knowledge of X as

$$H(Y|X) = - \sum_{x \in \mathcal{X}} \sum_{y \in \mathcal{Y}} p(y, x) \log_2 p(y|x) \quad (1.5)$$

The relation between the joint entropy and the conditional entropy is exhibited by the following *chain rule*

$$\begin{aligned} H(X, Y) &= H(X) + H(Y|X) \\ &= H(Y) + H(X|Y) \end{aligned} \quad (1.6)$$

For a continuous random variable X with a probability density function $p(x)$, the entropy is replaced by the differential entropy which is defined as

$$H(X) = - \int_{x \in \mathcal{X}} p(x) \log_2 p(x) dx \quad (1.7)$$

where \mathcal{X} is the support set of the random variable X .

Now, let us define the mutual information which is a measure of the amount of information that one random variable contains about another random variable. The mutual information $I(X, Y)$ is defined as the relative entropy between the joint distribution and the product distribution $p(x)p(y)$, *i.e.*,

$$I(X; Y) = - \sum_{x \in \mathcal{X}} \sum_{y \in \mathcal{Y}} p(x, y) \log_2 \frac{p(x, y)}{p(x)p(y)} \quad (1.8)$$

From the definitions of entropy and mutual information, one can easily show

$$\begin{aligned} I(X; Y) &= H(X) - H(X|Y) \\ &= H(Y) - H(Y|X) \end{aligned} \quad (1.9)$$

In the continuous domain, the mutual information is given by

$$I(X; Y) = - \int_{x \in \mathcal{X}} \int_{y \in \mathcal{Y}} p(x, y) \log_2 \frac{p(x, y)}{p(x)p(y)} dx dy \quad (1.10)$$

1.2.2 Channel Capacity and Outage Probability

The notion of channel capacity is established in the pioneering work of Shannon [Sha48]. The channel capacity defines the maximum amount of information that one

can *reliably* transmit over the channel. It is measured as the maximum of the mutual information between the input and output of the channel, with respect to the input distribution.

$$C = \max_{p(x)} I(X; Y) \quad (1.11)$$

The capacity of a coherent MIMO system where the CSI is known only at the receiver is achieved by an input distributed as a zero-mean circularly symmetric complex Gaussian random variable [Tel99, FG98]. The capacity of the random MIMO channel is given by

$$\begin{aligned} C &= E_{\mathbf{H}} [I(X; Y)] \\ C &= E_{\mathbf{H}} \left[\log_2 \det \left(\mathbf{I}_{N_r} + \frac{\rho}{N_t} \mathbf{H} \mathbf{H}^H \right) \right] \\ &= E_{\mathbf{H}} \left[\log_2 \det \left(\mathbf{I}_{N_t} + \frac{\rho}{N_t} \mathbf{H}^H \mathbf{H} \right) \right] \end{aligned} \quad (1.12)$$

where ρ is the average signal-to-noise ratio per receive antenna, the superscript H stands for conjugate transpose. The expectation is evaluated over the statistics of the matrix \mathbf{H} . The capacity can be computed by either analytical expression [Tel99, RV05] or Monte Carlo simulations.

The capacity of a MIMO system with uncorrelated Rayleigh fading channel achieves almost $r = \min(N_t, N_r)$ bps/Hz for every 3 dB increase in SNR while it achieves only one additional bps/Hz for every 3 dB increase for a *single-input single-output* (SISO) system [Tel99, FG98]. However, the correlation between antennas alter this capacity and may result to a substantial degradation of the MIMO capacity especially for high correlations [Loy01, RV05].

The outage probability is an important measure for the performance evaluation of communication systems over quasi-static fading channels. It is defined as the probability that a given realization of the channel cannot support a required data rate R . It can then be written as

$$\begin{aligned} P_{\text{out}} &= \Pr [I < R] \\ &= \Pr \left[\log_2 \det \left(\mathbf{I}_{N_r} + \frac{\rho}{N_t} \mathbf{H} \mathbf{H}^H \right) < R \right] \end{aligned} \quad (1.13)$$

In this case, we say that the channel is in outage. The computation of outage probabilities can be evaluated either by analytical expressions or by Monte Carlo simulations. However, exact analytical form of outage probabilities for any $N_t \times N_r$ are not easily tractable. Upper-bounds or Monte Carlo simulations are often used to compute these outage probabilities [Nar05, Nar06, OC07, RHGA10].

1.3 Diversity Techniques

Diversity techniques refer to methods of improving the reliability of a message by effectively transmitting different replicas of the same information over different independent branches, and thereby combating channel fading. Each replica experiences different channel conditions (fading, interference, etc.), in the hope that at least one of these replicas will be correctly received. The receiver wisely combines these replicas and try to recover the transmitted information. The *diversity order* d is defined as the number of independent received replicas. At high SNRs, the average error probability decays inversely with the d -th power of the SNR *i.e.*, SNR^{-d} [ZT03]. Thus, it is important to maximize this diversity order while maintaining, if possible, the same transmission rate. Several diversity methods can be distinguished:

Time diversity The same message is transmitted several times in different time intervals. The separation of these time intervals has to be sufficiently large, *i.e.*, greater than the *coherence time* of the channel, so that the fading channel coefficients change, and different channel gains are observed.

Frequency diversity Different replicas of the message are transmitted over different frequency bands. To ensure that the channel coefficients seen are different, the separation of these frequency bands has to be greater than the *coherence bandwidth* of the channel.

When using simple repetition coding, the price to pay for time diversity and frequency diversity methods is an increased bandwidth occupation or a reduced data rate. Another method to combat the effects of fading without wasting available resources is space diversity, also known as *antenna diversity*.

Space diversity The signal is transmitted via several transmit antennas and received via different receive antennas. These antennas should be placed at least half a wavelength of the carrier frequency apart to ensure that the signal undergoes different independent channel fades [WSG94]. The maximal achievable diversity order of a MIMO system, assuming the path gains between individual pairs are independent and identically distributed Rayleigh faded, is $d = N_t N_r$.

One way to exploit the diversity with the order d is to use repetition coding with a rate $1/d$. Coding techniques can be considered as more sophisticated forms to exploit the diversity. This coding can be done at several levels in the transmission chain. When considering space diversity, one can distinguish two major coding categories:

- *Channel coding* which consists of the addition of redundancy bits to the transmitted message, in order to detect and/or correct erroneous bits at the reception. Therefore, a higher reliability is achieved by exploiting the time diversity.
- *Space-time coding* for MIMO systems. It consists of the transmission on multiple antennas of a redundant and/or correlated version of the mapped symbols during several channel use periods, and thereby can exploit only space diversity or both space and time diversities.

Space-time coding for MIMO systems not only increases the diversity order, but also increases the spectral efficiency or the *multiplexing gain* of the channel. Indeed, it is possible to achieve simultaneously both diversity and multiplexing gains with a fundamental tradeoff known as *diversity-multiplexing tradeoff* (DMT) [ZT03].

1.3.1 Diversity-Multiplexing Tradeoff for MIMO systems

A MIMO system can provide two types of gains: diversity gain and multiplexing gain. In [ZT03], Zheng and Tse have proposed the DMT framework to characterize the interplay between reliability and rate at infinite SNR ($\text{SNR} \rightarrow \infty$). They have proved that both gains can be *simultaneously* obtained, but there is a fundamental tradeoff between them: a higher multiplexing gain comes at the price of sacrificing diversity. The DMT curve defines the upper-bound achievable by any space-time coding scheme over a $N_t \times N_r$ MIMO channel.

Let us consider a space-time code $\mathbf{X}_{[N_t \times T]}$ transmitting at rate $R(\rho)$ bits *per channel use* with a packet error probability $P_e(\rho)$. The asymptotic multiplexing gain $r_{\text{asymptotic}}$ is defined as the ratio of the achievable rate to the logarithm of ρ where $\rho \rightarrow \infty$. Asymptotically, an increase of 3 dB in ρ allows a data rate increase of $r_{\text{asymptotic}}$ bits.

$$r_{\text{asymptotic}} = \lim_{\rho \rightarrow \infty} \frac{R(\rho)}{\log \rho}. \quad (1.14)$$

The multiplexing gain is always less than or equal to $\min(N_t, N_r)$. Indeed, in the high SNR regime, the MIMO channel can be viewed as $\min(N_t, N_r)$ parallel spatial channels since $\min(N_t, N_r)$ is the total number of degrees of freedom available for communication [Fos96].

The asymptotic diversity gain $d_{\text{asymptotic}}$ is defined as the negative (asymptotic) slope of the packet error probability curve as a function of ρ in the log-log scale.

$$d_{\text{asymptotic}} = - \lim_{\rho \rightarrow \infty} \frac{\log P_e(\rho)}{\log \rho}. \quad (1.15)$$

Authors in [ZT03] have proven that the average packet error rate probability is lower-bounded by the outage probability at rate $R = r \log(\rho)$ *i.e.*, $P_e(\rho) \geq P_{\text{out}}(R)$, and then

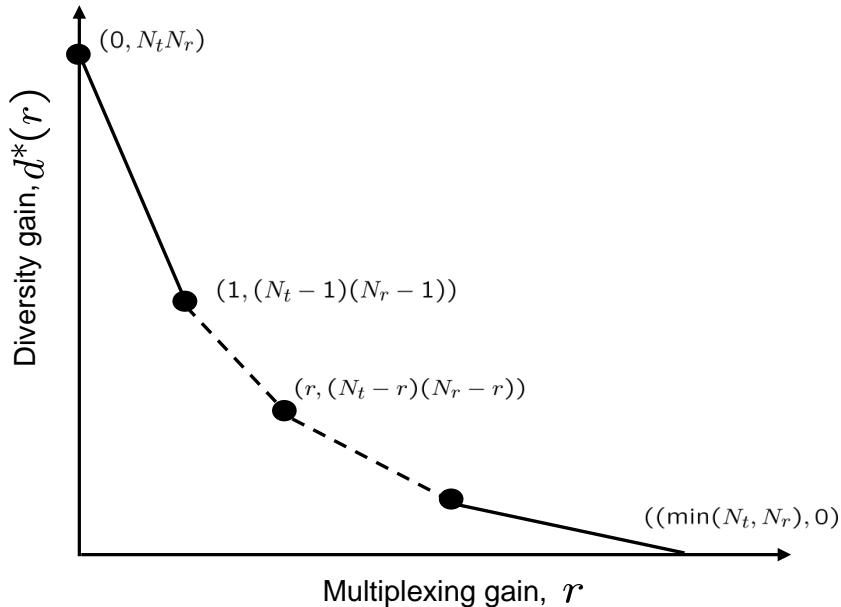


FIGURE 1.2: The optimal diversity-multiplexing tradeoff of a MIMO system.

the diversity gain can be defined based on the outage probability by

$$d_{\text{asymptotic}} = - \lim_{\rho \rightarrow \infty} \frac{\log P_{\text{out}}(\rho)}{\log \rho}. \quad (1.16)$$

For a coherent MIMO system with i.i.d. flat Rayleigh fading channel, the asymptotic optimal DMT is given by the piece-wise linear function connecting the points $(k, d^*(k))$ where $d^*(k)$ is given by [ZT03]

$$d^*(k) = (N_t - k)(N_r - k); k = 1, \dots, \min(N_t, N_r). \quad (1.17)$$

Authors in [ZT03] assume that the coherence time of the channel and T are greater than or equal to $N_t + N_r - 1$. Later, [EKP⁺06] has noted that $T \geq N_t$ is a sufficient condition. The DMT for a $N_t \times N_r$ uncorrelated flat Rayleigh fading MIMO channel is depicted in Figure 1.2. Furthermore, [CCL06] has proved that the spatial correlation does not affect the asymptotic DMT.

1.4 Space-Time Coding for MIMO Systems

At the transmitter, MIMO coding techniques are employed for data rate increase and/or better reliability. Spatial multiplexing schemes [WFGV98] aim at increasing the channel spectral efficiency while space-time codes are designed to exploit the channel diversity. The main idea of space-time coding is to introduce redundancy or correlation between transmitted symbols on spatial and temporal dimensions. A space-time code is

characterized by its rate, diversity gain and coding gain. The rate of a space-time code is equal to the average number of transmitted symbols per a channel use period. The diversity order is equal to the number of independent received replicas of transmitted symbols and the coding gain is the gain provided by coded system with respect to a non-coded one. A space-time code is said to be *full-rate* (FR) when the rate is equal to the total number of degrees of freedom available for communication *i.e.*, $\min(Nt, Nr)$. Besides, it is said to be *full-diversity* (FD) when it exploits all the available MIMO channel diversity $N_t N_r$.

One can distinguish two main types of space-time codes: *space-time trellis codes* (STTCs) and *space-time block codes* (STBCs). Space-time trellis coding consists of the coding on a trellis of transmitted symbols over multiple antennas and multiple channel uses. STTCs can provide both coding gain and diversity gain [TSC98]. The coding optimization is done for each targeted spectral efficiency value. The detection is done using the Viterbi algorithm by minimizing a cumulative likelihood metric then selecting the most likely path in the trellis. Due to their lack of flexibility and high *maximum likelihood* (ML)-detection complexity, they are excluded from practical communication system standards [SOZ11]. Therefore, they are beyond the scope of this thesis. On the other hand, STBCs enjoy relatively lower ML-detection complexity and are often incorporated in communication system standards. In the sequel, we introduce space-time block codes and their conventional design criteria. Then we focus on some well-known STBCs considered throughout this thesis. More details on coding for MIMO systems can be found in [DG07, SOZ11].

1.4.1 Space-Time Block Codes

Space-time block codes are usually represented by a $N_t \times T$ matrix where each row represents a transmit antenna and each column represents a channel use period. They were first introduced by Alamouti in [Ala98]. The scheme proposed by Alamouti is a low ML-detection STBC achieving full transmit diversity for 2×1 MISO systems with rate 1, equal to the rate of a SISO system. Thanks to its orthogonality property, the Alamouti code can be ML-detected by a simple linear processing on the set of received signals. Tarokh *et al.* in [TJC99] generalize the work of Alamouti and introduce orthogonal space-time block codes (OSTBCs). OSTBCs achieve full-diversity but, in order to maintain the orthogonality property, are not full-rate. To mitigate this problem, Hassibi *et al.* introduce in [HH02] linear dispersion STBCs (LD-STBCs) where they remove the orthogonality constraint. LD-STBCs are designed to maximize the symbol-wise mutual information. However, LD-STBCs in [HH02] do not guarantee the FR-FD properties, requisite to achieve lower error probabilities at high SNRs. The well-known *rank-determinant criteria* formulated in [TSC98] aim to design such space-time codes.

1.4.2 Conventional Rank-Determinant Design Criteria

The rank-determinant criteria are conventionally used while designing FR-FD STBCs for quasi-static flat Rayleigh fading MIMO channels. They aim to minimize the *pairwise error probability* (PEP) $\Pr(\mathbf{X}, \hat{\mathbf{X}})$, defined as the probability that the detector estimates an erroneous codeword $\hat{\mathbf{X}}$ instead of the transmitted codeword \mathbf{X} , between all possible transmitted codewords. The PEP is upper-bounded by [TSC98]

$$\Pr(\mathbf{X}, \hat{\mathbf{X}}) \leq \left(\prod_{i=1}^r \lambda_i \right)^{-N_r} (\rho/4)^{-rN_r}, \quad (1.18)$$

where r is the rank of matrix $\mathbf{\Delta} = (\mathbf{X} - \hat{\mathbf{X}})^H (\mathbf{X} - \hat{\mathbf{X}})$ and $\lambda_i; i = 1, \dots, r$ are the nonzero eigenvalues of matrix $\mathbf{\Delta}$.

The upper-bound on the PEP is tight at high SNRs. Based on this upper-bound, space-time codes design criteria are deduced.

Rank Criterion In order to achieve the maximum diversity, the rank r of matrix $\mathbf{\Delta}$ must be maximized for all possible transmitted codeword pairs $(\mathbf{X}, \hat{\mathbf{X}})$. The code diversity gain is defined as $d = rN_r$. When $r = N_t$, the space-time code benefits from the total degrees of freedom of the channel and a diversity order of $N_t N_r$ is achieved.

Determinant Criterion The minimum determinant of matrix $\mathbf{\Delta}$, defined as

$$\delta = \min_{\mathbf{X} \neq \hat{\mathbf{X}}} \prod_{i=1}^r \lambda_i \quad (1.19)$$

must be maximized.

However, the dominant parameter in STBC design is the diversity gain d which defines the slope of BER curves. Therefore, it is important to ensure the FD property of the STBC and then maximize its coding gain δ^{1/N_t} .

1.4.3 Conventional MIMO Codes

In this section, we introduce some well-known MIMO codes and we focus on the codes considered in the thesis, especially 2×2 WiMAX MIMO profiles specified in the IEEE 802.16e-2005 standard [IEE06]. Although we have restricted our study to the 2×2 MIMO schemes, the application of our work to any $N_t \times T$ MIMO scheme is straightforward.

Alamouti scheme (Matrix A) The Alamouti code is introduced as the first STBC exploiting the full transmit diversity for $2 \times N_r$ MIMO systems with a diversity d equal

to $2N_r$. A group of two data symbols (S_1, S_2) belonging to the complex constellation are transmitted by $N_t = 2$ antennas, during $T = 2$ channel use periods, as follows [Ala98]

$$\mathbf{X}^{\text{Alamouti}} = \begin{bmatrix} S_1 & -S_2^* \\ S_2 & S_1^* \end{bmatrix} \quad (1.20)$$

where S^* stands for the complex conjugate of S .

The Alamouti code was proved to be the only FR-FD STBC for 2×1 MISO systems when symbols belong to a complex constellation [TJC99]. For $N_r \geq 2$, it always offers full-diversity but not full-rate *e.g.*, it is only half-rate for a 2×2 MIMO system, because it only transmits two symbols during two channel use periods over two antennas. According to the IEEE 802.16e-2005 standard, the Alamouti code is a mandatory profile for the 2×2 mobile WiMAX system in the downlink and is referred to as *Matrix A* (MA) STBC.

The orthogonality of the Alamouti code makes its optimal ML-detection linear with a complexity in $\mathcal{O}(M)$. Orthogonal space-time block codes are extended in [TJC99] for a higher number of transmit antennas. In order to maintain the STBC orthogonality, OSTBCs sacrifice part of the data rate bearable by the MIMO system. Even though the orthogonality constraint is important from a complexity point of view, it imposes a wastage in one of the major benefits of MIMO techniques, the data rate increase.

Spatial multiplexing (Matrix B) The spatial multiplexing scheme, also known as *vertical Bell laboratories layered space-time* (V-BLAST) scheme, has been the first transmission technique employed in MIMO systems for the purpose of data rate increase [WFGV98]. It simply consists of transmitting simultaneously N_t symbols over the N_t antennas during one channel use period. According to the IEEE 802.16e-2005 standard, the *spatial multiplexing* (SM) is a mandatory profile for the 2×2 mobile WiMAX system in the downlink and referred to as *Matrix B* (MB). A group of two data symbols (S_1, S_2) are transmitted over $N_t = 2$ antennas as follows

$$\mathbf{X}^{\text{SM}} = \begin{bmatrix} S_1 \\ S_2 \end{bmatrix} \quad (1.21)$$

The spatial multiplexing scheme offers full-rate but does not benefit from any transmit diversity gain.

Zheng and Tse have shown in [ZT03] that both multiplexing gain and diversity gain can be simultaneously obtained with a fundamental tradeoff between them. Therefore, FR-FD STBCs are designed according to the rank-determinant criteria in a way achieving the optimal DMT frontier. FR-FD STBCs considered in the course of this thesis are briefly described in the following.

Golden code (Matrix C) *Perfect space-time block codes* (PSTBCs) [ORB06, BRV05] form an interesting family of full-rate full-diversity space-time block codes achieving the DMT frontier. Moreover, PSTBCs belong also to the family of linear-dispersion codes defined by Hassibi *et al.* [HH02] *i.e.*, they maximize the symbolwise mutual information between transmitted and received signals. Their structures are designed based on cyclic division algebras known as a powerful tool in designing STBCs. For a 2×2 MIMO system, the resulting PSTBC is well-known as the *Golden code* (GC) [BRV05]. At high SNRs, the GC is known to be the best 2×2 FR-FD STBC with non-vanishing determinants. The *non-vanishing determinant* (NVD) property guarantees a minimum determinant *i.e.*, a minimum MIMO coding gain independent of the modulation order M . This NVD property is a sufficient condition to design a STBC achieving the optimal DMT frontier [OBV07]. According to the GC structure, a group of four data symbols (S_1, S_2, S_3, S_4) is transmitted as follows

$$\mathbf{X}^{\text{GC}} = \frac{1}{\sqrt{5}} \begin{bmatrix} \alpha (S_1 + S_2\theta) & \alpha (S_3 + S_4\theta) \\ j\bar{\alpha} (S_3 + S_4\bar{\theta}) & \bar{\alpha} (S_1 + S_2\bar{\theta}) \end{bmatrix} \quad (1.22)$$

where $\theta = \frac{1+\sqrt{5}}{2}$, $\bar{\theta} = \frac{1-\sqrt{5}}{2}$, $\alpha = 1 + j - j\theta$ and $\bar{\alpha} = 1 + j - j\bar{\theta}$.

For higher number of antennas, PSTBCs can be found in [ORB06, OBV07, ESK07].

In order to benefit from both diversity and multiplexing gains, a variant version of the Golden code referred to as *Matrix C* (MC) is included in the IEEE 802.16e-2005 specification as an optional transmission MIMO profile.

Trace-orthonormal In [ZLW07], another approach has been considered to design FR-FD LD-STBC for coherent MIMO systems. Zhang *et al.* construct their STBC structure from both information-theoretic and detection error viewpoints leading to the *trace-orthonormal* (TO) STBC. For a 2×2 MIMO system, a group of four data symbols (S_1, S_2, S_3, S_4) is transmitted as follows [ZLW07]

$$\mathbf{X}^{\text{TO}} = \frac{1}{\sqrt{2}} \begin{bmatrix} X_{11} & X_{12} \\ X_{21} & X_{22} \end{bmatrix} \quad (1.23)$$

where

$$X_{11} = (S_1 + S_2) \cos \theta + (S_2^* - S_1^*) \sin \theta \quad (1.24a)$$

$$X_{12} = e^{\frac{j\pi}{4}} ((S_3 + S_4) \sin \theta + (S_4^* - S_3^*) \cos \theta) \quad (1.24b)$$

$$X_{21} = e^{\frac{j\pi}{4}} ((S_3 + S_4) \cos \theta + (S_3^* - S_4^*) \sin \theta) \quad (1.24c)$$

$$X_{22} = (S_1 + S_2) \sin \theta + (S_1^* - S_2^*) \cos \theta \quad (1.24d)$$

and θ is the code design parameter.

The trace-orthonormal STBC has a flexible structure where its design parameter θ is to be optimized according to the selected criterion. In [ZLW07], the rank-determinant criteria have been selected and an exhaustive search on θ has been performed in order to maximize the minimum determinant of the TO structure. This search leads to $\theta = \frac{1}{2} \arcsin \frac{1}{\sqrt{5}} \approx 13.28^\circ$ and the same coding gain as the Golden code gain is achieved. Therefore, in the context of a 2×2 MIMO system, the TO STBC guarantees the best performance at high SNRs.

Sezginer and Sari (Matrix D) Previously presented FR-FD STBCs benefit from both multiplexing and diversity gains of MIMO channels. However, their detection complexity can be tremendous especially for high order modulations.

For the 2×2 MIMO system, the complexity of the GC detector grows with the fourth power of the constellation order *i.e.*, $\mathcal{O}(M^4)$. Motivated by the proposal of a FR-FD STBC with reduced complexity, Sezginer and Sari have proposed in [SS07, SSB⁺08] the *Matrix D* (MD) STBC. The Matrix D code has been proposed as an alternative FR-FD STBC for the IEEE 802.16 standard with a substantial lower ML-detection complexity with respect to the MC code and a similar performance [SSB⁺08]. According to the MD structure, a group of four data symbols (S_1, S_2, S_3, S_4) is transmitted as follows

$$\mathbf{X}^{\text{MD}} = \begin{bmatrix} aS_1 + bS_3 & -cS_2^* - dS_4^* \\ aS_2 + bS_4 & cS_1^* + dS_3^* \end{bmatrix} \quad (1.25)$$

where $a = c = 1/\sqrt{2}$; $b = 1/\sqrt{2} \exp(j\varphi)$; $d = b \exp(-j\frac{\pi}{2})$ and $\varphi = \arg(b)$ is the code design parameter.

According to the rank-determinant criteria, an exhaustive search is performed in [SS07] in order to maximize the code minimum determinant. This search leads to $\varphi = \arg\left(\frac{[1 - \sqrt{7} + j(1 + \sqrt{7})]}{4\sqrt{2}}\right) \approx 114.29^\circ$. Unfortunately, its lower minimum determinant *i.e.*, coding gain leads to a slight loss in performance with respect to the GC.

Other 2×2 MIMO codes In this section, we provide a brief summary of the well-known full-rate 2×2 MIMO codes [ZLW07, BRV05, DV05, SR08, YW03, SS07, PGGA08, HTW03]. These codes are defined under the rank-determinant criteria. STBCs in [SR08, SS07, PGGA08, HTW03] are designed to reduce the ML-detection complexity, while STBCs in [ZLW07, BRV05, DV05, SR08] have the highest MIMO coding gain. Table 1.1 summarizes their characteristics. The minimum determinant is computed for symbols chosen from a regular M -QAM constellation [SR08].

MIMO Code \mathbf{X}	Minimum determinant for M -QAM modulations
Golden code (GC) [BRV05]	3.2000
Srinath-Rajan (SR) [SR08]	
Dayal-Varanasi (DV) [DV05]	
Trace-orthonormal (TO) [ZLW07]	
HTW-PGA [HTW03, PGGA08]	2.2857
Sezginer-Sari (MD) [SS07]	2.0000
Yao-Wornell (YW) [YW03]	0.8000
Spatial multiplexing (SM) [WFGV98]	0.0000

TABLE 1.1: Comparison between the minimum determinant of some well-known full-rate 2×2 MIMO codes.

1.4.3.1 ML-Detection of STBCs

At the receiver side, a MIMO detector is implemented to estimate the value of the transmitted symbols before space-time coding. Several detection techniques can be employed. The detection technique is selected based on two criteria: the performance must be as close as possible to the optimal one and the complexity should be tolerable. In order to obtain a fair comparison of MIMO codes performance, the optimal *maximum-likelihood* detector is employed while simulating all the presented MIMO codes. Besides by tolerating a small penalty performance, the complexity can be reduced using the list sphere decoder based on [HtB03]. This complexity can be further reduced with a higher performance penalty using a linear filter detector based on *minimum mean square error* (MMSE) criterion [FF73] or even a *zero forcing* (ZF) criterion [Pri72].

Full-rate full-diversity STBC The optimum receiver *i.e.*, the ML detector, evaluates the squared Euclidean distance $D(S_1, S_2, S_3, S_4)$ between the received noisy signal \mathbf{Y} and the noiseless transmitted codeword \mathbf{S} corresponding to all possible quadruplets of transmitted symbols (S_1, S_2, S_3, S_4) and selects the one which minimizes this distance, expressed by

$$D(S_1, S_2, S_3, S_4) = \|\mathbf{Y} - \mathbf{HS}\|_F^2 \quad (1.26)$$

where $\|\cdot\|_F$ is the Frobenius norm.

For FR-FD STBCs, the ML detector therefore makes an exhaustive search over all possible M^4 quadruplets and its complexity grows in $\mathcal{O}(M^4)$. In general, for a FR-FD STBC transmitting $N_t \times T$ symbols per block, the complexity grows in $\mathcal{O}(M^{N_t T})$. However, some FR-FD STBCs have been designed in a way permitting a ML-detection with low complexity *e.g.*, the Matrix D STBC [SS07]. The low ML-detection complexity of the MD code is described in Section 2.1.1.

Alamouti scheme For the Alamouti scheme, the ML-detection complexity grows linearly with the modulation order *i.e.*, $\mathcal{O}(M)$. Indeed, the received signals during the first and the second channel use periods can be written as

$$r_{11} = h_{11}S_1 + h_{12}S_2 + n_{11} \quad (1.27a)$$

$$r_{12} = -h_{11}S_2^* + h_{12}S_1^* + n_{12} \quad (1.27b)$$

for the first antenna, and

$$r_{21} = h_{21}S_1 + h_{22}S_2 + n_{21} \quad (1.28a)$$

$$r_{22} = -h_{21}S_2^* + h_{22}S_1^* + n_{22} \quad (1.28b)$$

for the second receive antenna. Based on an exhaustive search over all possible constellation points, the optimal ML detector estimates the transmitted symbols S_1 and S_2 using

$$\begin{aligned} \hat{S}_1 &= h_{11}^*r_{11} + h_{12}r_{12}^* + h_{21}^*r_{21} + h_{22}r_{22}^* \\ &= (|h_{11}|^2 + |h_{12}|^2 + |h_{21}|^2 + |h_{22}|^2) S_1 + \eta_1 \end{aligned} \quad (1.29)$$

$$\begin{aligned} \hat{S}_2 &= h_{12}^*r_{11} - h_{11}r_{12}^* + h_{22}^*r_{21} - h_{21}r_{22}^* \\ &= (|h_{11}|^2 + |h_{12}|^2 + |h_{21}|^2 + |h_{22}|^2) S_2 + \eta_2 \end{aligned} \quad (1.30)$$

with $\eta_1 = h_{11}^*n_{11} + h_{12}n_{12}^* + h_{21}^*n_{21} + h_{22}n_{22}^*$,

and $\eta_2 = h_{12}^*n_{11} - h_{11}n_{12}^* + h_{22}^*n_{21} - h_{21}n_{22}^*$.

These equations obviously show that the receiver exploits a diversity of order 4 which is the maximum diversity for a 2×2 MIMO system.

Spatial multiplexing The spatial multiplexing scheme uses only one period to transmit N_t symbols. On the first receive antenna, the received signal can be written as

$$r_1 = h_{11}S_1 + h_{12}S_2 + n_1 \quad (1.31)$$

Similarly, on the second receive antenna

$$r_2 = h_{21}S_1 + h_{22}S_2 + n_2 \quad (1.32)$$

The ML detector selects the couple (S_1, S_2) minimizing the distance $D(S_1, S_2)$ expressed by

$$D(S_1, S_2) = \|\mathbf{Y} - \mathbf{HS}\|_F^2 = \|r_1 - h_{11}S_1 - h_{12}S_2\|^2 + \|r_2 - h_{21}S_1 - h_{22}S_2\|^2. \quad (1.33)$$

The complexity of such a detector grows in $\mathcal{O}(M^2)$.

1.5 Background on Capacity-Approaching Channel Coding

In order to achieve reliable transmissions, channel coding is incorporated in digital communication systems. The basic principle of channel coding is to introduce redundancy bits to the transmitted data. The receiver uses these additional bits to, if possible, detect and/or correct erroneous bits in the received data, leading therefore to a more reliable transmission. However, the use of channel coding causes a reduction in the data rate or an expansion in the bandwidth. The multiplexing gain introduced by MIMO technologies can compensate this reduction.

For communication systems, the most relevant channel codes are *capacity-approaching codes* which closely approach the channel capacity defined by Shannon [Sha48] as the theoretical maximum limit at which reliable communication is still possible given a specific noise level. Among them, *turbo codes* [BGT93] and *low-density parity-check codes* [Gal62] are competing for adoption in recently standardized telecommunication systems.

In this section, we describe some well-known capacity-approaching channel codes considered throughout the thesis. We start by briefly describing convolutional codes, and then we present the 8-state double binary turbo code adopted in the WiMAX and *DVB-return channel via satellite* (DVB-RCS) standards [DB05, IEE06, Nua07, DVB09]. Thereafter, we describe a new turbo-like code known as FlexiCode [CTD⁺05]. Note that the work presented in this thesis is also applicable to LDPC codes and any channel code.

1.5.1 Convolutional Codes

Convolutional codes [Eli55] form a family of codes simple to implement based on *linear feedback shift registers*. They are widely used in various applications in order to increase the transmission reliability. A convolutional encoder receives at its input, at each instant i , a vector d_i of p bits and generates at its output a vector of q bits ($q > p$). This code is called p -binary code with rate p/q which corresponds to the ratio of the number of information bits p to the number of total coded bits q . The code is called systematic when the input d_i being encoded is included in the output sequence. Moreover, it is recursive if the current memory bits are fed back to compute the new memory bits. Figure 1.3 depicts the structure of a $p = 1$ *recursive systematic convolutional* (RSC) encoder with memory $\nu = 3$ and then $2^\nu = 8$ possible states, so-called 8-state binary RSC code. D represents the memory element, responsible of

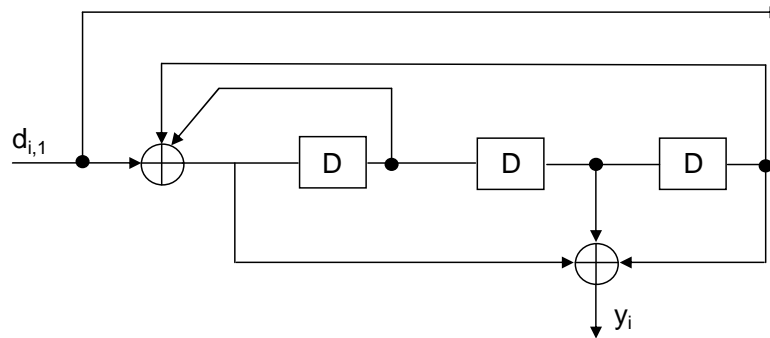


FIGURE 1.3: Structure of an 8-state binary encoder.

forwarding the bits with a delay of one time unit. The generator polynomials in octal form of this code are $(15, 13)_8$.

RSC code are characterized by a fixed code rate. When higher coding rates are required, puncturing *i.e.*, not transmitting certain coded bits, is applied [CCG79]. The code rate is then defined as the ratio of the number of information bits to the number of surviving coded bits.

Several algorithms are proposed to decode a convolutional code. We will focus on *soft-input soft-output* decoders. The most common algorithms are the *soft-output Viterbi algorithm* (SOVA) [HH89] and the BCJR algorithm [BCJR74]. The BCJR algorithm is also known as the *maximum a posteriori* (MAP) algorithm, as it maximizes the *a posteriori* probability. The log-MAP algorithm [RVH95] is a version of the MAP algorithm in the logarithmic domain. In order to decrease the log-MAP algorithm complexity, a less complex suboptimal variant of this algorithm called MAX-log-MAP, is proposed [RVH95] where the logarithmic operation is replaced by a maximization function ($\log(\exp(a) + \exp(b)) \approx \max(a, b)$). In this thesis, we use the MAP decoder for simulation results.

1.5.2 The WiMAX 8-State Double Binary Turbo Code

Turbo codes introduced by Berrou *et al.* consist of the parallel concatenation of two convolutional codes \mathcal{C}_1 and \mathcal{C}_2 with an interleaver Π between them [BGT93]. Figure 1.4 shows the structure of a turbo encoder. The designation, *turbo code*, is due to the iterative decoding at the receiver side. Non-binary turbo codes *i.e.*, the parallel concatenation of p -binary RSC leads to better global performance with respect to classical turbo codes ($p = 1$) [BJDK01, DB05]. The advantages of this construction are: better convergence of the iterative process, larger minimum distances (*i.e.*, larger asymptotic gains), less puncturing for a given rate, higher throughput, and reduced latency. Moreover, non-binary decoding is more robust towards the flaws of the decoding algorithm.

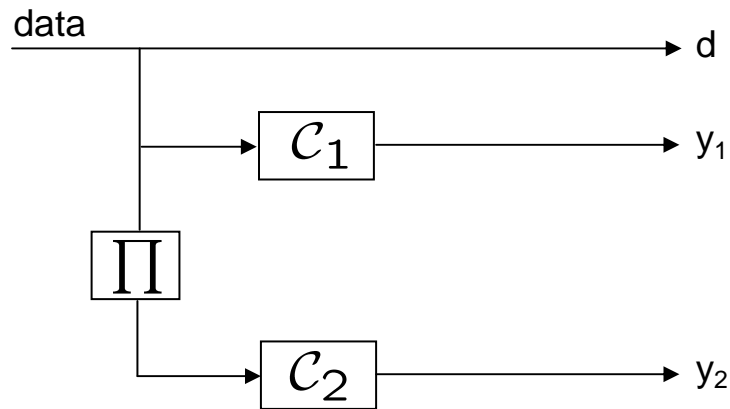


FIGURE 1.4: Structure of a turbo encoder.

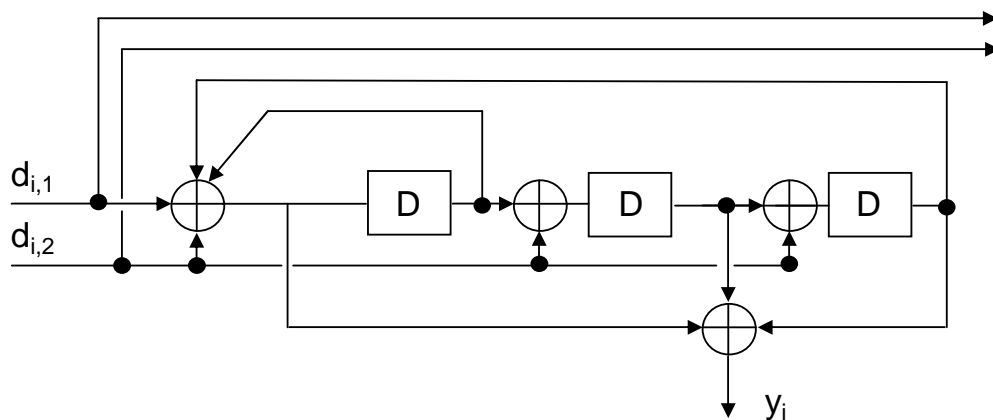


FIGURE 1.5: Structure of an 8-state double binary RSC encoder.

A very slight difference is observed between the decoding performance when using the MAP or the MAX-log-MAP algorithms.

A RSC code with $p = 2$ is called *double binary RSC*. Figure 1.5 depicts the structure of the 8-state double binary RSC encoder with generator polynomials $(15, 13)_8$. Due to its good performance and reasonable decoding complexity, the 8-state double binary turbo code based on this component encoder has been adopted in the WiMAX [IEE06], DVB-RCS [DVB09] and *DVB-Return Channel Terrestrial* (DVB-RCT) [DVB02] standards.

1.5.3 Log-Likelihood Ratios

A natural reliability value for the exchange of soft information in iterative decoding process is the *log-likelihood ratio* (LLR). Let b be a variable in a *Galois field* (GF) with the elements $\in \{0, 1\}$. Then, the *a priori* LLR of b is defined as [Hag04]

$$L_a(b) = \log \frac{P(b=0)}{P(b=1)} \quad (1.34)$$

$L_a(b)$ represents the *a priori* knowledge about the binary random variable b . For a transmission channel with transition probability $P(\mathbf{Y}|b)$, the *a posteriori* LLR value of b , conditioned on the received signal \mathbf{Y} , is

$$L(b|\mathbf{Y}) = \log \frac{P(b=0|\mathbf{Y})}{P(b=1|\mathbf{Y})} \quad (1.35)$$

The sign of $L(b|\mathbf{Y})$ provides the hard decision on b , and the magnitude $|L(b|\mathbf{Y})|$ tells the reliability of this decision.

Applying the Bayes' rule yields,

$$P(b=0|\mathbf{Y}) = \frac{P(\mathbf{Y}|b=0)}{P(\mathbf{Y})} P(b=0) \quad (1.36)$$

where $P(b=0)$ is the *a priori* probability that $b=0$ was transmitted. From equations (1.35) and (1.36), we obtain

$$L(b|\mathbf{Y}) = \log \frac{P(b=0)}{P(b=1)} + \log \frac{P(\mathbf{Y}|b=0)}{P(\mathbf{Y}|b=1)} = L_a(b) + L_{ch}(\mathbf{Y}|b) \quad (1.37)$$

For a Rayleigh fading MIMO channel with channel matrix \mathbf{H} , the channel LLR $L_{ch}(\mathbf{Y}|b)$ is given by

$$L_{ch}(\mathbf{Y}|b) = \log \frac{P(\mathbf{Y}|b=0)}{P(\mathbf{Y}|b=1)} = \log \frac{\sum_{\mathbf{S} \in \chi_0^i} P(\mathbf{Y}|\mathbf{S})}{\sum_{\mathbf{S} \in \chi_1^i} P(\mathbf{Y}|\mathbf{S})} \quad (1.38)$$

where χ_0^i (resp. χ_1^i) is the set of transmitted matrices \mathbf{S} having the bit b equal to 0 (resp. 1) and $P(\mathbf{Y}|\mathbf{S})$ is expressed as

$$\begin{aligned} P(\mathbf{Y}|\mathbf{S}) &\propto \exp\left(\frac{-\|\mathbf{Y} - \mathbf{H}\mathbf{S}\|_F^2}{\sigma^2}\right) \\ &= \exp\left(\frac{-D(S_1, S_2, S_3, S_4)}{\sigma^2}\right) \end{aligned} \quad (1.39)$$

1.5.4 Iterative (Turbo) Decoding

The iterative or turbo decoding principle of a parallel concatenated convolutional code is shown in Figure 1.6. \mathcal{C}_1^{-1} is the soft-input soft-output decoder corresponding to encoder \mathcal{C}_1 and \mathcal{C}_2^{-1} is the decoder corresponding to \mathcal{C}_2 .

Turbo decoding involves an exchange of information between two components decoders \mathcal{C}_1^{-1} and \mathcal{C}_2^{-1} . This exchange is enabled by linking the *a priori* LLR of one component decoder ($L_{a_1}(\mathbf{b})$ or $L_{a_2}(\tilde{\mathbf{b}})$) to the extrinsic LLR provided by the other component decoder ($L_{e_1}(\mathbf{b})$ or $L_{e_2}(\tilde{\mathbf{b}})$). Each decoder computes the extrinsic information related to the information word (\mathbf{b}), using its associated systematic and parity symbols (\mathbf{c}) coming from the transmission channel ($L_{ch}(\mathbf{c})$), and the *a priori* LLR. The decoding

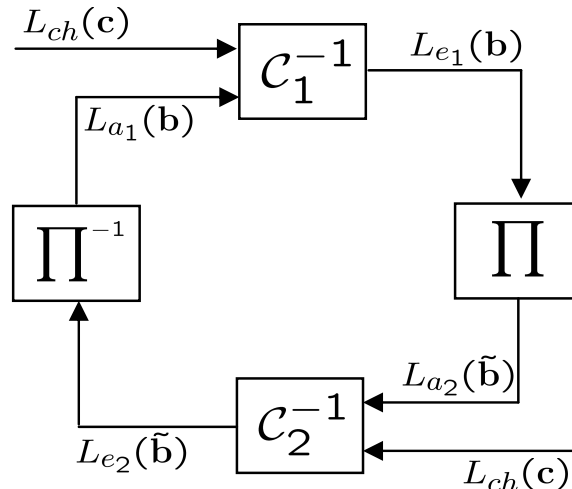


FIGURE 1.6: Iterative decoding of a parallel concatenated convolutional code.

process is usually executed in a sequential manner, and starts arbitrarily with either decoder, C_1^{-1} for example. C_1^{-1} computes the *a posteriori* LLRs $L(\mathbf{b})$ and the extrinsic information $L_{e_1}(\mathbf{b})$. At the first iteration, no *a priori* information $L_{a_1}(\mathbf{b})$ is available. Next, C_2^{-1} is processed. C_2^{-1} is fed by the channel observation from the detector $L_{ch}(\mathbf{c})$ and the *a priori* information $L_{a_2}(\tilde{\mathbf{b}})$ from C_1^{-1} . $L_{a_2}(\tilde{\mathbf{b}})$ is the interleaved version of $L_{e_1}(\mathbf{b})$ and $L_{e_1}(\mathbf{b}) = L(\mathbf{b}) - L_{a_1}(\mathbf{b})$. After C_1^{-1} processing is completed, C_2^{-1} starts processing. In turn, C_2^{-1} computes the *a posteriori* probability $L(\tilde{\mathbf{b}})$ and forwards extrinsic information $L_{e_2}(\tilde{\mathbf{b}}) = L(\tilde{\mathbf{b}}) - L_{a_2}(\tilde{\mathbf{b}})$ to C_1^{-1} . In the next iteration, this extrinsic information is deinterleaved and serves as *a priori* information for C_1^{-1} .

The turbo decoding process is repeated until a fixed maximum number of iterations N_{\max} is reached or an early stopping criterion is fulfilled.

1.5.5 EXtrinsic Information Transfer Charts

The turbo decoding algorithm does not generally converge to a maximum likelihood solution, although it gives good error correction performance in practice. One way to study the convergence behavior of FEC codes is to use EXIT charts, introduced by ten Brink in [tB01]. EXIT chart is a useful technique to describe the flow of extrinsic information between two (or more) constituent decoders. In an EXIT chart, the mutual information at the output of a component decoder is plotted as a function of the information at its input. If two decoders are exchanging messages, the behavior of the iterative process can be plotted in a two-dimensional chart. This chart permits the prediction of the SNR value corresponding to the convergence of the iterative process.

The mutual information between the transmitted bit $b \in \{0, 1\}$ and the channel LLR L_{ch} is computed by [Hag04]

$$I(L_{ch}, b) = 1 - E[\log_2(1 + \exp(-L_{ch}))] \quad (1.40)$$

where E is the mean function. By invoking the ergodicity theorem, the statistical mean can be evaluated by the time average and the mutual information can be then assessed by taking a large number N of samples. Therefore, $I(L_{ch}, b)$ can be computed by

$$I(L_{ch}, b) = 1 - \frac{1}{N} \sum_{n=1}^N \log_2(1 + \exp(-b_n \cdot L_{ch})) \quad (1.41)$$

$$\text{with } b_n = (-1)^b$$

For a component decoder, the information transfer function is measured as

$$I(L_e, b) = T(I(L_a, b)) \quad (1.42)$$

where $I(L_a, b)$ is the mutual information between b and the *a priori* LLR L_a and $I(L_e, b)$ is the mutual information between b and the extrinsic LLR L_e . $I(L_a, b)$ and $I(L_e, b)$ can be computed according to equation (1.41) where the *a priori* LLRs are modeled as independent Gaussian random variables [tB01]. Therefore, the transfer function of each component decoder \mathcal{C}_1^{-1} and \mathcal{C}_2^{-1} can be computed and then plotted in a two-dimensional chart. For decoder \mathcal{C}_1^{-1} , the *a priori* information $I_1(A)$ of the first decoder is plotted on the horizontal axis and its corresponding output extrinsic information $I_1(E)$ is plotted on the vertical axis. For decoder \mathcal{C}_2^{-1} , the *a priori* information $I_2(A)$, which is equal to $I_1(E)$, is plotted on the vertical axis and its output extrinsic $I_2(E)$, which becomes the *a priori* information $I_1(A)$ in the next iteration, is plotted on the horizontal axis. The decoding path is illustrated by stepping the two curves. For a successful decoding, there must be an open tunnel between the curves. The convergence threshold is defined as the minimum E_b/N_0 for which the tunnel begins to open and a clear decoding path is observed between the two curves.

Figure 1.7 plots the EXIT chart of the 8-state double binary turbo code with rate $R_c = 1/2$ combined with a 4-QAM modulation in a Rayleigh fading channel. At $E_b/N_0 = 2.6$ dB, an open tunnel is observed between the two curves, permitting the point (1, 1) to be reached. Therefore, $E_b/N_0 = 2.6$ dB corresponds to the convergence threshold for this turbo code.

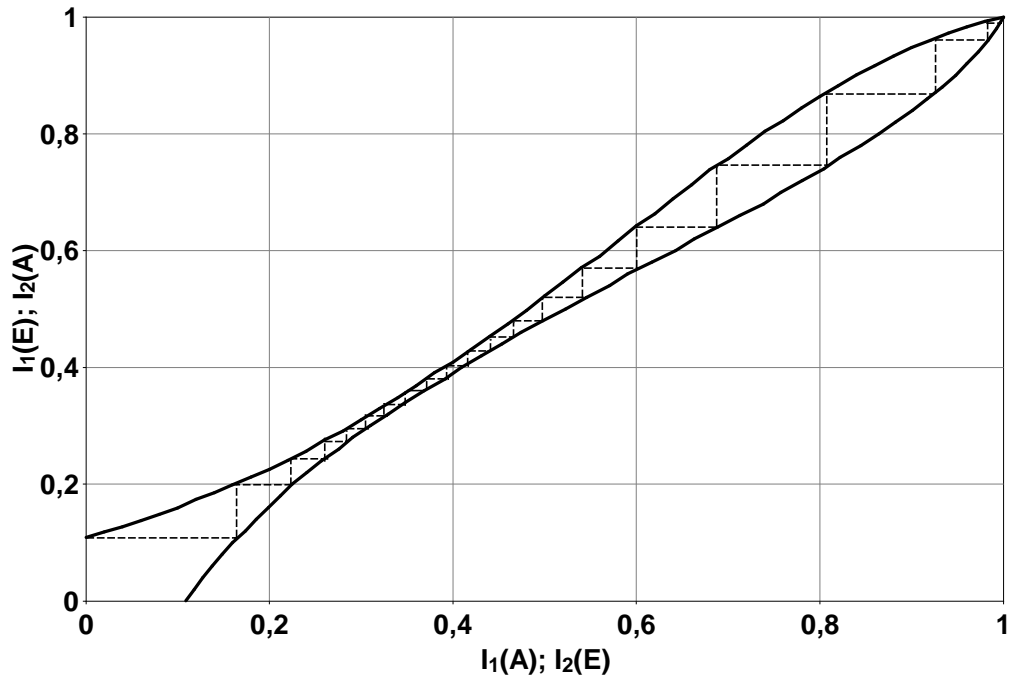


FIGURE 1.7: EXIT chart at $E_b/N_0 = 2.6$ dB of the 8-state double binary turbo code with rate $R_c = 1/2$; 4-QAM modulation; flat Rayleigh fading channel.

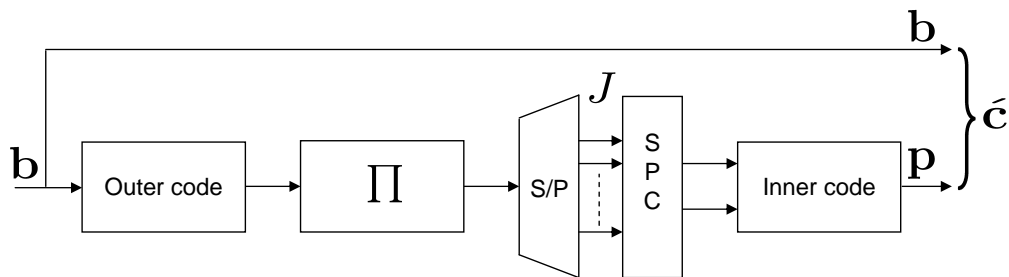


FIGURE 1.8: Structure of the Flexicode encoder.

1.5.6 FlexiCodes

FlexiCodes belong to the family of systematic serially concatenated codes, a new turbo-like introduced in [CTD⁺05]. Flexicodes intend to combine the advantages of both turbo and LDPC codes [CTD⁺05, DHP06]. They provide good performance over a wide range of operational scenarios and are simple to implement. Even for high code rates (> 0.9) and moderate block size ($< 4,096$), they can achieve a BER below 10^{-10} .

The structure of the FlexiCode encoder is depicted in Figure 1.8. The information word \mathbf{b} is first encoded by an outer code with rate $1/Q$. The bits at the output of the outer encoder are then interleaved and grouped into groups of J bits. Each group is passed to a *single parity check* (SPC) code which forms the sum modulo-2 of its J input bits. The bits at the SPC output are then encoded by an inner code with rate $1/L$ to generate parity word \mathbf{p} . FlexiCodes are systematic codes. Therefore the information

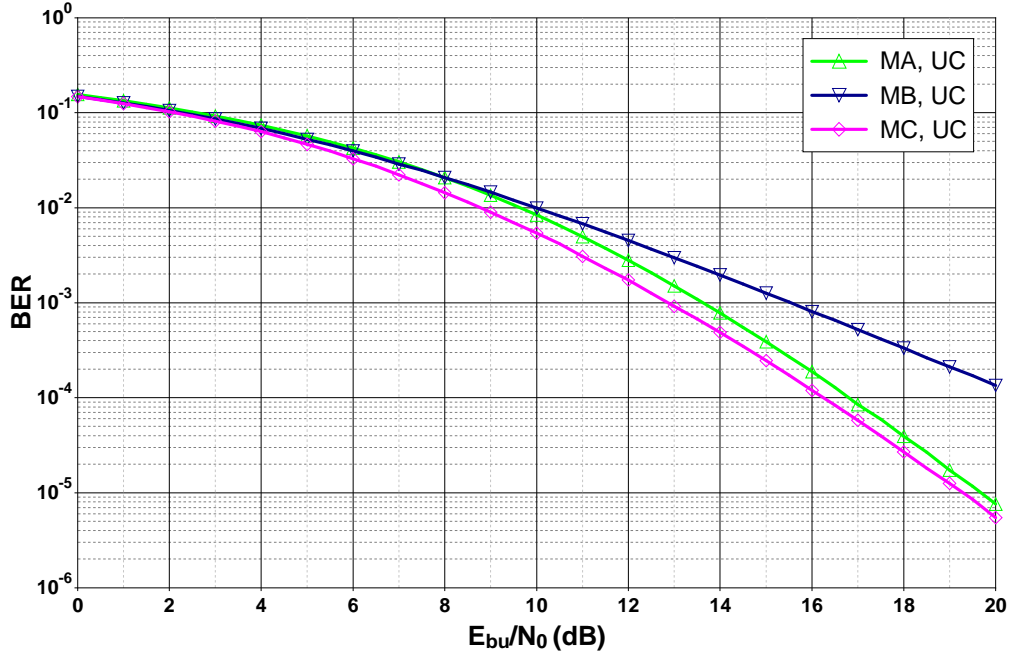


FIGURE 1.9: BER for 2×2 WiMAX MIMO profiles: MA with 16-QAM modulation and MB, MC with 4-QAM modulation; quasi-static flat Rayleigh fading MIMO channel.

word \mathbf{b} is concatenated with the parity word \mathbf{p} to form the codeword \mathbf{c} provided to the BICM interleaver. Thus, the rate of the overall code is:

$$R_c = \frac{J}{J + QL} \quad (1.43)$$

In the simulations of this thesis, we use the RSC $(5; 7)_8$ code with rate $1/2$ as outer code and a rate-1 convolutional encoder *i.e.*, an accumulator as inner encoder, leading to $R_c = J/(J + 2)$. The rate of the FlexiCode and therefore its performance can be controlled by varying parameter J .

1.6 An Example of Coded MIMO System: WiMAX

After having provided a background on MIMO codes and capacity-approaching FEC codes, we consider the 2×2 WiMAX system as an example of coded MIMO systems. We first provide the performance in terms of bit error rate for the uncoded system conventionally presented while classifying MIMO codes. Afterwards, we use the expression “uncoded”, with the understanding that a MIMO coding is used, to refer to the case of a MIMO system without any FEC code. Then, in order to assess the performance of the practical system, we provide the BER for the coded case.

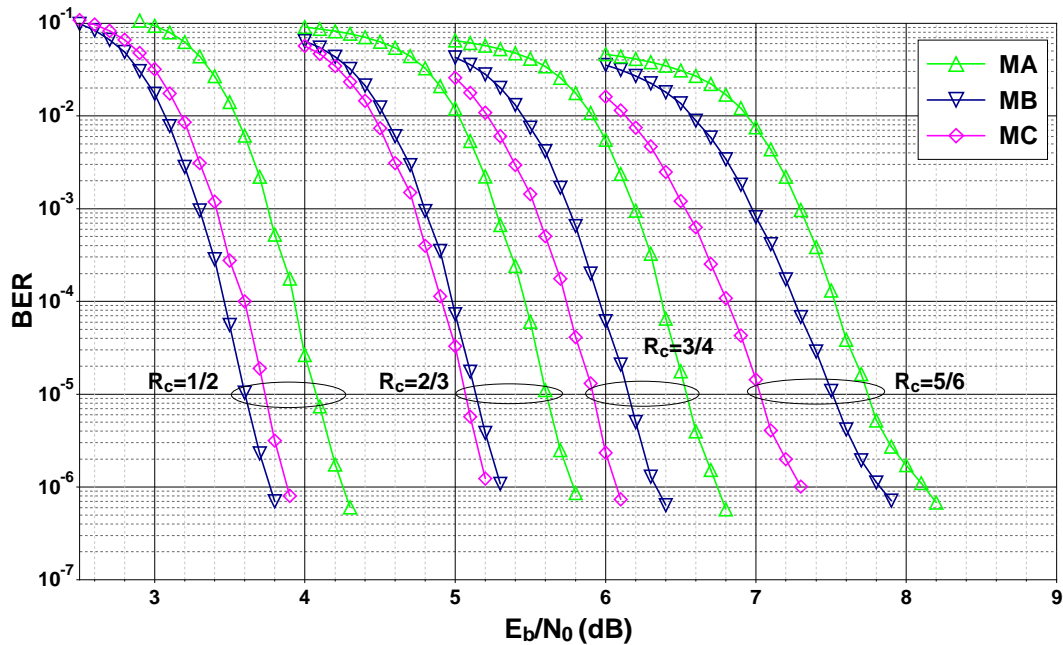


FIGURE 1.10: BER of turbo coded 2×2 WiMAX system; 8-state double binary turbo code ($R_c = 1/2, 2/3, 3/4, 5/6$) with 8 turbo decoding iterations; MIMO profiles: Alamouti code (MA) with 16-QAM and spatial multiplexing (MB), Golden code (MC) with 4-QAM; quasi-static flat Rayleigh fading MIMO channel.

1.6.1 Bit Error Rate of Uncoded Transmission

Figure 1.9 depicts the BER curves of the WiMAX 2×2 profiles over a quasi-static flat Rayleigh fading MIMO channel as a function of E_{bu}/N_0 , where E_{bu} denotes the energy per bit for uncoded MIMO system per receive antenna, and N_0 is the noise power spectral density. As they are referred to in the IEEE 802.16e-2005 standard [IEE06], MA denotes the Alamouti scheme, MB denotes the spatial multiplexing scheme and MC denotes the Golden code. A fair comparison between different profiles should be performed at the same spectral efficiency. Therefore, we use a 16-QAM modulation for the MA scheme and a 4-QAM modulation for the FR profiles.

Obtained results show that the slope of the BER curves are much higher for MA and MC with respect to MB scheme. Hence, these schemes substantially outperform MB at high SNRs. Based on the BER for uncoded transmission or *uncoded BER* (UBER), one can obviously select the MC transmission scheme due to its performance superiority.

1.6.2 Bit Error Rate of Coded Transmission

In order to evaluate the performance for the coded WiMAX system, BER curves have been plotted after 8 turbo decoding iterations for an information frame size equal to 4,800, as a function of E_b/N_0 where E_b is the energy per information bit. A random BICM interleaver is used and the gains are evaluated at a target BER equal to 10^{-5} .

Figure 1.10 shows the BER curves with a 4-QAM modulation for the FR profiles. For $R_c = 1/2$, MB code offers the best performance with a gain of 0.1 dB compared to MC code. From $R_c = 2/3$ to $R_c = 5/6$, the MC code surpasses all the presented codes with a gain increasing with the rate, from 0.05 dB at $R_c = 2/3$ to 0.25 dB at $R_c = 5/6$. The MA scheme always shows the worst performance.

Simulation results show that uncoded BER performance obtained in Section 1.6.1 is insufficient to predict the BER performance of the coded system. A selection of the transmission scheme for practical communication systems based only on UBER can be misleading. Indeed, UBER favors the selection of the MC (Golden code) scheme. However, the use of the MC would:

1. alter the performance of terminals for low coding rate profiles.
2. increase the MIMO detection complexity compared to MA and MB schemes.

Similar conclusions are obtained in [MRLRB07] in the context of the WiFi system based on the IEEE 802.11n standard, in [KSB09] in the context of the WiMAX system and in [MKV⁺12] in the context of the DVB-T2 standard.

Capacity-approaching FEC codes concatenated with MIMO techniques are used in most of the recently developed telecommunication systems *e.g.*, WiMAX, WiFi, LTE, LTE-Advanced and DVB. For these systems, a judicious method providing suitable transmission schemes, in terms of performance and complexity, must be addressed. This statement of fact motivates our work through this thesis.

1.7 Chapter Summary

In this chapter, we provided an introduction to coded MIMO systems. First, we described the considered MIMO system, the wireless channel environment and the system model. Thereafter, we presented a background knowledge about information theory, MIMO coding techniques and capacity-approaching channel coding. As an example of coded MIMO system, we considered the WiMAX system context. Uncoded performance are conventionally used to select the employed MIMO technique for coded MIMO system. However, obtained coded performance show that such a selection criterion is not suitable and may lead to a high complexity scheme with worse performance. In the sequel, an innovative method to select, and if possible design, an appropriate MIMO technique for coded MIMO systems is discussed.

Chapter 2

Improving Standardized STBCs for Coded MIMO Systems: Towards Adaptive STBCs

STBCs are conventionally designed according to the rank-determinant criteria suitable at high SNRs. Moreover, they are usually classified based on uncoded BER performance at high SNRs. The STBC offering the best uncoded BER performance is usually selected for practical communication systems. Recently, several papers have noted that such a selection is misleading and reveals to be insufficient to predict the performance of coded MIMO systems [MRLRB07, KSB09, LJ10, MKV⁺12, MRLB12]. Indeed, in Chapter 1, we have shown that the range of low to moderate SNRs should be targeted for the design of STBCs when a capacity-approaching FEC is used in the communication chain. In this chapter, we investigate the improvement of standardized STBCs for coded MIMO systems. Practical communication systems promote the usage of a low complexity receiver. Indeed, the receiver is implemented in the user terminal whose size and price should be kept reasonable.

Section 2.1 starts with the presentation of a low ML-detection complexity STBC called Matrix D [SS07, SSB⁺08]. Then we incorporate this structure into coded MIMO systems. In order to fully benefit from the power of capacity-approaching FEC codes, the FEC decoder requires soft decisions on transmitted bits on its input. Since the original detector for MD STBC provides hard decisions on received bits, we propose a soft detector for the MD STBC with the same complexity order as the original one. The low complexity detector is shown to be efficient even when the link between one or more antennas is lost or erased. Afterwards, in Section 2.2, we optimize the MD STBC according to the trace criterion [TC01, CYV01], instead of the determinant criterion. The trace criterion is efficient in the low SNRs region and therefore more appropriate for coded MIMO systems. Based on the MD STBC structure, we propose a new full-rate

full-diversity STBC with low ML-detection complexity and we show that it overcomes the original one in the context of WiMAX. In Section 2.3, we assess the computational complexity of MIMO detection and FEC decoding in a WiMAX receiver with different MIMO profiles.

Afterwards, we investigate the design of STBC codes for a large range of SNR. In Section 2.4, we propose a SNR-dependent STBC design criterion based on the *bitwise mutual information* (BMI) optimization between transmitted and soft detected bits at a specific target SNR. In Section 2.5, after the criterion validation, we optimize several standardized STBCs according to the BMI criterion. Their design parameters are SNR-dependent which leads to the proposal of *adaptive STBCs*. Adaptive Matrix D STBC overcomes or matches the original one for a wide range of SNRs. Furthermore, based on the trace-orthonormal STBC structure described in [ZLW07], we propose an adaptive trace-orthonormal STBC. The simulation results presented in Section 2.6 in the context of a WiMAX system and in Section 2.7 with a FlexiCode FEC code show that the adaptive trace-orthonormal STBC overcomes or matches conventional STBCs for all coding rates.

2.1 Matrix D Space-Time Block Code

In [SS07, SSB⁺08], the decoder complexity issue is included in the design criteria leading to the proposal of the MD STBC. In this section, we present the original hard detector for the MD STBC. Afterwards, we propose a soft detector for the Matrix D STBC with the same complexity order as the hard detector.

2.1.1 Original Low Complexity Detector

The original low complexity detector for the MD STBC proposed by Sezginer and Sari in [SS07] aims at providing the ML-detection on transmitted symbols with a reduced complexity. By transmitting a group of four data symbols (x_1, x_2, x_3, x_4) encoded according to the MD structure, the two signals received at the first and second channel use periods on the first receive antenna, are

$$r_1 = h_{11}(ax_1 + bx_3) + h_{12}(ax_2 + bx_4) + n_1, \quad (2.1a)$$

$$r_2 = h_{11}(-cx_2^* - dx_4^*) + h_{12}(cx_1^* + bx_3^*) + n_2, \quad (2.1b)$$

Similar expressions hold for the second receive antenna:

$$r_3 = h_{21}(ax_1 + bx_3) + h_{22}(ax_2 + bx_4) + n_3, \quad (2.2a)$$

$$r_4 = h_{21}(-cx_2^* - dx_4^*) + h_{22}(cx_1^* + bx_3^*) + n_4, \quad (2.2b)$$

where n_i , $i = 1, \dots, 4$, are additive noise terms.

A classical ML-detector makes an exhaustive search over all possible M^4 quadruplets (see section 1.4.3.1), whereas the MD STBC is designed in a special way permitting a low complexity implementation of the ML-detector [SS07]. From the received signals (r_1, r_2, r_3, r_4) , we compute for each pair (S_3, S_4)

$$w_1 = r_1 - b(h_{11}S_3 + h_{12}S_4), \quad (2.3a)$$

$$w_2 = r_2 - d(h_{12}S_3^* - h_{11}S_4^*), \quad (2.3b)$$

$$w_3 = r_3 - b(h_{21}S_3 + h_{22}S_4), \quad (2.3c)$$

$$w_4 = r_4 - d(h_{22}S_3^* - h_{21}S_4^*). \quad (2.3d)$$

Next, from (w_1, w_2, w_3, w_4) , we compute signals $h_{11}^*w_1$, $h_{12}w_2^*$, $h_{21}^*w_3$, $h_{22}w_4^*$. Then from these signals, we compute y_1 given by

$$y_1 = (h_{11}^*w_1 + h_{21}^*w_3)/a + (h_{12}w_2^* + h_{22}w_4^*)/c^*. \quad (2.4)$$

When $(S_3, S_4) = (x_3, x_4)$

$$y_1 = \alpha x_1 + \eta_1, \quad (2.5)$$

where $\alpha = (|h_{11}|^2 + |h_{12}|^2 + |h_{21}|^2 + |h_{22}|^2)$ and $\eta_1 = \frac{(h_{11}^*n_1 + h_{21}^*n_3)}{a} + \frac{(h_{12}n_2^* + h_{22}n_4^*)}{c^*}$.

Since y_1 has no term involving symbol x_2 , the ML-estimation of x_1 conditionally to (S_3, S_4) is obtained.

Similarly, after the computation of intermediate signals $h_{12}^*w_1$, $h_{11}w_2^*$, $h_{22}^*w_3$, $h_{21}w_4^*$, we have

$$y_2 = (h_{12}^*w_1 + h_{22}^*w_3)/a - (h_{11}w_2^* + h_{21}w_4^*)/c^*. \quad (2.6)$$

When $(S_3, S_4) = (x_3, x_4)$

$$y_2 = \alpha x_2 + \eta_2, \quad (2.7)$$

where $\eta_2 = (h_{12}^*n_1 + h_{22}^*n_3)/a - (h_{11}n_2^* + h_{21}n_4^*)/c^*$.

By sending signals y_1 and y_2 to a threshold detector, we get the ML-estimate of x_1 and x_2 conditionally to S_3 and S_4 , which we denote by $(S_1^{\text{ML}}, S_2^{\text{ML}}, S_3, S_4)$. α involves all the available channel coefficients and its expression shows that the estimates of transmitted symbols benefit from the 4-th order of spatial diversity. Instead of computing metric $D(S_1, S_2, S_3, S_4)$ for all (S_1, S_2, S_3, S_4) , we only need to compute it for $(S_1^{\text{ML}}, S_2^{\text{ML}}, S_3, S_4)$, with (S_3, S_4) spanning the constellation. In this way, the number of computed distances decreases from M^4 to M^2 and then the ML-detector complexity order is decreased from $\mathcal{O}(M^4)$ to $\mathcal{O}(M^2)$ [SS07]. More precisely, the ML-estimate of x_1 and x_2 , based on signals y_1 and y_2 , is done independently for each pair (S_3, S_4) and the ML-detection complexity order is therefore $\mathcal{O}(M^3)$. This complexity can be further

reduced to $\mathcal{O}(M^2\sqrt{M})$ for square QAM modulations *i.e.*, 4-QAM, 16-QAM, 64-QAM, etc., by detecting *separately* real and imaginary parts for some symbols [SR08].

2.1.2 Soft Detection for MD STBC

2.1.2.1 Original Detector Impairments

The low complexity detector presented in Section 2.1.1 provides, by its construction, the same hard decisions on transmitted symbols x_1 , x_2 , x_3 and x_4 as the classical ML-detector. In order to fully benefit from the power of capacity-approaching FEC codes, the FEC decoder requires soft decisions on transmitted bits. The probability $\hat{c}_i = P(c_i = 1)$ that the coded bit of index i is equal to 1 is computed as (see Section 1.5)

$$\hat{c}_i = \frac{\sum_{\mathbf{S} \in \chi_1^i} P(\mathbf{Y}|\mathbf{S})}{\sum_{\mathbf{S} \in \chi_1^i} P(\mathbf{Y}|\mathbf{S}) + \sum_{\mathbf{S} \in \chi_0^i} P(\mathbf{Y}|\mathbf{S})}, \quad (2.8)$$

where χ_0^i (resp. χ_1^i) is the set of transmitted matrices \mathbf{S} having bit c_i equal to 0 (resp. 1) and $P(\mathbf{Y}|\mathbf{S})$ is the likelihood function expressed as

$$\begin{aligned} P(\mathbf{Y}|\mathbf{S}) &\propto \exp\left(\frac{-\|\mathbf{Y} - \mathbf{H}\mathbf{S}\|_F^2}{\sigma^2}\right) \\ &= \exp\left(\frac{-D(S_1, S_2, S_3, S_4)}{\sigma^2}\right) \end{aligned} \quad (2.9)$$

In order to compute the soft estimate \hat{c}_i of each bit carried by x_3 and x_4 , a first solution involves using available distances $D(S_1^{\text{ML}}, S_2^{\text{ML}}, S_3, S_4)$. Simulations verify that soft estimates for x_3 and x_4 bits are very close to the ones obtained with classical soft ML-detection of complexity $\mathcal{O}(M^4)$, since (S_3, S_4) spans all the constellation. On the other hand, due to the low complexity detection, we have only the distances $y_1 - \alpha S_1$ and $y_2 - \alpha S_2$ to compute the estimates of the bits carried by x_1 and x_2 . This leads to less reliable soft estimates for these bits and to a performance loss when the MD STBC is concatenated with a capacity-approaching FEC code.

2.1.2.2 Proposed Soft Detector for MD STBC

Fortunately, the MD structure allows the low complexity ML-detector to work symmetrically *i.e.*, detect S_3 (or S_4) conditionally to S_1 and S_2 . Thus, to perform the soft detection on x_1 and x_2 bits, we propose to reuse the same approach used for the bits of symbols x_3 and x_4 . Then, the ML-detection complexity remains at the same order as the original detector since the exhaustive search is done only on two symbols.

The low complexity detection can be done *independently* for the bits of (x_1, x_2) and (x_3, x_4) . Indeed, taking S_i and S_j spanning the transmitted constellation, the ML-estimation of x_1 and x_2 conditionally to (S_3, S_4) is computed by

$$w_1 = r_1 - b(h_{11}S_i + h_{12}S_j), \quad (2.10a)$$

$$w_2 = r_2 - d(h_{12}S_i^* - h_{11}S_j^*), \quad (2.10b)$$

$$w_3 = r_3 - b(h_{21}S_i + h_{22}S_j), \quad (2.10c)$$

$$w_4 = r_4 - d(h_{22}S_i^* - h_{21}S_j^*). \quad (2.10d)$$

After the computation of these intermediate signals, we obtain the soft detection for bits of x_3 and x_4 as in Section 2.1.2.

Furthermore, the detection of x_3 and x_4 conditionally to (S_1, S_2) is done by

$$\tilde{w}_1 = r_1 - a(h_{11}S_i + h_{12}S_j), \quad (2.11a)$$

$$\tilde{w}_2 = r_1 - c(h_{12}S_i^* - h_{11}S_j^*), \quad (2.11b)$$

$$\tilde{w}_3 = r_3 - a(h_{21}S_i + h_{22}S_j), \quad (2.11c)$$

$$\tilde{w}_4 = r_4 - c(h_{22}S_i^* - h_{21}S_j^*). \quad (2.11d)$$

Similarly, from signals $\tilde{w}_1, \tilde{w}_2, \tilde{w}_3, \tilde{w}_4$, we compute the intermediate signals $h_{11}^* \tilde{w}_1, h_{12} \tilde{w}_2^*, h_{21}^* \tilde{w}_3, h_{22} \tilde{w}_4^*$. From these signals, we compute y_3

$$y_3 = (h_{11}^* \tilde{w}_1 + h_{21}^* \tilde{w}_3) / b + (h_{12} \tilde{w}_2^* + h_{22} \tilde{w}_4^*) / d^*. \quad (2.12)$$

When $(S_i, S_j) = (x_1, x_2)$

$$y_3 = \alpha x_3 + \eta_3, \quad (2.13)$$

where $\eta_3 = (h_{11}^* n_1 + h_{21}^* n_3) / b + (h_{12} n_2^* + h_{22} n_4^*) / d^*$.

Next, after the computation of the intermediate signals $h_{12}^* \tilde{w}_1, h_{11} \tilde{w}_2^*, h_{22}^* \tilde{w}_3, h_{21} \tilde{w}_4^*$, we evaluate

$$y_4 = (h_{12}^* \tilde{w}_1 + h_{22}^* \tilde{w}_3) / b - (h_{11} \tilde{w}_2^* + h_{21} \tilde{w}_4^*) / d^*. \quad (2.14)$$

When $(S_i, S_j) = (x_1, x_2)$

$$y_4 = \alpha x_4 + \eta_4, \quad (2.15)$$

where $\eta_4 = (h_{12}^* n_1 + h_{22}^* n_3) / b - (h_{11} n_2^* + h_{21} n_4^*) / d^*$.

Now, we have all the required distances to compute the soft estimate \hat{c}_i for the bits of x_1 and x_2 . Thus, the low complexity soft detection is done for all transmitted bits. The complexity of the proposed detector is still on the same order as the original detector since the pair (S_i, S_j) takes the constellation spanning role for (S_1, S_2) and (S_3, S_4) simultaneously. Only the number of computed intermediate signals is doubled. After

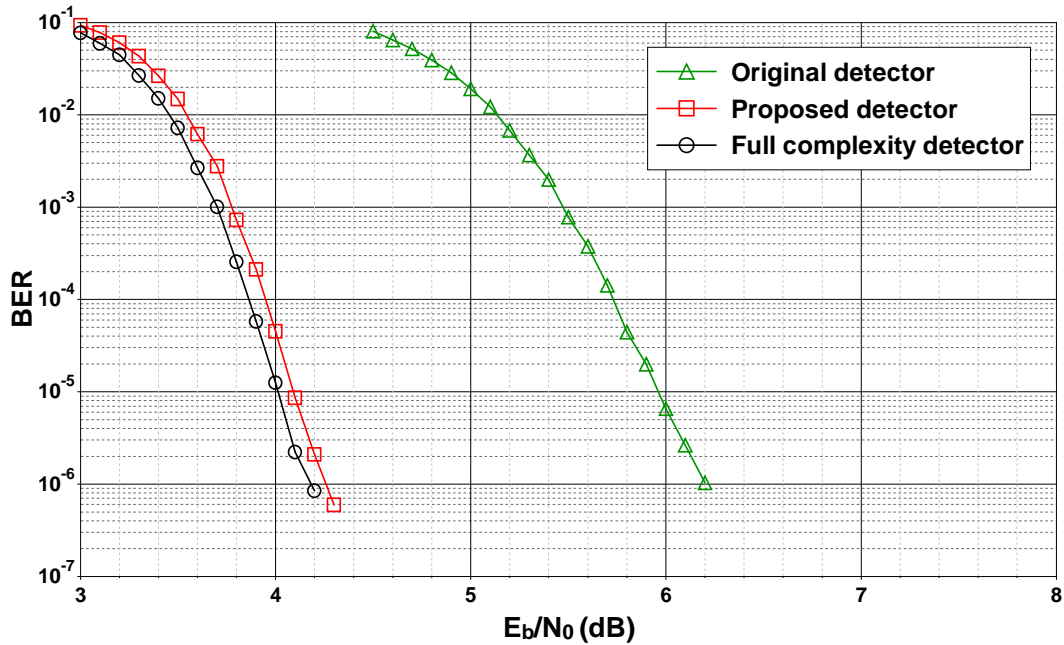


FIGURE 2.1: BER for the concatenation of the WiMAX 8-state double binary turbo code ($R_c = 1/2$, $k = 4,800$) and the MD STBC detected with: original, proposed and full complexity soft detectors; 4-QAM modulation; quasi-static flat Rayleigh fading MIMO channel.

the proposal of the soft detector for the MD STBC, we found that a hint on the used method was given in [SSB09]. However, [SSB09] has not considered a coded MIMO transmission using the MD STBC.

2.1.2.3 Comparison Between Detectors

Figure 2.1 plots the BER as a function of E_b/N_0 of the WiMAX 8-state double binary turbo code at rate $R_c = 1/2$, concatenated with the MD STBC and soft detected with the original, the proposed and the full complexity ML-detectors. The number of turbo decoding iterations is equal to 8. The transmission is done over a quasi-static flat Rayleigh fading MIMO channel. An information frame size of 4,800 bits and a 4-QAM modulation are considered. At a BER equal to 10^{-5} , a gain of 1.9 dB is obtained using the proposed detector with respect to the original one while a small loss of 0.1 dB is observed with respect to the full complexity detector. Due to its good performance and low complexity, the proposed detector is used in our work while simulating the MD STBC.

2.1.3 Robustness of the Detector with respect to Erasure Events

In some cases, the link between one transmit and one receive antenna might be erased. Without loss of generality, we assume that we lose the link between the first transmit and the first receive antenna *i.e.*, $h_{11} = 0$. By proceeding in the same manner as in

Section 2.1.1, we obtain

$$y_1 = \alpha^{\text{Er}} x_1 + \eta_1^{\text{Er}}, \quad (2.16a)$$

$$y_2 = \alpha^{\text{Er}} x_2 + \eta_2^{\text{Er}}, \quad (2.16b)$$

where $\alpha^{\text{Er}} = (|h_{12}|^2 + |h_{21}|^2 + |h_{22}|^2)$, $\eta_1^{\text{Er}} = (h_{21}^* n_3) / a + (h_{12} n_2^* + h_{22} n_4^*) / c^*$ and $\eta_2^{\text{Er}} = (h_{12}^* n_1 + h_{22}^* n_3) / a - (h_{21} n_4^*) / c^*$.

The expression α^{Er} obviously shows that the estimates of symbols x_1 and x_2 benefits from all the remaining spatial diversity.

Similarly, the low complexity ML-detection remains valid when more than one transmit or receive antennas are erased. Transmitted symbols always benefit from all the remaining spatial diversity.

For deep erasure events, FR-FD STBCs are more advantageous than spatial multiplexing schemes as the same information is transmitted several times over different paths and it could be recovered thanks to surviving paths. In contrast, the transmitted information following the spatial multiplexing scheme is totally lost during an erasure event. However, in a coded system, a part of this information can be recovered thanks to the correction power of employed capacity-approaching FEC codes especially at low coding rates.

2.2 Matrix D STBC for Coded MIMO Communication Systems

The MD STBC has been optimized according to the rank-determinant criteria [SS07] efficient at high SNRs. In the sequel, we investigate the optimization of the MD STBC in the range of low SNRs, more appropriate for coded MIMO systems.

2.2.1 Trace Criterion

As a substitute for the determinant criterion, authors in [TC01, CYV01] proposed the trace criterion to design space-time codes in the range of low SNRs. This criterion is based on the minimization of the upper bound for the PEP at low SNRs.

Trace Criterion The minimum trace of the matrix $\mathbf{\Delta} = (\mathbf{X} - \hat{\mathbf{X}})^H (\mathbf{X} - \hat{\mathbf{X}})$ is defined as

$$\xi = \min_{\mathbf{X} \neq \hat{\mathbf{X}}} \sum_{i=1}^r \lambda_i \quad (2.17)$$

where $\lambda_i; i = 1, \dots, r$ are the nonzero eigenvalues of matrix $\mathbf{\Delta}$. The minimum trace ξ must be maximized for all possible transmitted codeword pairs $(\mathbf{X}, \hat{\mathbf{X}})$. It is to noted that

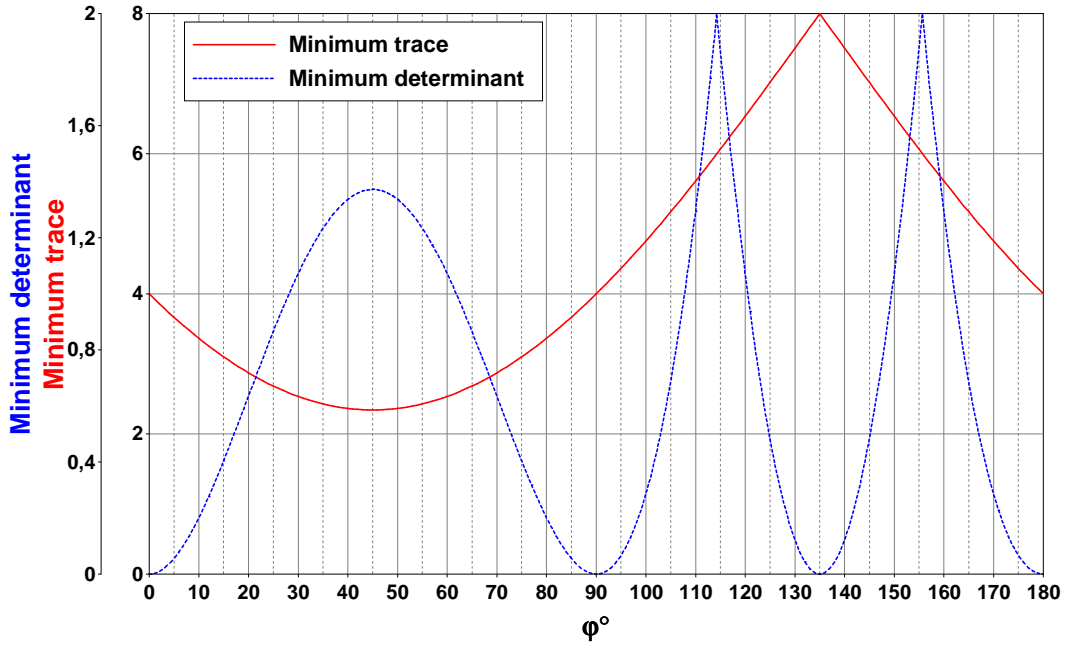


FIGURE 2.2: Minimum trace and minimum determinant of the MD STBC as a function of its design parameter φ ; 4-QAM modulation.

the minimum trace represents the minimum Euclidean distance between two space-time codewords.

2.2.2 MD STBC Optimization according to the Trace Criterion

In this section, the optimization of the MD STBC is done according to the trace design criterion instead of the classical determinant criterion. As in [SS07], an exhaustive search is done on the design parameter φ and the one maximizing the minimum trace is selected.

Figure 2.2 plots the minimum trace and the minimum determinant of the MD code as a function of φ for a 4-QAM modulation. It shows that the angle which maximizes the minimum trace is equal to $\varphi^{\text{Trace}} = 135^\circ$. The same angle is obtained for higher modulation order *i.e.*, 16-QAM, 64-QAM, etc. On the other hand, Figure 2.2 shows that $\varphi^{\text{Determinant}} = \arg(b) = \arg([(1 - \sqrt{7}) + j(1 + \sqrt{7})] / (4\sqrt{2})) \approx 114.29^\circ$ provides the highest minimum determinant [SS07]. Two different φ are obtained according to the trace criterion and the determinant criterion.

Unfortunately, the minimum determinant at $\varphi^{\text{Trace}} = 135^\circ$ is equal to 0 for many pairs $(\mathbf{X}, \hat{\mathbf{X}})$. Hence the matrix $\mathbf{\Delta} = (\mathbf{X} - \hat{\mathbf{X}})^H(\mathbf{X} - \hat{\mathbf{X}})$ is no longer full-rank *i.e.*, $r < N_t$ and the MD STBC loses its full-diversity property as $d = rN_r < N_tN_r$.

The full-diversity property guarantees a good behavior at high SNRs. In order to maintain the full-diversity property for the MD STBC, the minimum determinant should be different from 0. A tradeoff angle φ such that $\varphi^{\text{Determinant}} \leq \varphi \leq \varphi^{\text{Trace}}$ can be

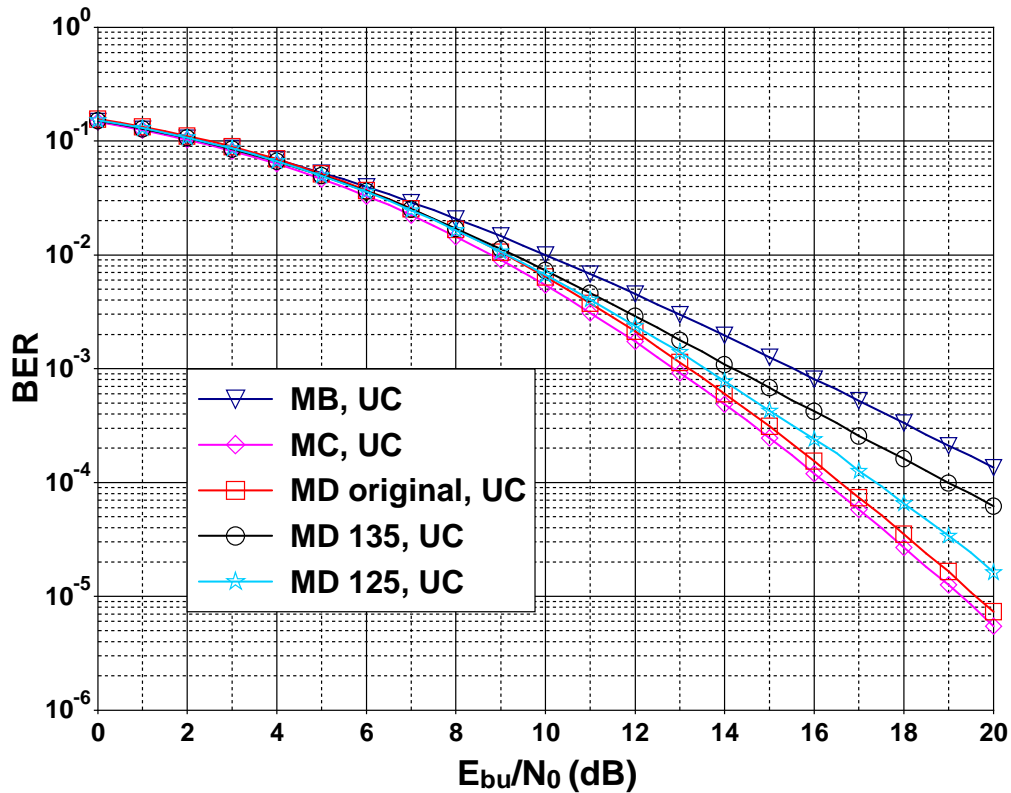


FIGURE 2.3: BER for the uncoded (UC) system (only MIMO system); MIMO profiles: Spatial multiplexing (MB), Golden code (MC), original MD [SS07], MD($\varphi = 135^\circ$) and MD($\varphi = 125^\circ$); 4-QAM modulation; quasi-static flat Rayleigh fading MIMO channel.

selected. Such a tradeoff aims to design a FR-FD STBC with low complexity detection, that performs well for a wide range of SNRs. As an example, we take the tradeoff angle $\varphi = 125^\circ$.

2.2.3 Performance Evaluation

In this section, we assess both uncoded and coded BER for the proposed MD codes and compare them with WiMAX MIMO profiles. We recall that the detection of MD codes is done using the proposed low complexity detector (see Section 2.1.2.2).

2.2.3.1 BER Curves of the Uncoded MIMO System

In order to validate the behavior of the proposed MD codes for high E_{bu}/N_0 , uncoded MIMO system is simulated. BER curves are plotted in Figure 2.3 for the spatial multiplexing (MB) code, the Golden code (MC), the original MD [SS07], the proposed MD($\varphi = 135^\circ$) and MD($\varphi = 125^\circ$) MIMO codes with 4-QAM modulation. It shows that the MD($\varphi = 135^\circ$) STBC loses its full-diversity property as the slope of its UBER curve is equal to the one of the MB code. Besides, the tradeoff MD($\varphi = 125^\circ$) maintains the full-diversity property as its UBER curve slope is equal to the one of the original

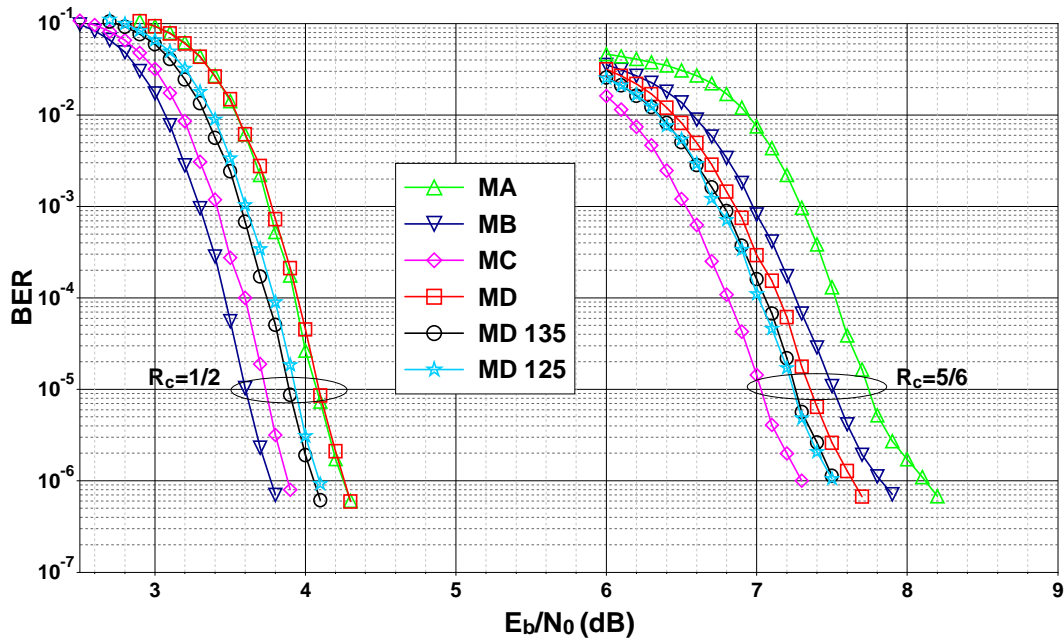


FIGURE 2.4: BER of turbo coded system; 8-state double binary turbo code ($R_c = 1/2$, $5/6$) with 8 turbo decoding iterations; MIMO profiles: Alamouti code (MA) with 16-QAM modulation and spatial multiplexing (MB), Golden code (MC), original MD [SS07], MD($\varphi = 135^\circ$) and MD($\varphi = 125^\circ$) with 4-QAM modulation; quasi-static flat Rayleigh fading MIMO channel.

MD STBC. However, since it is designed to be suitable for the range of low SNRs, a loss in MIMO coding gain is obtained with respect to original MD.

2.2.3.2 BER Curves of the Coded MIMO System

Figure 2.4 plots the BER as a function of E_b/N_0 for the coded WiMAX MIMO profiles *i.e.*, the Alamouti code (MA), the spatial multiplexing (MB), the Golden code (MC) and the low detection complexity MD-based codes: original MD [SS07], MD($\varphi = 135^\circ$) and MD($\varphi = 125^\circ$) STBCs concatenated with the 8-state double binary turbo code at coding rates $R_c = 1/2$ and $R_c = 5/6$. The frame size k is equal to 4,800 bits. The considered MIMO channel is a quasi-static flat Rayleigh fading channel ($T = 2$) with $N_t = 2$ transmit antennas and $N_r = 2$ receive antennas. A BER value equal to 10^{-5} is targeted.

At coding rate $R_c = 1/2$, a gain of 0.2 dB is obtained with the MD STBC optimized for low SNR *i.e.*, MD($\varphi = 135^\circ$) with respect to original MD. A slight loss is obtained with the tradeoff code MD($\varphi = 125^\circ$). Proposed MD codes outperform the original MD code and closes the gap to the MC code from 0.35 dB to 0.15 dB. The spatial multiplexing scheme surpasses the proposed MD codes with a gain of 0.3 dB.

At higher coding rate $R_c = 5/6$, a gain of 0.1 dB is obtained with proposed MD codes with respect to original MD. Indeed, when the coding rate increases, the turbo code

achieves its iterative convergence at higher SNRs where the original MD is optimized. The tradeoff code MD($\varphi = 125^\circ$) is slightly better than the MD($\varphi = 135^\circ$) optimized according to the trace criterion. The proposed MD codes outperforms the spatial multiplexing scheme with a gain of 0.25 dB while a loss of 0.2 dB is obtained with respect to the MC code.

Despite this slight loss of the tradeoff MD($\varphi = 125^\circ$) with respect to MD($\varphi = 135^\circ$) at low coding rates, the FR-FD version of the MD code or MD($\varphi = 125^\circ$) is favored for coded MIMO systems:

1. with capacity-approaching FEC codes operating at high coding rates,
2. without power control like broadcast systems.

Indeed, the MD($\varphi = 125^\circ$) works well regardless the radio conditions undergone by the terminals as it has a good performance for both low and high SNR. On the contrary, the use of the MD($\varphi = 135^\circ$) can alter the performance of terminals that are in good radio conditions.

The proposed soft detector and the optimization of the MD STBC according to the trace criterion have been published in [EALD11].

2.2.3.3 Erasure Effects on the BER of the Coded MIMO System

Throughout the communication, the link between one or more transmit/receive antennas might be lost. This phenomenon is modeled by the erasure of the channel coefficient between concerned antennas, $h_{ij} = 0$. MIMO codes spreading the transmitted information on more than one antenna and one channel use period are known to be more resistant against erasure events with respect to the spatial multiplexing scheme. For a coded MIMO system, a capacity-approaching FEC code tries to recover the transmitted information word based on detected bits where erased bits are considered as equiprobable such that $\hat{c}_i = \Pr(c_i = 1) = 0.5$.

Figure 2.5 plots the BER as a function of E_b/N_0 for the coded WiMAX MIMO profiles and the low complexity MD-based codes at a coding rate $R_c = 5/6$ with an erasure probability equal to 0.2 *i.e.*, a channel coefficient is erased ($h_{ij} = 0$) 20% of the transmission time. The comparison with Figure 2.4 shows the effect of erasures on the transmission. At a target BER = 10^{-5} , a loss of 1.6 dB is observed for the MC code, 1.8 dB for the MD-based codes, 0.8 dB for the MA code and a loss of 2.6 dB is obtained for the MB code. Indeed, the Alamouti code (MA) is more resistant against erasure events as transmitted symbols are sent twice on both antennas. On the contrary, transmitted symbols are lost during erasure events when the spatial multiplexing (MB) scheme is used. Nevertheless, the proposed MD($\varphi = 125^\circ$) code remains better than the original MD and MD($\varphi = 135^\circ$) STBCs.

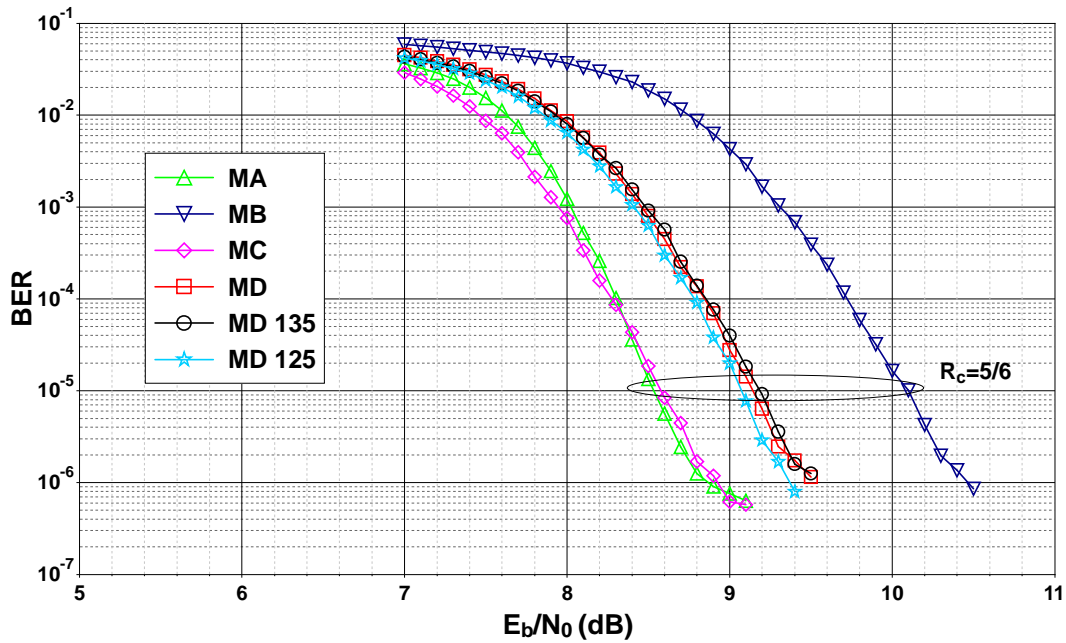


FIGURE 2.5: BER of turbo coded system; 8-state double binary turbo code ($R_c = 5/6$) with 8 turbo decoding iterations; MIMO profiles: Alamouti code (MA) with 16-QAM modulation and spatial multiplexing (MB), Golden code (MC), original MD [SS07], MD($\varphi = 135^\circ$) and MD($\varphi = 125^\circ$) with 4-QAM modulation; quasi-static flat Rayleigh fading erased MIMO channel with erasure probability = 0.2.

2.3 On the Complexity of the WiMAX Receiver

After the assessment of the performance for coded WiMAX MIMO profiles, a comparison of the receiver complexity between the WiMAX MIMO profiles shall be done. This comparison is assessed by evaluating the ML-detector and the FEC decoder complexities in terms of floating point (FP) additions and multiplications.

2.3.1 ML-Detection Complexity Assessment

The ML-detection complexity of STBCs is conventionally assessed by: the order of the number of computed distances required to detect a transmitted STBC [SR08]. FEC decoding needs the probability on coded bits \hat{c} at its input. Then, a deeper complexity study should take into account the number of required multiplications and additions per computed $P(c_i = 1)$. Table 2.1 provides the ML-detection complexity required for soft-decoding one bit (of the coded frame) at the output of the MIMO detector, in terms of number of FP additions and multiplications. The proposed soft detector in Section 2.1.2.2 is considered in the complexity assessment of the MD STBC. For square QAM, this complexity can be further reduced, as in [SR08], for all the presented codes by decoding independently real and imaginary parts of the complex symbols.

MIMO profiles	FP additions	FP multiplications
MA / Alamouti	$\frac{16M+M\log_2(M)+11}{\log_2(M)}$	$\frac{24M+\log_2(M)+8}{\log_2(M)}$
MB / SM	$\frac{38M^2+4N_tM\log_2(M)}{2N_t\log_2(M)}$	$\frac{40M^2+2N_t\log_2(M)}{2N_t\log_2(M)}$
MD [EALD11]	$\frac{4M^3+190M^2+4N_tM\log_2(M)+11}{2N_t\log_2(M)}$	$\frac{M^3+250M^2+2N_t\log_2(M)+8}{2N_t\log_2(M)}$
MC / GC	$\frac{36M^4+8N_tM\log_2(M)+2}{2N_t\log_2(M)}$	$\frac{40M^4+8N_t\log_2(M)+3}{2N_t\log_2(M)}$

TABLE 2.1: ML-detection complexity per coded bit of 2×2 WiMAX MIMO profiles in terms of floating point additions and multiplications.

2.3.2 Turbo Decoding Complexity Assessment

As done in [KDK10, Kba11] for the binary turbo code, the Max-Log-MAP based turbo decoding requires N_{symb} floating point additions for the processing of a turbo code information symbol per iteration, given by

$$N_{\text{symb}} = 3 \times 2^{\nu+p} + 5 \times 2^p + 2^{t+2} - 9 \quad (2.18)$$

where ν denotes the code memory, p is the number of information bits per turbo code information symbol and t is the number of coded bits provided by the encoder at each trellis stage. We obtain $N_{\text{symb}} = 171$ for the 8-state double binary turbo code ($\nu = 3$, $p = 2$, $t = 4$).

The number of turbo decoding iterations is usually fixed to a constant value equal to N_{max} . In contrast, in order to accurately assess the receiver complexity, we assume that the turbo decoder stops performing iterations when the frame is correctly decoded or the maximal number of iterations N_{max} is reached. The correct decoding of the frame can be detected based on a simple cyclic redundancy check (CRC) code added to the frame [Wic95, SSCL01].

Therefore, the number of FP additions per information bit is assessed by

$$\frac{\bar{N} \cdot N_{\text{symb}}}{p} \quad (2.19)$$

where \bar{N} is the average number of turbo decoding iterations required to correctly decode a received frame. \bar{N} is computed by

$$\bar{N} = \frac{\sum_{w=1}^W n_w}{W} \quad (2.20)$$

where W is the number of simulated frames, $n_w \leq N_{\text{max}}$ is the number of iterations per frame w required for correct decoding and N_{max} is the maximum number of turbo decoding iterations.

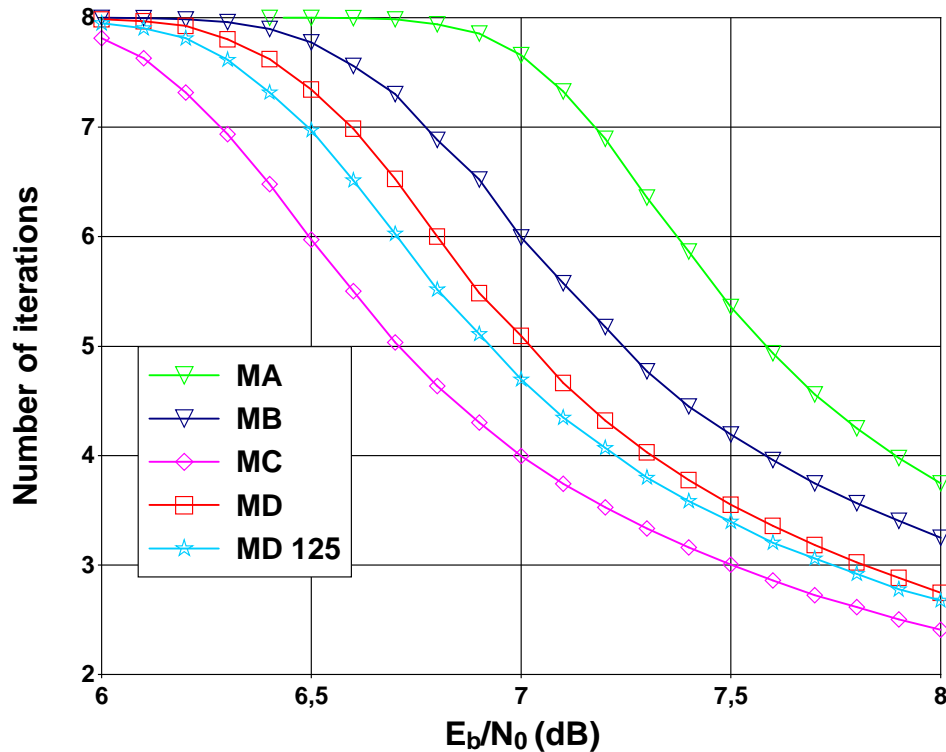


FIGURE 2.6: Average number of turbo decoding iterations per frame \bar{N} for $R_c = 5/6$; MIMO profiles: Alamouti code (MA) with 16-QAM modulation and spatial multiplexing (MB), Golden code (MC), original MD [SS07] and MD($\varphi = 125^\circ$) with 4-QAM modulation; $N_{\max} = 8$ decoding iterations.

The overall complexity per information bit is computed by adding the ML-detection detection complexity per coded bit, divided by the code rate R_c , to the FEC decoding complexity per information bit.

2.3.3 WiMAX Receiver Complexity Assessment

Figure 2.6 plots \bar{N} as a function of E_b/N_0 at $R_c = 5/6$ for presented MIMO profiles with a maximum number of turbo decoding iterations N_{\max} equal to 8. For each frame w , the turbo decoder performs n_w decoding iterations where $n_w \leq N_{\max}$. Indeed, the turbo decoder stops performing iterations when the frame is correctly decoded or the number of decoding iterations reaches N_{\max} . Figure 2.6 shows that the difference between the MC code and the proposed MD-based code is less than one iteration, *i.e.*, less than 85.5 additional additions per information bit whereas the original MD code needs one more iteration with respect to the MC code. The MB code needs around two more iterations, or 171 additional additions per information bit, with respect to the MC code.

Furthermore, Table 2.2 provides the ML-detection complexity per coded bit for 4-QAM and 16-QAM modulations. For a code rate R_c , the complexity per information bit is equal to the one per coded bit divided by R_c . Table 2.2 shows that the MC code

suffers from a high complexity, the MD-based codes have a moderate complexity while the MB and MA codes have a low complexity.

MIMO profiles	4-QAM		16-QAM	
	FP add.	FP mul.	FP add.	FP mul.
MA / Alamouti	41	53	82	99
MB / SM	84	81	640	641
MD [EALD11]	421	510	4,096	4,257
MC / GC	1,168	1,284	147,520	163,844

TABLE 2.2: ML-detection complexity per coded bit of 2×2 WiMAX MIMO profiles in terms of floating point additions and multiplications for 4-QAM and 16-QAM modulations.

Taking into consideration a number of quantization bits qb per floating point number, one multiplication can be converted to $qb - 1$ additions. Therefore, the ML-detection introduces the major part of the receiver complexity especially for high order modulations. And, the gain in terms of number of iterations obtained using the MC code does not compensate for the complexity of the ML-detection.

Practical communication systems promote the use of low complexity receivers. Thus, the proposed MD-based STBC could be a good choice trading off performance and detection complexity.

2.4 Bitwise Mutual Information Criterion

In the previous sections, we have found that conventional STBCs are not efficient for practical coded MIMO systems. Indeed, these STBCs are designed according to *asymptotic* rank-determinant criteria suitable in the range of high SNRs. As a substitute of the determinant criterion, we have used the trace criterion to optimize the matrix D STBC [EALD11]. However, the trace criterion is also restricted in the range of low SNRs. According to the used coding rate R_c , capacity-approaching FEC codes achieve desired performance at a specific SNR usually in the range of low to moderate SNRs. Based on the maximization of the bitwise mutual information (BMI) between transmitted and soft detected bits, we propose in the following a non-asymptotic SNR-dependent STBC design criterion aiming at choosing the appropriate design parameter value for STBCs at a specific target SNR.

2.4.1 Why Bitwise Mutual Information?

Uncoded BER performance is commonly used to classify and select the appropriate MIMO encoding for practical communication systems. However, we have shown in Section 1.6 that such a selection is misleading *e.g.*, the spatial multiplexing code is

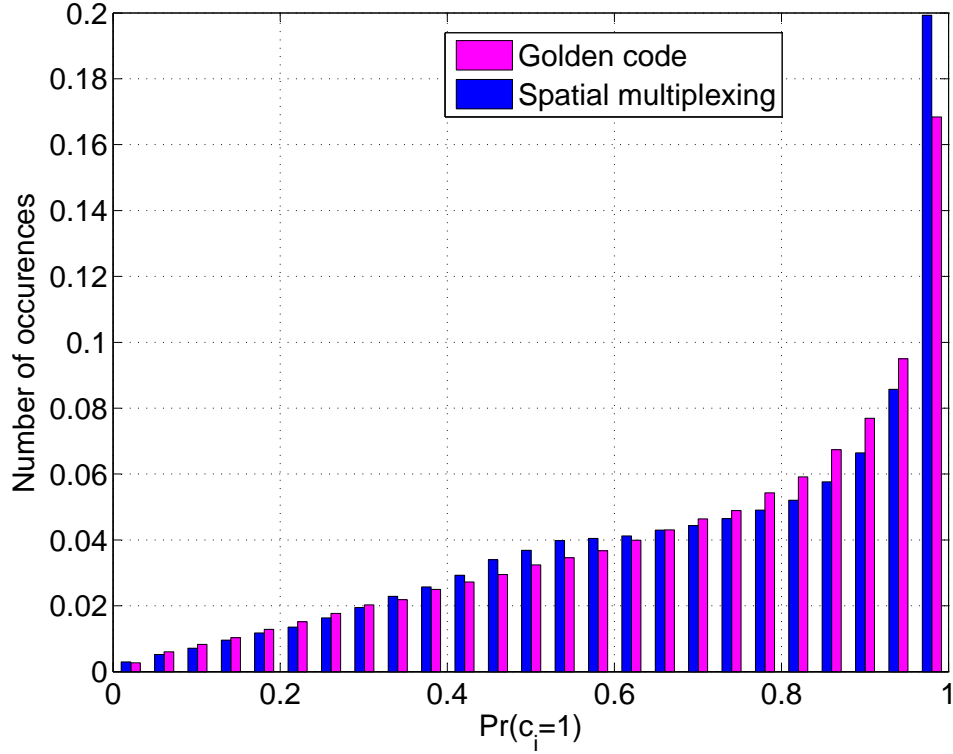


FIGURE 2.7: Normalized number of occurrences for the detected soft bit $\hat{c}_i = \Pr(c_i = 1)$ at $E_{bu}/N_0 = 0$ dB; MIMO profiles : spatial multiplexing (MB) and Golden code (MC); 4-QAM modulation.

better than the FR-FD Golden code for low coding rates. In order to understand the behavior of these MIMO codes in coded systems, we plot in Figure 2.7 the histogram or the normalized number of occurrences of detected soft bit \hat{c}_i for both codes at $E_{bu}/N_0 = 0$ dB, when the transmitted bit $c_i = 1$ and symbols belong to a 4-QAM modulation. At low SNRs, it shows that the SM detector produces more *strengthened* decisions on some bits and *weakened* ones for others with respect to the GC detector. Indeed, the GC encoder spreads four symbols on two antennas during two channel use periods. Due to this spreading, the GC will relatively *average* the decisions on transmitted bits. Therefore, it is wiser to use a metric containing information on soft detection for the classification, selection and design of MIMO codes for coded systems.

2.4.2 Criterion Definition

For any STBC the average *bitwise mutual information* between transmitted bits \mathbf{c} and soft detected bits $\hat{\mathbf{c}}$, $\text{BMI}(\hat{\mathbf{c}}; \mathbf{c})$; is computed as in [Hag04], by

$$\text{BMI}(\hat{\mathbf{c}}; \mathbf{c}) = 1 - E[\log_2(1 + \exp(-L))] \quad (2.21a)$$

$$\approx 1 - \frac{1}{N} \sum_{n=1}^N \log_2(1 + \exp(-u_n \cdot L_n)) \quad (2.21b)$$

$$\text{with } \begin{cases} L_n &= \ln \frac{1-\hat{c}_n}{\hat{c}_n} \\ u_n &= (-1)^{c_n} \end{cases}$$

where E is the mean function and L denotes the LLR. N is assumed to be large enough to accurately estimate the BMI. The BMI value is assessed at the output of the soft ML-detector by Monte Carlo simulations by passing a N -bit sequence into the mapper, the STBC encoder, the MIMO channel and the soft ML-detector.

At $E_{bu}/N_0 = 0$ dB, the average BMI for the SM code, $\text{BMI}^{\text{SM}} = 0.544$, is higher than the one for the GC, $\text{BMI}^{\text{GC}} = 0.537$. For low coding rates, the SM scheme then provides better performance than the GC when combined with several capacity-approaching FEC codes like turbo codes, LDPC codes, etc. as depicted in Figure 1.10 and also reported in [MRLRB07, KSB09, MKV⁺12]. The average BMI between transmitted bits \mathbf{c} and soft detected bits $\hat{\mathbf{c}}$ at the output of the MIMO detector is more appropriate to predict the performance of MIMO codes in the context of coded systems. Indeed, the higher the BMI at the FEC decoder input, the better the FEC decoding. Therefore, we propose to use the BMI to formulate a new STBC design criterion aiming at choosing the appropriate design parameter value at a specific target SNR for flexible STBCs *i.e.*, having a design parameter that can be optimized by exhaustive search.

Since the application of the BMI criterion to any $N_t \times T$ STBC is straightforward, we restrict our study in the following to 2×2 MIMO codes.

2.4.3 Criterion Validation

In order to validate the BMI criterion from a MIMO coding gain point of view, we have plotted in Figure 2.8 the BMI of the STBCs presented in Table 1.1 as a function of high E_{bu}/N_0 values for a 4-QAM modulation. Srinath-Rajan (SR) [SR08], Dayal-Varanasi (DV) [DV05], Trace-orthonormal (TO) [ZLW07] and GC STBCs show identical performance. Afterwards, the hierarchy from higher to lower BMI is: HTW-PGA [HTW03, PGGA08], Sezginer-Sari (MD) [SS07], Yao-Wornell (YW) [YW03] and spatial multiplexing (SM) [WFGV98]. Figure 2.8 shows that the hierarchy of the presented MIMO codes in terms of BMI is identical to their classification in Table 1.1 which validates the BMI criterion. At high E_{bu}/N_0 , the BMI and the rank-determinant criteria are equivalent.

2.5 Proposal of Adaptive Space-Time Block Codes

In the sequel, we present the optimization of some flexible STBCs according to the proposed BMI criterion. The obtained design parameter is SNR-dependent which leads to the proposal of *adaptive STBCs* optimized for a *wide range of SNRs*.

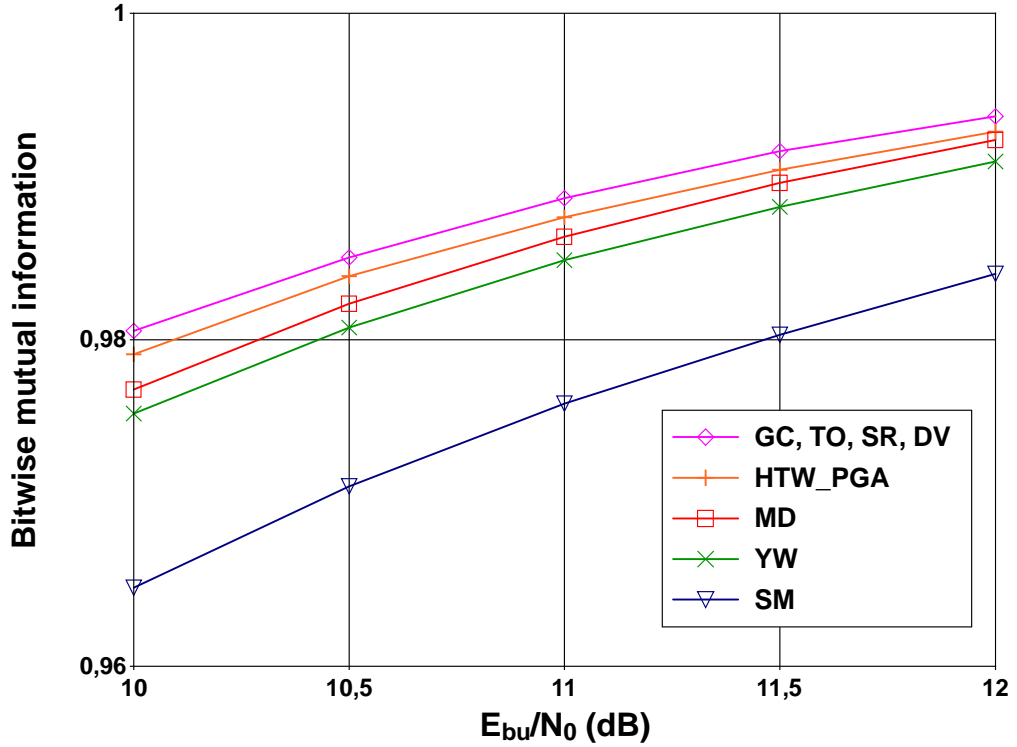


FIGURE 2.8: BMI of some well-known 2×2 MIMO codes at high E_{bu}/N_0 ; 4-QAM modulation.

2.5.1 Adaptive Matrix D STBC

The MD STBC, presented in [SS07], has $\varphi = \arg(b)$ as a design parameter. In [SS07], an exhaustive search is performed in order to maximize the minimum determinant. This search leads to $\varphi^{\text{Determinant}} = \arg\left(\frac{[(1 - \sqrt{7} + j(1 + \sqrt{7}))]}{(4\sqrt{2})}\right) \approx 114.29^\circ$. Original MD guarantees a good performance at high SNRs, but not necessarily at low and moderate SNRs regarding the used optimization criteria. In the range of low SNRs, the angle $\varphi^{\text{Trace}} = 135^\circ$ has already been proposed in Section 2.2.1 and [EALD11] for the MD STBC according to the trace criterion [TC01, CYV01].

In Figure 2.9 and Figure 2.10, the MD STBC minimum determinant and the BMI are plotted as a function of the design parameter φ , for a 4-QAM modulation, at $E_{bu}/N_0 = 12$ dB and $E_{bu}/N_0 = 0$ dB respectively. At high E_{bu}/N_0 (see Figure 2.9), the obtained φ under the BMI criterion is equal to 114.29° as the original one in [SS07]. While at low E_{bu}/N_0 , Figure 2.10 shows that the angle which maximizes the BMI is equal to $\varphi = 135^\circ$ different from the original one and equal to the one obtained according to the trace criterion. The optimization of the MD STBC according to the BMI criterion proves that:

- The value of φ is a function of E_{bu}/N_0 .
- The appropriate φ at any E_{bu}/N_0 can be obtained according the BMI criterion.

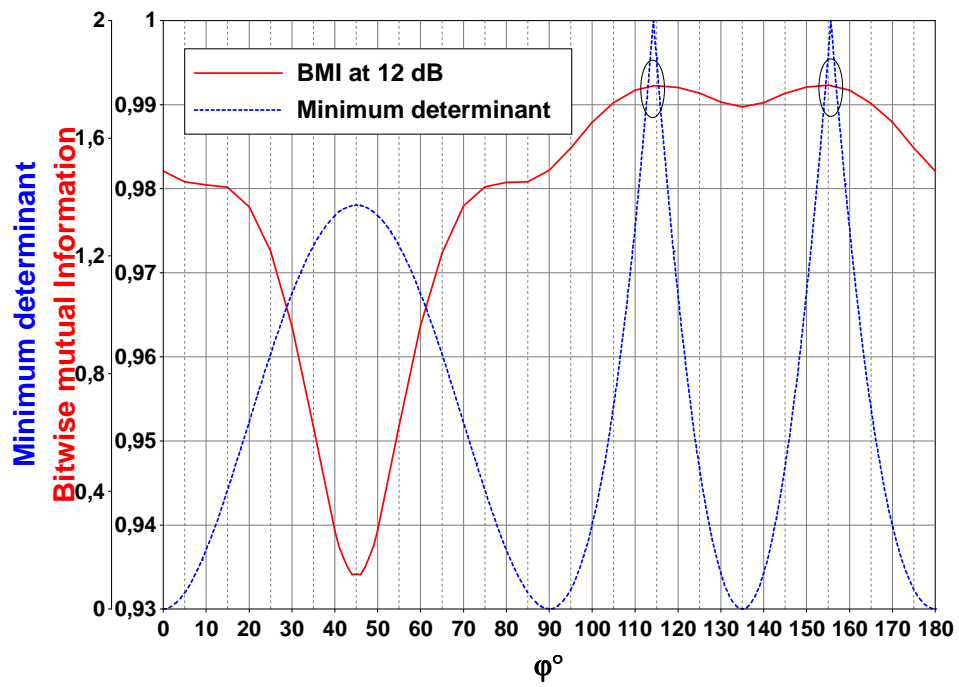


FIGURE 2.9: BMI at $E_{bu}/N_0 = 12$ dB and minimum determinant of MD STBC as a function of its design parameter φ ; 4-QAM modulation.

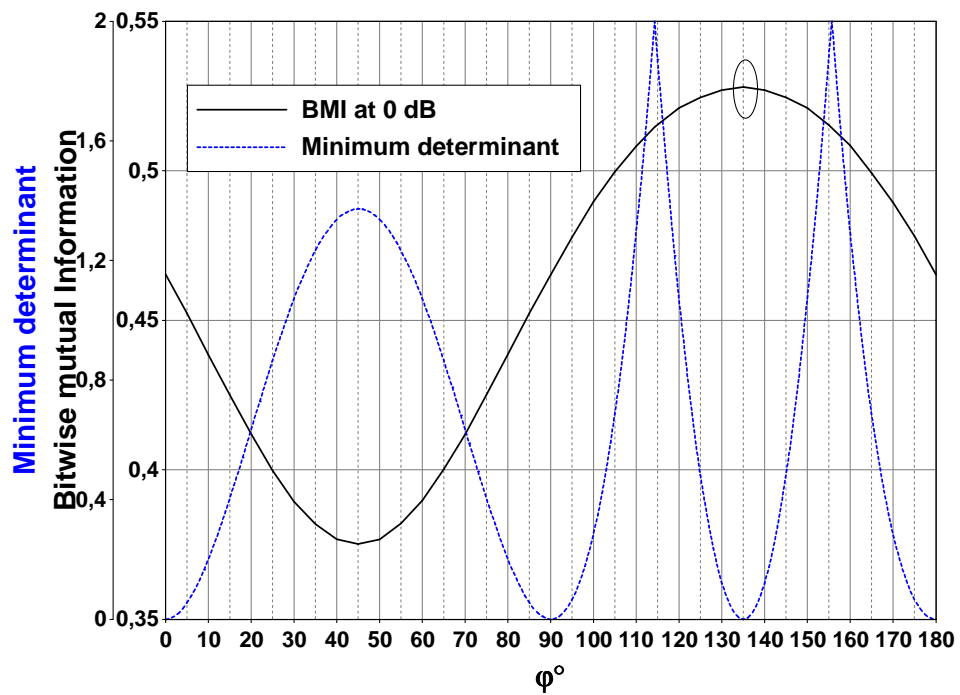


FIGURE 2.10: BMI at $E_{bu}/N_0 = 0$ dB and minimum determinant of MD STBC as a function of its design parameter φ ; 4-QAM modulation.

As we have already done in Figure 2.9 and Figure 2.10 at $E_{bu}/N_0 = 12$ dB and $E_{bu}/N_0 = 0$ dB respectively, we have computed for each E_{bu}/N_0 with a step of 0.25 dB, the appropriate φ which maximizes its BMI denoted by $\varphi_{\text{opt}}^{M\text{-QAM}}$. A polynomial interpolation is performed to obtain an analytical approximation of $\varphi_{\text{opt}}^{M\text{-QAM}}$ as a function of E_{bu}/N_0 .

For 4-QAM modulation, in the range $5.5 \text{ dB} < E_{bu}/N_0 < 11 \text{ dB}$, the analytical approximation of φ versus E_{bu}/N_0 , according to the BMI criterion, is given by (see Appendix A)

$$\varphi_{\text{opt}}^{4\text{-QAM}} = \begin{cases} \varphi^{\text{Trace}} = 135^\circ; \text{ For } E_{bu}/N_0 \leq 5.5 \text{ dB} \\ -0.46 \left(\frac{E_{bu}}{N_0}\right)^3 + 11.92 \left(\frac{E_{bu}}{N_0}\right)^2 - 102.64 \left(\frac{E_{bu}}{N_0}\right) \\ + 414; \text{ For } 5.5 < E_{bu}/N_0 < 11 \text{ dB} \\ \varphi^{\text{Determinant}} = 114.29^\circ; \text{ For } E_{bu}/N_0 \geq 11 \text{ dB} \end{cases} \quad (2.22)$$

Similarly, for 16-QAM modulation, the design parameter $\varphi_{\text{opt}}^{16\text{-QAM}}$ is computed by

$$\varphi_{\text{opt}}^{16\text{-QAM}} = \begin{cases} \varphi^{\text{Trace}} = 135^\circ; \text{ For } E_{bu}/N_0 \leq 11 \text{ dB} \\ -0.0973 \left(\frac{E_{bu}}{N_0}\right)^3 + 3.92 \left(\frac{E_{bu}}{N_0}\right)^2 - 54.05 \left(\frac{E_{bu}}{N_0}\right) \\ + 379.58; \text{ For } 10 < E_{bu}/N_0 < 17 \text{ dB} \\ \varphi^{\text{Determinant}} = 114.29^\circ; \text{ For } E_{bu}/N_0 \geq 17 \text{ dB} \end{cases} \quad (2.23)$$

For higher order modulations, the same method can be applied and a suitable $\varphi_{\text{opt}}^{M\text{-QAM}}$ can be chosen. Furthermore, a tradeoff value like the one proposed in Section 2.2.2 is not required anymore.

Figure 2.11 plots the BER of turbo coded WiMAX profiles, original MD and adaptive MD codes with 4-QAM modulation for FR profiles. The adaptive MD parameter $\varphi_{\text{opt}}^{4\text{-QAM}}$ is computed by: 1) passing from global system to uncoded MIMO system using $E_{bu}/N_0 = E_b/N_0 + 10 \log_{10}(R_c)$, 2) obtained E_{bu}/N_0 is then introduced in equation (2.22) to compute the suitable $\varphi_{\text{opt}}^{4\text{-QAM}}$. For $R_c = 1/2$, the MB offers the best performance. From $R_c = 2/3$ to $R_c = 5/6$, the MC surpasses all the presented codes. The MA always shows the worst performance. The proposed adaptive MD always overcomes the original MD with a gain between 0.1 and 0.2 dB while a loss less than 0.2 dB is observed with respect to the MC. Despite the fact that the adaptive MD STBC does not provide the best BER performance with respect to the MB code for low coding rates and the MC code for high coding rates, the proposed adaptive MD STBC could be a good choice for practical coded communication systems trading off performance and detection complexity. Our work on the adaptive MD STBC in the context of a WiMAX system has been published in [ELAD12b].

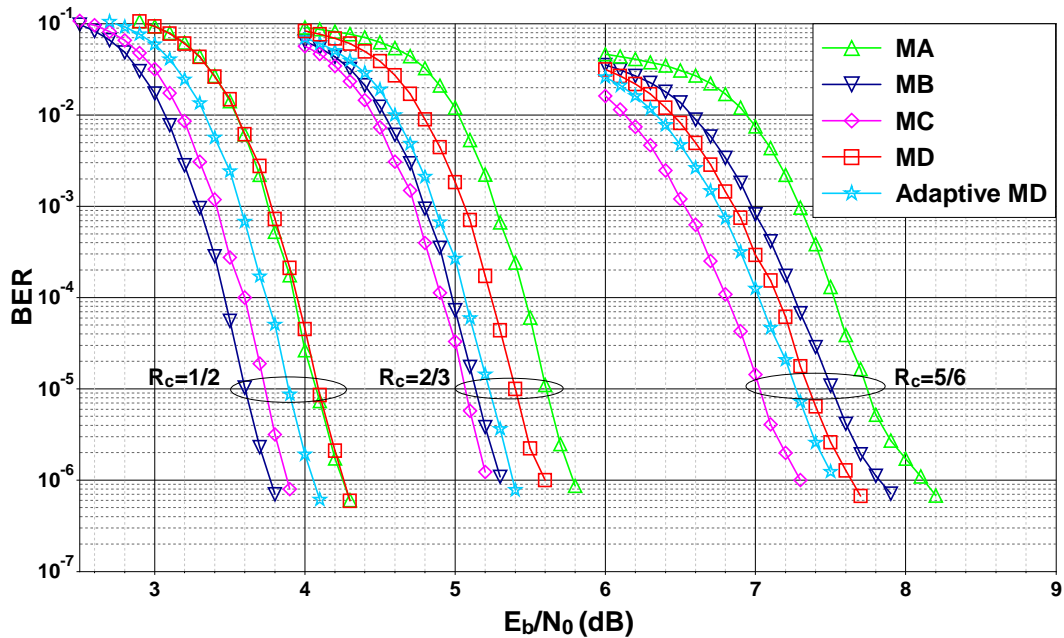


FIGURE 2.11: BER of turbo coded system; 8-state double binary turbo code ($R_c = 1/2, 2/3, 5/6$) with 8 turbo decoding iterations and information frame size $k = 4,800$ bits; MIMO profiles: Alamouti code (MA) with 16-QAM modulation and spatial multiplexing (MB), Golden code (MC), Matrix D (MD) and adaptive MD with 4-QAM modulation; quasi-static flat Rayleigh fading MIMO channel.

2.5.2 Adaptive Trace-Orthonormal STBC

In the previous section, we have proposed the adaptive MD code as a STBC for 2×2 coded MIMO systems trading off performance and ML-detection complexity. In this section, we look for a 2×2 adaptive STBC able to offer the best BER performance for all SNRs.

2.5.2.1 Presentation of Adaptive Trace-Orthonormal STBC

Among the codes presented in Table 1.1, the trace-orthonormal STBC has a flexible structure designed from both information-theoretic and detection error viewpoints [ZLW07]. By varying its design parameter θ , the performance of the TO STBC varies significantly. Therefore we propose to take advantage of this feature in order to design an adaptive TO-based STBC.

In [ZLW07], an exhaustive search is performed in order to maximize the TO minimum determinant. This search leads to $\theta = \frac{1}{2} \arcsin \frac{1}{\sqrt{5}} \approx 13.28^\circ$ and a coding gain equal to the one of the Golden code. Therefore, original TO guarantees the best performance at high SNRs, but not necessarily at low to moderate SNRs.

In Figure 2.12 and Figure 2.13, the minimum determinant and the BMI are plotted as a function of the design parameter θ , for a 4-QAM modulation, at $E_{bu}/N_0 = -3$ dB and $E_{bu}/N_0 = 12$ dB respectively. At low E_{bu}/N_0 , Figure 2.12 shows that the

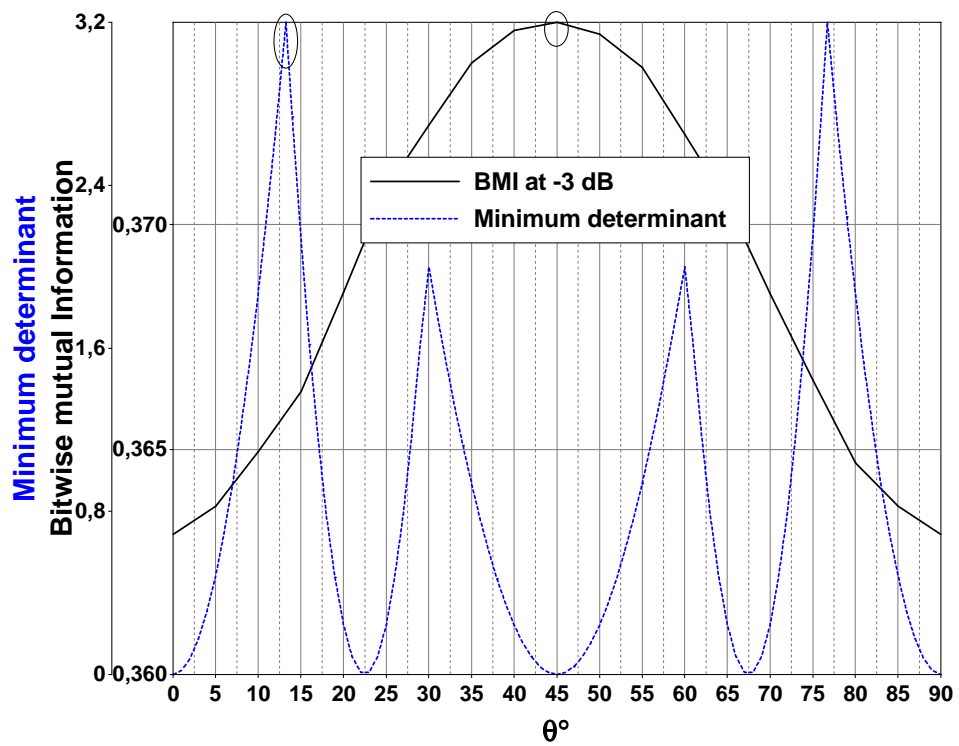


FIGURE 2.12: BMI at $E_{bu}/N_0 = -3$ dB and minimum determinant of TO STBC as a function of its design parameter θ ; 4-QAM modulation.

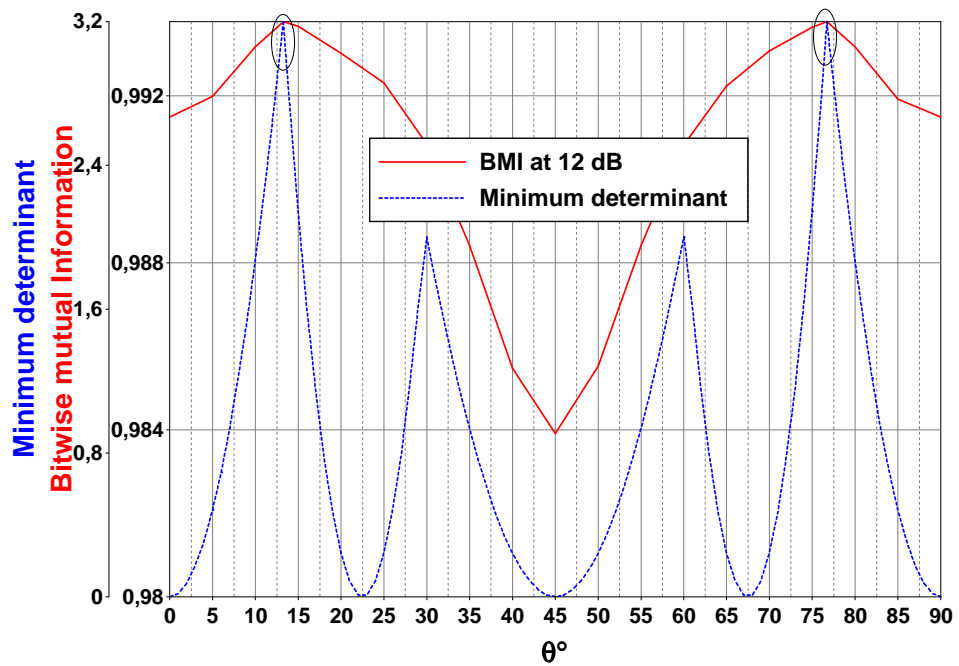


FIGURE 2.13: BMI at $E_{bu}/N_0 = 12$ dB and minimum determinant of TO STBC as a function of its design parameter θ ; 4-QAM modulation.

angle maximizing the BMI is equal to $\theta = 45^\circ$, different from the original one obtained according to the determinant criterion. For high E_{bu}/N_0 (see Figure 2.13), the obtained θ according to the BMI criterion is equal to 13.28° as the original one obtained in [ZLW07]. As already done in Figure 2.12 and Figure 2.13 for $E_{bu}/N_0 = -3$ dB and $E_{bu}/N_0 = 12$ dB respectively, we have computed the appropriate θ which maximizes the BMI for each E_{bu}/N_0 with a step of 0.25 dB. We denote the obtained θ by $\theta_{\text{opt}}^{M\text{-QAM}}$.

For 4-QAM modulation, in the range of -0.5 dB $< E_{bu}/N_0 < 4.25$ dB, a $\theta_{\text{opt}}^{4\text{-QAM}}$ is obtained for each E_{bu}/N_0 . Thanks to a polynomial interpolation, an analytical approximation of $\theta_{\text{opt}}^{4\text{-QAM}}$ as a function of E_{bu}/N_0 is derived (see Appendix B). Therefore, the design parameter of the proposed *adaptive TO STBC* which maximizes its BMI is computed, for all SNRs, by

$$\theta_{\text{opt}}^{4\text{-QAM}} = \begin{cases} 45^\circ; & \text{For } E_{bu}/N_0 \leq -0.5 \text{ dB} \\ -0.65 \left(\frac{E_{bu}}{N_0}\right)^3 + 4.79 \left(\frac{E_{bu}}{N_0}\right)^2 - 13.8 \left(\frac{E_{bu}}{N_0}\right) \\ + 36.47; & \text{For } -0.5 < E_{bu}/N_0 < 4.25 \text{ dB} \\ 13.28^\circ; & \text{For } E_{bu}/N_0 \geq 4.25 \text{ dB} \end{cases} \quad (2.24)$$

Similarly, for 16-QAM modulation, the design parameter $\theta_{\text{opt}}^{16\text{-QAM}}$ is computed by

$$\theta_{\text{opt}}^{16\text{-QAM}} = \begin{cases} 45^\circ; & \text{For } E_{bu}/N_0 \leq 9 \text{ dB} \\ 0.424 \left(\frac{E_{bu}}{N_0}\right)^2 - 14.936 \left(\frac{E_{bu}}{N_0}\right) \\ + 139; & \text{For } 9 < E_{bu}/N_0 < 13.5 \text{ dB} \\ 13.28^\circ; & \text{For } E_{bu}/N_0 \geq 13.5 \text{ dB} \end{cases} \quad (2.25)$$

For higher order modulations, the same method can be applied and a suitable $\theta_{\text{opt}}^{M\text{-QAM}}$ can be chosen. However, the ML-detection complexity of the TO STBC is $\mathcal{O}(M^4)$. Then the design of adaptive TO STBC for $M \geq 64$ becomes very complex as the BMI is computed based on Monte Carlo simulations (see Section 2.4). An analytical method to get the appropriate $\theta_{\text{opt}}^{M\text{-QAM}}$ as a function of E_{bu}/N_0 is still an open problem.

We notice that based on the Dayal-Varanasi (DV) [DV05] structure, an adaptive DV STBC code can also be proposed. The adaptive DV provides the same performance as the adaptive TO STBC.

2.5.2.2 Analysis of the Transmitted Constellations

According to the BMI criterion, the optimized parameter $\theta_{\text{opt}}^{M\text{-QAM}}$ for the adaptive TO STBC is $= 45^\circ$ in the range of low E_{bu}/N_0 and $\frac{1}{2} \arcsin \frac{1}{\sqrt{5}} \approx 13.28^\circ$ in the range of high E_{bu}/N_0 . In the context of coded MIMO systems, our simulation results in Section 1.6 have shown that the spatial multiplexing scheme provides the best performance at

low SNRs while the Golden code provides the best performance at high SNRs. In the following, we examine the transmitted constellation for both $\theta_{\text{opt}}^{M\text{-QAM}}$ values, 45° and 13.28° .

Low SNR Region

For $\theta = \pi/4 = 45^\circ$, we have $\cos \theta = \sin \theta = \frac{1}{\sqrt{2}}$. By substituting $\cos \theta$ and $\sin \theta$ for their values in the equations 1.24, one can show that

$$\begin{aligned}
X_{11} &= (S_1 + S_2) \cos \theta + (S_2^* - S_1^*) \sin \theta \\
&= (S_1 + S_2) \frac{1}{\sqrt{2}} + (S_2^* - S_1^*) \frac{1}{\sqrt{2}} \\
&= (\Re(S_1) + j\Im(S_1) + \Re(S_2) + j\Im(S_2)) \frac{1}{\sqrt{2}} \\
&\quad + (\Re(S_2) - j\Im(S_2) - \Re(S_1) + j\Im(S_1)) \frac{1}{\sqrt{2}} \\
&= \sqrt{2} (\Re(S_2) + j\Im(S_1))
\end{aligned} \tag{2.26}$$

and the transmitted signal on the first antenna during the first channel use period $\frac{1}{\sqrt{2}}X_{11}$ is

$$\frac{1}{\sqrt{2}}X_{11} = \Re(S_2) + j\Im(S_1) \tag{2.27}$$

Similarly, after the derivation of X_{12} , X_{21} and X_{22} , the structure of the TO STBC becomes

$$\mathbf{X}_{\theta=45^\circ}^{\text{TO}} = \begin{bmatrix} \Re(S_2) + j\Im(S_1) & e^{j\frac{\pi}{4}} [\Re(S_4) + j\Im(S_3)] \\ e^{j\frac{\pi}{4}} [\Re(S_3) + j\Im(S_4)] & \Re(S_1) + j\Im(S_2) \end{bmatrix} \tag{2.28}$$

If we consider

$$\begin{aligned}
S'_1 &= \Re(S_2) + j\Im(S_1) \\
S'_2 &= \Re(S_3) + j\Im(S_4) \\
S'_3 &= \Re(S_4) + j\Im(S_3) \\
S'_4 &= \Re(S_1) + j\Im(S_2)
\end{aligned} \tag{2.29}$$

where S'_1 , S'_2 , S'_3 and S'_4 belong to the M -QAM constellation.

The TO STBC for $\theta = 45^\circ$ reduces to

$$\mathbf{X}_{\theta=45^\circ}^{\text{TO}} = \begin{bmatrix} S'_1 & e^{j\frac{\pi}{4}} S'_3 \\ e^{j\frac{\pi}{4}} S'_2 & S'_4 \end{bmatrix} \tag{2.30}$$

Therefore, transmitted signals $\frac{1}{\sqrt{2}}X_{11}$ and $\frac{1}{\sqrt{2}}X_{22}$ are equivalent to the SM scheme and signals $\frac{1}{\sqrt{2}}X_{12}$ and $\frac{1}{\sqrt{2}}X_{21}$ are equivalent to a $\pi/4$ -rotated SM scheme. The adaptive TO STBC is equivalent to the SM scheme in the low SNR range.

High SNR Region

For $\theta = \frac{1}{2} \arcsin \frac{1}{\sqrt{5}} \approx 13.28^\circ$, we have $\cos \theta = \sqrt{\frac{1}{2} + \frac{1}{\sqrt{5}}}$ and $\sin \theta = \sqrt{\frac{1}{2} - \frac{1}{\sqrt{5}}}$. By substituting $\cos \theta$ and $\sin \theta$ for their values in equations 1.24, we obtain

$$\begin{aligned} X_{11} &= (S_1 + S_2) \cos \theta + (S_2^* - S_1^*) \sin \theta \\ &= (\Re(S_1) + j\Im(S_1) + \Re(S_2) + j\Im(S_2)) \sqrt{\frac{1}{2} + \frac{1}{\sqrt{5}}} \\ &\quad + (\Re(S_2) - j\Im(S_2) - \Re(S_1) + j\Im(S_1)) \sqrt{\frac{1}{2} - \frac{1}{\sqrt{5}}} \end{aligned} \quad (2.31)$$

The transmitted signal on the first antenna during the first channel use period $\frac{1}{\sqrt{2}}X_{11}$ is equivalent to a Golden code constellation rotated with an angle $\vartheta = \frac{\pi}{4} - \frac{1}{2} \arcsin \frac{1}{\sqrt{5}}$. Indeed, the rotation of this signal by $-\vartheta$, yields

$$\begin{aligned} \frac{1}{\sqrt{2}}X_{11}e^{-j\vartheta} &= \frac{1}{\sqrt{2}} [(S_1 + S_2) \cos \theta + (S_2^* - S_1^*) \sin \theta] e^{-j\vartheta} \\ &= \begin{bmatrix} (\Re(S_2) + j\Im(S_1)) \sqrt{\frac{1}{2} \left(1 + \frac{1}{\sqrt{5}}\right)} \\ + (\Re(S_1) + j\Im(S_2)) \sqrt{\frac{1}{2} \left(1 - \frac{1}{\sqrt{5}}\right)} \end{bmatrix} \\ &\times [\cos(-\vartheta) + j \sin(-\vartheta)] \\ &= \frac{1}{\sqrt{5}} \begin{bmatrix} (\Re(S_2) + j\Im(S_1)) \left(\frac{1+\sqrt{5}}{2} - j\right) \\ + (\Re(S_1) + j\Im(S_2)) \left(1 + j\frac{1-\sqrt{5}}{2}\right) \end{bmatrix} \\ &= \frac{1}{\sqrt{5}} \left[S'_1 \left(\frac{1+\sqrt{5}}{2} - j\right) + S'_2 \left(1 + j\frac{1-\sqrt{5}}{2}\right) \right] \end{aligned} \quad (2.32)$$

which is equivalent to the expression of the transmitted constellation with the GC [OV08].

Similarly, one can prove that $\frac{1}{\sqrt{2}}X_{12}e^{j\frac{1}{2}\arcsin\frac{1}{\sqrt{5}}}$ and $\frac{1}{\sqrt{2}}X_{21}e^{j\frac{1}{2}\arcsin\frac{1}{\sqrt{5}}}$, $\frac{1}{\sqrt{2}}X_{22}e^{-j\vartheta}$ belong to the GC constellation (see Appendix C). The adaptive TO STBC is equivalent to the GC in the high SNR range.

2.5.2.3 Complexity Reduction of ML-Detection

Practical communication systems promote the use of low complexity detection STBCs. In the range of low E_{bu}/N_0 , we have proved in Section 2.5.2.2 that the transmitted constellation for the adaptive TO STBC is equivalent to the spatial multiplexing one. Furthermore, (S'_1, S'_2, S'_3, S'_4) belong to the M -QAM constellation. (S'_1, S'_2) can be detected with a SM detector of complexity $\mathcal{O}(M^2)$ since their detection is *independent* of (S'_3, S'_4) . Similarly, (S'_3, S'_4) detection is independent of (S'_1, S'_2) . Then, the original

symbols can be easily reconstructed by

$$\begin{aligned}
 S_1 &= \Re(S'_4) + j\Im(S'_1) \\
 S_2 &= \Re(S'_1) + j\Im(S'_4) \\
 S_3 &= \Re(S'_2) + j\Im(S'_3) \\
 S_4 &= \Re(S'_3) + j\Im(S'_2)
 \end{aligned} \tag{2.33}$$

Besides, the ML-detection complexity of the GC and the original TO codes is always $\mathcal{O}(M^4)$ for all SNRs.

2.6 Performance Evaluation of the Proposed Adaptive TO STBC for a WiMAX System

In this section, we provide the performance evaluation in terms of BER for the proposed adaptive TO STBC in the context of a WiMAX system. Closed-loop and open-loop systems are considered.

In the closed-loop case, the transmitter has a prior knowledge on some parameters depending on the channel state at the receiver like E_b/N_0 . Depending on this E_b/N_0 , the modulation order M and the coding rate R_c are selected. This technique is well-known in the communication standards *e.g.*, WiMAX and HSDPA, by link adaptation or adaptive modulation and coding (AMC). The use of AMC techniques guarantees the user QoS as the suitable transmission scheme is selected depending on the channel state.

On the contrary, in the open-loop case as broadcast systems, the transmitter does not have any prior knowledge on the receiver channel state and the modulation and coding scheme (MCS) is selected regardless the receiver condition. Open-loop systems offer a best effort QoS.

2.6.1 Adaptive TO STBC Parameter Computation for Coded Systems

In the previous sections, we have proposed the adaptive TO STBC. Its appropriate $\theta_{\text{opt}}^{M\text{-QAM}}$ values depend on the coding rate R_c , the modulation order M and E_b/N_0 . For coded systems, $\theta_{\text{opt}}^{M\text{-QAM}}$ values are computed as follows

1. Passing from global system to uncoded MIMO by

$$E_{bu}/N_0 = E_b/N_0 + 10 \log_{10}(R_c) \tag{2.34}$$

2. The obtained E_{bu}/N_0 is introduced in equations (2.24) and (2.25) to compute the value of θ to be used for the proposed adaptive TO STBC.

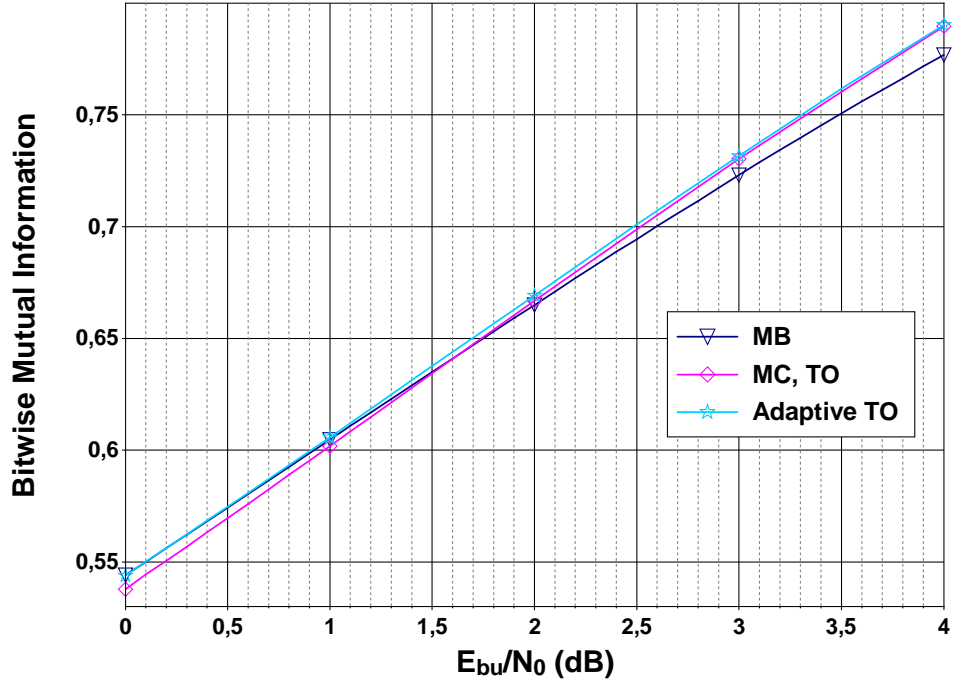


FIGURE 2.14: BMI of full-rate WiMAX MIMO profiles and adaptive TO code as a function of E_b/N_0 ; 4-QAM modulation.

For closed-loop systems, the value of E_b/N_0 is known at the transmitter. The computation of $\theta_{\text{opt}}^{M\text{-QAM}}$ values is straightforward using the above method.

On the contrary, for open-loop systems, the E_b/N_0 value is unknown at the transmitter. Such systems usually target a BER lower than a fixed value. Fortunately, the E_b/N_0 for which the FEC code achieves the targeted BER is known at each rate R_c . Therefore, the $\theta_{\text{opt}}^{M\text{-QAM}}$ can be also computed using the above based on this E_b/N_0 .

An example of the use of the adaptive TO STBC is provided in Section 2.6.3 for a closed-loop system and in Section 2.6.4 for an open-loop system.

2.6.2 BMI Study of the Adaptive TO STBC

Figure 2.14 illustrates the BMI of the MB, the MC (and hence the original TO) and the adaptive TO MIMO codes as a function of E_b/N_0 for a 4-QAM modulation. It shows that the adaptive TO code offers the highest BMI of all considered codes. Therefore, the adaptive TO code shall overcome the considered codes for coded MIMO systems. We notice that it also offers the highest BMI with respect to conventional 2×2 MIMO codes presented in Table 1.1.

2.6.3 Closed-Loop System

In this section, we first analyze the BER curves as a function of E_b/N_0 after 8 turbo decoding iterations for the turbo coded MIMO system with 4-QAM and 16-QAM

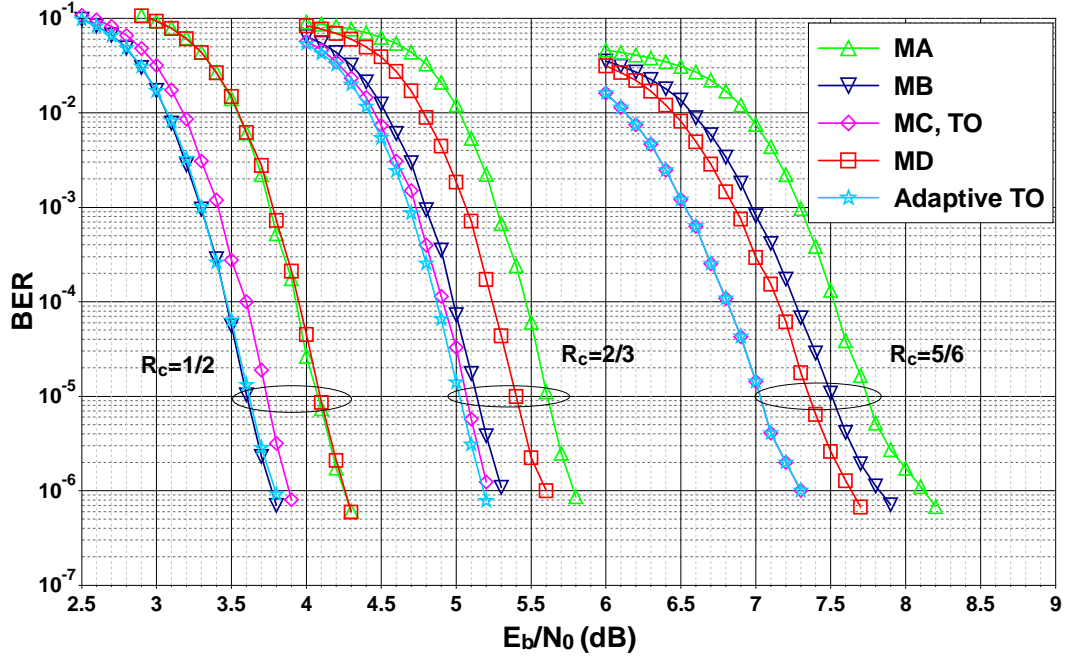


FIGURE 2.15: BER of turbo coded system; 8-state double binary turbo code ($R_c = 1/2$, $2/3$, $5/6$) with 8 turbo decoding iterations and information frame size $k = 4,800$ bits; MIMO profiles: Alamouti code (MA) with 16-QAM modulation and spatial multiplexing (MB), Golden code (MC) & original TO, Matrix D (MD) and adaptive TO with 4-QAM modulation; quasi-static flat Rayleigh fading MIMO channel.

modulations for full-rate WiMAX profiles. Then we investigate the case of *higher order modulations*.

2.6.3.1 4-QAM Modulation

For 4-QAM modulation, Figure 2.15 confirms the results obtained in Section 2.6.2 using the BMI study. Indeed, the adaptive TO code always provides the best BER performance for all coding rates with respect to WiMAX profiles. We evaluate the gains of the adaptive TO code at a target BER = 10^{-5} . For $R_c = 1/2$, the MB code matches the adaptive TO code, a gain of almost 0.15 dB is obtained with respect to the MC code (and hence to the original TO code) and 0.5 dB with respect to the MA and MD STBCs. For $R_c = 2/3$, the adaptive TO code surpasses all the presented codes, with a gain of 0.05 dB with respect to the MC code, 0.1 dB with respect to the MB code, 0.4 dB with respect to MD code and 0.6 dB with respect to the MA code. For $R_c = 5/6$, the MC code matches the adaptive TO code, while a gain of 0.45 dB is observed with respect to the MD code, 0.5 dB compared to the MB code and 0.75 dB compared to the MA code.

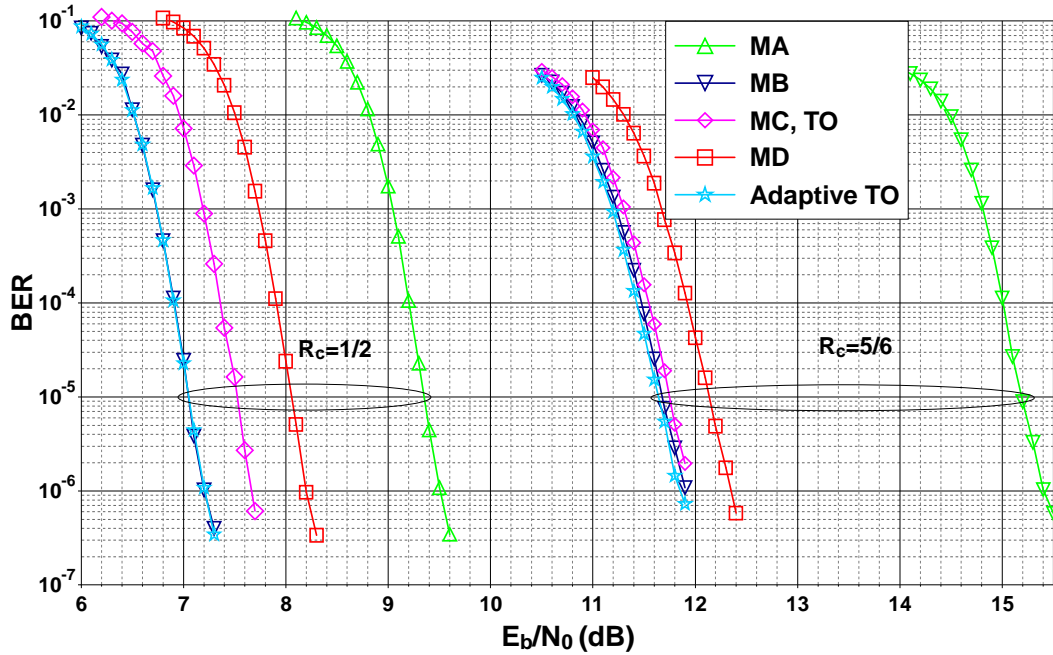


FIGURE 2.16: BER of turbo coded system; 8-state double binary turbo code ($R_c = 1/2$, $5/6$) with 8 turbo decoding iterations and information frame size $k = 10,800$ bits; MIMO profiles: Alamouti code (MA) with 256-QAM and spatial multiplexing (MB), Golden code (MC) & original TO, Matrix D (MD) and adaptive TO with 16-QAM; quasi-static flat Rayleigh fading MIMO channel.

2.6.3.2 16-QAM Modulation

Figure 2.16 plots the BER of the WiMAX MIMO profiles with 16-QAM modulation for full-rate profiles. In order to transmit at the same spectral efficiency, a 256-QAM modulation is used with the MA STBC. For low coding rate $R_c = 1/2$, the MB code matches the adaptive TO code, a gain of almost 0.5 dB is obtained with respect to the MC code, 1 dB with respect to the MD code and 2.4 dB with respect to the MA code. At high coding rate $R_c = 5/6$, the adaptive TO code surpasses all the presented codes, with a gain of 0.05 dB with respect to the MB code, 0.1 dB with respect to the MC code, 0.5 dB with respect to the MD code and 3.6 dB with respect to the MA code.

BER simulation results confirm that the adaptive TO based on the proposed angle $\theta_{\text{opt}}^{M\text{-QAM}}$ outperforms all STBC profiles of the WiMAX system.

2.6.3.3 Higher Order Modulations

Figure 2.17 plots the uncoded BER curves as a function of E_{bu}/N_0 for the MB, MC and MD MIMO codes with 4-QAM, 16-QAM and 64-QAM modulations. It shows that the E_{bu}/N_0 , for which BER curves for the MB and the MC codes cross, is increasing

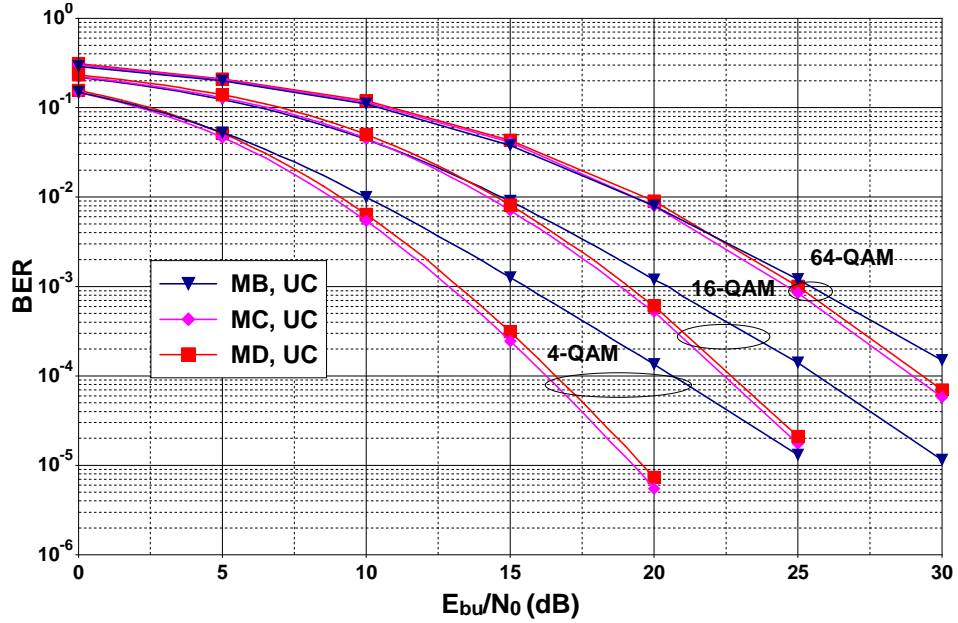


FIGURE 2.17: Uncoded BER for 2×2 MIMO profiles: Spatial multiplexing (MB), Golden code (MC) and Matrix D (MD); quasi-static flat Rayleigh fading channel.

with the increase of the modulation order M e.g., near to $E_{bu}/N_0 = 11$ dB with 16-QAM modulation and around $E_{bu}/N_0 = 20$ dB with 64-QAM modulation. Capacity-approaching FEC codes achieve low error rates even at low to moderate SNR region. For higher order modulations, the MB code (and hence the adaptive TO code) is then more effective than the MC and MD codes.

2.6.3.4 Conclusion

For any modulation order M , an adaptive TO STBC can be designed according to the BMI criterion. This is particularly of interest when an adaptive modulation and coding (AMC) is used as the appropriate angles are chosen for each rate R_c , modulation order M and E_b/N_0 . Moreover, the use of a non-adaptive MIMO code *i.e.*, MA, MB, MC or MD codes introduces a performance loss for some modulation and coding schemes. Indeed, the use of the well-known Golden code (MC code) [BRV05] will not only alter the performance of terminals at low coding rates but also increase their MIMO detection complexity.

Our work on the adaptive TO STBC in the context of a WiMAX system has been published in [ELAD12a].

2.6.4 Broadcast Transmission: Open-Loop System

A broadcast system does not employ a feedback channel from the receiver to the transmitter and the E_b/N_0 is then unknown at the transmitter. For open-loop systems,

the proposed adaptive STBCs are still useful. Indeed, the E_b/N_0 for which the FEC code achieves the targeted BER is known at each rate. For instance, for the 8-state double binary turbo code with 8 turbo decoding iterations at $R_c = 1/2$ and a target BER equal to 10^{-5} , $E_b/N_0 = 3.6$ dB (see Figure 2.15). The corresponding E_{bu}/N_0 is then computed by equation (2.34). Obtained E_{bu}/N_0 is introduced in the design parameter equations of adaptive STBCs to compute their appropriate values *e.g.*,

$$\theta_{\text{opt}}^{4\text{-QAM}}(3.6 + 10 \log_{10}(1/2)) = 30^\circ \quad (2.35)$$

For each rate, the target E_b/N_0 is known. E_{bu}/N_0 and then $\theta_{\text{opt}}^{4\text{-QAM}}$ can be computed thanks to the proposed method in Section 2.6.1. Afterwards, a *lookup table* (LUT) containing the appropriate θ to be used with each coding rate R_c is available at the transmitter. Table 2.3 provides $\theta_{\text{opt}}^{4\text{-QAM}}$ as a function of the coding rate R_c for the WiMAX 8-state double binary turbo code when the turbo decoder performs 8 turbo decoding iterations.

R_c	$\theta_{\text{opt}}^{4\text{-QAM}}$
1/2	30°
2/3	20°
5/6	13.28°

TABLE 2.3: LUT providing $\theta_{\text{opt}}^{4\text{-QAM}}$ as a function of the coding rate R_c for the 8-state double binary turbo code with 8 turbo decoding iterations at a target BER = 10^{-5} ; 4-QAM modulation.

Capacity-approaching FEC codes rapidly achieve their iterative convergence and the BMI has to be as high as possible in the SNR range of convergence. Actually, the BMI does not much vary with small variations of E_b/N_0 . Therefore, an open-loop transmission based on the TO STBC structure with the appropriate θ fixed for each rate R_c (LUT-based solution), provides about the same performance as the one with adaptive TO STBC where θ is computed adaptively with E_b/N_0 . This result is confirmed by simulations and the same BER curves as in Section 2.6.3 are obtained.

The main difference between closed-loop and open-loop systems is that, for open-loop systems, a LUT containing the appropriate design parameter for each rate R_c is to be computed, for each used FEC code. On the contrary, the adaptive STBCs can be directly used regardless of the FEC code, for closed-loop systems.

Discussion on the Importance of LUT Computation In general, the design of a LUT associated with the used FEC code is also important for closed-loop coded MIMO systems. Indeed, the estimated E_b/N_0 available at the transmitter might be erroneous due to an estimation error, noise and/or delay on the feedback channel, etc. When the feedback E_b/N_0 suggests a θ far from the LUT one's, the θ suggested by the LUT can be

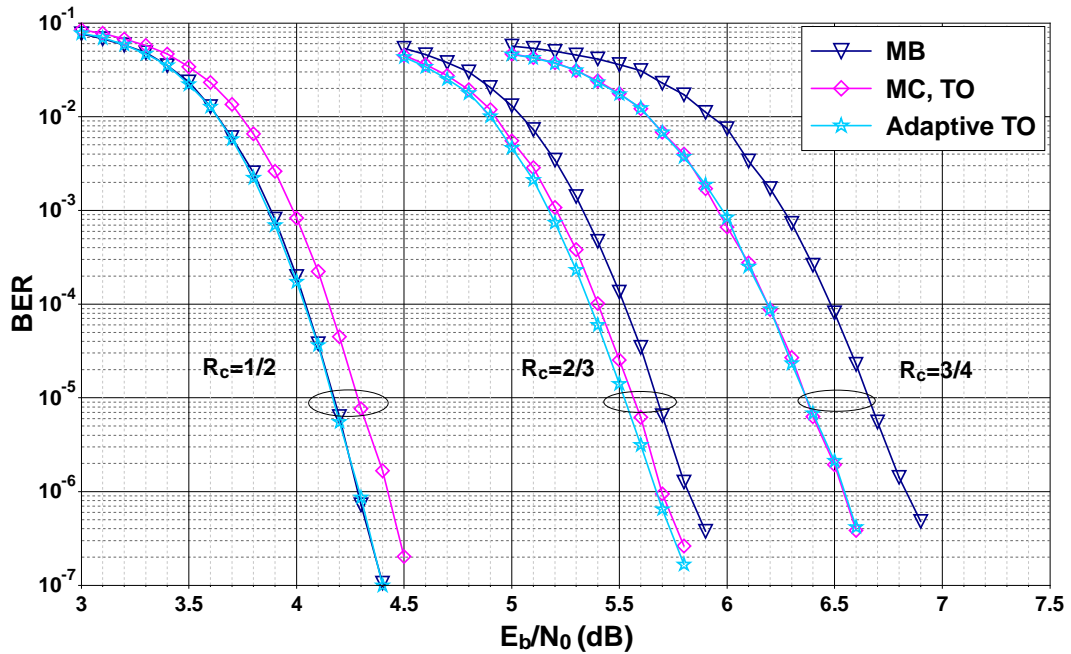


FIGURE 2.18: BER of coded MIMO system; FlexiCode ($R_c = 1/2, 2/3, 3/4$) with 10 turbo decoding iterations and an information frame size $k = 5,399$ bits; MIMO profiles: spatial multiplexing (MB), Golden code (MC) & original TO, and adaptive TO with 4-QAM modulation; quasi-static flat Rayleigh fading MIMO channel.

used, making the transmission resistant against E_b/N_0 estimation errors and preventing a non-efficient transmission.

2.7 Performance Evaluation with FlexiCode

We have shown in Section 2.6 the importance of adaptive STBCs structure where the proposed adaptive TO STBC shows a superiority with respect to well-known MIMO codes in the context of a WiMAX system. In order to prove the superiority of the adaptive TO STBC with any capacity-approaching FEC code, we have plotted in Figure 2.18 the BER for the concatenation of the FlexiCode with different coding rates ($R_c = 1/2, 2/3, 3/4$) and several MIMO profiles: the spatial multiplexing (MB), Golden code (MC) and the adaptive TO with 4-QAM modulation. Figure 2.18 shows that the adaptive TO STBC always provide the best performance with all coding rates R_c .

2.8 Chapter Summary

In this chapter, we have investigated the improvement of standardized STBCs for coded MIMO systems. We started by the presentation of the low complexity detector for the Matrix D STBC. FEC decoder requires soft decisions on transmitted bits while original MIMO detector only provides hard ones. Therefore, we proposed a soft detector

for the Matrix D STBC with the same complexity order. Afterwards, we optimized the Matrix D STBC in the region of low SNRs according to the trace criterion. Based on this optimization, we proposed a low ML-detection complexity FR-FD Matrix D-based STBC for coded MIMO systems and showed that it overcomes the original one in the context of WiMAX system. An assessment of the WiMAX receiver complexity and a comparison between different MIMO profiles were done.

Capacity-approaching FEC codes, usually present in the communication chain, achieve desired performance on a specific target SNR, in the low to moderate SNR range. Besides, conventional STBC design criteria target high SNRs and therefore are not necessarily efficient to design STBC for coded MIMO systems. To solve this problem, we proposed a new STBC design criterion based on the BMI maximization between transmitted and detected bits at a specific SNR. After the validation of the BMI criterion, we optimized several flexible STBCs according to the proposed criterion. We discovered that their design parameters are SNR-dependent, leading to the construction of adaptive STBCs. Adaptive matrix D STBC can be a good choice trading off performance and ML-detection complexity. Furthermore, we proposed the adaptive TO STBC which overcomes or matches the BMI offered by conventional STBCs. We gave a method to select the suitable design parameter for adaptive STBCs in the context of closed-loop and open-loop coded MIMO systems. The superiority of the adaptive TO STBC has been proved by BER simulations for 4-QAM and 16-QAM modulations. Thereafter, we discussed the case of higher order modulations as 64-QAM modulation.

The proposal of adaptive STBCs is important for practical coded MIMO systems especially those with adaptive modulation and coding *e.g.*, WiMAX, DVB, WiFi, HSPA+, as the appropriate design parameter is used with each coding rate, modulation order and E_b/N_0 . On the contrary, the use of a non-adaptive STBC like the well-known Golden code [BRV05], increases the MIMO detection complexity and alters the performance of terminals for low coding rate profiles. In addition, the use of the spatial multiplexing scheme [WFGV98] alters the performance of terminals for high coding rate profiles. The adaptive TO STBC always provides the best performance without any complexity increase with respect to conventional STBCs.

Chapter 3

Effect of Spatial Correlation and Antenna Selection on Coded MIMO Systems

In Chapter 2, we have examined the improvement of standardized STBCs for coded MIMO systems. We have proven that STBC design parameters are SNR-dependent. Therefore, we have proposed the BMI criterion and designed adaptive STBCs more suitable for coded MIMO systems.

In this chapter, we consider two independent issues encountered while designing coded MIMO systems. The chapter is split into two separate parts.

Until now, we have considered an uncorrelated Rayleigh MIMO channel. In the first part of this chapter, we examine the effect of the correlation between transmit and/or receive antennas on coded MIMO system performance and STBC design. The effect of spatial correlation on the MIMO channel capacity has been widely studied in the literature [Loy01, GSsS⁺03, RV05]. However, the effect of the spatial correlation on the performance and design of STBCs for coded MIMO systems is still to be addressed. Motivated by taking further steps towards practical systems, we extend our work presented in Chapter 2 to the case of correlated channels. In Section 3.1.1, the spatial correlated channel model is provided. Then, in Section 3.1.2, we investigate the effect of spatial correlation on the transmitter side, receiver side and both transmitter receiver based on a BMI study. Adaptive STBCs for spatially correlated channels are designed in Section 3.1.3. Recently, a new MIMO code called enhanced spatial multiplexing (eSM) has been proposed in [MKV⁺12] for full spatial correlation channels *i.e.*, when antennas are fully correlated. The eSM scheme is adopted for rate-2 transmission in the DVB-NGH standard. To serve as reference, the eSM scheme is presented in Section 3.1.4. Finally, BER curves are provided.

In the second part, we examine coded MIMO systems using more than dual transmit antennas. In order to limit the system complexity increase, we consider that an *antenna selection* (AS) is performed where the transmission is only done via selected best antennas. The AS technology is widely studied in the literature [WW99, NGP00, GP01, MW04]. However, previous works do not consider the existence of capacity-approaching FEC in the communication chain. Our work aims to assess the AS gains for coded MIMO systems. In Section 3.2.1, the system model, the AS algorithm and BER curves for the system without a FEC code are provided. In Section 3.2.3, adaptive STBCs are designed for MIMO systems employing the AS technology. Their BER curves are also provided in Section 3.2.4.

3.1 Effect of Spatial Correlation on Coded MIMO Systems

Until now, we have considered that antennas at transmitter and receiver sides were perfectly uncorrelated. This assumption is not always valid and largely depends on the communication environment *e.g.*, in indoor case. Furthermore, to ensure uncorrelated antennas, the spacing between them have to be greater than the half-wavelength $\lambda/2$ [WSG94, BEFN04]. In practice it is not always possible to space antennas far away from each others due to physical constraints. A high spatial correlation coefficient can be measured for small devices like mobile phones [BP12]. In the sequel, we examine the effect of spatial correlation on the system presented in Chapter 2. Also, we design adaptive STBCs for the coded system with spatial correlation between antennas.

3.1.1 Modeling Spatially Correlated Channels

Like in Chapter 2 we consider a coded MIMO system using an 8-state double binary turbo code concatenated with 2×2 MIMO codes. However, the channel is now assumed to be a *spatially correlated* quasi-static flat Rayleigh fading channel where transmit and/or receive antennas are correlated.

The MIMO spatially correlated Rayleigh channel is modeled by the matrix \mathbf{H} which can be factorized as

$$\mathbf{H} = \mathbf{R}_{\text{Rx}}^{1/2} \mathbf{H}_w \mathbf{R}_{\text{Tx}}^{1/2H} \quad (3.1)$$

where \mathbf{R}_{Rx} and \mathbf{R}_{Tx} are the $N_r \times N_r$ and $N_t \times N_t$ correlation matrices at the receiver and the transmitter respectively and $\mathbf{R}_{\text{Rx}}^{1/2}$ and $\mathbf{R}_{\text{Tx}}^{1/2}$ are computed by Cholesky factorization.

The correlation model is assumed to be exponential [Loy01]. The correlation matrix is constructed by a single coefficient and the correlation between antennas decreases exponentially with the distance between them. According to this model, the correlation matrices at the transmitter and the receiver sides are given, for a 2×2 MIMO system, by

$$\mathbf{R}_{\text{Tx}} = \begin{bmatrix} 1 & \rho_t \\ \rho_t^* & 1 \end{bmatrix} \quad (3.2)$$

$$\mathbf{R}_{\text{Rx}} = \begin{bmatrix} 1 & \rho_r \\ \rho_r^* & 1 \end{bmatrix} \quad (3.3)$$

where ρ_t and ρ_r are the correlation coefficients of neighboring transmit and receive antennas respectively ($0 \leq |\rho_t|, |\rho_r| \leq 1$).

3.1.2 BMI Study of the Effect of Spatial Correlation

In order to assess the effect of the correlation on coded MIMO systems, we have computed the BMI of the presented MIMO profiles *i.e.*, the Alamouti code, the spatial

multiplexing code and the Golden code, as a function of E_{bu}/N_0 for several correlation coefficients ρ_t and ρ_r . A M -QAM modulation is considered for the FR profiles and M^2 -QAM modulation for the Alamouti code in order to have the same spectral efficiency. We have found that the effect of spatial correlation differs depending on the used MIMO code and the correlation type. Also, we have designed adaptive MD and TO STBCs for each correlation value. In the sequel, to be concise, we only give the conclusions of our BMI study. BER simulations are provided in Section 3.1.5 and designed adaptive STBCs for the simulated cases are explicitly provided in Section 3.1.3.

Depending on the correlation type, several conclusions are obtained:

3.1.2.1 Correlation between Transmit Antennas

- An adaptive MD STBC can be always designed for all ρ_t in a way overcoming or matching the BMI of the original MD.
- At low to moderate correlations *e.g.*, $0 < |\rho_t| < 0.6$ for $M = 4$, an adaptive TO STBC can be always designed in a way providing the highest BMI with respect to conventional STBCs.
- The Alamouti code offers the highest BMI at high correlations *e.g.*, $0.6 < |\rho_t| < 1$ for $M = 4$.
- At very high correlations *e.g.*, $0.8 < |\rho_t| < 1$ for $M = 4$, the SM scheme has a BMI far from the one of FD STBCs leading to a performance loss with respect to other MIMO profiles. On the other hand, the trace-orthonormal with the value of $\theta = 45^\circ$ or $\mathbf{X}_{\theta=45^\circ}^{\text{TO}}$ is better than the SM scheme especially with high FEC coding rates R_c . In Section 2.5.2, we have proved that both codes have the same ML-detection complexity order.

3.1.2.2 Correlation between Receive Antennas

- An adaptive MD STBC can be always designed for all ρ_r in a way overcoming or matching the BMI of the original MD.
- At low to moderate correlations *e.g.*, $0 < |\rho_r| < 0.6$ for $M = 4$, an adaptive TO STBC can be always designed in a way providing the highest BMI with respect to conventional STBCs.
- The Alamouti code offers the highest BMI at high correlations *e.g.*, $0.6 < |\rho_r| < 1$ for $M = 4$.
- The $\mathbf{X}_{\theta=45^\circ}^{\text{TO}}$ code is always equivalent to the SM scheme.

3.1.2.3 Correlation between both Transmit and Receive Antennas

The same correlation value is assumed at the transmitter and the receiver *i.e.* $\rho_t = \rho_r$. A typical example of this case is a communication between two devices with similar physical environment and dimensions. For this case:

- An adaptive MD STBC can be always designed for all ρ_r, ρ_t in a way overcoming or matching the BMI of the original MD.
- At low correlations *e.g.*, $0 < \rho_t = \rho_r < 0.4$ for $M = 4$, an adaptive TO STBC can be always designed in a way providing the highest BMI with respect to conventional STBCs.
- The Alamouti code offers the highest BMI at moderate to high correlations *e.g.*, $0.4 < |\rho_t| = |\rho_r| < 1$ for $M = 4$.
- At very high correlations, the SM scheme has a BMI far from the one of FD STBCs while the $\mathbf{X}_{\theta=45^\circ}^{\text{TO}}$ preserves a BMI comparable to the one of FD profiles.

3.1.2.4 Discussion on the Obtained Results

The BMI study shows that the Alamouti code is more resistant against high correlations than other MIMO codes. This superiority is obtained thanks to its orthogonality property. As shown in Section 1.4.3.1, under the assumption of a perfect CSI knowledge at the receiver, the ML-detector estimates the transmitted symbols S_1 and S_2 using

$$\begin{aligned}\hat{S}_1 &= h_{11}^* r_{11} + h_{12} r_{12}^* + h_{21}^* r_{21} + h_{22} r_{22}^* \\ &= (|h_{11}|^2 + |h_{12}|^2 + |h_{21}|^2 + |h_{22}|^2) S_1 + \eta_1\end{aligned}\quad (3.4)$$

$$\begin{aligned}\hat{S}_2 &= h_{12}^* r_{11} - h_{11} r_{12}^* + h_{22}^* r_{21} - h_{21} r_{22}^* \\ &= (|h_{11}|^2 + |h_{12}|^2 + |h_{21}|^2 + |h_{22}|^2) S_2 + \eta_2\end{aligned}\quad (3.5)$$

Here, h_{ij} are the coefficients of the matrix $\mathbf{H} = \mathbf{R}_{\text{Rx}}^{1/2} \mathbf{H}_w \mathbf{R}_{\text{Tx}}^{1/2H}$. Therefore, the spatial correlation does not affect the estimation of transmitted symbols and every symbol is estimated independently of the others. The spatial correlation is equivalent to a SNR loss for this case.

Furthermore, the presented FR-FD STBCs have the non-vanishing determinant property [BRV05, SS07, ZLW07]. This property guarantees a separation between the STBC layers transmitted on the N_t antennas during one channel use period. Therefore, the constellation of transmitted symbols on the N_t antennas does not overlap due to transmit correlation and FR-FD STBCs work relatively well over correlated channels.

On the other hand, the SM scheme is shown to be weak against high spatial correlation, especially at the transmitter side, leading to an important performance loss. This

loss is caused by the fact that, according to the SM scheme, the same constellation is transmitted on the N_t antennas during one channel use period, and transmitted symbols overlap under fully spatial correlation between transmit antennas [MKV⁺12]. In return, as proved in Section 2.5.2.2, constellations of transmitted symbols according to the $\mathbf{X}_{\theta=45^\circ}^{\text{TO}}$ code are mutually phase-shifted by $\frac{\pi}{4}$, preventing this overlap. In [MKV⁺12], the *enhanced spatial multiplexing* (eSM) has been introduced for fully correlated channels where a rotation matrix is used as a precoding matrix for the SM scheme. The eSM is adopted as technical baseline for the DVB-NGH system.

In the sequel, we only consider the correlation on the transmitter side as its effect varies depending on the used MIMO code. On the other hand, the correlation on the receiver side can be seen as an SNR loss for all MIMO codes.

3.1.3 Adaptive TO STBC Design for Spatially Correlated Systems

Depending on the correlation value, adaptive STBCs can be designed according to the BMI criterion. For every transmit correlation ρ_t , we designed an adaptive TO code. The adaptive TO design parameter is denoted by $\theta_{\rho_t}^{M\text{-QAM}}$. In order to confirm our results obtained based on the BMI study in Section 3.1.2, we provide BER simulations in Section 3.1.5 for a low correlation as ρ_t equal to 0.3 and a high correlation as ρ_t equal to 0.7. In this Section, we explicitly provide the designed adaptive TO STBCs for simulated cases.

For a low correlation $\rho_t = 0.3$, the adaptive TO parameter is computed by

$$\theta_{\rho_t=0.3}^{4\text{-QAM}} = \begin{cases} 45^\circ; & \text{For } E_{bu}/N_0 \leq 0.25 \text{ dB} \\ -0.25 \left(\frac{E_{bu}}{N_0}\right)^3 + 3.37 \left(\frac{E_{bu}}{N_0}\right)^2 - 17.47 \left(\frac{E_{bu}}{N_0}\right) \\ \quad + 48.14; & \text{For } 0.25 < E_{bu}/N_0 < 5 \text{ dB} \\ 13.28^\circ; & \text{For } E_{bu}/N_0 \geq 5 \text{ dB} \end{cases} \quad (3.6)$$

And for a high correlation $\rho_t = 0.7$, $\theta_{\rho_t=0.7}^{4\text{-QAM}}$ is given by

$$\theta_{\rho_t=0.7}^{4\text{-QAM}} = \begin{cases} 45^\circ; & \text{For } E_{bu}/N_0 \leq 1.25 \text{ dB} \\ -0.39 \left(\frac{E_{bu}}{N_0}\right)^3 + 5.91 \left(\frac{E_{bu}}{N_0}\right)^2 - 30.8 \left(\frac{E_{bu}}{N_0}\right) \\ \quad + 76.14; & \text{For } 1.25 < E_{bu}/N_0 < 5.5 \text{ dB} \\ 13.28^\circ; & \text{For } E_{bu}/N_0 \geq 5.5 \text{ dB} \end{cases} \quad (3.7)$$

3.1.4 Enhanced Spatial Multiplexing Scheme

In [MKV⁺12], authors have proposed the enhanced spatial multiplexing (eSM) MIMO code. In this section, we present the eSM scheme then optimize its design parameter

according to the BMI criterion. Authors in [MKV⁺12] target to combine merits of both SM in terms of complexity and GC in terms of performance. High priority was put on the performance under full channel correlation *i.e.*, $\rho_t = 1$. A rotation matrix with angle Θ serves as a precoding matrix for the SM scheme. In the DVB-NGH standard, a phase hopping technique is adopted [PM10]. This technique periodically changes the phase of symbols transmitted by one of two antennas within one FEC frame. Moreover, a power imbalance between the two transmit antennas is supported. The power control is possible before and after the eSM encoding. Different sizes of QAM constellation can also be used to minimize the loss caused by the power imbalance. In [MKV⁺12], optimization parameters were found by simulations.

The resulting structure adopted for rate-2 MIMO in the DVB-NGH standard is:

$$\mathbf{X}^{\text{eSM}} = \begin{bmatrix} 1 & 0 \\ 0 & e^{j\phi(q)} \end{bmatrix} \begin{bmatrix} \sqrt{\beta} & 0 \\ 0 & \sqrt{1-\beta} \end{bmatrix} \begin{bmatrix} \cos \Theta & \sin \Theta \\ \sin \Theta & -\cos \Theta \end{bmatrix} \begin{bmatrix} \sqrt{\alpha} & 0 \\ 0 & \sqrt{1-\alpha} \end{bmatrix} \begin{bmatrix} S_1 \\ S_2 \end{bmatrix} \quad (3.8)$$

where $\phi(q)$ is the angle for phase hopping, Θ is the rotation angle for eSM precoding matrix, α and β are the power imbalance factor before and after eSM precoding.

Different parameters are obtained depending on the size of the constellation and the power imbalance between antennas. In [MKV⁺12], the eSM code is not defined when both S_1 and S_2 belong to the 4-QAM modulation. In order to compare the eSM with our proposed code we consider an equal power transmission across the two transmit antennas *i.e.*, $\alpha = \beta = \frac{1}{2}$, no phase hopping *i.e.*, $\phi(q) = 0$ and a 16-QAM modulation for both symbols S_1 and S_2 . For this case, and whatever is the correlation coefficient, $\Theta = \arctan\left(\frac{\sqrt{2+4}}{\sqrt{2+2}}\right)$ [MKV⁺12], and the eSM code is equivalent to a rotated SM code defined as

$$\mathbf{X}^{\text{eSM}} = \begin{bmatrix} \cos \Theta & \sin \Theta \\ \sin \Theta & -\cos \Theta \end{bmatrix} \begin{bmatrix} S_1 \\ S_2 \end{bmatrix} \quad (3.9)$$

For low correlations, the BMI offered by the eSM scheme is identical to the one offered by the conventional SM scheme. Indeed, under uncorrelated condition, similarly to the case of $\mathbf{X}_{\theta=45^\circ}^{\text{TO}}$ code, the rotation of the SM scheme does not provide any additional gain with respect to the unrotated case.

The eSM is proposed for a broadcast transmission. Therefore, we propose to optimize its design parameter, as already done in Section 2.6.4 for open-loop systems, for each rate R_c according to the BMI criterion with symbols belong to a 16-QAM modulation. At low correlations, the same BMI, equal to the one of the SM, is obtained for all Θ . At $\rho_t = 0.7$, the obtained rotation angle is $\Theta = \pi/4$ with $R_c = 1/2$ and $\Theta = \arctan\left(\frac{\sqrt{2+4}}{\sqrt{2+2}}\right)$ with $R_c = 2/3$ and $5/6$. At very high and full correlations, the BMI criterion provides the same rotation angle as the one obtained in [MKV⁺12] *i.e.*, $\Theta = \arctan\left(\frac{\sqrt{2+4}}{\sqrt{2+2}}\right)$ with all

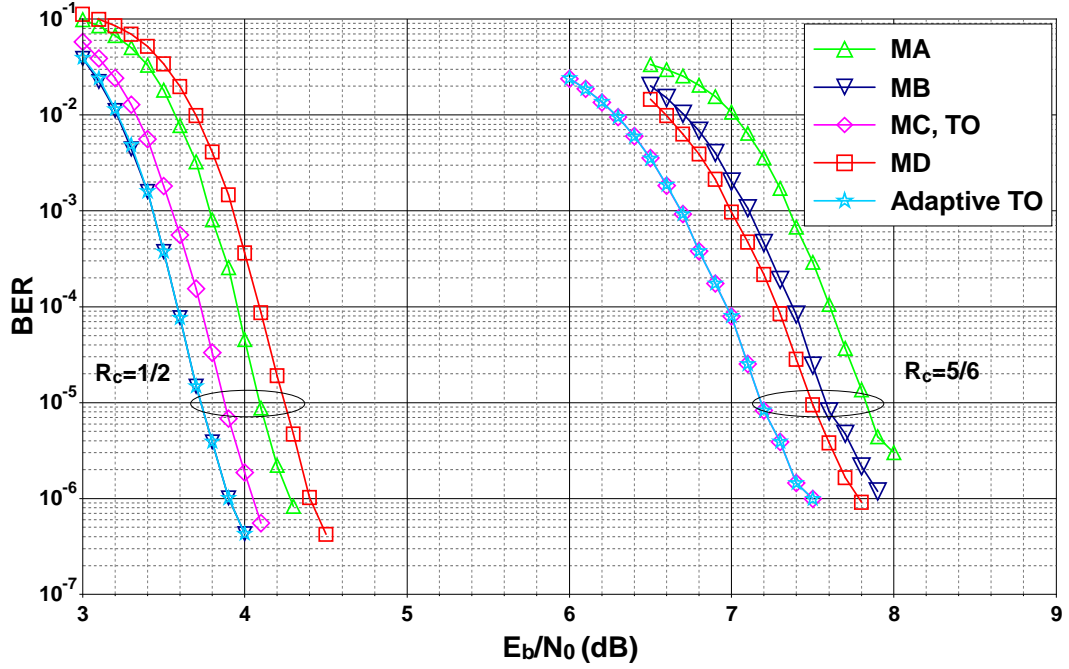


FIGURE 3.1: BER of turbo coded system; 8-state double binary turbo code with 8 turbo decoding iterations and information frame size $k = 4,800$ bits; MIMO profiles: Alamouti code (MA) with 16-QAM modulation and spatial multiplexing (MB), Golden code (MC) & original TO, Matrix D (MD) and adaptive TO with 4-QAM modulation; quasi-static flat correlated Rayleigh fading MIMO channel with $\rho_t = 0.3$.

rates $R_c = 1/2, = 2/3$ and $= 5/6$. For coded MIMO transmissions, the optimization of Θ according to the BMI criterion is more efficient than the criteria used in [MKV⁺12], as the suitable Θ is always selected. This result is confirmed by BER simulations provided in Section 3.1.6.

3.1.5 BER Performance of the Proposed Adaptive STBCs

In the sequel, we provide the BER of the presented and adaptive 2×2 MIMO codes at low and high transmit correlations *e.g.*, $\rho_t = 0.3$ and $\rho_t = 0.7$. As a reference, we consider the case of the system without correlation *i.e.*, $\rho_t = \rho_r = 0$ depicted in Figure 2.15. BER curves are evaluated after 8 turbo decoding iterations as a function of E_b/N_0 for a transmission over a quasi-static correlated Rayleigh fading MIMO channel. A random BICM interleaver is used. The number of transmit antennas is $N_t = 2$ and receive antennas is $N_r = 2$. A BER equal to 10^{-5} is targeted.

3.1.5.1 Low Transmit Correlation

Figure 3.1 depicts the BER for the case of low transmit correlation with $\rho_t = 0.3$. For $R_c = 1/2$, the MB code matches the adaptive TO code, a gain of almost 0.1 dB is obtained with respect to the MC code, 0.3 dB with respect to MA code and 0.4 with

respect to the MD code. For $R_c = 5/6$, the MC code matches the adaptive TO code, while a gain of 0.3 is observed compared to the MD code, 0.4 dB compared to the MB code and 0.65 dB compared to MA code.

The comparison between BER curves for the uncorrelated case depicted in Figure 2.15 and low correlation case depicted in Figure 3.1, shows that the low correlation is equivalent to a simple SNR loss, equal to 0.1 dB for $R_c = 1/2$ and 0.15 dB $R_c = 5/6$.

Figure 3.1 confirms the results obtained in Section 3.1.2 using the BMI study. For low correlations, as for uncorrelated case, the adaptive TO STBC always provides the best performance for all coding rates.

3.1.5.2 High Transmit Correlation

Figure 3.2 depicts the BER for the case of high transmit correlation with $\rho_t = 0.7$. For $R_c = 1/2$, the MA code surpasses all the presented codes, with a gain of 0.4 dB with respect to the MB and adaptive TO, 0.5 dB with respect to the MC and 0.8 dB with respect to the MD. For $R_c = 2/3$, the MA code also surpasses all the presented codes, with a gain of 0.25 dB with respect to the MC and adaptive TO, 0.4 dB with respect to the MB and 0.5 dB with respect to the MD. For $R_c = 5/6$, the MC code matches the adaptive TO code, while a gain of 0.1 dB is observed compared to the MA code, 0.3 dB compared to the MD code, and 0.6 dB with respect to the MB code.

For high correlations, the obtained performance largely depends on the MIMO code structure.

3.1.6 BER Performance of the Enhanced Spatial Multiplexing Scheme

In this section, we assess the performance of the eSM scheme, designed in [MKV⁺12] for a full correlation channel. It is to be noted that the eSM scheme provides the same performance as the conventional SM scheme at low correlations. Thus, we present the eSM performance at high transmit correlation like $\rho_t = 0.7$ and full transmit correlation *i.e.*, $\rho_t = 1$.

The complexity is an important issue for practical communication systems. In addition to the eSM scheme, we consider the SM and the $\mathbf{X}_{\theta=45^\circ}^{\text{TO}}$ schemes as they have the same detection complexity order as the eSM scheme, equal to $\mathcal{O}(M^2)$. Also, we consider the Alamouti code with symbols belonging to a M^2 -QAM constellation in order to compare all codes at the same spectral efficiency. Therefore, the Alamouti code has the same complexity order as the other profiles. In our simulations, a 16-QAM modulation is adopted for FR profiles and a 256-QAM modulation is used for the Alamouti code.

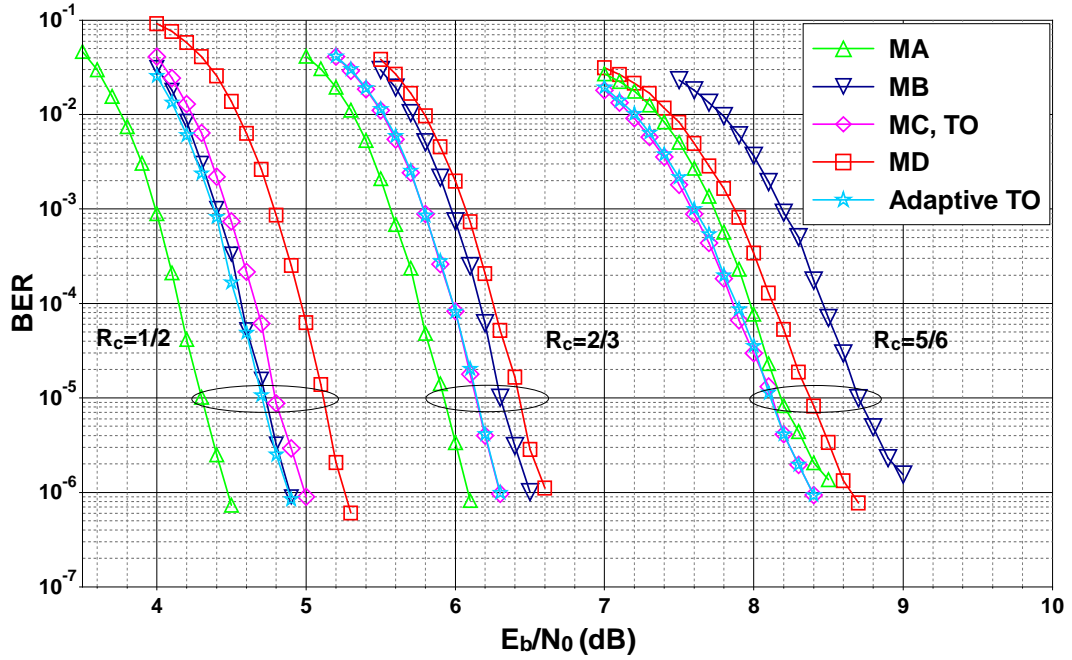


FIGURE 3.2: BER of turbo coded system; 8-state double binary turbo code with 8 turbo decoding iterations and information frame size $k = 4,800$ bits; MIMO profiles: Alamouti code (MA) with 16-QAM modulation and spatial multiplexing (MB), Golden code (MC) & original TO, Matrix D (MD) and adaptive TO with 4-QAM modulation; quasi-static flat correlated Rayleigh fading MIMO channel with $\rho_t = 0.7$.

3.1.6.1 High Transmit Correlation

Figure 3.3 depicts the BER performance of the considered codes for the case of $\rho_t = 0.7$ with coding rates $R_c = 1/2$ and $R_c = 5/6$. It shows that the eSM structure is more resistant against high correlations with respect to the other profiles. The $\mathbf{X}_{\theta=45^\circ}^{\text{TO}}$ is equivalent to the SM scheme. The Alamouti code has the worse performance among the presented codes as its symbols belong to the 256-QAM modulation. The eSM optimized according to the BMI criterion is shown to offer the best performance. At $R_c = 1/2$, a gain of 0.2 dB is obtained with respect to the original eSM scheme, 1 dB with respect to the SM scheme and $\mathbf{X}_{\theta=45^\circ}^{\text{TO}}$ and 1.6 dB with respect to the Alamouti code. At $R_c = 5/6$, both eSM schemes are equivalent while overcoming the SM and $\mathbf{X}_{\theta=45^\circ}^{\text{TO}}$ codes by 0.2 dB and the Alamouti code by 2.4 dB.

3.1.6.2 Full Transmit Correlation

Figure 3.4 depicts the BER performance for the full correlation case *i.e.*, $\rho_t = 1$ with a coding rate $R_c = 1/2$. It shows that the SM scheme has the worst performance. Also, it shows that the Alamouti code offers the best performance even though its symbols belong to the 256-QAM constellation. The Alamouti code overcomes the eSM code by 0.9 dB, the $\mathbf{X}_{\theta=45^\circ}^{\text{TO}}$ code by 5.8 dB and the SM code by 9 dB.

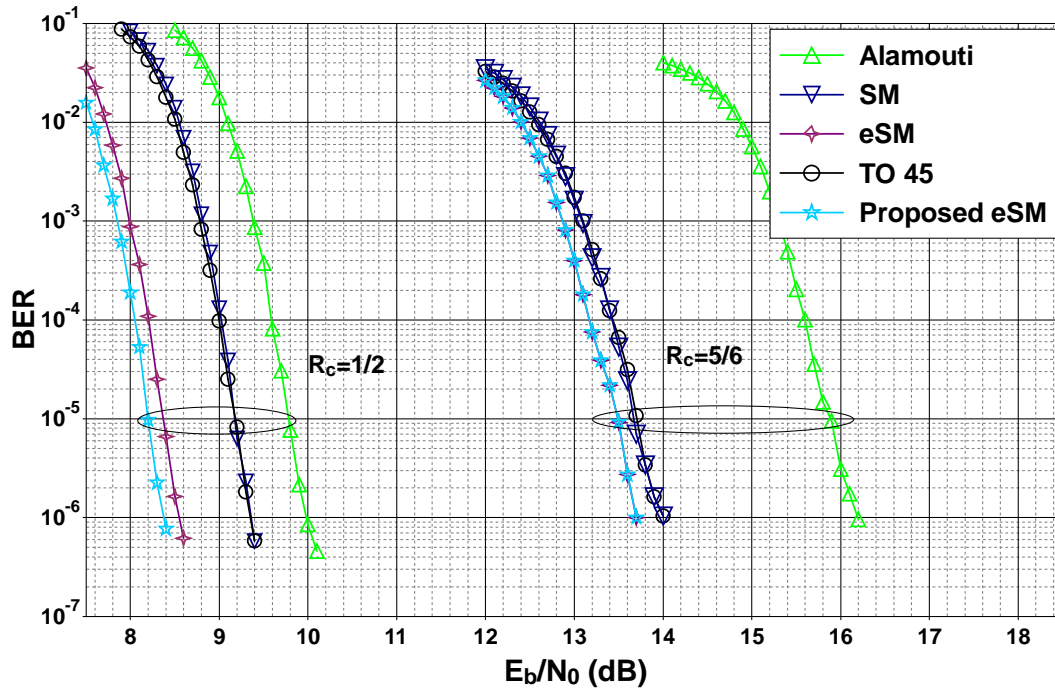


FIGURE 3.3: BER of turbo coded system; 8-state double binary turbo code with 8 turbo decoding iterations and information frame size $k = 4,800$ bits; MIMO profiles: Alamouti code with 256-QAM modulation and spatial multiplexing (SM), $\mathbf{X}_{\theta=45^\circ}^{\text{TO}}$ (TO 45), enhanced spatial multiplexing (eSM) [MKV⁺12], proposed eSM with 16-QAM modulation; quasi-static flat correlated Rayleigh fading MIMO channel with $\rho_t = 0.7$.

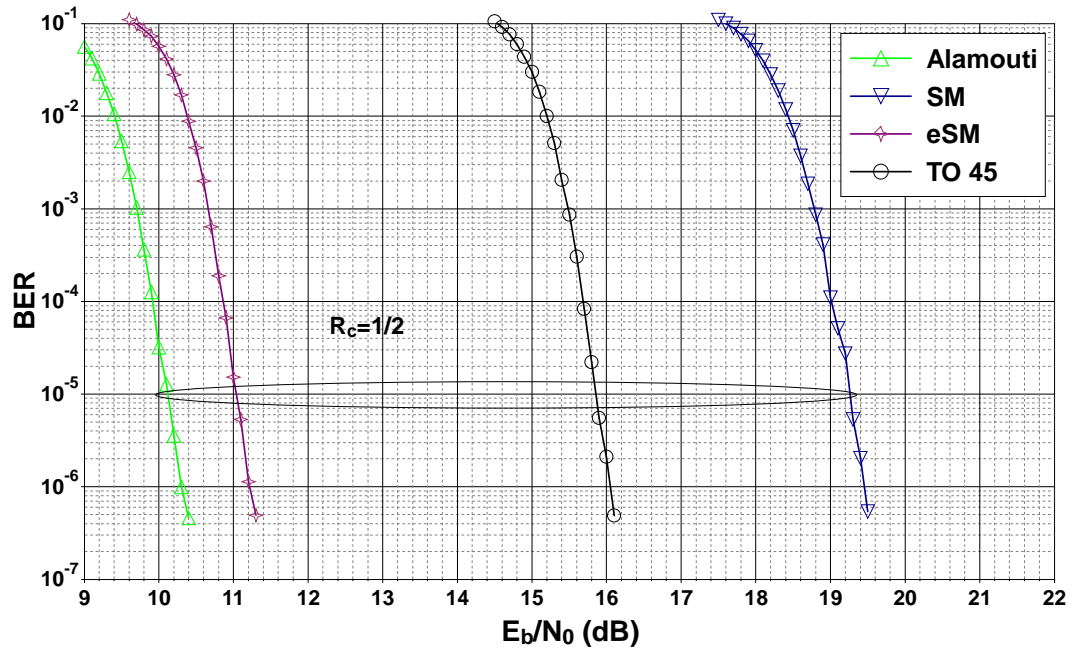


FIGURE 3.4: BER of turbo coded system; 8-state double binary turbo code ($R_c = 1/2$) with 8 turbo decoding iterations and information frame size $k = 4,800$ bits; MIMO profiles: Alamouti code with 256-QAM modulation and spatial multiplexing (SM), $\mathbf{X}_{\theta=45^\circ}^{\text{TO}}$ (TO 45), enhanced spatial multiplexing (eSM) [MKV⁺12] with 16-QAM modulation; quasi-static flat correlated Rayleigh fading MIMO channel with $\rho_t = 1$.

As stated in Section 3.1.2, the SM scheme is weak against full correlation due to the overlapping of its symbol and the Alamouti code is resistant against correlations thanks to its orthogonality property. Also, the eSM scheme preserves a good performance as it is designed for a full correlation case. We recall that the BMI optimization of the eSM for full correlation gives the same angle as the original eSM. The $\mathbf{X}_{\theta=45^\circ}^{\text{TO}}$ code is better than the SM code due to the rotation between the constellation of its transmitted symbols.

3.1.7 Conclusions on the Effect of Spatial Correlation

In this part, we study the effect of spatial correlation on coded MIMO systems. We showed that low correlations are equivalent to a SNR loss with respect to uncorrelated case. The adaptive TO STBC always provides the best performance at low correlations.

On the other hand, at high correlations, the performance largely depends on the correlation value and the MIMO code structure. The choice of the suitable MIMO code is not obvious and requires further information on the communication environment (correlation value, code rates R_c , modulation order M). Fortunately, the BMI can be used as a tool to classify and select the suitable MIMO code.

3.2 Antenna Selection for Coded MIMO Systems

In our previous works, we have examined the improvement of standardized STBCs for coded MIMO systems with dual antennas at transmitter and receiver sides. Telecommunication standards define the use of more than dual antennas *e.g.*, up to 4×4 for the WiMAX and 8×8 for the LTE-A [SOZ11]. In contrast, the use of MIMO techniques lead to a complexity and cost increase with respect to SISO systems at both transmitter and receiver sides. Transmitting on multiple antennas require multiple analog *radio-frequency* (RF) chains which comprise expensive hardware blocks. The implementation of a high number of RF chains is not always possible due to physical and economic constraints *e.g.*, small handsets. Furthermore, the detection complexity of transmitted signals increases with the number of transmit antennas for a full-rate transmission (see Section 1.4.3.1).

Antenna selection techniques have been proposed as a means to benefit from expected MIMO gains with tolerable cost and complexity [WW99, NGP00, GP01, MW04]. Here, transmission and reception is performed only through a subset of the available antennas, thereby reducing the system complexity and the number of required RF chains. In our work, we focus on AS at the transmitter side. Indeed, AS at the receiver side is not recommended as it can lead to a considerable reduction in the system capacity. Transmit AS is a good approach to benefit from MIMO system gains with low cost and complexity [WLB09].

For a MIMO system employing the AS technology, it has been shown that FD STBCs like the Alamouti code [Ala98] can benefit from the maximal channel diversity *i.e.*, $N_t N_r$ at high SNRs [GP01]. Our work focuses on the study of the effect of transmit AS technique for practical coded MIMO communication systems *e.g.*, the WiMAX system.

We start by presenting the transmit antenna selection technology and the employed selection algorithm. Then we design efficient adaptive STBCs for coded MIMO system with AS. Afterwards, we assess the gain provided by an AS on transmit antennas, with respect to classical WiMAX coded system.

3.2.1 Transmit Antenna Selection

Again, we consider a coded MIMO system with N_t transmit antennas, N_r receive antennas operating over a quasi-static uncorrelated flat Rayleigh fading channel. In addition to the previous system, we assume that a low-rate error-free zero-delay feedback channel feeds the set of best transmit antennas to the transmitter every T channel use periods. This set is determined by a selection algorithm operating at the receiver side. Afterwards, encoder output \mathbf{X} is only transmitted via the selected best transmit antennas. The unselected transmit antennas are deactivated.

In the sequel, we denote by Ψ the set of best antennas. The cardinality ψ of the set Ψ is chosen depending on the tolerable complexity. The system transmitting over ψ selected transmit antennas of N_t is denoted by $(\psi/N_t) \times N_r$.

3.2.1.1 Antenna Selection Algorithm

In this section, we present the used selection algorithm. The channel is defined by the matrix

$$\mathbf{H} = \begin{bmatrix} h_{11} & h_{12} & \cdots & h_{1N_t} \\ h_{21} & h_{22} & \cdots & h_{2N_t} \\ \vdots & \vdots & \ddots & \vdots \\ h_{N_r1} & h_{N_r2} & \cdots & h_{N_rN_t} \end{bmatrix} \quad (3.10)$$

Depending on the channel conditions, many selection algorithms exist in the literature [WW99, NGP00, GP01, GP02]. When a STBC is used, it is clear that the best AS algorithm is done by choosing the ψ transmit antennas with highest norms [GP01, GP02, WLB09]. Every T periods, the receiver selects ψ of N_t columns as

$$\max_{j \in \{1, \dots, N_t\} - \Psi, j \leq \psi} \sum_{i=1}^{N_r} |h_{ij}|^2 \quad (3.11)$$

where Ψ is the set of already selected antennas. When $j = \psi$, the selected set Ψ is fed to the transmitter. The selection algorithm requires a computation of the channel coefficients norms $|h_{ij}|^2$ and their summation. Its complexity is $\mathcal{O}(N_t N_r)$ which is small compared to the detection complexity equal to $\mathcal{O}(M^{N_t T})$ (see Section 1.4.3.1) especially for high order modulations.

In order to assess the transmit AS gains and compare them with our previous work, we only consider the selection of dual antennas of the N_t available ones ($\psi = 2 \leq N_t$).

3.2.2 BER Curves of the Uncoded MIMO System with Transmit AS

In this section, we assess the gain obtained by transmit AS technology for MIMO systems without any FEC codes. Authors in [GP02, WLB09] have shown that the FD Alamouti code benefits from the full available channel diversity equal to $N_t N_r$. Thus, we consider other FD STBCs like the GC [BRV05] and compare its performance with the SM scheme [WFGV98].

Figure 3.5 depicts uncoded BER curves for SM scheme with dashed curves and GC with solid curves as a function of E_{bu}/N_0 with 4-QAM modulation. Dual transmit antennas are selected out of $N_t = 2, 3, 4$ and 5. The channel is assumed to be quasi-static uncorrelated flat Rayleigh fading.

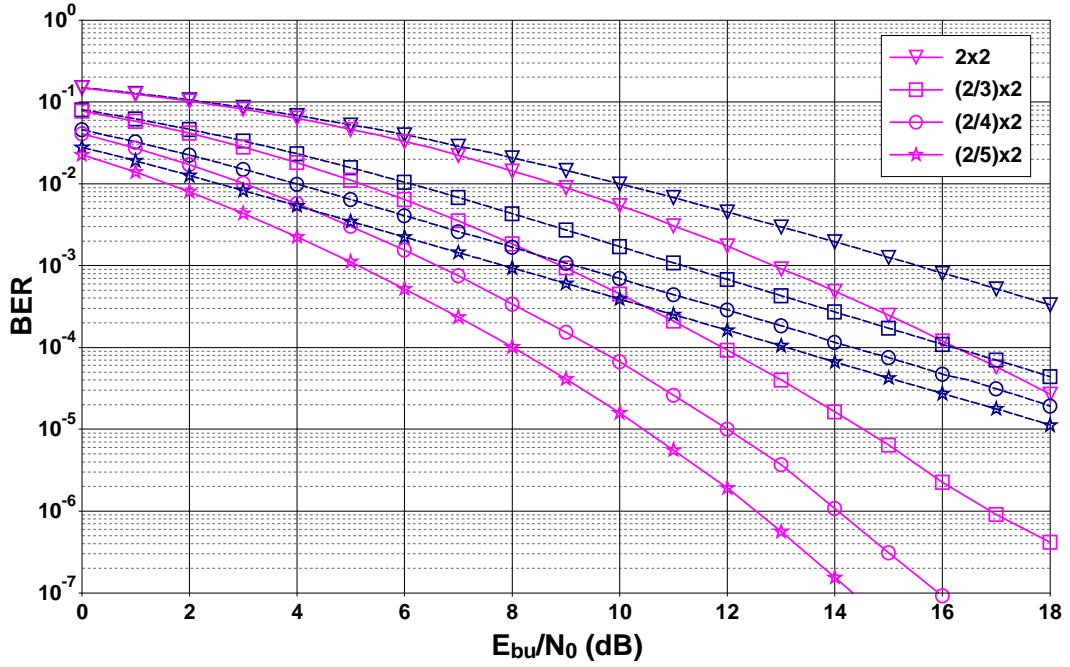


FIGURE 3.5: Uncoded BER of spatial multiplexing with dashed blue curves and Golden code with solid pink curves; dual transmit AS among $N_t = 2, 3, 4$ and 5 ; 4-QAM modulation; quasi-static uncorrelated flat Rayleigh fading MIMO channel.

Figure 3.5 shows that the FR-FD GC benefits from both diversity and SNR gains. The slope of BER curves for the GC is steeper for higher number of available transmit antennas. Indeed, the GC benefits from all the available channel diversity equal to $N_t N_r$. On the other hand, the slope of BER curves for the SM scheme remains the same. This result is expected as the SM scheme does not provide any transmit diversity. The SM scheme only benefits from SNR gains. Obtained SNR gains increase with the increase of the number of transmit antennas N_t for both MIMO codes.

At a target BER equal to 10^{-5} , the GC overcomes the SM with a gain of 7.5 dB for $(2/5) \times 2$ system. The gap between the GC and the SM increases with the SNR as the slope of BER curves for the GC is steeper than the SM one. In the sequel, we study the transmit AS gains in the context of a turbo-coded WiMAX system.

Note that [GBM09] considers transmit antenna and code selection (TACS) in the context of MIMO WiMAX systems. TACS consists of a selection, depending on the channel feedback, of best antennas and MIMO WiMAX code (MA, MB, MC) to be used for transmission. A similarity between [GBM09] and our work exists, as we select also the best antennas and the parameter of adaptive STBCs based on the channel feedback. In contrast, an uncoded WiMAX system is considered in [GBM09] and symbols are estimated based on a MMSE equalizer. Even if we consider their approach for coded WiMAX system and use a ML-detector, our approach provides better performance. Indeed, depending on the parameter value, the adaptive TO STBC can transmit based

on MB or MC codes (see Section 2.5.2.2) and it overcomes both in some case which makes our approach more suitable for coded MIMO systems.

3.2.3 Transmit AS for Coded MIMO systems: Adaptive STBCs design

Following the method proposed in Section 2.5, the design parameter of the presented STBCs is optimized for each $(2/N_t) \times N_r$ system, leading to the construction of adaptive MD and TO codes.

3.2.3.1 Adaptive Matrix D STBC

The parameter of adaptive MD STBC is denoted by $\varphi_{(2/N_t) \times N_r}^{M\text{-QAM}}$. For 4-QAM modulation, the adaptive MD design parameter is computed for $(2/3) \times 2$ by

$$\varphi_{(2/3) \times 2}^{4\text{-QAM}} = \begin{cases} 135^\circ; \text{ For } E_{bu}/N_0 \leq 2 \text{ dB} \\ -2.43 \left(\frac{E_{bu}}{N_0} \right)^3 + 26.06 \left(\frac{E_{bu}}{N_0} \right)^2 - 95.17 \left(\frac{E_{bu}}{N_0} \right) \\ + 240; \text{ For } 2 < E_{bu}/N_0 < 4.75 \text{ dB} \\ 114.29^\circ; \text{ For } E_{bu}/N_0 \geq 4.75 \text{ dB} \end{cases} \quad (3.12)$$

And for $(2/5) \times 2$ by

$$\varphi_{(2/5) \times 2}^{4\text{-QAM}} = \begin{cases} 135^\circ; \text{ For } E_{bu}/N_0 \leq -1.5 \text{ dB} \\ -7.27 \left(\frac{E_{bu}}{N_0} \right)^3 - 10.29 \left(\frac{E_{bu}}{N_0} \right)^2 - 10.38 \left(\frac{E_{bu}}{N_0} \right) \\ + 118.32; \text{ For } -1.5 < E_{bu}/N_0 < 0.25 \text{ dB} \\ 114.29^\circ; \text{ For } E_{bu}/N_0 \geq 0.25 \text{ dB} \end{cases} \quad (3.13)$$

The same optimization can be done for each number of available transmit antennas and the suitable parameter is selected. Based on the MD STBC structure, a low complexity ML-detection adaptive STBC can be always designed for coded $(2/N_t) \times N_r$ MIMO systems.

3.2.3.2 Adaptive Trace-Orthonormal STBC

Similarly, the suitable design parameter is selected for the adaptive TO STBC and denoted by $\theta_{(2/N_t) \times N_r}^{M\text{-QAM}}$. For 4-QAM modulation, the adaptive TO STBC design parameter

is computed for $(2/3) \times 2$ by

$$\theta_{(2/3) \times 2}^{4\text{-QAM}} = \begin{cases} 45^\circ; & \text{For } E_{bu}/N_0 \leq -3.25 \text{ dB} \\ 0.52 \left(\frac{E_{bu}}{N_0}\right)^3 + 2.51 \left(\frac{E_{bu}}{N_0}\right)^2 - 5.74 \left(\frac{E_{bu}}{N_0}\right) \\ + 17; & \text{For } -3.25 < E_{bu}/N_0 < 0.75 \text{ dB} \\ 13.28^\circ; & \text{For } E_{bu}/N_0 \geq 0.75 \text{ dB} \end{cases} \quad (3.14)$$

And $\theta_{(2/5) \times 2}^{4\text{-QAM}}$ is given by

$$\theta_{(2/5) \times 2}^{4\text{-QAM}} = \begin{cases} 45^\circ; & \text{For } E_{bu}/N_0 \leq -5.75 \text{ dB} \\ 0.23 \left(\frac{E_{bu}}{N_0}\right)^3 + 4.85 \left(\frac{E_{bu}}{N_0}\right)^2 + 18.26 \left(\frac{E_{bu}}{N_0}\right) \\ + 32.5; & \text{For } -5.75 < E_{bu}/N_0 < -2.5 \text{ dB} \\ 13.28^\circ; & \text{For } E_{bu}/N_0 \geq -2.5 \text{ dB} \end{cases} \quad (3.15)$$

Based on the TO structure, an adaptive STBC can be designed for every $(2/N_t) \times N_r$ system. In the sequel, we only consider adaptive TO STBCs while assessing the benefits of AS for coded MIMO systems as they always provide the best performance for any $(2/N_t) \times N_r$ system.

3.2.4 BER Performance of the Coded MIMO System with Transmit AS

The same simulation conditions as in Section 2.6.3.1 are considered. The information frame size is equal to 4,800 bits. A random BICM interleaver is used. The number of receive antennas is $N_r = 2$ and the number of selected antennas is $\psi = 2$ out of $N_t = 2, 3, 5$ transmit antennas. A 4-QAM modulation is used for the FR codes and a 16-QAM modulation for the Alamouti code.

Figure 3.6 and Figure 3.7 plot the BER curves for $\psi = 2$ selected transmit antennas out of $N_t = 3$ and $N_t = 5$ available ones, respectively. The comparison between both figures shows that the AS technique does not provide any additional diversity gain as the same slope for BER curves, equal to the one for 2×2 system without AS (see Figure 2.15), is obtained at the same coding rate R_c . Indeed, the capacity-approaching FEC code achieves iterative convergence in the low SNR region where the effect of additional spatial diversity is not paramount.

Moreover, both figures confirm that adaptive STBCs are more suitable for practical communication systems since they offer the best performance for both code rates. We evaluated the gain of AS between different N_t values based on the best transmission *i.e.*, the adaptive TO STBC and at a target BER equal to 10^{-5} . Compared to the classical turbo coded 2×2 WiMAX system (see Figure 2.15), the gain of $(2/3) \times 2$ system is more

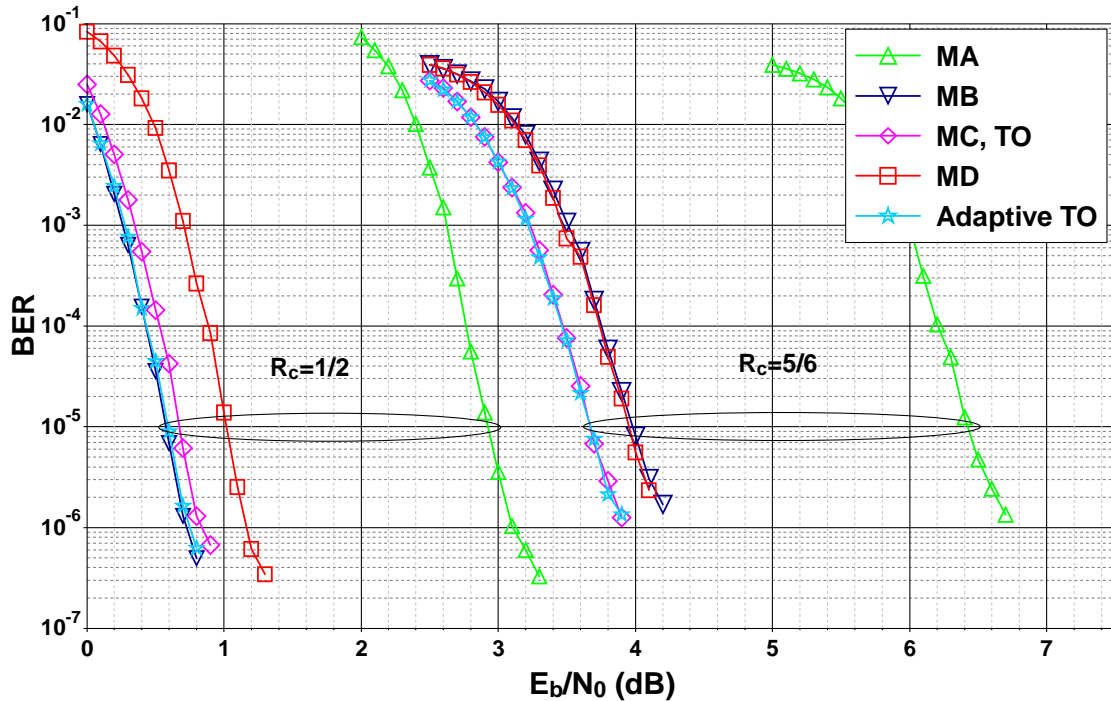


FIGURE 3.6: BER of turbo coded $(2/3) \times 2$ system; 8-state double binary turbo code ($R_c = 1/2, 5/6$) with 8 turbo decoding iterations and information frame size $k = 4,800$ bits; MIMO profiles: Alamouti code (MA) with 16-QAM modulation and spatial multiplexing (MB), Golden code (MC) & original TO, Matrix D (MD) and adaptive TO with 4-QAM modulation; quasi-static uncorrelated flat Rayleigh fading channel.

than 3 dB and the one of $(2/5) \times 2$ system is more than 6.35 dB. The AS gain is obtained due to the SNR gain. Furthermore, this SNR gain increases with the total number of transmit antennas. Table 3.1 summarizes transmit AS gains for a $(2/N_t) \times 2$ system with respect to classical turbo coded WiMAX system, for several number of antennas $N_t = 3, 4, 5$ and coding rates $R_c = 1/2, 5/6$.

The AS technique is a promising approach for coded MIMO systems as it offers a substantial SNR gain with a low additional cost and complexity increase.

MIMO system	$R_c = 1/2$	$R_c = 5/6$
$(2/3) \times 2$	3	3.4
$(2/4) \times 2$	5.1	5.4
$(2/5) \times 2$	6.35	6.8

TABLE 3.1: Transmit AS gains in dB with respect to a coded WiMAX MIMO system at a target BER = 10^{-5} .

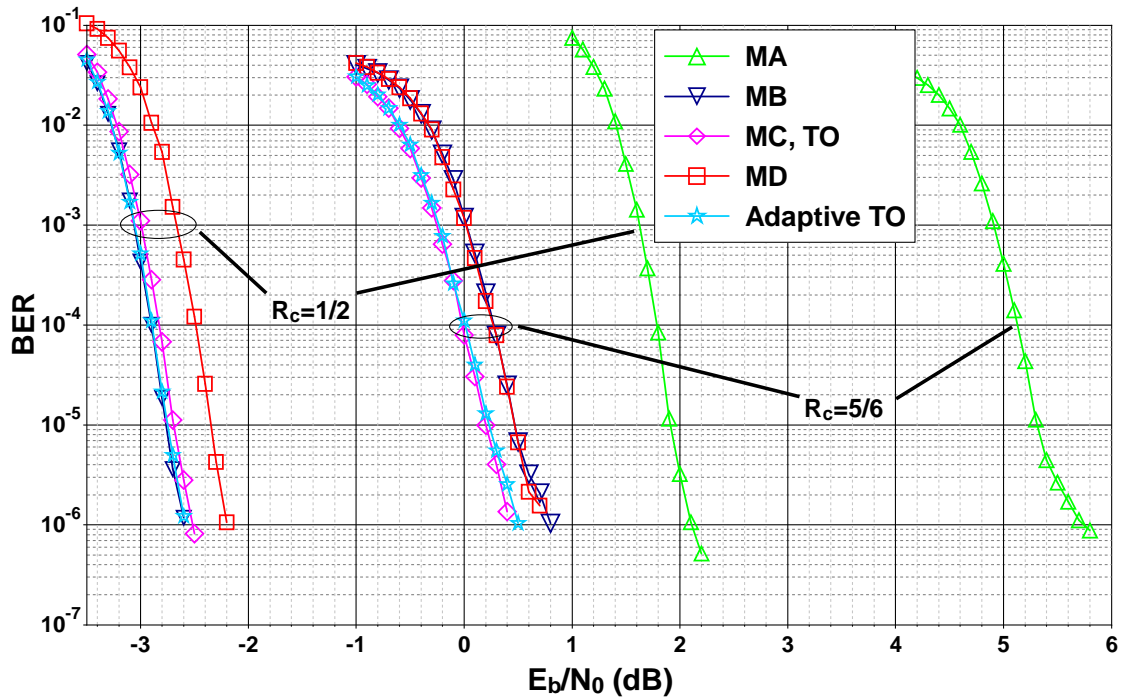


FIGURE 3.7: BER of turbo coded $(2/5) \times 2$ system; 8-state double binary turbo code ($R_c = 1/2, 5/6$) with 8 turbo decoding iterations and information frame size $k = 4,800$ bits; MIMO profiles: Alamouti code (MA) with 16-QAM modulation and spatial multiplexing (MB), Golden code (MC) & original TO, Matrix D (MD) and adaptive TO with 4-QAM modulation; quasi-static uncorrelated flat Rayleigh fading channel.

3.3 Chapter Summary

In this chapter, we investigated two independent topics encountered while designing coded MIMO systems: the effect of spatial correlation between antennas and the AS technique for MIMO systems with more than dual antennas.

In the first part, we studied the effect of spatial correlation on the performance of coded MIMO systems. We showed that the effect of low correlations is similar to an SNR loss with respect to uncorrelated systems. For this case, adaptive codes can be designed in a way providing the best performance. In contrast, high correlations can lead to a substantial degradation on system performance even for adaptive codes. This degradation differs depending on the used MIMO profile. The choice of the suitable MIMO profile for correlated channels is strongly linked to the communication environment (correlation value, coding rate, modulation order).

In the second part, we recalled the AS technology known as a technology providing MIMO gains with low cost and complexity. The performance of AS for MIMO system without powerful FEC codes is largely studied in the literature where FD STBCs can achieve the maximum diversity at high SNRs. However, coded MIMO systems operate at low to moderate SNRs. For each considered system, we have designed adaptive STBCs in a way overcoming conventional STBCs. In the context of a turbo coded WiMAX

system, we have shown that AS technology provides a significant SNR gain of more than 3 dB by simply increasing the number of available transmit antennas N_t . This gain increases with the increase of N_t . Thanks to transmit AS technology, a substantial performance improvement can be obtained for coded MIMO systems with a low cost and complexity increase.

Chapter 4

Finite-SNR Diversity-Multiplexing Tradeoff for Rayleigh MIMO Channels

The diversity-multiplexing tradeoff (DMT), formulated in [ZT03] by Zheng and Tse, represents the upper bound on the diversity gain at a multiplexing gain r achievable by any transmission over a $N_t \times N_r$ MIMO system. STBCs are conventionally designed according to rank-determinant criteria. A nonzero lower bound on the coding gain *i.e.*, a nonzero minimum determinant is a sufficient condition to reach the frontier of the asymptotic DMT [EKP⁺06, ORBV06]. In the previous chapters, we have shown that conventional STBCs designed in a way achieving the diversity-multiplexing gain tradeoff are not necessarily efficient for practical communication systems. Indeed, the DMT framework [ZT03] and rank determinant criteria [TSC98] have been developed under asymptotic conditions where the SNR tends to infinity.

Another framework has been proposed in [NEC05, Nar05, Nar06] to characterize the tradeoff between diversity and multiplexing gains at finite SNRs. This finite-SNR DMT could provide new insights to design MIMO systems optimized at operational SNRs. In section 1.3.1, we have provided the definition of conventional asymptotic multiplexing and diversity gains based on the outage probability. At high SNR ρ , the average packet error rate probability $P_e(\rho)$ is lower bounded by the outage probability at rate $R = r \log(\rho)$ *i.e.*, $P_e(\rho) \geq P_{\text{out}}(R)$ [ZT03]. At low to moderate SNR, by assuming the use of capacity-approaching FEC codes such as turbo codes or LDPC codes in the communication chain, the average packet error rate probability can be approximated by the channel outage probability as well [NEC05, Nar05, Nar06]. Therefore, Narasimhan has used the outage probability to define multiplexing and diversity gains at finite SNR. Moreover, he has mentioned that exact form of the outage probability and therefore the finite-SNR DMT for any $N_t \times N_r$ MIMO channels is not tractable. Estimates of

the finite-SNR DMT are given in [Nar05, Nar06, RHGA10] for uncorrelated, correlated Rayleigh and Rician fading $N_t \times N_r$ MIMO channels where $N_r \geq N_t$. For special cases, the exact outage probability and the finite-SNR DMT can be derived. To the best of our knowledge, the exact expression of the finite-SNR DMT is derived only for 2×2 MIMO systems in [EM07a] with uncorrelated Rayleigh fading channels and for both multiple-input single-output (MISO) and single-input multiple-output (SIMO) systems with uncorrelated [EM07b] and correlated [RHGA10] Rayleigh fading channels. Inspired from the method in [EM07a], we derive in this chapter the exact finite-SNR DMT for both uncorrelated and correlated Rayleigh fading MIMO channels with dual antennas *i.e.*, $N_t \times 2$ and $2 \times N_r$ MIMO channels.

The remainder of this chapter is organized as follows. In Section 4.1, we provide a background on finite-SNR DMT where we recall the definition of multiplexing and diversity gains at finite SNR and present this framework for orthogonal space-time block codes (OSTBCs). Afterwards, in Section 4.2, we derive the outage probability and the exact finite-SNR DMT for any transmission over uncorrelated and correlated flat Rayleigh fading channels with dual antennas. Numerical results are provided in Section 4.3.

4.1 Background on Finite-SNR DMT

Motivated by the characterization of the DMT at realistic SNRs, data rates and packet error rates, non-asymptotic definitions of multiplexing and diversity gains have been introduced in [NEC05, Nar05, Nar06]. The multiplexing gain r is defined as the ratio of the system data rate R to the capacity of an AWGN channel at SNR ρ with array gain G [Nar06]

$$r = \frac{R}{\log(1 + G\rho)} \quad (4.1)$$

The array gain is chosen such that G is equal to N_r . Its introduction is motivated by considering the MIMO mutual information I at low SNR. In the limit of $\rho \rightarrow 0$, $I \approx \log\left(1 + \frac{\rho}{N_t} \|\mathbf{H}\|_F^2\right)$. Thus, for a fair comparison of diversity and outage performance across different N_t and N_r at low to medium SNRs, the array gain G is chosen to such that $G = \frac{1}{N_t} E\left[\|\mathbf{H}\|_F^2\right] = N_r$ [Nar05]. As many researchers investigating the finite-SNR DMT, we follow these definitions in our work. We note that additional definitions of the multiplexing gain at finite SNR have been considered in [LL10].

By assuming the use of capacity-approaching channel codes in the communication chain, the probability of error is well approximated by the channel outage probability [NEC05, Nar05, Nar06]. Therefore, the diversity gain $d(r, \rho)$ of a system with a fixed multiplexing gain r at SNR ρ is defined by the negative slope of the log-log curve of

outage probability versus SNR, leading to

$$d(r, \rho) = -\frac{\partial \log P_{\text{out}}(r, \rho)}{\partial \log \rho} = -\frac{\rho}{P_{\text{out}}(r, \rho)} \frac{\partial P_{\text{out}}(r, \rho)}{\partial \rho} \quad (4.2)$$

where $P_{\text{out}}(r, \rho)$ is the outage probability as a function of the multiplexing gain r and SNR ρ . As no CSI is available at the transmitter, an equal power across transmit antennas is adopted and $P_{\text{out}}(r, \rho)$ is then defined for a given target data rate R by

$$P_{\text{out}}(r, \rho) = \Pr[I \leq R] = \Pr[I \leq r \log(1 + G\rho)]. \quad (4.3)$$

This definition of diversity gain is important for system design as the diversity gain at a particular operating SNR can be used to estimate the additional SNR required to decrease the outage probability by a specified amount, for a given data rate represented by the multiplexing gain.

Due to the fact that the exact form of the finite-SNR DMT for $N_t \times N_r$ MIMO channels is not tractable, estimates of finite-SNR DMTs are derived in [Nar06, RHGA10] for both flat Rayleigh fading and Rician fading for $N_r \geq N_t$. Moreover, an estimate of the finite-SNR DMT for the *spatial multiplexing with horizontal encoding* scheme in uncorrelated flat Rayleigh fading channel is derived in [NEC05].

On the other hand, exact finite-SNR DMT has been derived for some cases *e.g.*, for 2×2 uncorrelated flat Rayleigh fading MIMO channel in [EM07a] and for both MISO and SIMO systems with uncorrelated [EM07b] and correlated [RHGA10] flat Rayleigh fading. Moreover, exact finite-SNR DMT has been derived for OSTBCs in [NEC05] over uncorrelated flat Rayleigh fading channel and in [Nar06] over correlated flat Rayleigh fading and Rician fading channels. In the sequel, we focus on exact finite-SNR DMT. We present the derivation of exact finite-SNR DMT for OSTBCs and then we derive the exact finite-SNR DMT for systems with dual transmit and/or receive antennas. We consider both uncorrelated and correlated flat Rayleigh fading MIMO channels.

4.1.1 Finite-SNR DMT for Orthogonal Space-time Block Codes

In order to derive the finite-SNR DMT, the outage probability has to be derived. The mutual information for OSTBC with spatial code rate R_s is given by [NEC05]

$$I_{\text{OSTBC}} = R_s \log \left(1 + \frac{\rho}{N_t} \|\mathbf{H}\|_F^2 \right), \quad (4.4)$$

where R_s is the MIMO rate equal to the average number of transmitted symbols per channel use period through the N_t transmit antennas *e.g.*, $R_s = 1$ for the Alamouti code [Ala98], and $R_s = 1/2$ or $R_s = 3/4$ for the complex OSTBC given in [TJC99].

Therefore, the outage probability for OSTBC is computed as follows

$$\begin{aligned} P_{\text{out}}^{\text{OSTBC}}(r, \rho) &= \Pr [I_{\text{OSTBC}} \leq r \log(1 + G\rho)] \\ &= \Pr \left[\|\mathbf{H}\|_F^2 \leq \frac{N_t}{\rho} ((1 + G\rho)^{r/R_s} - 1) \right]. \end{aligned} \quad (4.5)$$

The distribution of $\|\mathbf{H}\|_F^2$ depends on the channel type.

For uncorrelated flat Rayleigh fading channel, $\|\mathbf{H}\|_F^2$ is gamma distributed with parameters $(N_t N_r, 1)$ [NEC05]. Therefore, $P_{\text{out,OSTBC}}^{\text{uncorr}}(r, \rho)$ is computed as follows

$$\begin{aligned} P_{\text{out,uncorr}}^{\text{OSTBC}}(r, \rho) &= \Pr \left[\|\mathbf{H}\|_F^2 \leq \frac{N_t}{\rho} ((1 + G\rho)^{r/R_s} - 1) \right]. \\ &= \frac{\gamma(N_t N_r, \frac{N_t}{\rho} ((1 + G\rho)^{r/R_s} - 1))}{(N_t N_r - 1)!}. \end{aligned} \quad (4.6)$$

where $\gamma(a, x)$ is the incomplete gamma function defined by $\int_0^x t^{a-1} e^{-t} dt$.

Next, from (4.2), the exact finite-SNR DMT for OSTBC is [NEC05]

$$\begin{aligned} d_{\text{OSTBC}}^{\text{uncorr}}(r, \rho) &= \frac{\left(\frac{N_t}{\rho} ((1 + G\rho)^{r/R_s} - 1) \right)^{N_t N_r - 1}}{\gamma(N_t N_r, \frac{N_t}{\rho} ((1 + G\rho)^{r/R_s} - 1))} \\ &\times e^{-\frac{N_t}{\rho} \left(\frac{N_t}{\rho} ((1 + G\rho)^{r/R_s} - 1) \right)} \left((1 + G\rho)^{r/R_s} - 1 - \frac{r G N_t}{R_s} (1 + G\rho)^{r/R_s - 1} \right). \end{aligned} \quad (4.7)$$

Note that the array gain G was not included in [NEC05] while deriving the finite-SNR DMT. We introduce the array gain G in these equations in order to follow its introduction by the same author in [Nar05, Nar06] and compare them with our derived exact finite-SNR for 2×2 MIMO channel.

By considering a full-rank transmit covariance matrix \mathbf{R}_{Tx} with ordered eigenvalues $\mu_1, \mu_2, \dots, \mu_{N_t}$ ($\mu_{N_t} \geq \dots \geq \mu_2 \geq \mu_1$), the exact finite-SNR DMT for OSTBC over correlated flat Rayleigh fading channel is given by [Nar06]

$$\begin{aligned} d_{\text{OSTBC}}^{\text{corr}}(r, \rho) &= \left(\frac{N_t}{\rho} (1 + G\rho)^{r/R_s} - 1 - \frac{r G N_t}{R_s} (1 + G\rho)^{r/R_s - 1} \right) \\ &\times \frac{F' \left(\frac{N_t}{\rho} (1 + G\rho)^{r/R_s - 1} \right)}{F \left(\frac{N_t}{\rho} (1 + G\rho)^{r/R_s - 1} \right)}, \end{aligned} \quad (4.8)$$

where

$$F(x) = \prod_{n=1}^{N_t} \left(\frac{\mu_1}{\mu_n} \right)^{N_r} \sum_{k=0}^{\infty} \frac{\tilde{\delta}_k \gamma(N_r N_t + k, x/\mu_1)}{\Gamma(N_t N_r + k)}, \quad (4.9)$$

$\Gamma(n)$ is the gamma function defined by $\gamma(n, x \rightarrow \infty) = \int_0^\infty t^{n-1} e^{-t} dt$, and

$$\begin{aligned} \tilde{\delta}_0 &= 1 \\ \tilde{\delta}_k &= \frac{N_r}{k+1} \sum_{i=1}^{k+1} \left[\sum_{j=1}^{N_t} \left(1 - \frac{\mu_1}{\mu_j} \right)^i \right] \tilde{\delta}_{k+1-i}. \end{aligned} \quad (4.10)$$

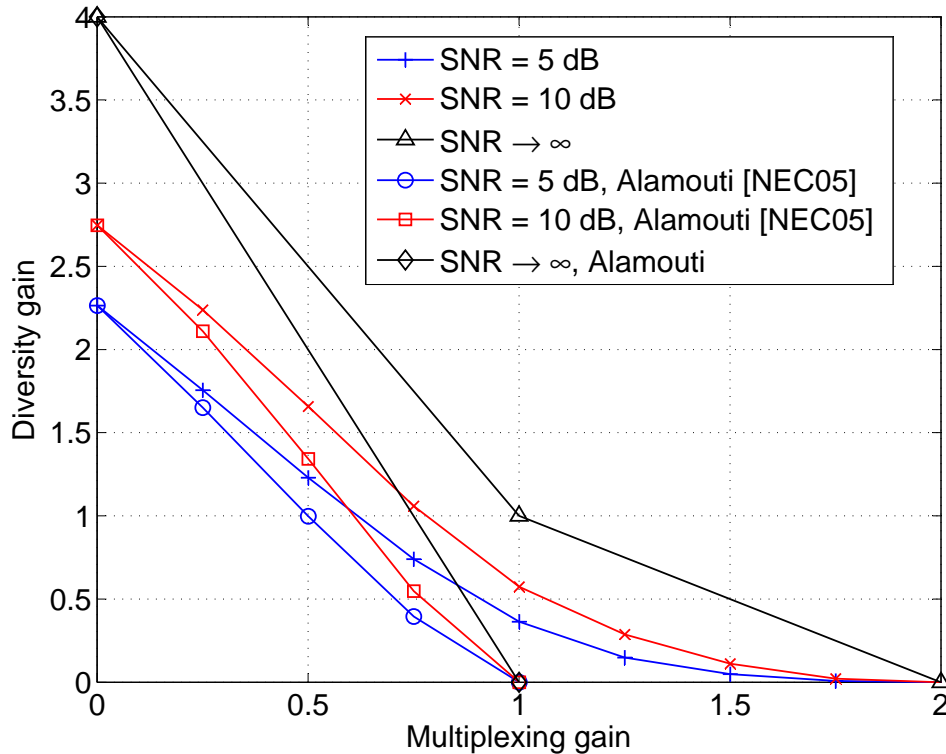


FIGURE 4.1: Asymptotic and exact finite-SNR DMT curves for 2×2 uncorrelated flat Rayleigh MIMO channel with and without Alamouti code at various SNRs.

The asymptotic DMT for OSTBCs for both uncorrelated and correlated flat Rayleigh fading channel is given by [ZT03, Nar06]

$$d_{\text{OSTBC}}^*(r) = N_t N_r \left(1 - \frac{r}{R_s}\right); 0 \leq r \leq R_s. \quad (4.11)$$

4.1.2 Finite-SNR DMT for 2×2 MIMO Channels

In [EM07a], the authors have derived the exact finite-SNR DMT for the 2×2 uncorrelated flat Rayleigh fading MIMO channel. Figure 4.1 depicts the exact finite-SNR DMT curves [EM07a] for uncorrelated flat Rayleigh fading channel for 2×2 MIMO systems at SNR = 5 and 10 dB and the asymptotic DMT [ZT03]. It shows that the achievable diversity gains at finite SNRs are significantly lower than asymptotic values when the SNR tends to infinity. We note that the resulting DMT curves are identical to the ones obtained in [Nar05] by Monte Carlo simulations, which validates that derived finite-SNR DMT is exact. Besides the Monte Carlo estimates of the finite-SNR DMT, a non exact expression of finite-SNR DMT is also given in [Nar05] based on the lower bound on outage probability. Their numerical results showed that this non exact expression overestimates the achievable DMT.

Furthermore, in order to discuss the achievability of exact finite-SNR DMT, we also plotted the exact finite-SNR DMT for the Alamouti code derived in [NEC05]. Figure 4.1

shows that the Alamouti code always benefits from all the available diversity of the system (when the multiplexing gain r approaches to zero), not only at asymptotic SNRs, but also at realistic SNRs.

4.2 Finite-SNR DMT for MIMO Channels with Dual Antennas

Motivated by the characterization of MIMO channels at finite SNRs and inspired by the work in [EM07a], we derive in this section the exact finite-SNR DMT for MIMO systems with dual uncorrelated and correlated antennas. We recall that the exact finite-SNR DMT has been derived only for MISO, SIMO systems with uncorrelated [EM07b] and correlated [RHGA10] Rayleigh fading channels and 2×2 MIMO systems with uncorrelated Rayleigh fading channels [EM07a]. Our work extends the literature on finite-SNR DMT by the derivation of the exact finite-SNR DMT for MIMO systems with dual antennas *i.e.*, $N_t \times 2$ and $2 \times N_r$ systems for a transmission over an uncorrelated and correlated flat Rayleigh fading channels.

We start by deriving the analytical expression of the pdf of mutual information between received and transmitted signals; then we provide the outage probability for both uncorrelated and correlated flat Rayleigh fading channels. Finally, we derive the exact finite-SNR DMT for both cases.

4.2.1 Mutual Information for $N_t \times 2$ and $2 \times N_r$ MIMO Systems

In this section, we derive an analytical expression for the pdf of mutual information between received and transmitted signals for $N_t \times 2$ and $2 \times N_r$ MIMO systems. By assuming that the transmitted codeword \mathbf{X} is a zero-mean white complex Gaussian random variable, the MIMO mutual information conditioned on the channel realization \mathbf{H} is given by [Tel99]

$$\begin{aligned} I &= \log \det \left(\mathbf{I}_{N_r} + \frac{\rho}{N_t} \mathbf{H} \mathbf{H}^H \right) \\ &= \log \det \left(\mathbf{I}_{N_t} + \frac{\rho}{N_t} \mathbf{H}^H \mathbf{H} \right) \end{aligned} \quad (4.12)$$

It is to be noted that in (4.12) we use \log_e then the mutual information is measured in nats. If we use \log_2 then the mutual information is measured in bits. Passing from \log_e to \log_2 in the expressions of outage probability and DMT is straightforward. The same DMT curves are obtained for both cases.

Let us define $m \triangleq \min(N_t, N_r)$ and $n \triangleq \max(N_t, N_r)$. When $m = 2$, the mutual information I is expressed by

$$I = \log \left(1 + \lambda_1 \frac{\rho}{N_t} \right) + \log \left(1 + \lambda_2 \frac{\rho}{N_t} \right). \quad (4.13)$$

where λ_1 and λ_2 are the two nonzero ordered eigenvalues ($\lambda_1 \geq \lambda_2$) of $\mathbf{H}\mathbf{H}^H$ for $N_t \times 2$ systems or $\mathbf{H}^H\mathbf{H}$ for $2 \times N_r$ systems.

Let us define new variables x and y as

$$x \triangleq \log \left(1 + \lambda_1 \frac{\rho}{N_t} \right) \text{ and } y \triangleq \log \left(1 + \lambda_2 \frac{\rho}{N_t} \right). \quad (4.14)$$

From the definition in (4.14), the mutual information between received and transmitted signals is

$$I = x + y. \quad (4.15)$$

The analytical expressions for the pdf of I , the outage probability and the finite-SNR DMT depend on the channel type. In the sequel, we derive them for both uncorrelated and correlated flat Rayleigh fading channels with dual antennas.

4.2.2 Finite-SNR DMT for Uncorrelated Flat Rayleigh Channels

4.2.2.1 Mutual Information pdf Derivation

For uncorrelated flat fading Rayleigh channels, the channel matrix $\mathbf{H} = \mathbf{H}_w$ is complex normally distributed. Therefore, matrices $\mathbf{H}\mathbf{H}^H$ and $\mathbf{H}^H\mathbf{H}$ are central complex Wishart distributed [Jam64, RV05] (and references therein). For $m = 2$, the joint pdf of their two nonzero ordered eigenvalues λ_1 and λ_2 ($\lambda_1 \geq \lambda_2$) is given by [RV05]

$$f^{\text{uncorr}}(\lambda_1, \lambda_2) = \frac{(\lambda_1 \lambda_2)^{n-2}}{\Gamma(n) \Gamma(n-1)} (\lambda_1 - \lambda_2)^2 e^{-(\lambda_1 + \lambda_2)} \quad (4.16)$$

Using rules in [PP02], the joint pdf of x and y can be derived from the one of λ_1 and λ_2 by (see Appendix D)

$$\begin{aligned} f^{\text{uncorr}}(x, y) &= \left(\frac{N_t}{\rho} \right)^{2n} \frac{1}{\Gamma(n)\Gamma(n-1)} e^{x+y} (e^x - e^y)^2 \\ &\times (e^x - 1)^{n-2} (e^y - 1)^{n-2} e^{-\frac{N_t}{\rho}(e^x + e^y - 2)} \end{aligned} \quad (4.17)$$

where $x \geq y \geq 0$.

From (4.15), the joint pdf of I and y is obtained by

$$\begin{aligned} f^{\text{uncorr}}(I, y, \rho) &= \left(\frac{N_t}{\rho} \right)^{2n} \frac{1}{\Gamma(n)\Gamma(n-1)} e^I (e^{I-y} - e^y)^2 \\ &\times (e^y - 1)^{n-2} (e^{I-y} - 1)^{n-2} e^{-\frac{N_t}{\rho}(e^{I-y} + e^y - 2)} \end{aligned} \quad (4.18)$$

where $I/2 \geq y \geq 0$.

The pdf of I can be derived by integrating the function $f(I, y, \rho)$ in (4.18) over y from 0 to $I/2$ which leads to

$$f^{\text{uncorr}}(I, \rho) = \left(\frac{N_t}{\rho}\right)^{2n} \frac{1}{\Gamma(n)\Gamma(n-1)} e^I \times \int_0^{I/2} g^{\text{uncorr}}(y, I, \rho) dy \quad (4.19)$$

where $g^{\text{uncorr}}(y, I, \rho)$ is expressed by

$$g^{\text{uncorr}}(y, I, \rho) = (e^{I-y} - e^y)^2 (e^{I-y} - 1)^{n-2} \times (e^y - 1)^{n-2} e^{-\frac{N_t}{\rho}(e^{I-y} + e^y - 2)}. \quad (4.20)$$

For each value of I and ρ , the expression $\int_0^{I/2} g^{\text{uncorr}}(y, I, \rho) dy$ can be calculated by numerical integration.

Numerical integration algorithm Many algorithms for numerical integration exist in the literature. In our numerical results, we have used the composite Simpson's rule given by

$$\int_a^b f(x) dx \approx \frac{h}{3} \left[f(x_0) + 2 \sum_{i=1}^{k/2-1} f(x_{2i}) + 4 \sum_{i=1}^{k/2} f(x_{2i-1}) + f(x_k) \right], \quad (4.21)$$

where $x_i = a + ih$ for $i = 0, 1, \dots, k-1, k$ with $h = (b-a)/k$ and k an even number; in particular $x_0 = a$ and $x_k = b$, and the formula (4.21) can be written as

$$\int_a^b f(x) dx \approx \frac{h}{3} [f(x_0) + 4f(x_1) + 2f(x_2) + \dots + 4f(x_{k-1}) + f(x_k)]. \quad (4.22)$$

4.2.2.2 Outage Probability Derivation

In this section, we use the results in Section 4.2.2.1 to obtain the outage probability at a multiplexing gain r and SNR ρ . From the expression of the pdf of I obtained in (4.19), and thanks to numerical integration, the outage probability $P_{\text{out}}(r, \rho)$ is computed for each ρ and r by

$$\begin{aligned} P_{\text{out}}^{\text{uncorr}}(r, \rho) &= \int_0^R f^{\text{uncorr}}(I, \rho) dI \\ &= \left(\frac{N_t}{\rho}\right)^{2n} \frac{1}{\Gamma(n)\Gamma(n-1)} \\ &\times \int_0^{r \log(1+G\rho)} e^I \left(\int_0^{I/2} g^{\text{uncorr}}(y, I, \rho) dy \right) dI \end{aligned} \quad (4.23)$$

The outage probability curves describe the performance over MIMO channels and their slopes define the finite-SNR DMT.

4.2.2.3 Analytical Expression of Finite-SNR DMT

The finite-SNR DMT is computed using (4.2). Using the well-known Leibniz integral rule [PP02] in (4.23), $\frac{\partial P_{\text{out}}^{\text{uncorr}}(r, \rho)}{\partial \rho}$ is given by (see Appendix D)

$$\frac{\partial P_{\text{out}}^{\text{uncorr}}(r, \rho)}{\partial \rho} = A_1^{\text{uncorr}}(r, \rho) + A_2^{\text{uncorr}}(r, \rho) + A_3^{\text{uncorr}}(r, \rho) \quad (4.24)$$

where

$$\begin{aligned} A_1^{\text{uncorr}}(r, \rho) &= -2n(N_t)^{2n} \frac{1}{\rho^{2n+1}} \frac{1}{\Gamma(n)\Gamma(n-1)} \\ &\times \int_0^r \log(1+G\rho) e^I \left(\int_0^{I/2} g^{\text{uncorr}}(y, I, \rho) dy \right) dI \\ &= -\frac{2n}{\rho} P_{\text{out}}^{\text{uncorr}}(r, \rho), \end{aligned} \quad (4.25)$$

$$\begin{aligned} A_2^{\text{uncorr}}(r, \rho) &= \left(\frac{N_t}{\rho} \right)^{2n} \frac{1}{\Gamma(n)\Gamma(n-1)} \frac{rG}{1+G\rho} e^{r \log(1+G\rho)} \\ &\times \left(\int_0^{r \log(1+G\rho)/2} g^{\text{uncorr}}(y, r \log(1+G\rho), \rho) dy \right), \end{aligned} \quad (4.26)$$

and

$$\begin{aligned} A_3^{\text{uncorr}}(r, \rho) &= \left(\frac{N_t}{\rho} \right)^{2n} \frac{1}{\Gamma(n)\Gamma(n-1)} \\ &\times \int_0^{r \log(1+G\rho)} e^I \left(\int_0^{I/2} \frac{\partial g^{\text{uncorr}}(y, I, \rho)}{\partial \rho} dy \right) dI \end{aligned} \quad (4.27)$$

where

$$\begin{aligned} \frac{\partial g^{\text{uncorr}}(y, I, \rho)}{\partial \rho} &= (e^{I-y} - e^y)^2 (e^{I-y} - 1)^{n-2} (e^y - 1)^{n-2} \\ &\times e^{-\frac{N_t}{\rho}(e^{I-y} + e^y - 2)} \frac{N_t}{\rho^2} (e^{I-y} + e^y - 2). \end{aligned} \quad (4.28)$$

The above expressions can also be calculated by numerical integration. After deriving $P_{\text{out}}^{\text{uncorr}}(r, \rho)$ and $\frac{\partial P_{\text{out}}^{\text{uncorr}}(r, \rho)}{\partial \rho}$, the finite-SNR DMT can be easily computed using (4.2).

$$d^{\text{uncorr}}(r, \rho) = -\frac{\rho}{(4.23)} (4.24). \quad (4.29)$$

Note that for $n = 2$, our equations are identical to the ones obtained in [EM07a] for a 2×2 uncorrelated Rayleigh fading MIMO channel.

4.2.3 Finite-SNR DMT for Correlated Flat Rayleigh Channel

In this section, we consider the case of MIMO systems with correlated dual antennas. We derive the exact finite-SNR DMT for the correlated flat Rayleigh fading channel where we assume that the dual antennas are correlated at the transmitter side or at the receiver side only. A typical example of a system with correlation at one side only is a communication between a mobile station and a base station. Here, the antennas at the base station can be spaced sufficiently far apart to achieve uncorrelation but, due to physical size constraints, it is more difficult to space antennas far apart at the mobile station.

4.2.3.1 Mutual Information pdf Derivation

When correlation between dual antennas is assumed at the transmitter or at the receiver, matrices $\mathbf{H}\mathbf{H}^H$ and $\mathbf{H}^H\mathbf{H}$ are complex Wishart distributed and the joint pdf of their two nonzero ordered eigenvalues λ_1 and λ_2 ($\lambda_1 \geq \lambda_2$) is given by [RV05]

$$f^{\text{corr}}(\lambda_1, \lambda_2) = \frac{(a_1 a_2)^n (\lambda_1 \lambda_2)^{n-2} (\lambda_1 - \lambda_2)}{(a_2 - a_1) \Gamma(n) \Gamma(n-1)} \left[e^{-(a_1 \lambda_1 + a_2 \lambda_2)} - e^{-(a_1 \lambda_2 + a_2 \lambda_1)} \right] \quad (4.30)$$

where a_1 and a_2 are the ordered eigenvalues ($a_2 \geq a_1$) of $\mathbf{R}_{\text{Rx}}^{-1}$ (downlink) or $\mathbf{R}_{\text{Tx}}^{-1}$ (uplink).

We note that the case of correlation at both transmitter and receiver side leads to a more complicated form of the pdf for the two nonzero ordered eigenvalues λ_1 and λ_2 [RV05]. Therefore, the exact finite-SNR DMT is not easily tractable for this case.

Similarly to Section 4.2.2.1, the joint pdf of x and y can be derived from the one of λ_1 and λ_2 by

$$f^{\text{corr}}(x, y) = \frac{(a_1 a_2)^n \left(\frac{N_t}{\rho}\right)^{2n-1}}{(a_2 - a_1) \Gamma(n) \Gamma(n-1)} e^{x+y} (e^x - e^y) (e^x - 1)^{n-2} (e^y - 1)^{n-2} \times \left[e^{-\frac{N_t}{\rho}(a_1 e^x + a_2 e^y - a_1 - a_2)} - e^{-\frac{N_t}{\rho}(a_1 e^y + a_2 e^x - a_1 - a_2)} \right], \quad (4.31)$$

where $x \geq y \geq 0$.

and the joint pdf of I and y is obtained by

$$f^{\text{corr}}(I, y, \rho) = \frac{(a_1 a_2)^n \left(\frac{N_t}{\rho}\right)^{2n-1}}{(a_2 - a_1) \Gamma(n) \Gamma(n-1)} e^I (e^{I-y} - e^y) (e^{I-y} - 1)^{n-2} (e^y - 1)^{n-2} \times \left[e^{-\frac{N_t}{\rho}(a_1 e^{I-y} + a_2 e^y - a_1 - a_2)} - e^{-\frac{N_t}{\rho}(a_1 e^y + a_2 e^{I-y} - a_1 - a_2)} \right], \quad (4.32)$$

where $I/2 \geq y \geq 0$.

The pdf of I can be derived by integrating the function $f^{\text{corr}}(I, y, \rho)$ in (4.32) over y from 0 to $I/2$, leading to

$$f^{\text{corr}}(I, \rho) = \frac{(a_1 a_2)^n \left(\frac{N_t}{\rho}\right)^{2n-1}}{(a_2 - a_1) \Gamma(n) \Gamma(n-1)} e^I \times \int_0^{I/2} g^{\text{corr}}(y, I, \rho) dy, \quad (4.33)$$

where $g^{\text{corr}}(y, I, \rho)$ is expressed by

$$g^{\text{corr}}(y, I, \rho) = (e^{I-y} - e^y) (e^{I-y} - 1)^{n-2} (e^y - 1)^{n-2} \times \left[e^{-\frac{N_t}{\rho}(a_1 e^{I-y} + a_2 e^y - a_1 - a_2)} - e^{-\frac{N_t}{\rho}(a_1 e^y + a_2 e^{I-y} - a_1 - a_2)} \right]. \quad (4.34)$$

A numerical integration is used to compute the expression of $\int_0^{I/2} g^{\text{corr}}(y, I, \rho) dy$ for each value of I and ρ .

4.2.3.2 Outage Probability Derivation

From the expression of the pdf of I obtained in (4.33), the outage probability $P_{\text{out}}^{\text{corr}}(r, \rho)$ is computed for each ρ and r by

$$\begin{aligned} P_{\text{out}}^{\text{corr}}(r, \rho) &= \int_0^R f^{\text{corr}}(I, \rho) dI \\ &= (a_1 a_2)^n \left(\frac{N_t}{\rho}\right)^{2n-1} \frac{1}{(a_2 - a_1)\Gamma(n)\Gamma(n-1)} \\ &\times \int_0^{r \log(1+G\rho)} e^I \left(\int_0^{I/2} g^{\text{corr}}(y, I, \rho) dy \right) dI \end{aligned} \quad (4.35)$$

4.2.3.3 Analytical Expression of Finite-SNR DMT

Similarly to Section 4.2.2.3, we apply the Leibniz integral rule [PP02] in (4.23) to derive $\frac{\partial P_{\text{out}}^{\text{corr}}(r, \rho)}{\partial \rho}$ as follows

$$\frac{\partial P_{\text{out}}^{\text{corr}}(r, \rho)}{\partial \rho} = A_1^{\text{corr}}(r, \rho) + A_2^{\text{corr}}(r, \rho) + A_3^{\text{corr}}(r, \rho) \quad (4.36)$$

where

$$\begin{aligned} A_1^{\text{corr}}(r, \rho) &= (-2n + 1) (N_t)^{2n-1} \frac{1}{\rho^{2n}} (a_1 a_2)^n \frac{1}{(a_2 - a_1)\Gamma(n)\Gamma(n-1)} \\ &\times \int_0^{r \log(1+G\rho)} e^I \left(\int_0^{I/2} g^{\text{corr}}(y, I, \rho) dy \right) dI \\ &= -\frac{2n-1}{\rho} P_{\text{out}}(r, \rho), \end{aligned} \quad (4.37)$$

$$\begin{aligned} A_2^{\text{corr}}(r, \rho) &= (a_1 a_2)^n \left(\frac{N_t}{\rho}\right)^{2n-1} \frac{1}{(a_2 - a_1)\Gamma(n)\Gamma(n-1)} \frac{rG}{1+G\rho} e^{r \log(1+G\rho)} \\ &\times \left(\int_0^{r \log(1+G\rho)/2} g^{\text{corr}}(y, r \log(1+G\rho), \rho) dy \right), \end{aligned} \quad (4.38)$$

and

$$\begin{aligned} A_3^{\text{corr}}(r, \rho) &= (a_1 a_2)^n \left(\frac{N_t}{\rho}\right)^{2n-1} \frac{1}{(a_2 - a_1)\Gamma(n)\Gamma(n-1)} \\ &\times \int_0^{r \log(1+G\rho)} e^I \left(\int_0^{I/2} \frac{\partial g^{\text{corr}}(y, I, \rho)}{\partial \rho} dy \right) dI \end{aligned} \quad (4.39)$$

where

$$\begin{aligned} \frac{\partial g^{\text{corr}}(y, I, \rho)}{\partial \rho} &= (e^{I-y} - e^y) (e^{I-y} - 1)^{n-2} (e^y - 1)^{n-2} \\ &\times \left[\begin{aligned} &\frac{N_t}{\rho^2} (a_1 e^{I-y} + a_2 e^y - a_1 - a_2) e^{-\frac{N_t}{\rho} (a_1 e^{I-y} + a_2 e^y - a_1 - a_2)} \\ & - \frac{N_t}{\rho^2} (a_2 e^{I-y} + a_1 e^y - a_1 - a_2) e^{-\frac{N_t}{\rho} (a_2 e^{I-y} + a_1 e^y - a_1 - a_2)} \end{aligned} \right]. \end{aligned} \quad (4.40)$$

The above expressions can also be calculated by numerical integration. After deriving $P_{\text{out}}^{\text{corr}}(r, \rho)$ and $\frac{\partial P_{\text{out}}^{\text{corr}}(r, \rho)}{\partial \rho}$, the finite-SNR DMT can be easily computed using (4.2).

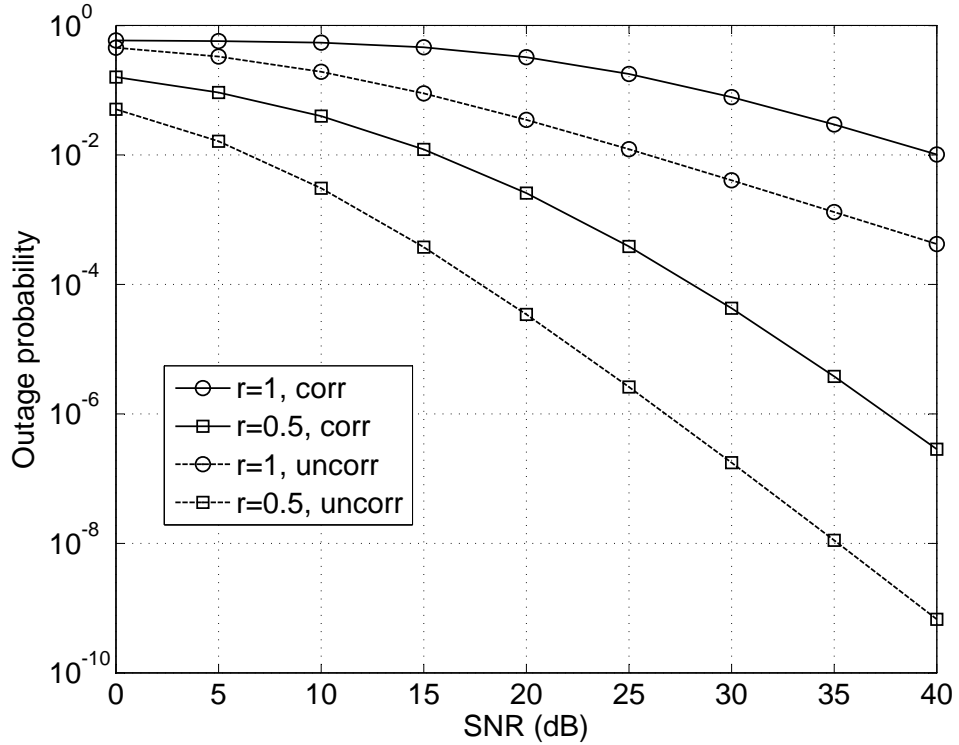


FIGURE 4.2: Outage probability for different multiplexing gains $r = 0.5, 1$; $N_t = N_r = 2$, uncorrelated and correlated ($\rho_t = 0.0043 + j0.9789$ as in [Nar06]) flat Rayleigh fading with dashed and solid lines respectively.

4.3 Numerical Results

In this section, we provide numerical results for the outage probability and the exact finite-SNR DMT. We start by the assessment of outage probability and finite-SNR DMT for 2×2 MIMO system. Then we consider the case of higher number of antennas *i.e.*, $n \geq 3$.

4.3.1 2×2 MIMO System

Figure 4.1 depicted in Section 4.1.2 for 2×2 uncorrelated Rayleigh fading MIMO channels showed that achievable DMT at finite SNRs are significantly lower than asymptotic DMT. Moreover, it showed that derived exact finite-SNR DMT are identical to the ones obtained by Monte Carlo simulations, which validates the derivation method.

Afterwards, we consider the correlated flat Rayleigh MIMO channel case. We recall that the correlation between the dual transmit antennas is modeled by the matrix

$$\mathbf{R}_{\text{Tx}} = \begin{bmatrix} 1.0000 & \rho_t \\ \rho_t^* & 1.0000 \end{bmatrix} \quad (4.41)$$

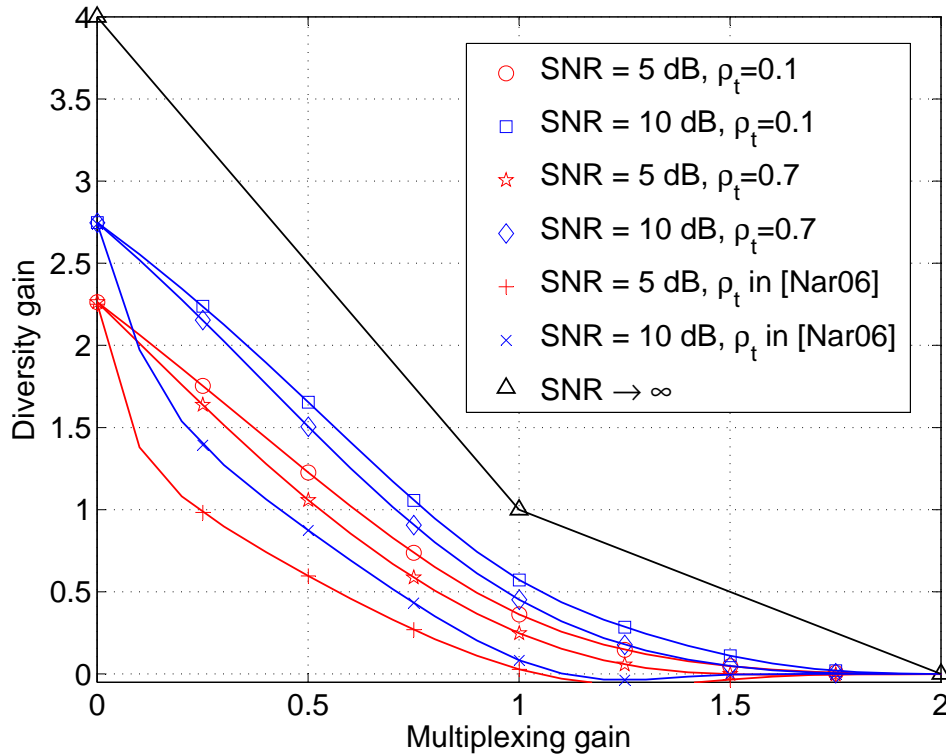


FIGURE 4.3: Asymptotic and exact finite-SNR DMT curves for 2×2 correlated flat Rayleigh MIMO channel with low $\rho_t = 0.1$, medium $\rho_t = 0.7$ and high $\rho_t = 0.0043 + j0.9789$ (as in [Nar06]) correlations at various SNRs.

In order to assess the derived DMT, we assume for the high spatial correlation case that ρ_t is equal to $0.0043 + j0.9789$, as in [Nar06].

Figure 4.2 depicts the outage probability for multiplexing gain values r equal to 0.5 and 1 as a function of SNR, for both uncorrelated and correlated flat Rayleigh fading channels with dashed and solid lines respectively. The resulting curves are identical to the ones obtained in [Nar05, Nar06, RHGA10] by Monte Carlo simulations, which validates the derived exact outage probability for both cases. Nevertheless, low outage probabilities can be easily assessed using our derived equations while authors in [Nar05, Nar06, RHGA10] were limited to outage probabilities higher than 10^{-6} because of simulation complexity. Moreover, Figure 4.2 shows that a lower outage probability is reached in the uncorrelated case. At $r = 0.5$ and $r = 1$, a steeper slope of the outage probability curves is observed for the uncorrelated channel with respect to the correlated channel especially at low to moderate SNRs. Thus, at the same multiplexing gain r and at finite SNR, one can expect that a higher diversity gain is obtained for the uncorrelated channel compared to the correlated channel.

Figure 4.3 depicts the exact finite-SNR DMT curves for $n = 2$ at SNR = 5 and 10 dB over correlated flat Rayleigh channel with low $\rho_t = 0.1$, medium $\rho_t = 0.7$ and high $\rho_t = 0.0043 + j0.9789$ correlations. At $\rho_t = 0.1$, almost the same finite-SNR DMT

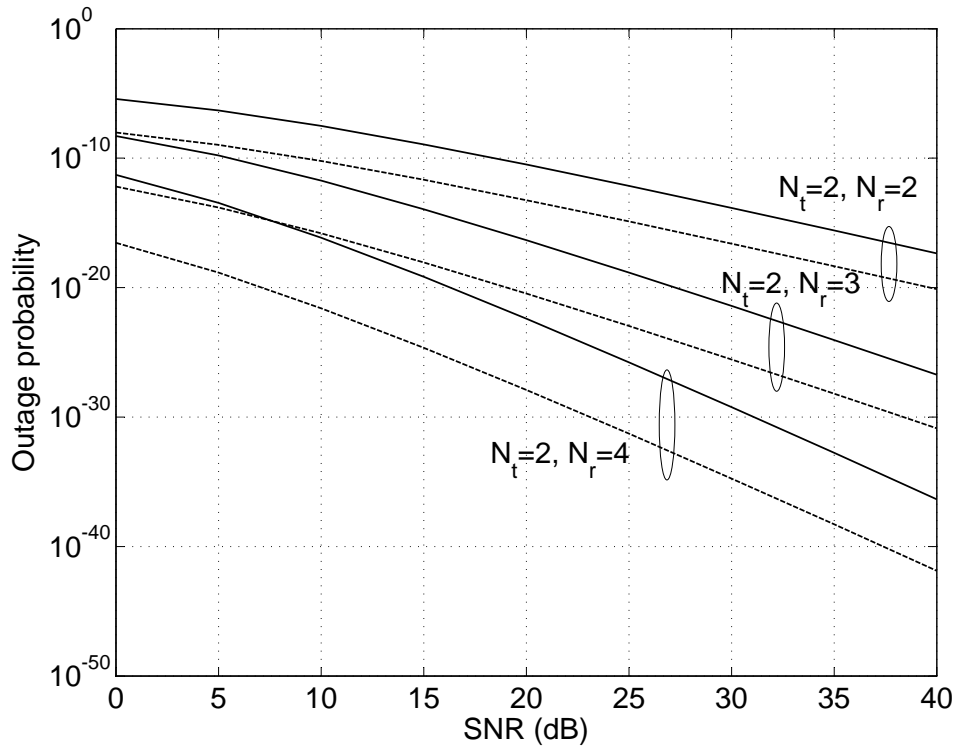


FIGURE 4.4: Outage probability for MIMO systems with multiplexing gain $r \rightarrow 0$; 2×2 , 2×3 and 2×4 , in uncorrelated and correlated ($\rho_t = 0.0043 + j0.9789$) flat Rayleigh fading channels (dashed and solid lines respectively).

is obtained for both uncorrelated (Figure 4.1) and correlated channels. As expected, when the correlation coefficient increases, the diversity gain decreases. However, the diversity gain is only slightly degraded at low to moderate values of spatial correlation. On the contrary, the diversity gain is severely degraded for high correlations. We observed that our derived exact DMT curves are identical to the ones obtained in [RCHG06, Nar06, RHGA10] by Monte Carlo simulations, which validates the derived exact DMT for correlated channels. Besides, their numerical results showed that non exact expressions overestimate the achievable DMT. Also, Figure 4.3 shows that the maximum achievable diversity *i.e.*, the diversity gain for $r \rightarrow 0$, at finite SNR is the same for both correlated and uncorrelated channels. Similar conclusions have also been found in [RHGA10] based on their estimates of finite-SNR DMT.

4.3.2 MIMO System with $n \geq 3$

Based on estimated finite-SNR DMT, authors in [RHGA10] have proven that the estimated maximum diversity at finite SNR is the same for both uncorrelated and correlated channels. In order to prove that the exact maximum diversity at finite SNR is the same for both cases, we have plotted in Figure 4.4 the corresponding outage

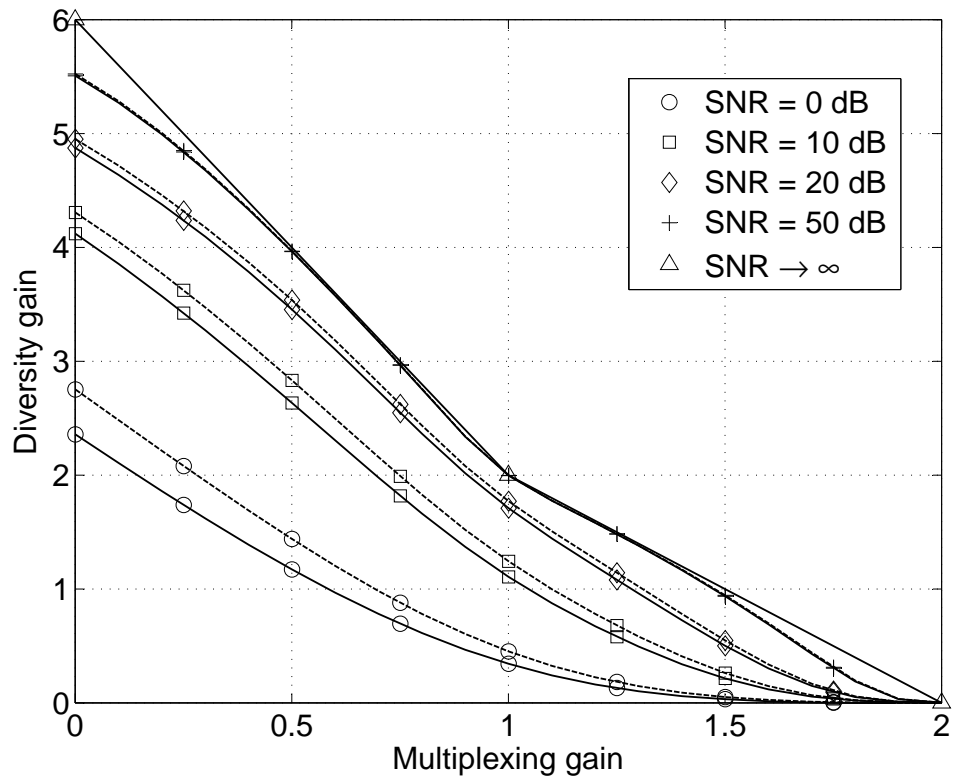


FIGURE 4.5: Asymptotic and exact finite-SNR DMT curves for 3×2 MIMO channel with solid lines and 2×3 MIMO channel with dashed lines at various SNRs.

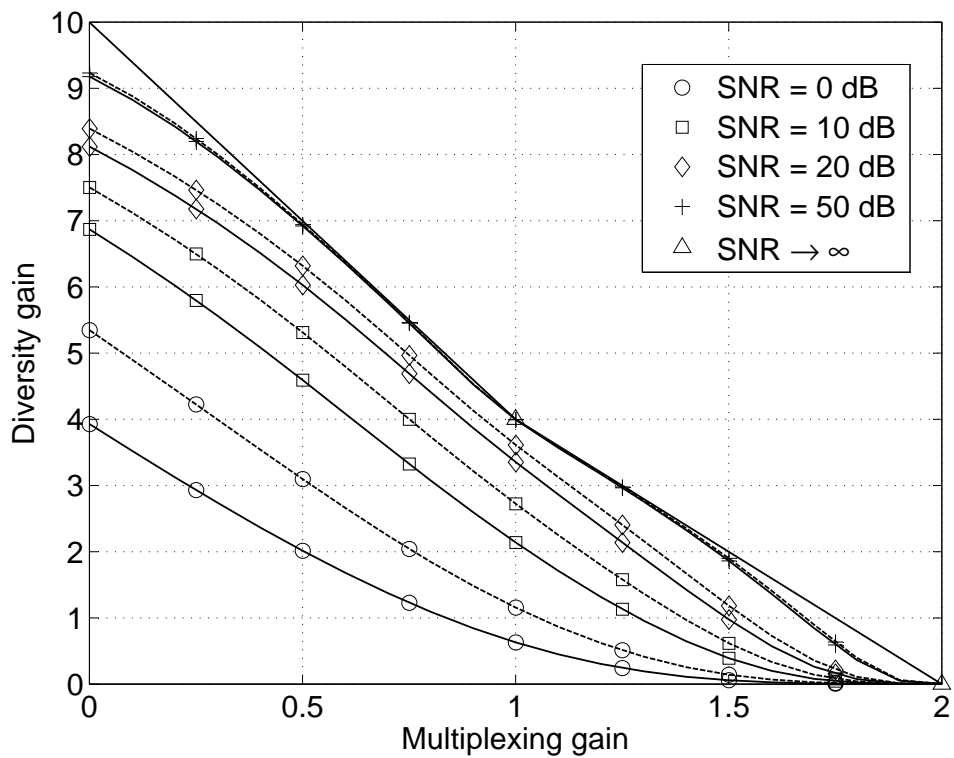


FIGURE 4.6: Asymptotic and exact finite-SNR DMT curves for 5×2 MIMO channel with solid lines and 2×5 MIMO channel with dashed lines at various SNRs.

probability curves when the multiplexing gain r tends to 0. A high spatial correlation ($\rho_t = 0.0043 + j0.9789$) at the transmitter and several uncorrelated antennas ($N_r = 2, 3, 4$) at the receiver are considered. We recall that the maximum diversity gain is defined by the negative slope of the log-log curve of the outage probability versus SNR when $r \rightarrow 0$. At any SNR, Figure 4.4 obviously shows that outage probability curves for uncorrelated and correlated channels have the same slope and therefore the same diversity with only SNR loss. Furthermore, lower outage probabilities can be achieved for the uncorrelated case. The SNR loss between uncorrelated and correlated channels increases with the increase of the number of receive antennas.

In order to discuss the difference between finite-SNR DMT for $N_t \times 2$ and $2 \times N_r$ systems, we plot, in Figure 4.5 for $n = 3$ and in Figure 4.6 for $n = 5$, the asymptotic and exact finite-SNR DMT for $n \times 2$ and $2 \times n$ uncorrelated flat Rayleigh channels with dashed and solid lines respectively. The results show that receive antennas provide higher diversity gains than transmit antennas especially at low to medium SNRs. We recall that no CSI is available at the transmitter and an equal power across transmit antennas is adopted. Under this assumption, the outage probability is defined by (4.3) and the finite-SNR DMT by (4.2). Therefore, the superiority of $N_r \times 2$ with respect to $2 \times N_t$ can be explained by the fact that receive diversity is always obtained regardless of the transmission technique. On the other hand, a judicious transmission technique is required to benefit from transmit diversity, and an equal power across transmit antennas is not necessarily the best strategy at low to moderate SNRs. It is to be noted that the gap between $N_t \times 2$ and $2 \times N_r$ systems increases with the increase of n . Also, this gap decreases with the SNR increase where both systems converge to the asymptotic DMT [ZT03] *e.g.*, SNR = 50 dB. This convergence is not uniform. It is faster for higher multiplexing gains.

Afterwards, we investigate the effect of increasing the number of antennas on the finite-SNR DMT for correlated Rayleigh fading channels. Figure 4.7 depicts, with dashed and solid lines respectively, the exact finite-SNR DMT curves for 2×5 correlated flat Rayleigh MIMO channel with low $\rho_t = 0.1$ and high $\rho_t = 0.0043 + j0.9789$ [Nar06] correlation at various SNRs. A comparison with the results of Figure 4.3 shows that the gap between finite-SNR DMT for low and high spatial correlations curves increases with the increase of the number of receive antennas. Moreover, this gap decreases with the SNR increase especially for low multiplexing gains. When $r \rightarrow 0$, the same maximum diversity is achieved regardless of the spatial correlation value as proved in Figure 4.4. A comparison between Figure 4.6 and Figure 4.7 shows that the same finite-SNR DMT curves are obtained over uncorrelated and correlated channels for a low correlation value as $\rho_t = 0.1$.

In addition, all presented finite-SNR DMT figures show that the achievable diversity gains at finite SNR are significantly lower than the asymptotic values. A convergence of

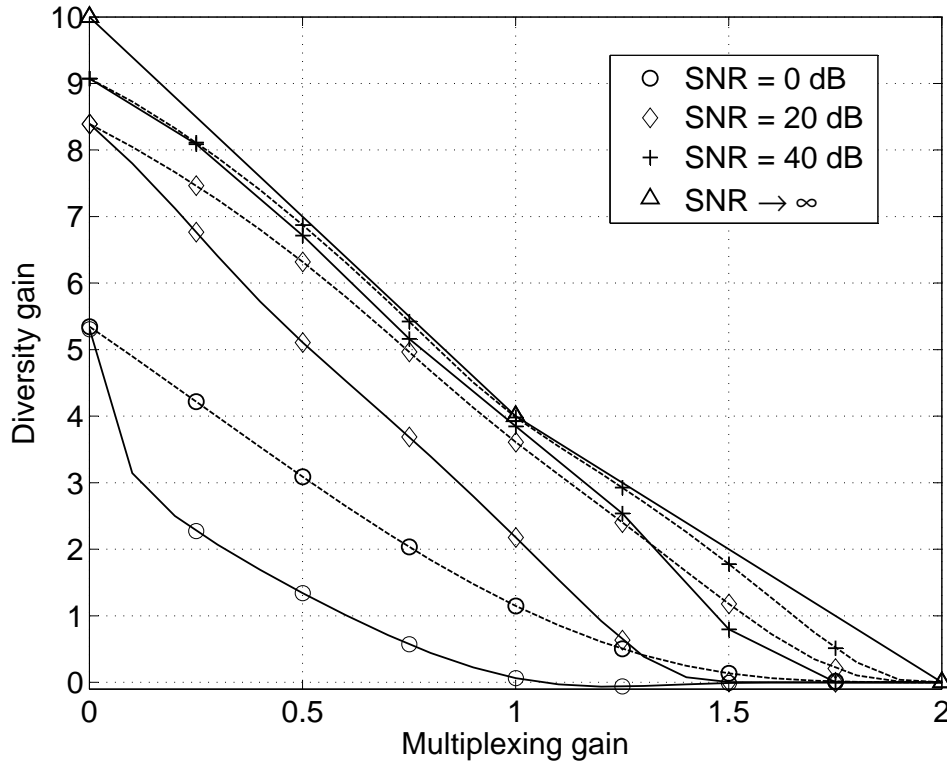


FIGURE 4.7: Exact finite-SNR DMT curves for 2×5 correlated flat Rayleigh MIMO channel with a low $\rho_t = 0.1$ and high $\rho_t = 0.0043 + j0.9789$ correlations at various SNRs (dashed and solid lines respectively).

the finite-SNR DMT to the asymptotic DMT is obtained at high SNRs typically greater than 50 dB. Unfortunately, an analytical proof of this convergence, by letting the SNR tends towards infinity, is not easily tractable due to the presence of integrals.

4.4 Chapter Summary

In this chapter, we derived the exact finite-SNR diversity-multiplexing tradeoff for uncorrelated and correlated flat Rayleigh MIMO channels with dual antennas. The finite-SNR DMT characterizes the MIMO system at operational SNRs where available diversity gains are computed. In order to derive the finite-SNR DMT, we have computed the outage probability by manipulating the pdf of the channel mutual information between transmitted and received signals. Then we have computed the diversity gain defined as the negative slope of the log-log curve of outage probability versus SNR.

We showed, for 2×2 system, that our results either in terms of outage probability or finite-SNR DMT are identical to the ones obtained by Monte Carlo simulations for both uncorrelated and correlated channels. Based on outage probability curves, we proved that the maximum achievable diversity at finite SNRs, obtained when r tends to 0, is the same for both uncorrelated and correlated channels with several antennas

regardless of the spatial correlation value. Then we plotted the finite-SNR DMT for correlated channels. We showed that the diversity gain is only slightly degraded at low to moderate spatial correlations while it is severely degraded for high correlations. In addition, we showed that the gap between DMT curves for low and high correlations increases with the increase of the number of antennas. Furthermore, we investigated the difference between $N_t \times 2$ and $2 \times N_r$ systems. We showed that receive antennas provide higher diversity gains with respect to transmit antennas especially at low to moderate SNRs. In all cases, the finite-SNR DMT converges to the conventional asymptotic DMT at high SNRs.

Generally, the analysis on finite-SNR DMT shows that the achievable diversity gains are significantly lower than asymptotic values when the SNR tends to infinity. STCs for MIMO systems are conventionally designed to achieve the asymptotic DMT frontier and therefore are not efficient at realistic SNRs. This finite-SNR DMT characterizes the achievable performance by any transmission over MIMO channels at finite SNRs and could provide new insights on the design STCs for practical MIMO systems.

The derivation of the finite-SNR DMT for uncorrelated Rayleigh fading channels with dual antennas has been published in [EHL⁺13].

Conclusions and perspectives

Most of modern wireless communication systems such as WiMAX, DVB, WiFi, HSPA+, LTE and 4G, adopt the concatenation of capacity approaching FEC codes with MIMO codes, so-called coded MIMO system. However, the existence of such FEC codes has not been yet considered while designing standardized space-time codes for MIMO systems. In this thesis, we investigated the analysis and design of space-time block codes (STBCs) for MIMO systems using capacity approaching FEC codes.

Conclusions

In **Chapter 1**, we motivated our work by showing that conventional STBCs are not efficient for coded MIMO systems. Afterwards, in **Chapter 2**, we started our study by the proposal of a soft detector for the low ML-detection complexity Matrix D code [SS07, SSB⁺08]. Then we optimized the Matrix D code at low SNRs according to the trace criterion [TC01, CYV01]. Based on this optimization and the structure of Matrix D code, we proposed a low ML-detection complexity FR-FD STBC suitable for coded MIMO systems. The proposed code overcomes the original one in the context of a WiMAX system. Furthermore, we assessed the complexity of the WiMAX receiver by evaluating both FEC decoder and MIMO detector complexities. A comparison between different WiMAX transmission profiles was also done.

In general, capacity approaching FEC codes achieve their desired performance at a specific SNR while conventional STBCs are designed based on asymptotic criteria. Therefore, we proposed an SNR-dependent STBC design criterion based on the bitwise mutual information (BMI) maximization between transmitted and detected bits. After its validation, we optimized several flexible STBCs according to the proposed BMI criterion. We showed that their design parameters are SNR-dependent, leading to the proposal of adaptive STBCs. Based on the matrix D STBC structure, we designed an adaptive matrix D STBC which can be used as a good choice trading off performance and detection complexity. Furthermore, based on the trace-orthonormal STBC structure [ZLW07], we proposed the adaptive TO STBC. The adaptive TO STBC overcomes or matches conventional STBCs in terms of BER performance and complexity with all coding rates. The proposal of adaptive STBCs is important for coded MIMO systems as

the appropriate design parameter is used with each coding rate, modulation order and E_b/N_0 . On the contrary, the use of conventional non-adaptive STBCs like the Alamouti code [Ala98], the spatial multiplexing [WFGV98] and the Golden code [BRV05], increases the MIMO detection complexity and alters the performance of terminals for some transmission profiles.

Thereafter, in **Chapter 3**, we studied the effect of the spatial correlation on the performance of coded MIMO systems. We showed that low correlations are similar to a SNR loss with respect to the uncorrelated system. For this case, adaptive TO STBC can always be designed in a way providing the best performance. In contrast, we showed that high correlations can lead to substantial performance degradation. This degradation differs depending on the used MIMO profile. The choice of the suitable MIMO profile for correlated channels is strongly linked to the communication environment.

Also in **Chapter 3**, we considered the case of coded MIMO systems using more than dual transmit antennas. The antenna selection (AS) technology was identified to be an effective technique to improve performance while keeping reasonable system complexity. Actually, in the MIMO literature, the performance of AS for MIMO system without FEC codes is well-studied where SNR and diversity gains are obtained. For coded MIMO system with AS, we started by designing adaptive STBCs then we showed that the AS technology provides a significant SNR gain of more than 3 dB by simply increasing the number of available transmit antennas. With low cost and low complexity increase, a substantial performance improve can be obtained using the AS technology for coded MIMO systems.

We highlight that the proposed BMI criterion is a useful tool to design STBC optimized at a target specific SNR. Furthermore, it serves to predict the performance of a particular STBC, classify STBCs and select the suitable STBC for a coded MIMO system.

Conventional STBCs designed according to the rank-determinant criteria achieve the asymptotic DMT tradeoff formulated in [ZT03] by Zheng and Tse [EKP⁺06, ORBV06]. Recently, the finite-SNR DMT was proposed to characterize the interplay between diversity and multiplexing at finite SNR [Nar06]. Our last contribution in **Chapter 4** consists of the derivation of the exact finite-SNR DMT for MIMO systems with dual antennas. We considered both uncorrelated and correlated Rayleigh fading channels. For 2×2 system, we showed that our results either in terms of outage probability or finite-SNR DMT are identical to the ones obtained by Monte Carlo simulations. Afterwards, we proved that the maximum achievable diversity at finite SNRs, obtained when r tends to 0, is independent from spatial correlation. For correlated channels, we showed that the diversity gain is slightly degraded at low to moderate spatial correlations while it is severely degraded at high correlations. Furthermore, we investigated

the difference between $N_t \times 2$ and $2 \times N_r$ systems. We showed that receive antennas provide higher diversity gains with respect to transmit antennas especially at low to moderate SNRs. Finally, we observed that achievable diversity gains at realistic SNRs are significantly lower than asymptotic values. Anyway, the finite-SNR DMT converges to the conventional asymptotic DMT at high SNRs.

Finally, we highlight several interesting perspectives of our work.

Perspectives

The first perspective consists in the extension of the work *i.e.*, the design of adaptive STBCs, for coded MIMO systems with higher number of antennas. Actually, recent wireless communication system standards define the use of up to 4×4 antennas for the WiMAX and 8×8 for the LTE-A.

Second, we showed that the proposed BMI criterion is an efficient tool to design and select STBCs for coded MIMO systems. However, it remains an empirical criterion as it is based on Monte Carlo simulations. Besides, the finite-SNR DMT is an analytical framework to characterize MIMO channels at finite-SNR. This finite-SNR DMT could provide new insights on the design of STBCs at operational SNRs. Furthermore, the finite-SNR DMT for the proposed adaptive TO STBC has still to be computed and to be compared with the MIMO channel finite-SNR DMT.

Third, through our work, we only considered an optimal ML-detector. Practical communication systems promote the use of low complexity detectors *e.g.*, list sphere detector [HtB03] and MMSE. It is important to examine the optimization of standardized STBCs according to the BMI criterion for systems implementing low complexity detectors. Recently, some papers address the design of STBCs for MIMO systems with a turbo MMSE equaliser [SHA12].

Also, we only considered Rayleigh fading channels. A further step could involve considering other channel types as Rician fading and introduce the Doppler effect in the channel model.

Furthermore, we assumed that a perfect CSI is available at the receiver and considered parameters (E_b/N_0 , correlation, AS feedback values) are perfectly estimated. It is worth examining the effect of estimation errors on the system performance.

In the same context, the work on the BMI criterion and the adaptive STBCs can be extended to the precoded MIMO systems, where a perfect or a partial CSI is assumed at the transmitter.

The last perspective consists of the application of the proposed work in the context of cooperative systems. Cooperative communications have been proposed to exploit the spatial diversity gains inherent in multiuser wireless systems without the need of multiple antennas at each node. Therefore, the cooperation between communication

nodes is equivalent to a distributed MIMO system. Several papers have proposed the use of distributive space-time codes where the space-time code is split into parts and each part is transmitted by a transmit node [LW03, JHHN04, YB07]. On the other hand, distributed capacity-approaching FEC coding where the encoder is split into parts and each part is transmitted by a transmit node, is also investigated [ZV03, JHHN04, YG11]. A scheme using distributive space-time coding associated to a conventional/distributive capacity-approaching FEC coding is to be addressed. The proposed works like the BMI criterion and the adaptive STBCs are to be extended to the coded cooperation system.

Appendix A

Optimization of Matrix D STBC Parameter according to the BMI Criterion

For 4-QAM modulation, the optimization of the MD STBC according to the BMI criterion provides $\varphi_{\text{opt}}^{4\text{-QAM}} = 135^\circ$ for $E_{bu}/N_0 \leq 5.5$ dB and $\varphi_{\text{opt}}^{4\text{-QAM}} = 114.29^\circ$ for $E_{bu}/N_0 \geq 11$ dB. In the range $5.5 \text{ dB} < E_{bu}/N_0 < 11$ dB, a $\varphi_{\text{opt}}^{4\text{-QAM}}$ is obtained at each E_{bu}/N_0 . Table A.1 provides obtained φ for each E_{bu}/N_0 with a step of 5° in φ and 0.25 dB in E_{bu}/N_0 .

In order to obtain an analytical approximation of $\varphi_{\text{opt}}^{4\text{-QAM}}$ as a function of E_{bu}/N_0 , we have performed a polynomial interpolation between values in Table A.1. We have found that a polynomial of degree 3 can be a good estimate passing by the points in Table A.1 (see Figure A.1). Note that polynomials with degree greater than 3 provide almost identical curve as the polynomial with degree 3. This interpolation leads to

$$\varphi_{\text{opt}}^{4\text{-QAM}} = \begin{cases} \varphi^{\text{Trace}} = 135^\circ; \text{ For } E_{bu}/N_0 \leq 5.5 \text{ dB} \\ -0.46 \left(\frac{E_{bu}}{N_0}\right)^3 + 11.92 \left(\frac{E_{bu}}{N_0}\right)^2 - 102.64 \left(\frac{E_{bu}}{N_0}\right) \\ + 414; \text{ For } 5.5 < E_{bu}/N_0 < 11 \text{ dB} \\ \varphi^{\text{Determinant}} = 114.29^\circ; \text{ For } E_{bu}/N_0 \geq 11 \text{ dB} \end{cases}$$

E_{bu}/N_0 in dB	φ
5.5	135°
5.75	130°
6	125°
6.25	125°
6.5	125°
6.75	125°
7	125°
7.25	120°
7.5	120°
7.75	120°
8	120°
8.25	120°
8.5	120°
8.75	120°
9	120°
9.25	120°
9.5	120°
9.75	120°
10	120°
10.25	120°
10.5	120°
10.75	115°
11	114.29°

TABLE A.1: MD STBC parameter φ optimized according to the BMI criterion as a function of E_{bu}/N_0 ; 4-QAM modulation.

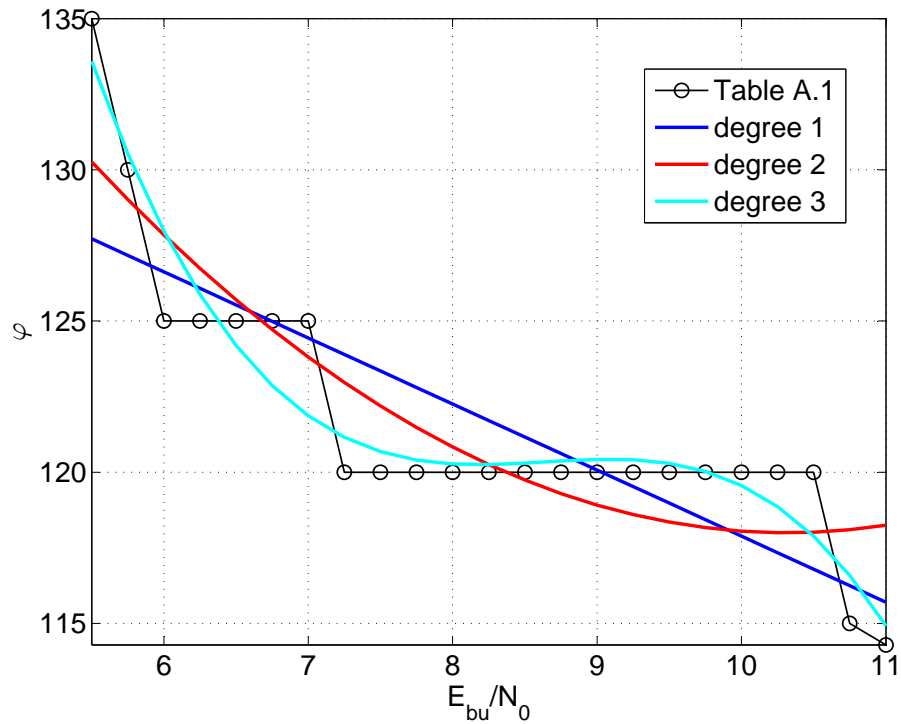


FIGURE A.1: Polynomial interpolation between φ values obtained according to the BMI criterion.

Appendix B

Optimization of Trace-Orthonormal STBC Parameter according to the BMI Criterion

For 4-QAM modulation, the optimization of the TO STBC according to the BMI criterion provides $\theta_{\text{opt}}^{4\text{-QAM}} = 45^\circ$ for $E_{bu}/N_0 \leq -0.5$ dB and $\theta_{\text{opt}}^{4\text{-QAM}} = 13.28^\circ$ for $E_{bu}/N_0 \geq 4.25$ dB. In the range -0.5 dB $< E_{bu}/N_0 < 4.25$ dB, a $\theta_{\text{opt}}^{4\text{-QAM}}$ is obtained at each E_{bu}/N_0 . Table B.1 provides obtained θ for each E_{bu}/N_0 with a step of 5° in θ and 0.25 dB in E_{bu}/N_0 .

In order to obtain an analytical approximation of $\theta_{\text{opt}}^{4\text{-QAM}}$ as a function of E_{bu}/N_0 , we have performed a polynomial interpolation between values in Table B.1. This interpolation is depicted in Figure B.1. A polynomial with degree equal to 3 is chosen. Note that polynomials with degree greater than 3 provide almost identical curve as the polynomial with degree 3. This interpolation leads to

$$\theta_{\text{opt}}^{4\text{-QAM}} = \begin{cases} 45^\circ; & \text{For } E_{bu}/N_0 \leq -0.5 \text{ dB} \\ -0.65 \left(\frac{E_{bu}}{N_0}\right)^3 + 4.79 \left(\frac{E_{bu}}{N_0}\right)^2 - 13.8 \left(\frac{E_{bu}}{N_0}\right) \\ \quad + 36.47; & \text{For } -0.5 < E_{bu}/N_0 < 4.25 \text{ dB} \\ 13.28^\circ; & \text{For } E_{bu}/N_0 \geq 4.25 \text{ dB} \end{cases}$$

E_{bu}/N_0 in dB	θ
-0.5	45°
-0.25	40°
0	35°
0.25	35°
0.5	30°
0.75	30°
1	25°
1.25	25°
1.5	25°
1.75	25°
2	25°
2.25	20°
2.5	20°
2.75	20°
3	20°
3.25	20°
3.5	20°
3.75	20°
4	15°
4.25	13.28°

TABLE B.1: TO STBC parameter θ optimized according to the BMI criterion as a function of E_{bu}/N_0 ; 4-QAM modulation.

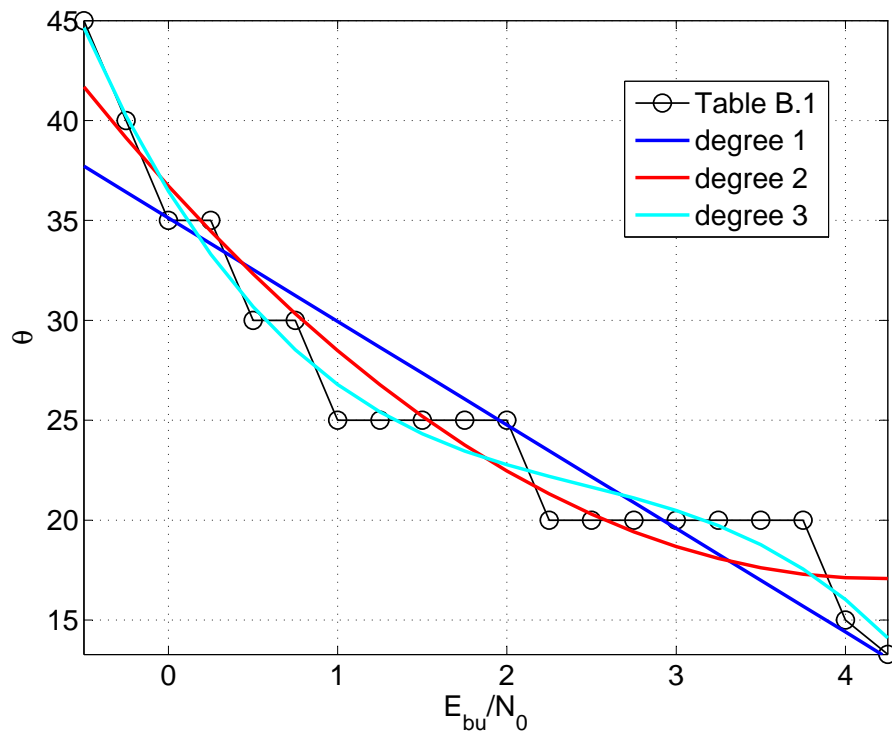


FIGURE B.1: Polynomial interpolation between θ values obtained according to the BMI criterion.

Appendix C

Transmitted Constellation for Trace-Orthonormal STBC

The constellation of transmitted signals encoded by the original trace-orthonormal STBC [ZLW07] is equivalent to a rotated version of the GC constellation. Indeed, one can prove that

$$\begin{aligned}
\frac{1}{\sqrt{2}} X_{12} e^{j\frac{1}{2} \arcsin \frac{1}{\sqrt{5}}} &= \frac{1}{\sqrt{2}} e^{j\frac{\pi}{4}} \left((S_3 + S_4) \sin \theta + (S_4^* - S_3^*) \cos \theta \right) e^{j\frac{1}{2} \arcsin \frac{1}{\sqrt{5}}} \\
&= \begin{bmatrix} (\Re(S_4) + j\Im(S_3)) \sqrt{\frac{1}{2} \left(1 + \frac{1}{\sqrt{5}}\right)} \\ -(\Re(S_3) + j\Im(S_4)) \sqrt{\frac{1}{2} \left(1 - \frac{1}{\sqrt{5}}\right)} \end{bmatrix} \\
&\times \left[\cos \left(\frac{\pi}{4} + \frac{1}{2} \arcsin \frac{1}{\sqrt{5}} \right) + j \sin \left(\frac{\pi}{4} + \frac{1}{2} \arcsin \frac{1}{\sqrt{5}} \right) \right] \\
&= \frac{1}{\sqrt{5}} \begin{bmatrix} (\Re(S_4) + j\Im(S_3)) \left(1 + j\frac{1+\sqrt{5}}{2}\right) \\ +(\Re(S_3) + j\Im(S_4)) \left(\frac{1-\sqrt{5}}{2} - j\right) \end{bmatrix}
\end{aligned} \tag{C.1}$$

Similarly,

$$\begin{aligned}
\frac{1}{\sqrt{2}} X_{21} e^{j\frac{1}{2} \arcsin \frac{1}{\sqrt{5}}} &= \frac{1}{\sqrt{2}} e^{j\frac{\pi}{4}} \left((S_3 + S_4) \cos \theta + (S_3^* - S_4^*) \sin \theta \right) e^{j\frac{1}{2} \arcsin \frac{1}{\sqrt{5}}} \\
&= \begin{bmatrix} (\Re(S_3) + j\Im(S_4)) \sqrt{\frac{1}{2} \left(1 + \frac{1}{\sqrt{5}}\right)} \\ +(\Re(S_4) + j\Im(S_3)) \sqrt{\frac{1}{2} \left(1 - \frac{1}{\sqrt{5}}\right)} \end{bmatrix} \\
&\times \left[\cos \left(\frac{\pi}{4} + \frac{1}{2} \arcsin \frac{1}{\sqrt{5}} \right) + j \sin \left(\frac{\pi}{4} + \frac{1}{2} \arcsin \frac{1}{\sqrt{5}} \right) \right] \\
&= \frac{1}{\sqrt{5}} \begin{bmatrix} (\Re(S_3) + j\Im(S_4)) \left(1 + j\frac{1+\sqrt{5}}{2}\right) \\ -(\Re(S_4) + j\Im(S_3)) \left(\frac{1-\sqrt{5}}{2} - j\right) \end{bmatrix}
\end{aligned} \tag{C.2}$$

and

$$\begin{aligned}
\frac{1}{\sqrt{2}} X_{22} e^{-j\vartheta} &= \frac{1}{\sqrt{2}} [(S_1 + S_2) \sin \theta + (S_1^* - S_2^*) \cos \theta] e^{-j\vartheta} \\
&= \begin{bmatrix} (\Re(S_1) + j\Im(S_2)) \sqrt{\frac{1}{2} \left(1 + \frac{1}{\sqrt{5}}\right)} \\ -(\Re(S_2) + j\Im(S_1)) \sqrt{\frac{1}{2} \left(1 - \frac{1}{\sqrt{5}}\right)} \end{bmatrix} \\
&\times [\cos(-\vartheta) + j \sin(-\vartheta)] \\
&= \frac{1}{\sqrt{5}} \begin{bmatrix} (\Re(S_1) + j\Im(S_2)) \left(\frac{1+\sqrt{5}}{2} - j\right) \\ -(\Re(S_2) + j\Im(S_1)) \left(1 + j\frac{1-\sqrt{5}}{2}\right) \end{bmatrix}
\end{aligned} \tag{C.3}$$

These equations are equivalent to the ones of the Golden code [OV08, BRV05].

Appendix D

Derivation of Finite-SNR DMT for uncorrelated Rayleigh MIMO Channels

In this Appendix, we provide the computation of the joint pdf of x and y . Then, we compute $\frac{\partial P_{\text{out}}^{\text{uncorr}}(r, \rho)}{\partial \rho}$ employed in the derivation of the finite-SNR DMT for uncorrelated Rayleigh MIMO Channels.

Joint pdf of x and y

The joint pdf of the two nonzero ordered eigenvalues λ_1 and λ_2 ($\lambda_1 \geq \lambda_2$) is given by

$$f^{\text{uncorr}}(\lambda_1, \lambda_2) = \frac{(\lambda_1 \lambda_2)^{n-2}}{\Gamma(n) \Gamma(n-1)} (\lambda_1 - \lambda_2)^2 e^{-(\lambda_1 + \lambda_2)} \quad (\text{D.1})$$

The joint pdf of x and y can be derived from the one of λ_1 and λ_2 by

$$f^{\text{uncorr}}(x, y) = f^{\text{uncorr}}(\lambda_1, \lambda_2) \frac{\partial \lambda_1}{\partial x} \frac{\partial \lambda_2}{\partial y} \quad (\text{D.2})$$

where

$$\lambda_1 \triangleq \frac{N_t}{\rho} (e^x - 1) \quad \text{and} \quad \lambda_2 \triangleq \frac{N_t}{\rho} (e^y - 1). \quad (\text{D.3})$$

By replacing λ_1 and λ_2 in equation (D.1) and computing

$$\frac{\partial \lambda_1}{\partial x} = \frac{e^x N_t}{\rho} \quad \text{and} \quad \frac{\partial \lambda_2}{\partial y} = \frac{e^y N_t}{\rho}. \quad (\text{D.4})$$

leads to

$$\begin{aligned} f^{\text{uncorr}}(x, y) &= \left(\frac{N_t}{\rho}\right)^{2n} \frac{1}{\Gamma(n)\Gamma(n-1)} e^{x+y} (e^x - e^y)^2 \\ &\times (e^x - 1)^{n-2} (e^y - 1)^{n-2} e^{-\frac{N_t}{\rho}(e^x + e^y - 2)} \end{aligned} \quad (\text{D.5})$$

Computation of $\frac{\partial P_{\text{out}}^{\text{uncorr}}(r, \rho)}{\partial \rho}$

The Leibniz integral rule is used to compute the derivative of an integral and expressed by

$$\frac{\partial}{\partial \rho} \int_{a(\rho)}^{b(\rho)} f(I, \rho) dI = \int_{a(\rho)}^{b(\rho)} \frac{\partial f(I, \rho)}{\rho} dI + f(b(\rho), \rho) \frac{\partial b(\rho)}{\partial \rho} - f(a(\rho), \rho) \frac{\partial a(\rho)}{\partial \rho} \quad (\text{D.6})$$

In our case,

$$P_{\text{out}}^{\text{uncorr}}(r, \rho) = \int_0^R f^{\text{uncorr}}(I, \rho) dI \quad (\text{D.7})$$

where

$$\begin{aligned} f^{\text{uncorr}}(I, \rho) &= \left(\frac{N_t}{\rho}\right)^{2n} \frac{1}{\Gamma(n)\Gamma(n-1)} e^I \\ &\times \int_0^{I/2} g^{\text{uncorr}}(y, I, \rho) dy \end{aligned} \quad (\text{D.8})$$

and $g^{\text{uncorr}}(y, I, \rho)$

$$\begin{aligned} g^{\text{uncorr}}(y, I, \rho) &= (e^{I-y} - e^y)^2 (e^{I-y} - 1)^{n-2} \\ &\times (e^y - 1)^{n-2} e^{-\frac{N_t}{\rho}(e^{I-y} + e^y - 2)}. \end{aligned} \quad (\text{D.9})$$

Afterwards,

$$\frac{\partial P_{\text{out}}^{\text{uncorr}}(r, \rho)}{\partial \rho} = \frac{\partial}{\partial \rho} \int_0^R f^{\text{uncorr}}(I, \rho) dI \quad (\text{D.10})$$

can be computed using the Leibniz integral rule where $a(\rho) = 0$ and $b(\rho) = R = r \log(1 + G\rho)$. Therefore,

$$f^{\text{uncorr}}(a(\rho), \rho) \frac{\partial a(\rho)}{\partial \rho} = 0, \quad (\text{D.11})$$

and

$$\begin{aligned} \frac{\partial P_{\text{out}}^{\text{uncorr}}(r, \rho)}{\partial \rho} &= \int_{a(\rho)}^{b(\rho)} \frac{\partial f^{\text{uncorr}}(I, \rho)}{\rho} dI + f^{\text{uncorr}}(b(\rho), \rho) \frac{\partial b(\rho)}{\partial \rho} \\ &= A_1^{\text{uncorr}}(r, \rho) + A_2^{\text{uncorr}}(r, \rho) + A_3^{\text{uncorr}}(r, \rho) \end{aligned} \quad (\text{D.12})$$

Indeed,

$$\begin{aligned} f^{\text{uncorr}}(b(\rho), \rho) \frac{\partial b(\rho)}{\partial \rho} &= f^{\text{uncorr}}(r \log(1 + G\rho), \rho) \frac{rG}{1+G\rho} \\ &= \left(\frac{N_t}{\rho}\right)^{2n} \frac{1}{\Gamma(n)\Gamma(n-1)} e^{r \log(1+G\rho)} \\ &\times \left(\int_0^{r \log(1+G\rho)/2} g^{\text{uncorr}}(y, r \log(1 + G\rho), \rho) dy \right) \frac{rG}{1+G\rho} \\ &= A_2^{\text{uncorr}}(r, \rho) \end{aligned} \quad (\text{D.13})$$

and

$$\begin{aligned}
\int_{a(\rho)}^{b(\rho)} \frac{\partial f^{\text{uncorr}}(I, \rho)}{\rho} dI &= \left[\begin{aligned} &\left(\frac{N_t}{\rho}\right)^{2n} \frac{1}{\Gamma(n)\Gamma(n-1)} \\ &\times \int_0^{r \log(1+G\rho)} e^I \left(\int_0^{I/2} \frac{\partial g^{\text{uncorr}}(y, I, \rho)}{\partial \rho} dy \right) dI \end{aligned} \right] \\
&+ \left[\begin{aligned} &-2n \left(\frac{N_t}{\rho}\right)^{2n} \frac{1}{\rho^{2n+1} \Gamma(n)\Gamma(n-1)} \\ &\times \int_0^{r \log(1+G\rho)} e^I \left(\int_0^{I/2} g^{\text{uncorr}}(y, I, \rho) dy \right) dI \end{aligned} \right] \\
&= A_3^{\text{uncorr}}(r, \rho) + A_1^{\text{uncorr}}(r, \rho)
\end{aligned} \tag{D.14}$$

List of Publications

1. **A. El Falou**, C. Langlais, C. Abdel Nour and C. Douillard. Codage spatio-temporel adaptatif pour les systèmes MIMO utilisant un codage de canal à fort pouvoir de correction. In *Proc. GRETSI*, September 2013.
2. **A. El Falou**, W. Hamouda, C. Langlais, C. Abdel Nour and C. Douillard. Finite-SNR Diversity-Multiplexing Tradeoff for Rayleigh MIMO Channels. *IEEE Commun. Lett.*, vol. 17, no. 4, pp. 753-756, April 2013.
3. **A. El Falou**, C. Langlais, C. Abdel Nour and C. Douillard. Adaptive trace-orthonormal STBC for MIMO system with capacity approaching FEC codes. In *Proc. IEEE Vehicular Technology Conference (VTC)*, September 2012.
4. **A. El Falou**, C. Langlais, C. Abdel Nour and C. Douillard. Low ML-detection complexity, adaptive 2×2 STBC, with powerful FEC codes. In *Proc. Int. Symp. on Turbo Codes & Iterative Information Processing*, August 2012.
5. **A. El Falou**, C. Abdel Nour, C. Langlais and C. Douillard. Low decoding complexity STBC design for turbo coded broadcast transmission. In *Proc. IEEE Int. Symp. on Broadband Multimedia Syst. and Broadcast. (BMSB)*, June 2011.

Bibliography

- [Ala98] S.M. Alamouti. A simple transmit diversity technique for wireless communications. *IEEE J. Sel. Areas in Commun.*, 16(8):1451–1458, October 1998.
- [BCC⁺07] E. Biglieri, R. Calderbank, A. Constantinides, A. Goldsmith, A. Paulraj, and H.V. Poor. *MIMO Wireless Communications*. Cambridge Univ. Press, 2007.
- [BCJR74] L. Bahl, J. Cocke, F. Jelinek, and J. Raviv. Optimal decoding of linear codes for minimizing symbol error rate. *IEEE Trans. Inf. Theory*, 20(2):284–287, March 1974.
- [BEFN04] B. Bisla, R. Eline, and L.M. Franca-Neto. RF system and circuit challenges for WiMAX. *Intel Tech. J.*, 8(3):189–200, 2004.
- [BGT93] C. Berrou, A. Glavieux, and P. Thitimajshima. Near Shannon limit error correcting coding and decoding: turbo-codes. In *Proc. IEEE Int. Conf. Commun. (ICC)*, pages 1064–1070, May 1993.
- [BJDK01] C. Berrou, M. Jezequel, C. Douillard, and S. Kerouedan. The advantages of non-binary turbo codes. In *Proc. IEEE Inf. Theory Workshop*, pages 61–63, September 2001.
- [BP12] S.C. Del Barrio and G.F. Pedersen. Correlation evaluation on small LTE handsets. In *Proc. IEEE Vehicular Technology Conference (VTC)*, September 2012.
- [BRV05] J.-C. Belfiore, G. Rekaya, and E. Viterbo. The golden code: a 2×2 full-rate space-time code with nonvanishing determinants. *IEEE Trans. Inf. Theory*, 51(4):1432–1436, April 2005.
- [CCG79] J.B. Cain, G.C. Clark, and J.M. Geist. Punctured convolutional codes of rate $(n - l)/n$ and simplified maximum likelihood decoding. *IEEE Trans. Inf. Theory*, 25(1):97–100, January 1979.

- [CCL06] W. Chang, S.-Y. Chung, and Y.H. Lee. Diversity-multiplexing tradeoff in rank-deficient and spatially correlated MIMO channels. In *Proc. IEEE Int. Symp. Inf. Theory (ISIT)*, pages 1144–1148, 2006.
- [CTB98] G. Caire, G. Taricco, and E. Biglieri. Bit-interleaved coded modulation. *IEEE Trans. Inf. Theory*, 44(3):927–946, May 1998.
- [CTD⁺05] K.M. Chugg, P. Thiennviboon, G.D. Dimou, P. Gray, and J. Melzer. New class of turbo-like codes with universally good performance and high-speed decoding. In *Proc. IEEE Military Communications Conference (MILCOM)*, pages 3117–3126, October 2005.
- [CYV01] Z. Chen, J. Yuan, and B. Vucetic. Improved space-time trellis coded modulation scheme on slow rayleigh fading channels. *Electron. Lett.*, 37(7):440–441, March 2001.
- [DB05] C. Douillard and C. Berrou. Turbo codes with rate- $m/(m+1)$ constituent convolutional codes. *IEEE Trans. Commun.*, 53(10):1630–1638, October 2005.
- [DG07] T.M. Duman and A. Ghayeb. *Coding for MIMO communication systems*. John Wiley & Sons, 2007.
- [DHP06] J.-B. Dore, M.-H. Hamon, and P. Penard. High speed decoding of serial concatenated codes. In *Proc. IEEE Global Commun. Conf. (GLOBECOM)*, pages 1–5, December 2006.
- [DV05] P. Dayal and M.K. Varanasi. An optimal two transmit antenna space-time code and its stacked extensions. *IEEE Trans. Inf. Theory*, 51(12):4348–4355, December 2005.
- [DVB02] Interaction channel for digital terrestrial television. DVB, ETSI EN 301 985, 2002.
- [DVB09] Interaction channel for satellite distribution systems. DVB, ETSI EN 301 790, v1.5.1, May 2009.
- [EALD11] A. El Falou, C. Abdel Nour, C. Langlais, and C. Douillard. Low decoding complexity STBC design for turbo coded broadcast transmission. In *Proc. IEEE Int. Symp. on Broadband Multimedia Syst. and Broadcast. (BMSB)*, June 2011.
- [EHL⁺13] A. El Falou, W. Hamouda, C. Langlais, C. Abdel Nour, and C. Douillard. Finite-SNR diversity-multiplexing tradeoff for rayleigh MIMO channels. *IEEE Commun. Lett.*, 17(4):753–756, April 2013.

- [EKP⁺06] P. Elia, K.R. Kumar, S.A. Pawar, P.V. Kumar, and H.-F. Lu. Explicit space-time codes achieving the diversity-multiplexing gain tradeoff. *IEEE Trans. Inf. Theory*, 52(9):3869–3884, September 2006.
- [ELAD12a] A. El Falou, C. Langlais, C. Abdel Nour, and C. Douillard. Adaptive trace-orthonormal STBC for MIMO system with capacity approaching FEC codes. In *Proc. IEEE Vehicular Technology Conference (VTC)*, September 2012.
- [ELAD12b] A. El Falou, C. Langlais, C. Abdel Nour, and C. Douillard. Low ML-detection complexity, adaptive 2×2 STBC, with powerful FEC codes. In *Proc. Int. Symp. on Turbo Codes & Iterative Information Processing*, August 2012.
- [ELAD13] A. El Falou, C. Langlais, C. Abdel Nour, and C. Douillard. Codage spatio-temporel adaptatif pour les systèmes MIMO utilisant un codage de canal à fort pouvoir de correction. In *Proc. GRETSI*, September 2013.
- [Eli55] P. Elias. Coding for noisy channel. *I.R.E Conv.Rec.*, 3:37–46, March 1955.
- [EM07a] H. Ebrahimzad and A. Mohammadi. Diversity-multiplexing tradeoff in MIMO system with finite SNR. In *European Conference on Wireless Technologies*, pages 146–149, October 2007.
- [EM07b] H. Ebrahimzad and A. Mohammadi. Diversity-multiplexing tradeoff in MISO/SIMO systems at finite SNR. In *Proc. IEEE Vehicular Technology Conference (VTC)*, pages 594–598, April 2007.
- [ESK07] P. Elia, B.A. Sethuraman, and P. Vijay Kumar. Perfect space-time codes for any number of antennas. *IEEE Trans. Inf. Theory*, 53(11):3853–3868, November 2007.
- [FF73] D.D. Falconer and G.J. Foschini. Theory of minimum mean-square-error qam systems employing decision feedback equalization. *Bell Syst. Techn. J.*, pages 1821–1849, December 1973.
- [FG98] G.J. Foschini and M.J. Gans. On limits of wireless communications in a fading environment when using multiple antennas. *Wireless Personal Communications*, 6:311–335, March 1998.
- [Fos96] G.J. Foschini. Layered space-time architecture for wireless communication in a fading environment when using multi-element antennas. *Bell Labs Tech. J.*, 1(2):41–59, 1996.

- [Gal62] R. Gallager. Low-density parity-check codes. *IEEE Trans. Inf. Theory*, 8(1):21–28, January 1962.
- [GBB08] N. Gresset, L. Brunel, and J.J. Boutros. Space-time coding techniques with bit-interleaved coded modulations for MIMO block-fading channels. *IEEE Trans. Inf. Theory*, 54(5):2156–2178, May 2008.
- [GBM09] I. Gutierrez, F. Bader, and A. Mourad. Joint transmit antenna and space-time coding selection for wimax mimo systems. In *Proc. IEEE Int. Symp. on Personal, Indoor and Mobile Radio Commun. (PIMRC)*, pages 3138–3143, 2009.
- [GP01] D. Gore and A. Paulraj. Space-time block coding with optimal antenna selection. In *Proc. IEEE Int. Conf. Acoust., Speech, and Signal Processing*, May 2001.
- [GP02] D.A. Gore and A.J. Paulraj. MIMO antenna subset selection with space-time coding. *IEEE Trans. Signal Processing*, 50(10):2580–2588, 2002.
- [GSsS⁺03] D. Gesbert, M. Shaf, Da shan Shiu, P.J. Smith, and A. Naguib. From theory to practice: an overview of MIMO space-time coded wireless systems. *IEEE J. Sel. Areas in Commun.*, 21(3):281–302, April 2003.
- [Hag04] J. Hagenauer. The EXIT chart—introduction to EXtrinsic Information Transfer in iterative processing. In *Proc. European Signal Processing Conf.*, pages 1541–1548, September 2004.
- [HH89] J. Hagenauer and P. Hoeher. A viterbi algorithm with soft-decision outputs and its applications. In *Proc. IEEE Global Commun. Conf. (GLOBECOM)*, pages 1680–1686, November 1989.
- [HH02] B. Hassibi and B.M. Hochwald. High-rate codes that are linear in space and time. *IEEE Trans. Inf. Theory*, 48(7):1804–1824, July 2002.
- [HtB03] B.M. Hochwald and S. ten Brink. Achieving near-capacity on a multiple-antenna channel. *IEEE Trans. Commun.*, 51(3):389–399, March 2003.
- [HTW03] A. Hottinen, O. Tirkkonen, and R. Wichman. *Multi-antenna Transceiver Techniques for 3G and Beyond*. John Wiley & Sons, 2003.
- [IEE06] IEEE 802.16-2005: IEEE standard for local and metropolitan area networks - Part 16: Air Interface for Fixed and Mobile Broadband Wireless Access Systems – Amendment 2: Physical Layer and Medium Access Control Layers for Combined Fixed and Mobile Operation in Licensed Bands, February 2006.

- [Ism11] A. Ismail. *Codes Espace-Temps à Faible Complexité pour Systèmes MIMO*. PhD thesis, Supélec, 2011.
- [ITU12] ITU. International telecommunication union: Key global telecom indicators for the world telecommunication service sector. http://www.itu.int/ITU-D/ict/statistics/at_glance/KeyTelecom.html, 2012.
- [Jam64] A.T. James. Distributions of matrix variates and latent roots derived from normal samples. *The Annals of Mathematical Statistics*, 35(2):475–501, June 1964.
- [JHHN04] M. Janani, A. Hedayat, T.E. Hunter, and A. Nosratinia. Coded cooperation in wireless communications: space-time transmission and iterative decoding. *IEEE Trans. Signal Processing*, 52(2):362–371, February 2004.
- [Kba11] D. Kbaier. *Towards ideal codes : looking for new turbo code schemes*. PhD thesis, September 2011.
- [KDK10] D. Kbaier, C. Douillard, and S. Kerouedan. Reducing the convergence loss of 3-dimensional turbo codes. In *Proc. Int. Symp. on Turbo Codes & Iterative Information Processing*, September 2010.
- [KSB09] R. Kobeissi, S. Sezginer, and F. Buda. Downlink performance analysis of full-rate STCs in 2×2 MIMO WiMAX systems. In *Proc. IEEE Vehicular Technology Conference (VTC)*, April 2009.
- [KSP⁺02] J.P. Kermoal, L. Schumacher, K.I. Pedersen, P.E. Mogensen, and F. Frederiksen. A stochastic MIMO radio channel model with experimental validation. *IEEE J. Sel. Areas in Commun.*, 20(6):1211–1226, August 2002.
- [LJ10] A. Lozano and N. Jindal. Transmit diversity vs. spatial multiplexing in modern MIMO systems. *IEEE Trans. Wireless Commun.*, 9(1):186–197, January 2010.
- [LL10] S. Loyka and G. Levin. Finite-SNR diversity-multiplexing tradeoff via asymptotic analysis of large MIMO systems. *IEEE Trans. Inf. Theory*, 56(10):4781–4792, October 2010.
- [Loy01] S.L. Loyka. Channel capacity of MIMO architecture using the exponential correlation matrix. *IEEE Commun. Lett.*, 5(9):369–371, September 2001.
- [LW03] J.N. Laneman and G.W. Wornell. Distributed space-time-coded protocols for exploiting cooperative diversity in wireless networks. *IEEE Trans. Inf. Theory*, 49(10):2415–2425, October 2003.

- [MKV⁺12] S. Moon, W.S. Ko, D. Vargas, G. Serrano, M.D. Nisar, and V. Pauli. Enhanced spatial multiplexing for rate-2 MIMO of DVB-NGH system. In *19th Int. Conf. on Telecommun. (ICT)*, April 2012.
- [MN96] D.J.C. MacKay and R.M. Neal. Near shannon limit performance of low density parity check codes. *Electron. Lett.*, 32(18):1645–1646, 1996.
- [MRLB12] L. Mroueh, S. Rouquette-Leveil, and J.-C. Belfiore. Application of perfect space time codes: PEP bounds and some practical insights. *IEEE Trans. Commun.*, 60(3):747–755, 2012.
- [MRLRB07] L. Mroueh, S. Rouquette-Leveil, G. Rekaya, and J.-C. Belfiore. On the performance of the golden code in BICM-MIMO and in IEEE 802.11n cases. In *Asilomar Conf. on Signals, Systems and Computers (ACSSC)*, November 2007.
- [MW04] A.F. Molisch and M.Z. Win. MIMO systems with antenna selection. *IEEE Microwave Mag.*, 5(1):46–56, 2004.
- [Nar05] R. Narasimhan. Finite-SNR diversity performance of rate-adaptive MIMO systems. In *Proc. IEEE Global Commun. Conf. (GLOBECOM)*, December 2005.
- [Nar06] R. Narasimhan. Finite-SNR diversity-multiplexing tradeoff for correlated Rayleigh and Rician MIMO channels. *IEEE Trans. Inf. Theory*, 52(9):3965–3979, September 2006.
- [NEC05] R. Narasimhan, A. Ekbal, and J.M. Cioffi. Finite-SNR diversity-multiplexing tradeoff of space-time codes. In *Proc. IEEE Int. Conf. Commun. (ICC)*, pages 458 – 462, May 2005.
- [NGP00] R. Nabar, D. Gore, and A. Paulraj. Optimal selection and use of transmit antennas in wireless systems. In *Proc. Int. Conf. Telecommun. (ICT)*, 2000.
- [Nua07] L. Nuaymi. *WiMAX: Technology for Broadband Wireless Access*. John Wiley & Sons, 2007.
- [OBV07] F. Oggier, J.-C. Belfiore, and E. Viterbo. Cyclic division algebras: A tool for space-time coding. *Foundations and Trends in Communications and Information Theory*, 4(1):1–95, 2007.
- [OC07] C. Oestges and B. Clerckx. *MIMO Wireless Communications: From Real-World Propagation to Space-Time Code Design*. Academic Press (Elsevier), 2007.

- [ORBV06] F. Oggier, G. Rekaya, J.-C. Belfiore, and E. Viterbo. Perfect space-time block codes. *IEEE Trans. Inf. Theory*, 52(9):3885–3902, September 2006.
- [OV08] F. Oggier and E. Viterbo. The golden code. http://www.ecse.monash.edu.au/staff/eviterbo/perfect_codes/Golden_Code.html, 2008.
- [Pät02] M. Pätzold. *Mobile fading channels*. John Wiley, 2002.
- [PGGA08] J.M. Paredes, A.B. Gershman, and M. Gharavi-Alkhansari. A new full-rate full-diversity space-time block code with nonvanishing determinants and simplified maximum-likelihood decoding. *IEEE Trans. Signal Processing*, 56(6):2461–2469, June 2008.
- [PK94] A.J. Paulraj and T. Kailath. Increasing capacity in wireless broadcast systems using distributed transmission/directional reception (DTDR), 1994. US Patent 5,345,599.
- [PM10] P. Petrov and Y. Murakami. The effect of LoS components on MIMO performance. DVB TM-H document TM-NGH591, 2010.
- [PP02] A. Papoulis and S.U. Pillai. *Probability, random variable, and stochastic processes, Fourth edition*. McGraw-Hill. Press, 2002.
- [Pri72] R. Price. Nonlinearly feedback-equalizer PAM vs. capacity from noisy filter channel. In *Proc. IEEE Int. Conf. Commun. (ICC)*, June 1972.
- [RCHG06] Z. Rezki, B. Cotruta, D. Haccoun, and F. Gagnon. Finite diversity multiplexing tradeoff over spatially correlated channels. In *Proc. IEEE Vehicular Technology Conference (VTC)*, September 2006.
- [RHGA10] Z. Rezki, D. Haccoun, F. Gagnon, and W. Ajib. Diversity-multiplexing tradeoff over correlated Rayleigh fading channels: a non-asymptotic analysis. *Wirel. Commun. Mob. Comput.*, 10(2):188–199, February 2010.
- [RV05] T. Ratnarajah and R. Vaillancourt. Quadratic forms on complex random matrices and multiple-antenna systems. *IEEE Trans. Inf. Theory*, 51(8):2976–2984, August 2005.
- [RVH95] P. Robertson, E. Villebrun, and P. Hoeher. A comparison of optimal and sub-optimal map decoding algorithms operating in the log domain. In *Proc. IEEE Int. Conf. Commun. (ICC)*, volume 2, pages 1009–1013, June 1995.
- [Sha48] C.E. Shannon. A mathematical theory of communication. *Bell Syst. Techn. J.*, 27(1):79–423, July 1948.

- [SHA12] M. Sayed-Hassan and K. Amis. On the design of full-rate full-diversity space-time block codes for multiple-input-multiple-output systems with a turbo minimum mean square error equaliser at the receiver side. *IET Communications*, 6(18):3065–3074, December 2012.
- [Skl01] B. Sklar. *Digital Communications: Fundamentals and Applications*. Prentice-Hall PTR, second edition, 2001.
- [SOZ11] A. Sibille, C. Oestges, and A. Zanella. *MIMO: From Theory to Implementation*. Elsevier Inc., 2011.
- [SR08] K.P. Srinath and B.S. Rajan. A low-complexity, full-rate, full-diversity 2×2 STBC with golden code’s coding gain. In *Proc. IEEE Global Commun. Conf. (GLOBECOM)*, December 2008.
- [SS07] S. Sezginer and H. Sari. Full-rate full-diversity 2×2 space-time codes of reduced decoder complexity. *IEEE Commun. Lett.*, 11(12):973–975, December 2007.
- [SSB⁺08] S. Sezginer, H. Sari, B. Muquet, F. Buda, S. Labonte, and J. Gosteau. Matrix D: full-rate, full-diversity 2×2 space-time code with low-complexity ML detection. *IEEE 802.16 Broadband Wireless Access Working Group*, May 2008.
- [SSB09] S. Sezginer, H. Sari, and E. Biglieri. On high-rate full-diversity 2×2 space-time codes with low-complexity optimum detection. *IEEE Trans. Commun.*, 57(5):1532–1541, May 2009.
- [SSCL01] Ming-Der Shieh, Ming-Hwa Sheu, Chung-Ho Chen, and Hsin-FU Lo. A systematic approach for parallel CRC computations. *Journal of information science and engineering*, 17(1):445–461, September 2001.
- [tB01] S. ten Brink. Convergence behavior of iteratively decoded parallel concatenated codes. *IEEE Trans. Commun.*, 49(10):1727–1737, October 2001.
- [TC01] M. Tao and R.S. Cheng. Improved design criteria and new trellis codes for space-time coded modulation in slow flat fading channels. *IEEE Commun. Lett.*, 5(7):313–315, July 2001.
- [Tel99] I.E. Telatar. Capacity of multi-antenna gaussian channels. *Europ. Trans. Telecommun.*, 10:585–595, 1999.
- [TJC99] V. Tarokh, H. Jafarkhani, and A.R. Calderbank. Space-time block codes from orthogonal designs. *IEEE Trans. Inf. Theory*, 45(5):1456–1467, July 1999.

- [TSC98] V. Tarokh, N. Seshadri, and A.R. Calderbank. Space-time codes for high data rate wireless communications: Performance criterion and code construction. *IEEE Trans. Inf. Theory*, 44(2):744–765, March 1998.
- [vNP00] R. van Nee and R. Prasad. *OFDM for Wireless Multimedia Communications*. Artech House, 2000.
- [WFGV98] P.W. Wolniansky, G.J. Foschini, G.D. Golden, and R.A. Valenzuela. V-BLAST: an architecture for realizing very high data rates over the rich-scattering wireless channel. In *Proc. IEEE Int. Symp. on Signals, Syst. and Electronics (ISSSE)*, September 1998.
- [Wic95] S.B. Wicker. *Error Control Systems for Digital Communications and Storage*. Englewood Cliffs, XJ: Prentice Hall, 1995.
- [Win87] J. H. Winters. On the capacity of radio communication systems with diversity in a rayleigh fading environment. *IEEE J. Sel. Areas in Commun.*, 5(5):871–878, June 1987.
- [WLB09] Feng Wang, Xia Liu, and M.E. Bialkowski. Space time block coded MIMO system with redundant antennas. In *Int. Conf. on Information Assurance and Security (IAS)*, volume 2, pages 204–207, August 2009.
- [WSG94] J.H. Winters, J. Salz, and R.D. Gitlin. The impact of antenna diversity on the capacity of wireless communication systems. *IEEE Trans. Commun.*, 42(2):1740–1751, April 1994.
- [WW99] M.Z. Win and J.H. Winters. Analysis of hybrid selection/maximal-ratio combining in rayleigh fading. *IEEE Trans. Commun.*, 47(12):1773–1776, December 1999.
- [YB07] S. Yang and J.-C. Belfiore. Optimal space-time codes for the MIMO amplify-and-forward cooperative channel. *IEEE Trans. Inf. Theory*, 53(2):647–663, February 2007.
- [YBO⁺04] K. Yu, M. Bengtsson, B. Ottersten, D. McNamara, P. Karlsson, and M. Beach. Modeling of wide-band MIMO radio channels based on NLoS indoor measurements. *IEEE Trans. on Vehicular Technology*, 53(3):655–665, May 2004.
- [YG11] R. Youssef and A. Graell i Amat. Distributed serially concatenated codes for multi-source cooperative relay networks. *IEEE Trans. Wireless Commun.*, 10(1):253–263, 2011.

- [YW03] H. Yao and G.W. Wornell. Achieving the full MIMO diversity-multiplexing frontier with rotation-based space-time codes. In *Proc. Allerton Conf. Comm. Control and Computing*, October 2003.
- [ZLW07] J.-K. Zhang, J. Liu, and K.M. Wong. Trace-orthonormal full-diversity cyclotomic space-time codes. *IEEE Trans. Signal Processing*, 55(2):618–630, February 2007.
- [ZT03] L. Zheng and D.N.C. Tse. Diversity and multiplexing: a fundamental tradeoff in multiple-antenna channels. *IEEE Trans. Inf. Theory*, 49(5):1073–1096, May 2003.
- [ZV03] B. Zhao and M.C. Valenti. Distributed turbo coded diversity for relay channel. *Electron. Lett.*, 39(10):786–787, 2003.